A COMPARISON OF ANALOG AND DIGITAL DATA FOR MEASUREMENTS OF TURBULENCE PARAMETERS

by

Laura G. Ozimek

A thesis
presented to the University of Manitoba
in partial fulfillment of the
requirements for the degree of
Master of Science
in
Mechanical Engineering

Winnipeg, Manitoba

ISBN 0-315-37162-5

A COMPARISON OF ANALOG AND DIGITAL DATA FOR MEASUREMENTS OF TURBULENCE PARAMETERS

BY

LAURA G. OZIMEK

A thesis submitted to the Faculty of Graduate Studies of the University of Manitoba in partial fulfillment of the requirements of the degree of

MASTER OF SCIENCE

ABSTRACT

An experimental investigation of analog and digital data for measurement of various flow parameters has been undertaken. Comparative measurements of skewness, flatness and velocity spectra taken by different experimenters were examined for a turbulent boundary layer flow at a free stream velocity of 8 m/sec. Comparative measurements of skewness, flatness, mixed moments and spectra were examined for flow in an 8° conical diffuser with fully developed pipe flow at at entry. The Reynolds number based on the pipe diameter and pipe bulk velocity at entry to the diffuser was 130,000. Measurements in the boundary layer tunnel and the diffuser were taken perpendicular to the wall.

Single wire measurements taken in the boundary layer flow show no significant difference between analog and digital measurements. Single wire and cross wire measurements taken in the diffuser flow show the digital results cross the zero value ahead of corresponding analog results in such measurements as skewness and certain fourth order mixed moments. A greater amount of scatter between data points is seen in some higher order moments. Digital data for super skewness, super flatness and probability density functions of some parameters are also examined.

Based on the measurements presented in this research, it can be concluded that there is no difference between analog and digital values obtained for any physical quantity in turbulent flow provided adequate analog and digital systems are properly used.

ACKNOWLEDGEMENTS

I would like to thank Dr. R. S. Azad who initiated the project and guided me throughout this work, fellow student Robert W. Derksen who wrote the data acquisition and analysis programs for use with the PDP-11 computer, and Ken Tarte who helped ink some of the final drawings. To them, my appreciation, and most of all, my thanks.

NOMENCLATURE

A	a constant
B	a constant
C	a constant
d	pipe diameter, or diameter of hot wire
D	Preston tube outer diameter
f( )	a function of ( )
f(K)	Kolmogorov frequency, $f = U / 2\pi\eta$
h( )	a function of ( )
k	Karman constant, k=0.41
k_1	yaw correction for X-wire, $k_1 = 0.23$
k_2	pitch correction for X-wire, $k_2 \approx 1$
K( )	flatness factor or kurtosis
K_5	nondimensional 5th moment, super skewness
K_6	nondimensional 6th moment, super flatness
l	sensitive length of hot wire
m	a constant
n	a constant
p	static pressure
p_0	total pressure
p( )	probability density
PDF	probability density function
Re	Reynolds number, ud/ν
Re(λ)	turbulent Reynolds number, $u'\lambda/\nu$
rms	root mean square

S( )	skewness factor
T	time
u	axial velocity flow component
u'	rms of fluctuating axial velocity component
u_+	nondimensional velocity, u /u*
u*	friction velocity
$\overline{uv}$	Reynolds shear stress
U	mean axial velocity component
U_∞	free stream velocity
U_1	velocity parallel to probe supports
U_2	velocity parallel to probe sensor
U_3	binormal velocity
U(eff)	effective velocity
v	transverse or radial velocity flow component
v'	rms of transverse velocity component
V	voltage
$W(y/\delta)$	wake function
x	axial position
x*	nondimensional argument, $\log(\Delta p\ D^2/4\rho\nu^2)$
y	distance from a surface
y_+	nondimensional distance from a surface, yu^*/ν
y*	nondimensional function, $\log(\tau_0\ D^2/4\rho\nu^2)$
α	flow angle
γ	intermittency
δ	boundary layer thickness
Δ	inner pressure gradient parameter, $(\nu/\rho u^{*3})(dp/dx)$
Δp	pressure difference

ΔPc	contraction cone pressure drop
$\bar{\epsilon}$	dissipation rate, $15\ u'^2\ \nu\ /\lambda^2$
η	Kolmogorov length scale, $(\nu^3\ /\ \epsilon)^{1/4}$
λ	Taylor microscale
μ	dynamic viscosity
ν	kinematic viscosity, μ/ρ
π	a constant, 3.14159...
Π	pressure gradient parameter
ρ	fluid density
σ	standard deviation
σ^2	variance
τ	shear stress
τ_0	wall shear stress
$\partial u/\partial t$	axial velocity derivative

TABLE OF CONTENTS

Appendix page

LIST OF FIGURES

Chapter I

INTRODUCTION

1.1 HISTORICAL BACKGROUND

The origins of thermal anemometry can be traced to the last decade of the nineteenth century when Overbeck [1895] attempted velocity measurements in an air stream. The constant current anemometer he invented has since undergone vigorous development. Morris [1912] had invented the first constant temperature anemometer with manual adjust. Freymuth [1982] states that by 1921 the first constant temperature anemometer with automatic feedback, designed by Hill, Hargood-Ash and Griffiths, had been commercially sold. A step-up transformer for hot wire signal amplification was used as early as 1926 by Tyler, and Gupta [1927] reported the first electronic amplification of hot wire signals. Ziegler invented, but did not build, the first constant temperature anemometer with electronic feedback and linearizer in 1934. In 1931, three years earlier, he introduced square wave testing of the constant current anemometer. Square wave testing of the constant temperature anemometer was introduced much later by Staritz in 1960.

The original thermal anemometers were difficult to use and required expert care. In the period following the second World War, thermal anemometry developed from an art into a standard method of experimental flow research. Solid state electronics turned the hot wire anemometer from a troublesome instrument into a device easily used in simple flows after only a few hours training.

Although many of the basic analog instruments used in hot wire anemometry have not changed fundamentally since the 1960s, the methodology of extracting information from the turbulent signals has changed. Originally, most statistical measurements in turbulent flows were obtained with analog devices. Special circuits were constructed to add, subtract, multiply, integrate, differentiate, time delay, and filter the fluctuating electrical signals. Statistics determined from discretized values of the instantaneous fluctuations obtained from chart or oscillograph records were rarely done. The early computers were too slow and too small for analysis of wide band digital records to be practical. The development of analog-to-digital converters over the past twenty years has made digital computing of turbulent signals practical.

Due to the rapid development and implementation of high speed computers and digital sampling techniques, it is not possible to catalog all past applications of sampling techniques in turbulence research. However, an overview of some initial efforts in the use of discretized sampling and digital data handling in experimental turbulence is presented.

Bearman [1968] described digital methods and equipment required to compute root mean square values, auto correlation and cross correlation functions, power spectral density functions and cross power spectral density functions. Aliasing errors due to digitally sampling an analog signal below that of twice the signal frequency, and quantization distortions due to the discretization of a continuous signal into a finite number of subranges were also discussed. There was, however, no mention of the fast Fourier transform technique.

The development of the fast Fourier transform technique greatly reduced the computer time required to calculate various statistics from that of the discrete Fourier transform method. In addition, the fast Fourier transform method preserved the phase information in the signal, information lost in a spectral measurement. The discrete Fourier transform was not practical for wide bandwidth turbulence signals. For statistical accuracy, the discrete Fourier transform technique required transformations of long time series or many averages of shorter ones. Blackman and Tukey [1958] described another technique whereby lagged products were computed, smoothed with a lag window and then transformed in order to reduce the computing time required for spectral estimates. Cooley and Tukey [1965] have shown that both the energy spectrum and autocorrelation, by using the fast Fourier transform algorithm to compute the Fourier coefficients of a time series and then to fast Fourier retransform a sequence made up of complex Fourier coefficients to determine the mean lagged products of the series, required less time than to compute the correlation function alone by direct computation of lagged products.

Other aspects of digital processing and analysis have been discussed by Bendat and Piersol [1966], Oppenheim and Schafer [1975], Chen [1979], Beauchamp and Yuen [1979], and many others.

Frenkiel and Klebanoff [1967a, b] were among the first to publish papers presenting results obtained from digital techniques for data evaluation. Using constant current anemometry, digital sampling and high speed computing techniques, two-point time correlations up to the eighth order and associated skewness and flatness factors were determined for the streamwise fluctuating component in grid turbulence. The results were obtained using samples of 160020 digitized data recorded at 1/12800 second intervals during 12.5 second time periods.

Van Atta and Chen [1968], using constant temperature anemometry, digital sampling and computer analysis to measure two-point time correlations in grid turbulence, found that results for all even order correlations were in close agreement with those of Frenkiel and Klebanoff while the odd order correlations were different. The differences in the odd order moments were attributed to the different modes of anemometer operation and confirmed in studies by Compte-Bellot [1965], and Helland and Van Atta [1976] which show that there is a difference in the odd order velocity statistics when measured by the constant current anemometer and constant temperature anemometer. Van Atta and Chen also checked several double and triple correlation results obtained from a fast Fourier transform method against calculations from mean lagged products, the method used by Frenkiel and Klebanoff, and found no significant differences.

Geophysical measurements, such as those by Gibson, Stegen and Williams [1970] and Gibson, Stegen and McConnell [1970], presented special problems due to wide spectral bandwidth. The anemometer signals were preconditioned prior to recording on FM tape. The anemometer signal was first band pass filtered between 2 Hz and 2 KHz, amplified, recorded on tape, and then analyzed.

Kendal [1970] used a 512-channel digital averaging educator to measure the periodic components of wave induced fluctuations and Reynolds stresses. To improve the accuracy of some of the measurements, the cyclically repetitive components were subtracted from the signal leaving only the turbulent component for analysis.

Tennekes and Wyngaard [1972] performed digital sampling and computer analysis of the fine structure of atmospheric turbulence. Their findings showed that the spread in the tails of the probability densities of the velocity derivatives and other variables increased with Reynolds number. They found that accurate measurements of the fourth moment of the velocity derivative at a turbulent Reynolds number in the order of 5000 required a dynamic range of forty standard deviations. They concluded that measurement of moments beyond the fourth for velocity derivatives in geophysical turbulence were practically impossible with the current instrumentation, design and executation of the experiments. On-line, real-time digitization was suggested in order to increase the dynamic range, but for records of atmospheric turbulence longer than an hour, integration times of higher order moments would extend beyond the time intervals over which reasonably stationary atmospheric conditions could be expected. Ensemble averages, by repeated experiments, would be necessary to achieve statistical stability in the extreme tails of the probability distributions.

Digital measurements by Frenkiel and Klebanoff [1971] and Pierce [1972] showed that laboratory measurements for smaller values of turbulent Reynolds number were less scattered than data for skewness or flatness plotted against higher values of turbulent Reynolds number. Pierce found that only twelve standard deviations of the signal for measurement of the streamwise velocity derivative were required to determine kurtosis at the centerline of a free jet with a turbulent Reynolds number of 640, considerably lower than in the atmospheric turbulence studies conducted by Tennekes and Wyngaard [1972].

1.2 OBJECTIVE OF THE STUDY

Prior to the mid 1960s, analog instrumentation techniques were used to process turbulence signals from hot wires. Digital techniques or combination analog/digital techniques have since developed. Gibson, Stegen and McConnell [1970], in their studies of atmospheric turbulence, state that "digital data processing techniques were used, permitting a substantial improvement in the quality" of the data points. Other than a recent attempt by Sastry [1984], for measurements in the wake of a flat plate, no direct comparison between analog and digital methods is available. His analog and digital results up to Reynolds stresses showed good agreement, while differences in the triple velocity correlations were attributed to the small size of the sample sets. However, neither the sampling rate nor the number of samples per data set in the study were mentioned. Sastry's results were inconclusive.

Since the recent development of the digital facilities in the turbulence laboratory at the University of Manitoba, only one previous investigator, Derksen [1986], has used digital sampling to study the statistical behavior of wall bounded turbulence parameters. Although digital results obtained from sampling sine waves, square waves, and gaussian noise signals compared well with their known mathematical values, no direct comparison between analog instrumentation and digital techniques for the study of turbulence parameters was undertaken at that time.

A direct comparison of some experimental turbulence parameters obtained through analog and digital techniques was undertaken in this study. Measurements were taken in a simple boundary layer flow and in a more complex flow, like that through a conical diffuser, in order to determine possible differences in the parameters obtained by the two sampling methods.

1.2.1 Parameters Measured

Skewness and flatness factors of the streamwise velocity component from single wire hot-wire analog measurements by Derksen [1981] and Kassab [198_] were compared with the digital results throughout the boundary layer of the flow. Analog spectral measurements by Kassab [198_] were compared with digitally obtained spectral results. Measurements across the turbulent boundary were taken perpendicular to the pipe wall, 15 cm from the pipe exit for a free stream velocity of 8 m/sec. A few additional skewness measurements were taken in the sublayer of a boundary layer flow with a free stream velocity of 4 m/sec.

The analog and digital measurements of the flow in the conical diffuser were taken simultaneously. Single wire measurements of third and fourth order moments of the velocity and the velocity derivative were taken and compared. In addition, the fifth and sixth order moments were digitally obtained. Measurements for five spectra were taken by both analog and digital means: the first very close to the wall, the second at the 'blue line' where skewness is zero, flatness is minimal and the rms of the turbulent velocity is at a maximum, the third at the longitudinal axis of the conical diffuser, the fourth between the wall and the blue line, and the fifth between the blue line and the diffuser axis. From cross wire measurements, mixed moments up to the fourth order, and five spectra each of the longitudinal velocity and the transverse velocity fluctuations were obtained. The single and cross wire measurements were taken normal to the wall, 9 cm from the diffuser exit. All tests were conducted with fully developed pipe flow at the diffuser entry. Most tests were conducted at a Reynolds number of 130,000 based on the entry pipe diameter and pipe bulk velocity.

Chapter II

WIND TUNNELS AND SPECIALIZED INSTRUMENTATION

A wind tunnel is a device used to blow a steady uniform stream of air through a working section of the tunnel in order to record and study various flow characteristics. An open return, or open circuit wind tunnel, draws in fresh air from the atmosphere into the settling chamber of the wind tunnel and discharges its entire flow to the atmosphere at the end of a pipe or a diffuser. As a rule, most open return wind tunnels are of the low speed type, restricted to speeds well below the speed of sound.

Two low speed, open return wind tunnels were used in the experiments: a boundary layer tunnel and a fully developed pipe flow tunnel with an 8° conical diffuser at its outlet. Various pressure sensing devices and electronic equipment used with the hot-wire anemometer were employed to study the air flow in the boundary layer tunnel and in the diffuser.

2.1 FLOW FACILITIES

Since the performance of an open return wind tunnel and hot wire anemometer are affected by variations in room environment, the following section will attempt to describe the laboratory room conditions.

2.1.1 The Laboratory

Both wind tunnels were housed in the same laboratory, a room approximately 21 m long, 11 m wide and 4 m high. In addition to the two wind tunnels, the laboratory also held a technician's office and drafting table, a PDP-11 computer, a DISA nozzle calibration unit, and various small work areas. The wind tunnels were located side-by-side, parallel to the long edge of the room. At times, both wind tunnels could be in operation.

The laboratory had two rows of cold air ducts in the ceiling and steam radiators along the floor. Since open return tunnels are sensitive to draughts, care was taken to position neither the input nor the venting end of either wind tunnel beneath a working cold air duct.

On any day, the temperature distribution throughout the room was moderately uniform. Day-to-day temperatures varied from 22°C to 28°C, with 23°C to 25°C being the most common. The barometric pressures varied approximately 20 mm Hg, from approximately 730 mm Hg to approximately 750 mm Hg. The day-to-day fluctuations resulted in approximately 1% variation in air density, and as seen from tables in Goldstein [1938] approximately 2% variation in kinematic viscosity.

2.1.2 The Boundary Layer Wind Tunnel

The boundary layer tunnel is made up of a wooden inlet cone, a radial vane damper, four stage axial fans driven by two-speed four-pole ball bearing motors, a Woods type silencer, two 8° total angle rectangular diffusers with two turning sections, a settling duct with copper wire screens, an area ratio 16:1 plywood circular contraction cone, a number 4 grit sandpaper flow trip, and a 2.67 m length of 27.1 cm ID brass pipe at the exit. The horizontal axis of the brass pipe was approximately 1.05 m above the laboratory floor.

Briefly, air at room atmospheric conditions was drawn in through the inlet cone by the axial fans, driven through the two diffusers and into the settling chamber. The copper wire screens in the settling chamber broke down any large scale lateral components of the flow prior to the flow entering the circular contraction cone. The velocity of the air flow leaving the contraction cone increased due to the reduced cross sectional area of the contraction. Upon leaving the circular contraction cone, the air flow was driven over the sandpaper trip and through the working section of the brass pipe before being discharged to the atmosphere and recycled to the inlet cone and axial flow fans. The course grit sandpaper flow trip located after the contraction cone forced transition to turbulent flow and thickened the turbulent boundary layer in the brass pipe.

Rings of static pressure taps circled the inlet and outlet of the contraction cone. These rings of static pressure taps were used to measure the pressure drop across the contraction cone. The speed of the airflow through the boundary layer tunnel was increased with increased pressure drop. The pressure drop across the contraction cone was thus used to set the operating point of the boundary layer tunnel.

Detailed descriptions of the boundary layer tunnel, its various components, and its operation may be found in Serag [1978] and Burhanuddin [1980]. A plan view of the boundary layer tunnel is shown in Figure 2.1.

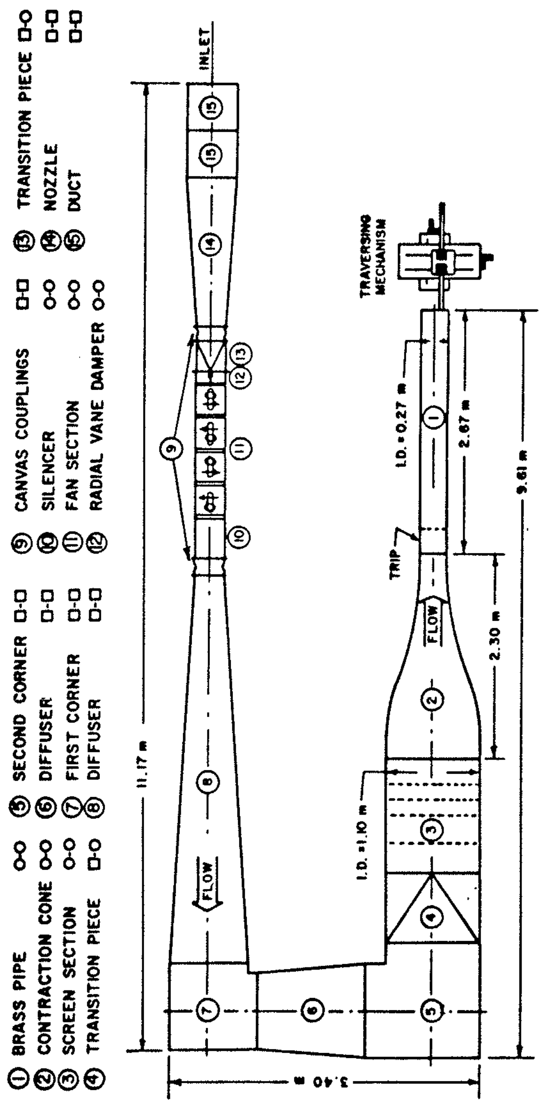

Figure 2.1: The Boundary Layer Tunnel

2.1.3 Wind Tunnel and Diffuser

The second wind tunnel was a straight open return tunnel. It consisted of a radial flow fan driven by a 25 Hp DC electric motor, a rectangular diffuser, three sets of copper wire screens in a settling chamber, a contraction cone of area ratio of 89:1, a combined vibration isolater and flow trip, and two straight sections of 10.16 cm ID steel pipe with a combined length of 7.95 m. The flow vented to the atmosphere through a diffuser at the end of the steel pipe. The length of steel pipe was supported on wheeled jack posts placed on wooden benches. The pipe axis was approximately 2.1 m above the floor of the laboratory.

Briefly, air at room conditions was drawn into the radial flow fan then driven through the diffuser and into the settling chamber where the wire screens broke down any large scale flow structures from the fan. The air then flowed through the contraction cone, over the flow trip in the vibration isolater, and then through the steel pipe and diffuser before being discharged to the laboratory and recycled to the fan.

The flow trip was a number 4 grit sandpaper, similar to that of the boundary layer tunnel. The course grit sandpaper flow trip was used to immediately force transition to turbulent flow upon entering the pipe. The forced transition reduced the subsequent length of pipe necessary to obtain fully developed turbulent pipe flow as the inlet condition to the diffuser. Further details of the various wind tunnel components are described in Derksen [1986]. A schematic of the wind tunnel is shown in Figure 2.2.

2.1.3.1 The 8° Diffuser

A subsonic diffuser is a device of diverging cross sectional area which causes an increase in static pressure and a decrease in fluid velocity. In order to prevent separation of the flow, the included angle of the diffuser is generally small.

The diffuser used in the experiments had a conical expansion of 8° included angle and a 4:1 area ratio. Sovran and Klomp [1967] have shown that such a diffuser has the largest possible pressure recovery without flow separation and therefore has the largest efficiency of all conical diffusers. The diffuser was machined from cast aluminum. At the inlet, it had an inside diameter of 10.16 cm matching the diameter of the mating steel pipe, and at the outlet it had an inside diameter of 20.22 cm. The overall length of the diffuser was 72 cm. Static pressure holes, 0.6 mm in diameter, spaced 90° apart were connected by plastic tubing to form static pressure rings. Eleven rings of static pressure taps were spaced at 6 cm intervals along the wall of the conical diffuser. The diffuser had fully developed pipe flow at the inlet and a free exhaust at the outlet. The diffuser geometry is shown in Figure 2.3.

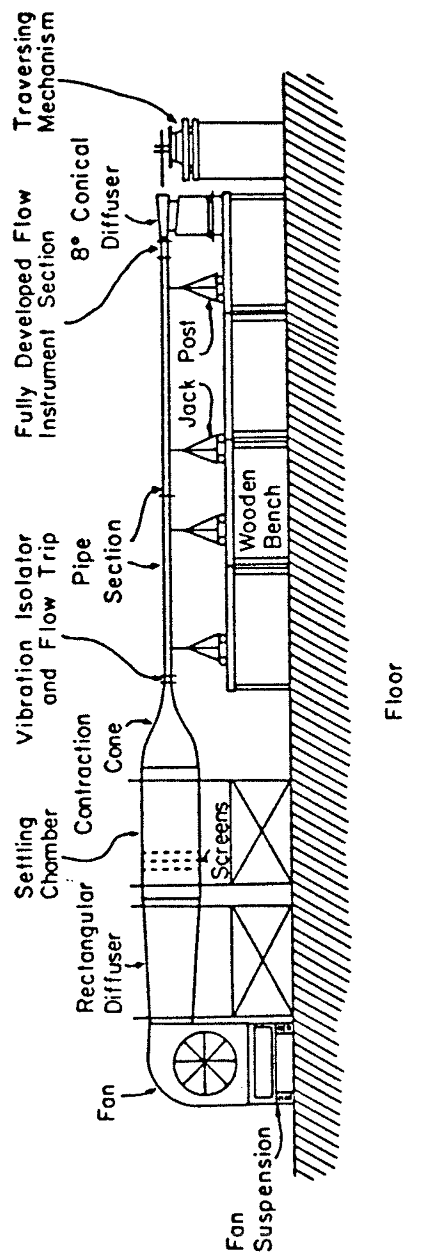

Figure 2.2: Wind Tunnel Layout

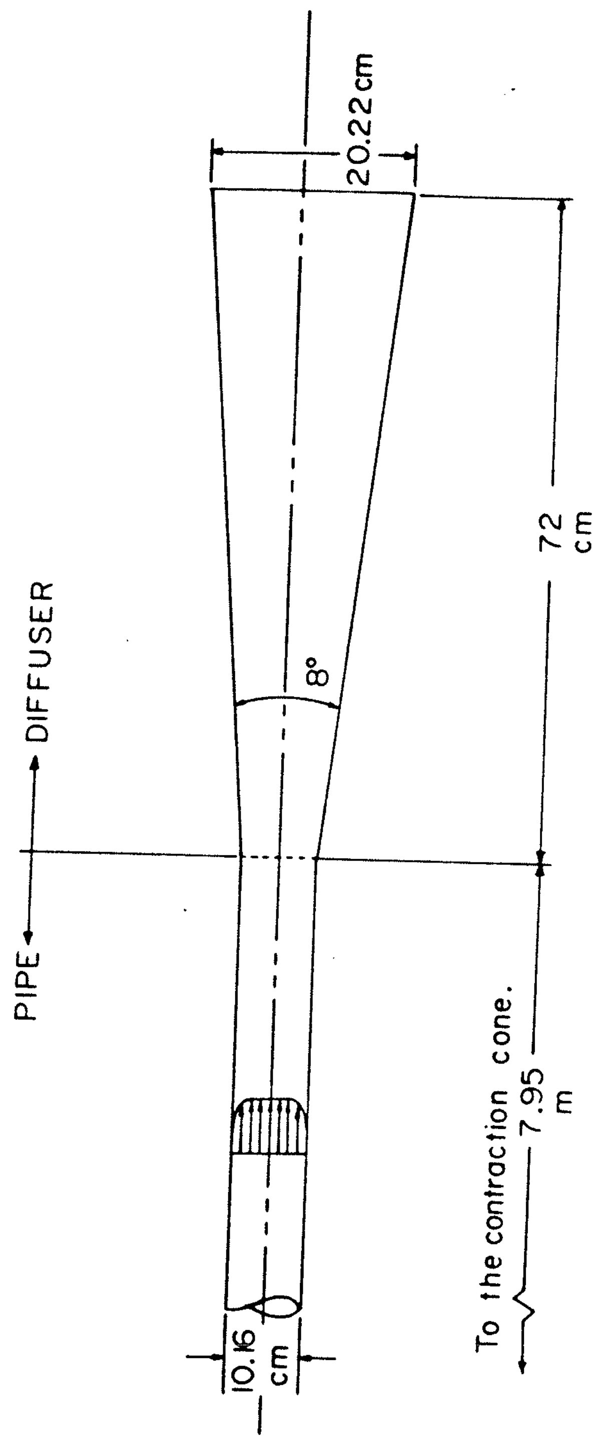

Figure 2.3: Diffuser Geometry

2.1.4 Traversing Mechanisms

Milling tables were used to position the various pressure sensing probes and hot-wire probes in the flow through both the boundary layer tunnel and the diffuser. Both milling tables were Model FB102, M. S. Tool Supplies coordinate tables having a longitudinal feed of 37 cm and a cross feed of 15 cm.

The coordinate table at the diffuser station was also mounted on a circular milling table enabling rotation as well as x-y motion. The circular milling table allowed the probe to be moved at any angle to the wall or axis of the diffuser. The coordinate table at the boundary layer tunnel supported x-y motion only, thereby allowing only probe motion parallel and normal to the tunnel wall.

The coordinate table at the diffuser station was also equiped with a DISA Type 55E40 traversing mechanism. The DISA traversing mechanism consisted of a drive gear arranged to permit the probe guide tube 100 mm of longitudinal travel with a resolution of 0.1 mm. The DISA traversing mechanism was mounted in such a way as to allow travel along the guide slots in the milling table. The combined longitudinal travel was well in excess of the 72 cm length of the diffuser.

2.1.5 Wind Tunnel Operation

The pressure drop across the contraction cone was used to set the operating point of the boundary layer wind tunnel. The boundary layer tunnel was calibrated for centerline velocity in the brass pipe. Rings of static pressure taps, just before and just after the contraction cone, were connected to an Airflow Developments Ltd. inclined manometer which was graduated in increments of 0.002 inches H_2O. The manometer ranged from 0.000 to 0.500 inches H_2O. By selecting various combinations of one to four of the four stage axial flow fans and varying the air flow intake opening on the radial vane damper between 0° and 180°, the operating point of the boundary layer tunnel could be controled. The speed of the airflow through the tunnel, and hence the Reynolds number, was proportional to the square root of the pressure drop across the contraction cone.

The flow in the second wind tunnel and diffuser was calibrated in terms of both the pressure drop across the contraction cone and the fan speed of the tunnel. The contraction cone pressure drop was measured with a Trimount inclined manometer which was calibrated from 0.00 to 8.00 inches H_2O in increments of 0.02 innches H_2O. The fan speed was monitored by counting pulses produced when magnetic field lines from a magnet and pickup on a rotating shaft were interrupted as the motor turned. Since the system was slightly dependent on room temperature and the external power source, the control settings had to be carefully monitored or the tunnel Reynolds number could drift. The Reynolds number, based on the pipe diameter and either the centerline or the bulk velocity of the flow in the pipe, was found to be proportional to the square root of the contraction cone pressure drop, and proportional to the fan speed.

2.2 PRESSURE DEVICES

Various pressure sensing and pressure measuring devices were used to measure static, total, and Preston pressures. Static and total pressures were recorded for different Reynolds numbers in the boundary layer tunnel and in the diffuser. Preston pressures were recorded at 3 cm intervals along the diffuser wall for a flow at Reynolds number of 137,000 based on the centerline velocity and pipe diameter at the diffuser inlet.

2.2.1 Pressure Probes

The static pressure tubes used in the experiments were cylindrical, forward facing impact tubes which were placed parallel to the flow. The tip of the static pressure tube was hemispherical and closed to the flow. A ring of four static pressure holes, 90° apart around the 1 mm diameter tube, was drilled 14.35 mm from the rounded tip. Two static pressure tubes were used: a straight static pressure tube was used along the axis of the diffuser, and a wall-type static pressure tube with a double $60°-30°$ bend was used in the boundary layer tunnel and along the wall of the $8°$ conical diffuser.

The Pitot tube or total pressure tube used in the experiments was a wall-type, forward facing impact tube. The cylindrical body of the tube was flattened at the tip but remained open to the flow. The Pitot tube and static tube measurements were used to calibrate the tunnels and to record the velocity distributions in the boundary layer tunnel and in the diffuser. The velocity distributions served as calibration standards for the hot-wire measurements. The Pitot and static pressure tubes were United Sensor forward facing impact tubes.

The Preston tube used in the experiments was a forward facing, round Pitot tube of inhouse manufacture. The Preston tube was used to measure skin friction at various locations along the diffuser wall. The Preston tube used was made from a 1.1 mm OD hypodermic tubing.

The pressure tubes were held in place by holders mounted to the milling tables. Plastic tubing connected the pressure tubes to one or more of the pressure measuring devices.

2.2.2 Manometer Systems

A manometer is a device used to measure a pressure difference, usually between a point in a flow and the atmosphere. A liquid filled manometer operates on the principle that the height of a column of liquid in the manometer is proportional to the difference in pressure acting on the upper and lower surfaces of the fluid column. Manometers vary in range and sensitivity as determined by the gauging fluid, length and inclination of the liquid holding tubes, and method of measuring the liquid heights.

An alternative to the liquid filled manometer is the pressure transducer. The pressure difference across a diaphragm is converted into an electrical signal which is proportional to the deflection of the diaphragm. Various manometers and manometer systems are discussed in Bradshaw [1970] and Bryer and Pankhurst [1971].

2.2.2.1 Combist and Betz Manometers

Combist and Betz manometers were used to obtain static and total pressure measurements. Of the two manometers, the Betz had the larger range and required the longer response time. The Betz manometer ranged from -17 to 400 mm H_2O in increments of 0.1 mm H_2O. The Combist micromanometer ranged from 0 to 30 mm H_2O in increments of 0.01 mm H_2O.

2.2.2.2 Pressure Transducer

As previously mentioned, a pressure transducer is a device used to convert pressure changes into electrical signals. An MKS Instruments Baratron pressure transducer, type 223BH-A-1, with PDR-D-1 external power supply and digital readout was used for the first time in this series of tests. The Baratron pressure transducer provided a 0 to ±1 volt output signal which is linear with pressure. It has a full scale range of 0 to ±10 Torr. The pressure transducer is comprised of an Inconel sensor, printed circuit board, and cover. A metal diaphragm supported by thick walled Inconel rings, a dimensionally stable ceramic electrode which senses the deflection of the metal diaphragm, and a reference cover through which a glass-to-metal feedthrough terminal passes an electrical signal to the printed circuit board make up the sensor part of the pressure transducer. The MKS Baratron pressure transducer was calibrated at the factory using a transfer standard calibrated with a CEC Air Dead-Weight Tester traceable to the National Bureau of Standards.

The PDR-D-1 is a power supply and digital readout. The power supply provides ±15 VDC at 35 mA, and supplies power to the digital readout as well as power for the pressure transducer.

The only adjustment necessary for operating the pressure transducer is trimming the zero potentiometer. A coarse zero control is located on the pressure transducer while a fine zero control for the pressure gauge is located on the front panel of the digital readout. Zeroing is done when there is no pressure differential across the sensor.

The pressure transducer has two $^3/_{16}$" OD inlet tubes, one on each side of the casing housing the metal diaphragm. The manufacture has designated the two ports as Pr and Px. The Pr port, located on the same side of the diaphragm as the coarse zero control, remained open to the atmospheric pressure throughout the experiments. The Px port, located on the opposite side of the casing, was connected via PVC plastic tubing to the pressure probe placed in the airflow. The variable pressure at the Px port was taken relative to the atmospheric pressure at the Pr port.

The pressure readings registered by the transducer arrangement were read directly as mm Hg or Torr. The pressure transducer had linear output between ±10 VDC, or ±10 Torr, and saturated at ±12 VDC or ±12 Torr.

The pressure transducer readings were first compared to pressure readings taken with the Combist manometer for airflow in the boundary layer tunnel. Upon converting the pressure transducer readings from Torr into mm H_2O, no significant difference between the two sets of readings was found. For the airflow through the conical diffuser, the instantaneous pressure differential across the the sensor fluctuated rapidly. In order to obtain a stable reading, the electrical signal was sent through an integrator set for a sixty second time constant. The readout was then taken from the digital display of a voltmeter connected to the integrator. The pressure reading was recorded to 3 $^1/_2$ digits of accuracy.

2.3 ELECTRONIC MEASURING DEVICES

2.3.1 The Anemometer System

An anemometer is a device used for measuring the speed of a fluid. There are three types of anemometers: those that depend on a pressure differential between two points, those that use the cooling of a heated body exposed to the flow, and those that use the momentum of the fluid to drive a set of cups or small windmill facing the direction of flow. The principle of operation behind the hot-wire anemometer is based on the measure of convective heat loss from a heated sensing element to the surrounding fluid. A complete system consists of sensing elements, anemometer units, linearizers, signal manipulating equipment, and metering equipment.

2.3.1.1 Hot-Wire Probes

The sensing element of the anemometer is the hot-wire probe. It is comprised of the hot-wire itself, and a means of support together with the electrical leads. The probe contains either one or more sensing elements.

The hot-wire probes used in the experiments were DISA hot-wire probes: type 55P05 gold plated, single wire, boundary layer type probes, and type 55P51 gold plated, X-array probes. The X-array or cross wire probes are so named because of their geometric configuration. Two oppositely oriented inclined hot wires, separated by a small distance, are combined into a single probe capable of responding to velocity fluctuations coming from two perpendicular planes. The 55P51 X-array probe has the sensor plane parallel to the probe axis. These probes are mounted with the probe axis parallel to the direction of the main flow.

Standard gold plated hot-wire probes have platinum plated tungsten wires, 5 μm in diameter, with an overall length of 3 mm and a sensitive length of 1.25 mm. The wires are suspended between two prongs and are welded in place. The wire ends welded to the prongs are copper and gold plated in order to accurately define the sensitive length of the hot-wire and to reduce the amount of heat dissipated by the prongs. The prongs are stainless steel, 0.5 mm in diameter, and taper off towards the sensor. The prongs are embedded in a ceramic tube and extend approximately 2 mm beyond the end of the ceramic tube. The prong extensions are gold plated and serve as plug pins through which the electrical connection to the probe is made.

Two-pin and four-pin DISA shorting probes were used to short circuit the probe support and 5 m probe cable in order to cancel their resistances during alignment of the anemometer system.

The hot-wires were operated at an overheat ratio of 0.8 in the constant temperature mode. The 0.8 overheat ratio was selected in order to obtain maximum sensitivity without damage to the probe. Special care was taken to match the frequency response and sensitivity of the two sensors in the X-array probe in an attempt to minimize the contamination of one component by the other when their outputs were fed into the various signal manipulators.

2.3.1.2 Constant Temperature Units

Two different circuits are available for the measurement of thermal losses to determine speed of flow. Their modes of operation are constant current and constant temperature.

The constant current anemometer uses a probe powered by a constant current. In operation, the current through the probe is independent of any resistance changes in the bridge. The probe resistance changes are the result of flow changes acting on the probe. The measure of the flow velocity is a result of the voltage difference across the bridge.

The constant temperature anemometer is the more widely used of the two types of hot-wire anemometers. In the constant temperature mode, the resistance of the sensor, and therefore its temperature, is held constant. Basically, the anemometer consists of a Wheatstone bridge, a servo amplifier and feedback loop. When the bridge is in balance, no voltage difference will exist between the end points of the bridge. A change in the flow acting on the the probe will cause an unbalance in the bridge, introducing an error voltage at the input of the servo amplifier. The amplified voltage is used to adjust the bridge operating voltage and hence the current through the probe thereby restoring the bridge balance.

The anemometers used in the series of comparative tests were the DISA 55M system anemometers. A DISA 55M01 main unit set to the 'wire' mode of operation was used with a DISA 55M10 standard bridge equiped with a plug-in 5 m cable compensation unit. By adjusting the cable compensation unit, bridge unbalance due to differences in probe cable parameters could be compensated. A square wave generator incorporated into the 55M01 main unit was used to aid adjustment of the anemometer system to attain maximum flat frequency response. The maximum obtainable upper frequency limit with the 55M10 standard bridge is approximately 200 kHz. The DISA 55M01 main unit was connected by a power cable to a remotely located DISA 55M05 power supply. By setting up the power pack separately, the amount of electromagnetic noise or hum could be reduced as well as lessen heating of the 55M01 main unit and reduce the possibility of temperature drift in the anemometer.

2.3.1.3 Linearizers

The output voltage of a constant temperature anemometer is a non-linear function of the flow velocity. The relationship between the flow velocity, U, and the anemometer output voltage, V, can be expressed by a form of King's law:

$$V^2 = A + B\,U^n$$

where A, B, and n are constants whose values depend on the dimensions and operating conditions of the probe, on the physical properties of the fluid, and on the the flow conditions. A linearizer is basically an electronic analog computer capable of transforming the non-linear input voltage to a linearized output voltage proportional to the flow velocity. When the anemometer output is not linearized, distortion of the output signal results in errors in both the mean and the fluctuating velocity measurements.

Two types of DISA linearizers were used in the tests: a DISA type 55D10 linearizer and DISA type 55M25 linearizers. The 55D10 linearizer was used for the flow in the boundary layer tunnel. Linearization of the anemometer signal could be accomplished for a range of one octave, that is, the anemometer signal could only be linearized for half the flow range of interest. The 55M25 linearizers were used for the flow in the conical diffuser. Due to a combination of exponential and square root functions on the 55M25 linearizer, the anemometer signal could be linearized over a flow range of 2.5 decades. Both types of linearizers had a linear response for an output voltage range of 0 to 10 volts and saturated at 12 volts.

2.3.1.4 RMS Meter

A DISA type 55D35 rms voltmeter was used to measure the local turbulence components of the flow. The degree of turbulence in the flow can be determined from the ratio of the rms voltage to the mean voltage. The 55D35 rms voltmeter measures the true rms value of an AC voltage on the basis of the equation

$$u(rms) = \left(1/T \int_0^T u^2 \, dt \right)^{1/2} \quad .$$

The DC components of the signal, usually corresponding to the local mean velocity, are eliminated by the rms voltmeter and must be determined from another voltmeter.

The DISA type 55D35 rms voltmeter measures rms values of AC voltages between 300 μVrms and 300 Vrms inside the frequency range 0.1 Hz to 700 kHz. The 55D35 rms voltmeter has an integrator with a time constant which can be varied from 0.3 to 100 seconds. In most applications, a 30 second time constant gave a stable output. The exception was the spectra measurements where a 100 second time constant was necessary to achieve stable readings in the low frequency range of the spectrum. A waiting period of four time constants was allowed to pass before a reading was taken from the analog equipment.

2.3.1.5 Signal Processors

Flow condition information from the anemometer must be mathematically processed before a numerical value representing a required parameter may be determined. Turbulence processors are small analog computers used to make such mathematical calculations.

Two turbulence processors were available for laboratory use: a DISA type 52B25 turbulence processor and a Tri-Met Instruments model type TM 377 multifunction turbulence processor. The DISA processor has several different functions available depending upon use of single or cross wire input, generally from linearized anemometer output. The DISA processor has a rotary gain switch for the two channels, each with seven discrete settings ranging from $10^{0.5}/10$ to $100/10^{0.5}$ used to amplify the input signal, and is equiped with separate pilot lamps which light to indicate when the amplitude of the input signal is clipped. A built-in integration circuit with time constants from 0.1 to 100 seconds could be activated to determine the mean value of a selected function who's value is read from an external DC voltmeter. The DISA processor can accept input voltages in the range ±30 volts and has an output voltage in the range ±10 volts.

The Tri-Met turbulence processor was developed specifically for use in the turbulence laboratory at the University of Manitoba. The circuit description may be found in Hummel

[1978]. The Tri-Met processor may be used for single or cross wire measurements. The linearized anemometer output signal is fed into the processor input where for single wire measurements voltage readings are taken with the processor in the "A" mode of operation, and for cross wire measurements the linearized anemometer signals used to determine the "u" and "v" flow components are formed with separate add and subtract circuits. The cross wire signals are taken with the "(A+B)/2" setting for the u flow component and with the "(A-B)/2" setting for the v flow component. The negative of both flow components from the cross wire signals is available on the front panel of the processor.

The Tri-Met turbulence processor is equiped with a multiplier network comprised of Burr Brown 4205-K multipliers. This network produces an output signal equal in amplitude to the product of the magnitudes of the input signals. In this way, all possible combinations of the uv products up to the fourth order are formed. Simultaneous output signals may be taken three at a time, the particular products dependent upon the selected function settings.

A series of amplifiers coupled together is used to control the signal amplitude. The pregain amplifier can be set to 1, 2, 5 or 10. Course post gains of 1, 10 or 100 are available to each channel. A ten turn precision potentiometer in each channel varies the signal gain from 0 to 1.000.

The Tri-Met processor will accept an input signal in the range of 0 to +10 volts. The input signal is generally the linearized output from the anemometers. The output signal is in the range ±10 volts. As the "u" channel overload indicator light is nonfunctional, an oscilloscope trace of the output was necessary to monitor the signal. All outputs, the u component, the v component, and their products, are instantaneous values and as such were averaged with an external integrator before a numerical value could be read from the external DC voltmeter in the analog series of measurements.

Of the two turbulence processors, the Tri-Met processor is the easier to use. Studies by Derksen [1981] state there is no significant difference between results obtained through the Tri-Met and DISA turbulence processors. As the Tri-Met processor was in use elsewhere when this investigation began, preliminary analog measurements in the boundary layer tunnel were conducted using the DISA processor. The Tri-Met processor was subsequently used in both the analog and digital diffuser flow measurements.

Although the Tri-Met processor has a built-in signal differentiation option, an external differentiator based on a design by Wyngaard and Lumley [1967] was adopted for use in the turbulence laboratory. The Linear Systems Ltd. model SP2 spectral processor can produce the first and second differentials of the input signal. It is the first velocity derivative that is used in the isotropic relation with Taylor's hypothesis to determine the dissipation.

2.3.2 Auxiliary Instruments

2.3.2.1 Signal Conditioner

DISA 55D26 signal conditioners were used to force the input signal between the voltage limits of the PDP-11 computer. Although the input signal levels to the signal conditioners may be between +30 volts and -15 volts, the computer can only accept an input signal between ±5 volts. Using the signal conditioner to force the input signal between the ±5 volt limits, a mean DC voltage was first subtracted from the signal leaving only the fluctuating component of the signal to be amplified within the desired limits.

The conditioner is equiped with a zero suppression circuit which permits the suppression of the DC component input voltage. Once the mean component is eliminated, the turbulence signal is stepped up in the amplifier circuit for a peak to peak range of ±5 volts before the signal is fed into the computer for acquisition and analysis.

The amplifier circuit has a seven position gain selection switch. Gains range between 1 and 100. In addition, the circuit is equiped with a screwdriver operated potentiometer thereby permitting continuously variable adjustment between individual switch settings. The overall control range of the amplifier circuit is from 0.8 to 200.

2.3.2.2 Other Equipment

In addition to the equipment previously mentioned, a pair of Krohn-Hite model 3550 filters and an assortment of oscilloscopes were used.

The Krohn-Hite model 3550 filter is a multifunction filter. It can be operated in a low-pass, high-pass, band-pass, or band-reject mode. The cutoff frequencies may be independently adjusted between 2 Hz and 200 KHz. The filters were necessary in such measurements as spectra and the velocity derivative.

Three oscilloscopes were used throughout the testing. One scope was necessary to monitor the data sent to the computer in order to assure the input signal was amplified to within the allowable ±5 volt limits. The remaining two scopes were used to monitor the analog signals. The three oscilloscopes used were a Tektronix 466 storage 'scope, a Tektronix model 2213A oscilloscope, and a Telequipment Oscilloscope Type D1011.

2.4 COMPUTER FACILITIES

The computer facilities developed in the Turbulence laboratory at the University of Manitoba consisted of a PDP-11/34a central processing unit, an FP11-A floating point processor, two RL01 random access disk drives for secondary storage, and a VT-100 video display terminal. The computer was equiped with an LPA-11k laboratory peripheral accelerator with a KW-11k dual programmable clock and an AD-11k 12 bit A/D converter for data acquisition. An RSX-11M operating system was used with a DEC FORTRAN compiler to run the computer. The software packages for data acquisition and analysis of the turbulent signal were developed in the laboratory. Hard copy output was obtained through an LA-180, 180 character per second line printer and an HP 7475a, six pen plotter. Further details on the computer facilities and adapted programs used in the current study may be found in Derksen [1986].

Chapter III

THEORETICAL CONSIDERATIONS

Turbulence is defined as a three dimensional time-dependent motion characterized by high levels of fluctuating vorticity. In the time domain, a turbulence signal is characterized by a randomly fluctuating amplitude or intensity. In the frequency domain, it is a continuum phenomenon of considerable bandwidth. Turbulence is a feature of the fluid flow, not of the fluid, and is the usual state of fluid motion except at low Reynolds numbers. Statistical analysis has developed into a fundamental tool for studying turbulence properties.

The central limit theorem of statistics states that the probability distribution of a continuous variable which is the sum of a number of independent random variables approaches the normal or Gaussian distribution as the number of such variables increases. The properties of a Gaussian distribution are stable and predictable. Nearly all random processes occuring in nature are Gaussian. Turbulence, however, is an exception.

3.1 TURBULENCE MEASUREMENTS

In turbulent flows, average values with respect to time and space exist. A way of 'scaling' turbulence is necessary to quantitatively describe turbulent motion. However, this alone is insufficient to characterize turbulent motion. The violence of the motion must also be represented. Since the 1930s, the ratio of the root mean square turbulence velocity component to the time mean velocity value has defined the relative turbulent intensity of a flow.

3.1.1 Probability Density Distributions and Moments

The probability density distribution of a turbulent signal can be used to define the structure of the signal. Properties of the turbulent signal that can be obtained from the probability density distribution are:

1. symmetry of the signal.
2. agreement with gaussian signals.
3. intermittency of the signal.

The probability density function has the properties

$$p(u) \geq 0 \quad ,$$

$$\int_{-\infty}^{+\infty} p(u)\, du = 1$$

where p(u) is the probability density. The probability density provides a way of describing the probability distribution of a random variable. A signal or process is said to be Gaussian if the bell shaped curve of the probability density has the form

$$p(u) = \frac{1}{\sigma\sqrt{(2\pi)}} e^{-u\ /2\sigma^2}$$

where the signal has zero mean value and the variance of the signal is σ^2.

3.1.1.1 Moments

The moments describe the shape of the distribution. The first moment, or mean, is taken to be zero for turbulent signals. The second moment, or variance, is a measure of spread or dispersion. A small variance is characterized by a narrow probability density curve and a steep distribution function while a large variance is characterized by a broad probability density curve.

The even moments generally describe width, peakedness or spread of the distribution while the odd moments describe the symmetry of the distribution. The probability density function, p(u), of a normal of Gaussian distribution is symmetric about the mean and all odd order moments are zero. In general the value of an n^{nt} even order moment about the mean of a Gaussian distribution can be found by

$$\overline{u^n(t)}/(\overline{u^2(t)})^{n/2} = 1*3*5*...(n-1).$$

Moments about the mean are refered to as central moments.

The nondimensionalized third central moment is called skewness and is denoted by S(u) where

$$S(u) = \overline{u^3(t)}/(\overline{u^2(t)})^{3/2}.$$

The skewness describes the symmetry of the distribution about the mean. Generally, skewness is defined as positive for a 'long tail' on the positive side of the mean and a 'short tail' on the other side, and vice versa. For turbulent signals, the skewness indicates a preferred fluctuation of the velocity. For a normal Gaussian distribution, skewness is zero.

The nondimensionalized fourth central moment is known as the flatness factor or kurtosis and is denoted by K(u).

$$K(u) = \overline{u^4(t)} \;/\; (\;\overline{u^2(t)}\;)^2 \;.$$

Kurtosis is a measure of the flatness of the tails of the density curve. The higher moments weight the higher amplitude parts of the probability density distribution curve more. A flatness factor greater than the Gaussian normal value of three means the distribution is more peaked around the mean than for a normal distribution. This indicates that the probability of small amplitudes is higher than the probability of large amplitudes. The flatness factor may thus be used to indicate the degree of intermittency of the signal. An intermittency factor, γ, is defined as a fraction of time during which periods of activity exist. A signal with two different magnitudes of fluctuations appearing in an intermittent manner can produce a large flatness factor. An estimate of the intermittency can be found by

$$\gamma = 3 \;/\; [\; \overline{u^4(t)} \;/\; (\; \overline{u^2(t)})^2 \;] \;.$$

where three is the Gaussian normal value.

In an oscilloscope trace of the electrical signal, an intermittent signal has bursts of activity followed by periods of relative silence. The time derivative of the turbulent signal is usually used to estimate the intermittency. Unfortunately, a high value of the flatness factor does not necessarily indicate intermittency. If, however, intermittency is shown to occur by some other means, then the flatness factor can be used to estimate the degree of intermittency of the signal.

Super skewness and hyper skewness have been defined by Frenkiel and Klebanoff [1976] as the nondimensionalized central fifth and seventh order moments respectively. Their Gaussian values are zero. The nondimensionalized central sixth order moment, super flatness, has a Gaussian value of fifteen.

3.1.1.2 Mixed Moments

Moments and central moments of joint distributions may be expressed in a similar way. In general, the moment of a joint distribution may be defined by:

$$\overline{u^n v^m} = \int_{-\infty}^{+\infty}\int u^n v^m p(u,v)\, du\, dv \quad .$$

The first central moment, n=1 and m=1, is called the correlation or covariance. When nondimensionalized by the standard deviation of each variable, it is called the correlation coefficient.

3.1.2 Spectral Analysis

The statistical techniques previously described are concerned with the general characteristics of the turbulent signals. The next step is to consider the characteristics of the signal specifically in the frequency domain. Two of the most commonly used quantities in a frequency analysis are the amplitude of the signal and the power contained in the signal at each frequency.

There are a number of reasons why the power spectrum of a signal is computed. One reason is that due to the random nature of the turbulence signal, it is necessary to determine some average quantities which are relatively stable and meaningful to interpret. The power spectrum is an average quantity which is used to measure the power or energy content of a turbulence signal distributed over different frequencies or wavenumbers. Integration of the power spectral density provides information about the total power of the signal.

Four of the most common techniques used to determine the power spectral density are:

1. band pass filtering.
2. direct Fourier transform.
3. Fourier transform of the auto correlation function.
4. Fourier transform after segmentation.

Traditionally, analog filtering methods take the form of a set of parallel band pass filters set to the frequency range of interest. The signal to be analyzed is applied to the filter inputs. To obtain discrete points on the frequency spectrum, the filtered output signals are then squared and averaged.

The direct method of obtaining a power spectrum involves computing the Fourier transform of the time series and taking the mean square value of the transform. Until the development of the fast Fourier transform technique, the direct method was not generally used due to the long computation time.

G. I. Taylor introduced the calculation of correlation functions in the 1920s. Later work showed that the auto correlation and the power spectra form a Fourier pair. Thus, by calculating the auto correlation and then taking its Fourier transform the power spectrum could be indirectly determined. Blackman and Tukey [1958] developed a practical approach to this indirect method of determining the power spectrum.

The easiest way to view the spectrum is as a function that produces the proper energy when integrated over all wavenumbers. That is:

$$u^2 = \int_0^\infty F_1(\ k\ )\ dk \quad .$$

where $F_1(\ k\ )$ and the auto correlation are Fourier transforms of each other.

In turbulent flows, a measurement of $F_1(\ k\ )$ will show how the energy is distributed among the various eddy sizes in the flow. Most of the energy is at the low frequencies or wavenumbers, in the larger eddies, and decreases at the higher wavenumbers due to the decreased severity of the velocity fluctuations. The energy, converted to turbulence, is transfered through the spectrum to the high frequency components and due to the rapid viscous decay of the smaller eddies is dissipated into heat there.

In addition to determining information about the structure of the turbulent field from the shape of the spectrum, the 'scales' of turbulence may also be obtained from the smoothed spectrum.

3.1.3 Turbulence Scales

The Taylor microscale of turbulence, λ, is a measure of the size of those eddies in which the dissipation of the turbulent energy into heat is taking place. The Taylor microscale may be determined from certain velocity correlations, from the energy spectrum, or through the measurement of the root mean square values of the timewise differentiated velocity fluctuation.

In practice, however, neither the correlation function nor the energy spectrum measurements offer the most convenient means of experimentally determining the Taylor microscale. A simple and direct method of determining λ has evolved from measurements of the velocity derivative where

$$\lambda = u' \; / \; (\; \partial u/\partial x \;)^{0.5} \quad .$$

By applying Taylor's hypothesis, the microscale, λ, may be calculated directly from

$$\lambda^2 = U^2 \; [u'^2 \; / \; (\; \partial u/\partial t)^2 \;] \; .$$

For isothermal turbulence, the mean dissipation rate, ϵ, can be calculated from the relationship

$$\overline{\epsilon} = 15 \; u'^2 \; \nu \; /\lambda^2$$

where ν is the kinematic viscosity.

The Taylor microscale is also used to determine the turbulence Reynolds number, Re(λ), where

$$Re(\lambda) = u' \; \lambda \; / \; \nu \quad .$$

The Kolmogorov length scale, η, provides a measure of the smallest eddies in the turbulence responsible for dissipation. The Kolmogorov length scale may be defined by

$$\eta = (\nu^3 / \overline{\epsilon})^{1/4} \quad .$$

The Kolmogorov length is the smallest turbulent fluctuation that can withstand the damping effect of viscosity.

Chapter IV

PRESSURE MEASUREMENTS - RESULTS AND DISCUSSION

Pressure measurements were taken in both the boundary layer tunnel and the conical diffuser. These measurements were necessary as a performance comparison between the various pressure measuring devices and as a calibration standard for the hot-wire measurements.

Static and total pressure readings were taken in the boundary layer tunnel in order to, first, calibrate the tunnel, second, obtain velocity profiles, and third, compare the performance of the two liquid filled manometers and the pressure transducer. Two velocity distributions, one at a free stream velocity of 8 m/sec, and one at a free stream velocity of 4 m/sec, were taken in the boundary layer tunnel.

Static and total pressure readings were taken along the diffuser wall and diffuser axis at various contraction cone pressure drops in order to determine Reynolds number independence in the diffuser flow. In addition to the static and pitot pressure readings, Preston pressure readings were taken along the diffuser wall in order to determine the wall shear stresses and friction velocities. Velocity profiles and Preston pressures, at one tunnel operating point, were taken at 3 cm intervals along the diffuser wall. The twenty-three velocity distributions in the diffuser were taken at right angles to the diverging conical wall.

4.1 THE BOUNDARY LAYER TUNNEL

The boundary layer tunnel was calibrated for tunnel centerline velocity by measuring the static and total pressures 15 cm upstream of the pipe outlet against the contraction cone pressure drop. The static pressure and total pressure, plotted in Figure 4.1 and Figure 4.2, both show a linear relationship from 0.010 to 0.350 in H_2O of contraction cone pressure drop. The centerline velocity was determined from Bernouilli's equation for steady, incompressible flow along a streamline:

$$U = [\, 2 \,(\, p_0 - p \,) \,/\, \rho \,]^{0.5}$$

where p is the static pressure and p_0 is the total pressure. The calculated velocity was plotted against the contraction cone pressure drop, ΔPc, and against $(\, \Delta Pc \,/\, \rho \,)^{0.5}$ in Figure 4.3 and Figure 4.4 respectively. As shown by Figure 4.4, the speed of the airflow through the tunnel, and hence the tunnel Reynolds number, is proportional to the square root of the contraction cone pressure drop.

By using the linear relationship between the centerline velocity and $(\, \Delta Pc \,/\, \rho \,)^{0.5}$, the boundary layer tunnel could be set to the desired tunnel operating point based on the centerline velocity. For example, contraction cone pressure drops of 0.025 and 0.110 in H_2O resulted in centerline velocities of 4 and 8 m/sec respectively.

A comparison of the different manometers showed that although the Betz manometer has a larger range, the Combist micromanometer allowed greater precission for pressure measurements in the boundary layer tunnel. As with similar results from Derksen [1981], use of the Combist micromanometer provided the more constant results. Later tests using the Baratron pressure transducer and Combist micromanometer showed no difference between the results obtained with either pressure measuring device.

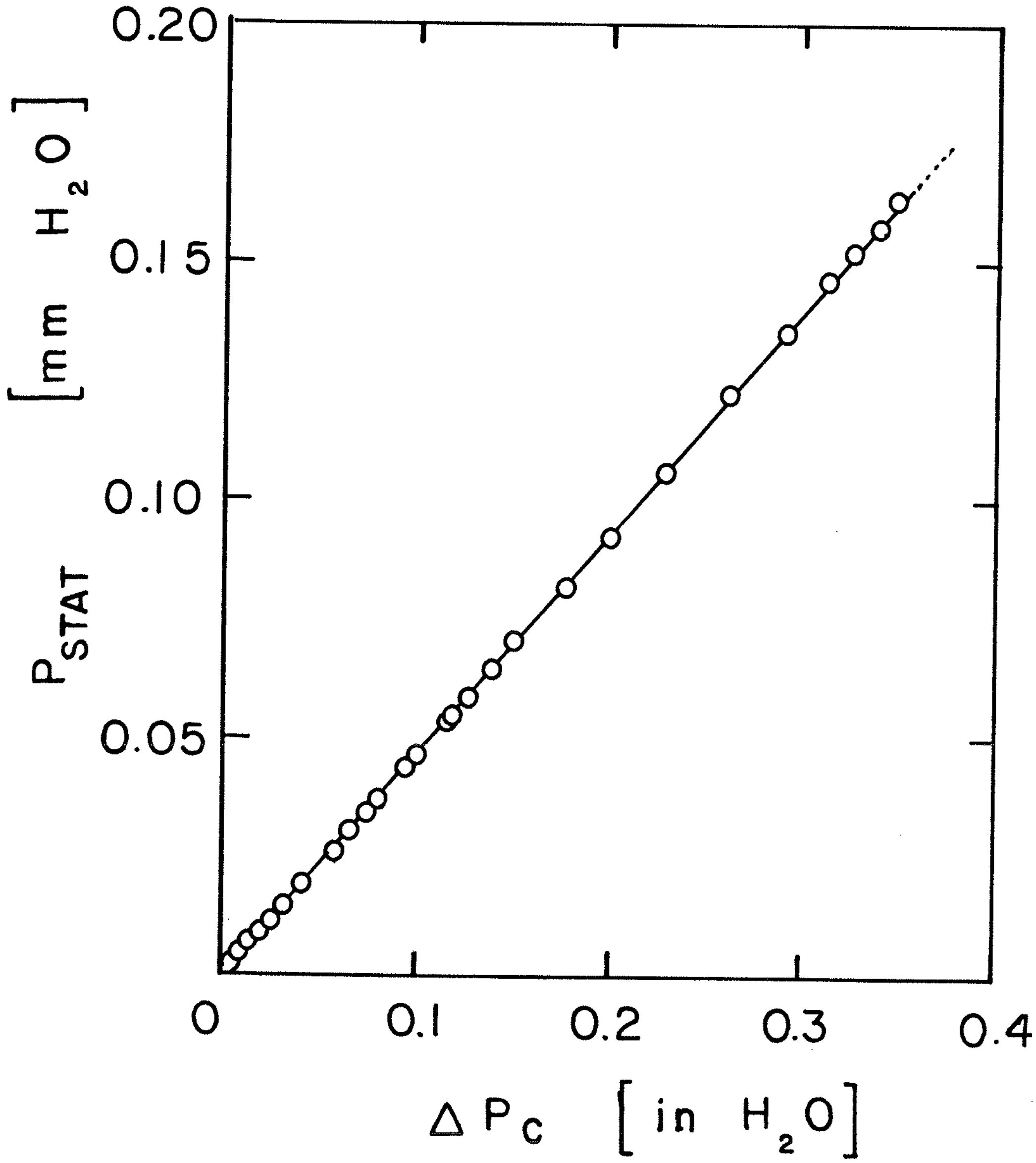

Figure 4.1: Static Pressure versus Cone Pressure Drop

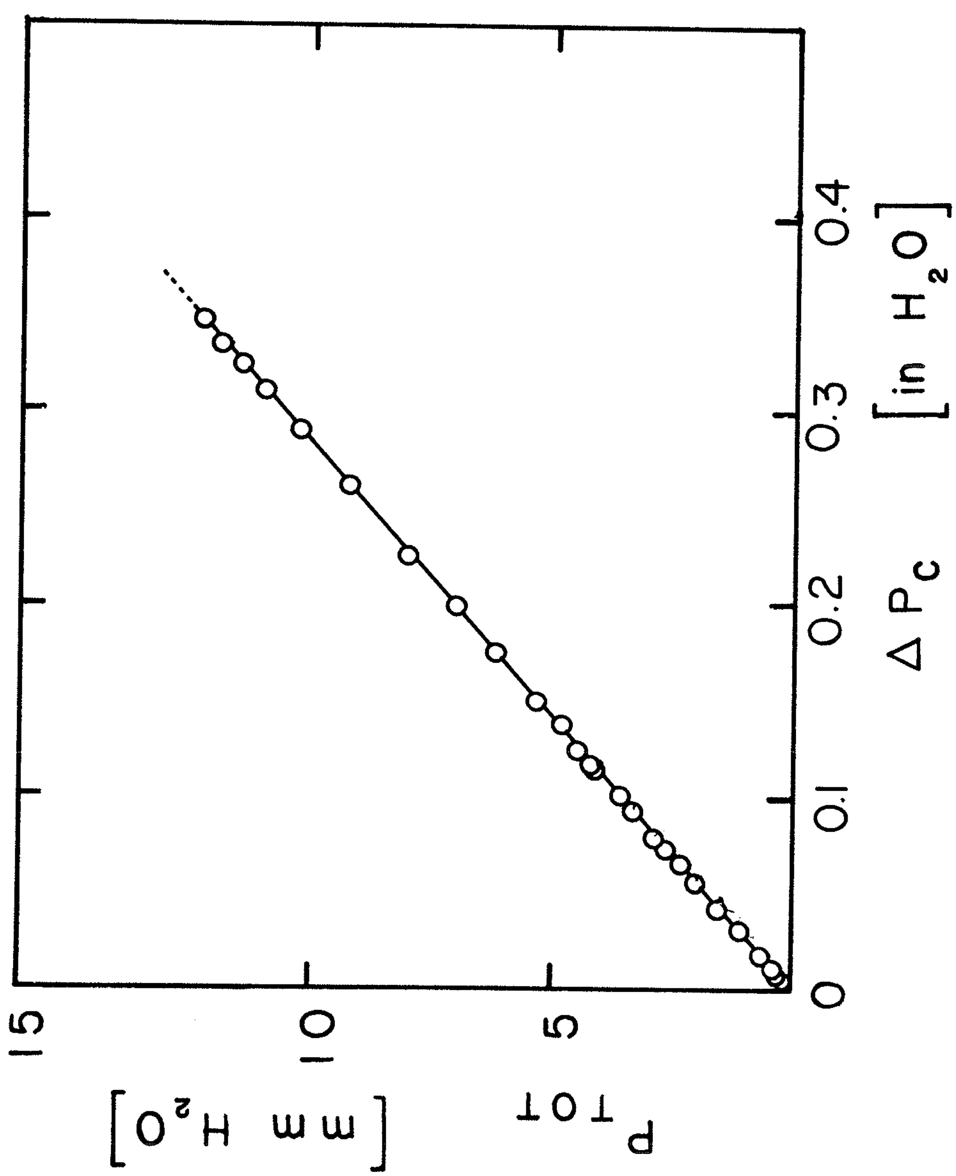

Figure 4.2: Total Pressure versus Cone Pressure Drop

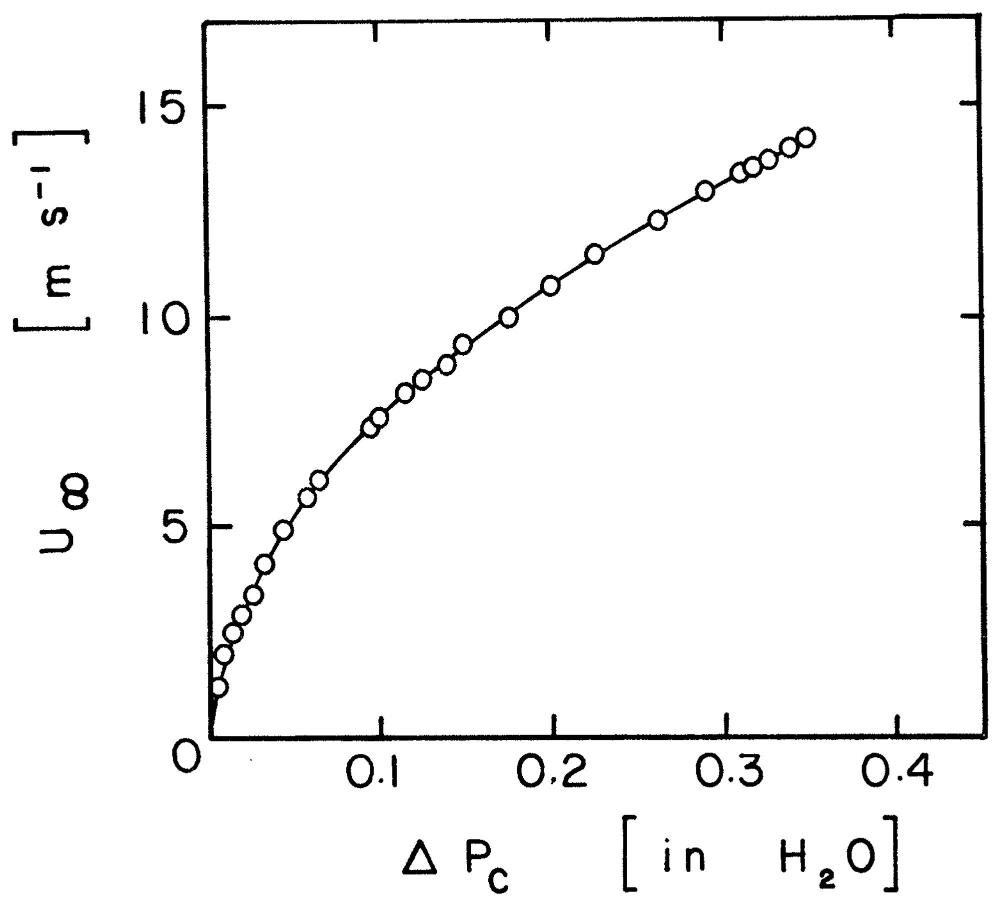

Figure 4.3: Velocity Calibration Curve I

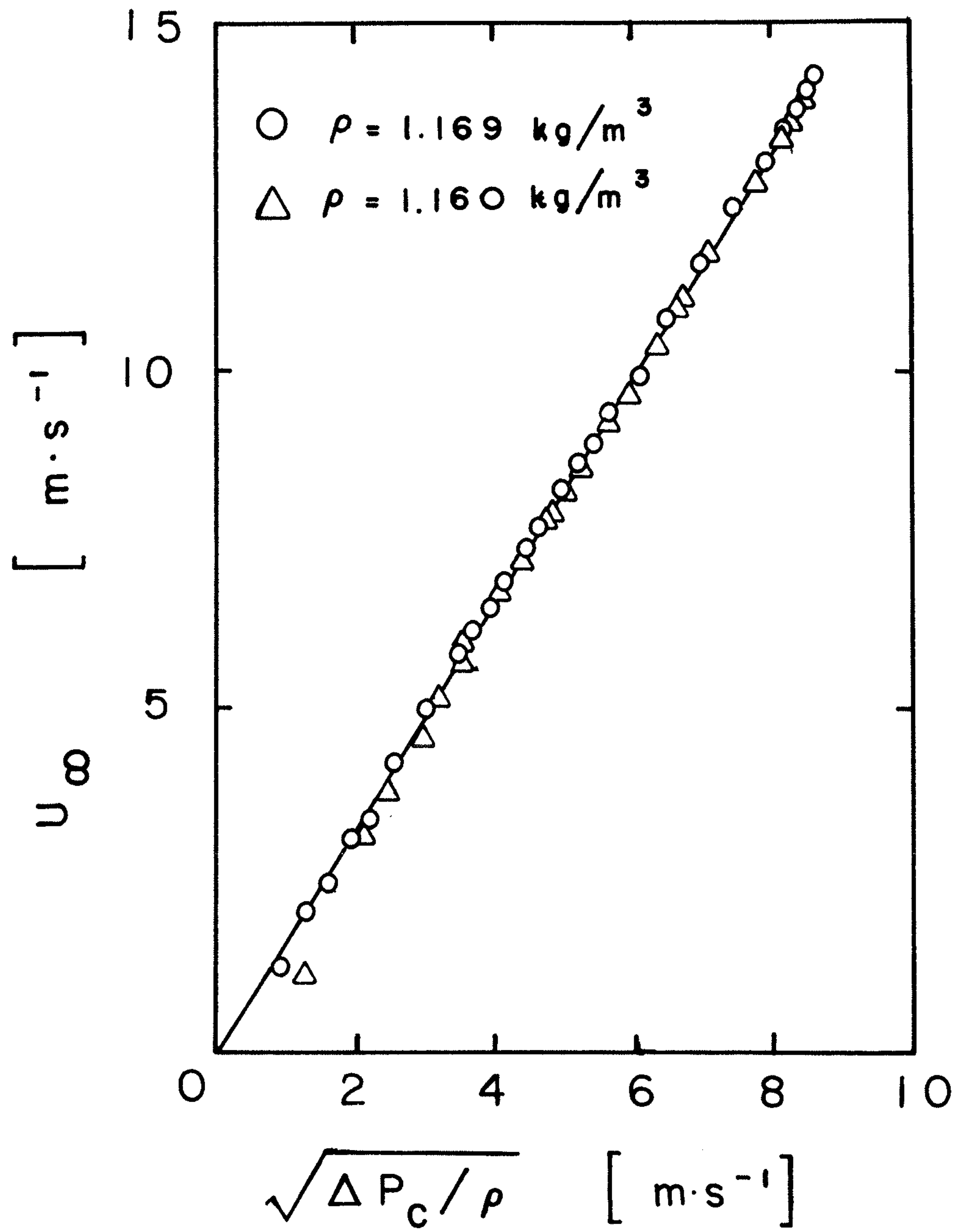

Figure 4.4: Velocity Calibration Curve II

4.2 THE DIFFUSER

The pressure measurements in the diffuser were taken with fully developed pipe flow as the inlet condition to the diffuser. Studies by Laufer [1954] have shown that a pipe length of 50 diameters is adequate for complete flow development in a pipe. The pipe entry length to the diffuser inlet is 78 pipe diameters in length. This is well in excess of the 50 diameters needed for fully developed pipe flow at the diffuser entry. Recent studies by Dang [198_] have shown that, for this tunnel, the pipe flow at 78 pipe diameters is indeed fully developed flow.

4.2.1 Static and Total Pressures

Static and total pressures measurements were taken at four different tunnel operating points. The contraction cone pressure drops, in inches of water, were 0.5 , 1.0, 2.0, and 4.0. These pressure drops corresponded to Reynolds numbers of 92,000, 130,000, 184,000, and 260,000 respectively, based on the pipe diameter and pipe bulk velocity. The pressure results, when divided by the operating contraction cone pressure, would collapse onto the same curve thereby indicating a Reynolds number similarity for the flow in the diffuser.

From the plot of static pressures in the diffuser shown in Figure 4.5, the diffuser is shown to be a pressure recovery device. The negative valued static pressures in the diffuser increase continuously, approaching atmospheric pressure towards the diffuser outlet. The rate of recovery is greatest near the diffuser inlet and gradually decreases in the downstream direction. Static pressures at the diffuser wall measured by means of the eleven static pressure wall taps and the static pressure tubes were found to be the same.

Static pressure measurements were taken along both the diffuser wall and the diffuser axis. As with similar results from Okwuobi [1972] and Arora [1978] for the same diffuser but different operating points, the radial variation in static pressure was very small.

Total pressure measurements were taken along the diffuser axis for three different tunnel operating points. As with static pressure measurements, the total pressure measurements collapsed onto the same curve when scaled by the appropriate contraction cone pressure drop. Unlike the static pressure measurements, the total pressure measurements were positive valued. The axial total pressure measurements in the downstream direction linearly decreased in value to a position approximately 15 cm from the venting end of the diffuser. An increased bending of the axial total pressure curve occured in the last 15 cm of the diffuser flow.

Due to the highly fluctuating nature of the diffuser flow, pressure results using the Combist micromanometer were difficult to read without a significant loss in precision. With the wind tunnel operating at the higher Reynolds numbers, the pressures were beyond the range of the Combist micromanometer. The Betz manometer, due to its large internal volume, would be slow to respond to the pressure changes. This was advantageous in that the pressure fluctuations at any point in the flow would be considerably damped. The disadvantage lay in the long settling time required to obtain a stable reading at a new location in the flow. The Baratron pressure transducer readings were in excellent agreement with those of the liquid filled manometers. However, the output from the Baratron pressure transducer is an instantaneous result. Before a stable reading could be obtained, the electrical signal was sent through an integrator set for a sixty second time constant. A waiting period of at least four times the time constant was allowed to pass before an averaged reading could be taken from the display of an externally connected voltmeter.

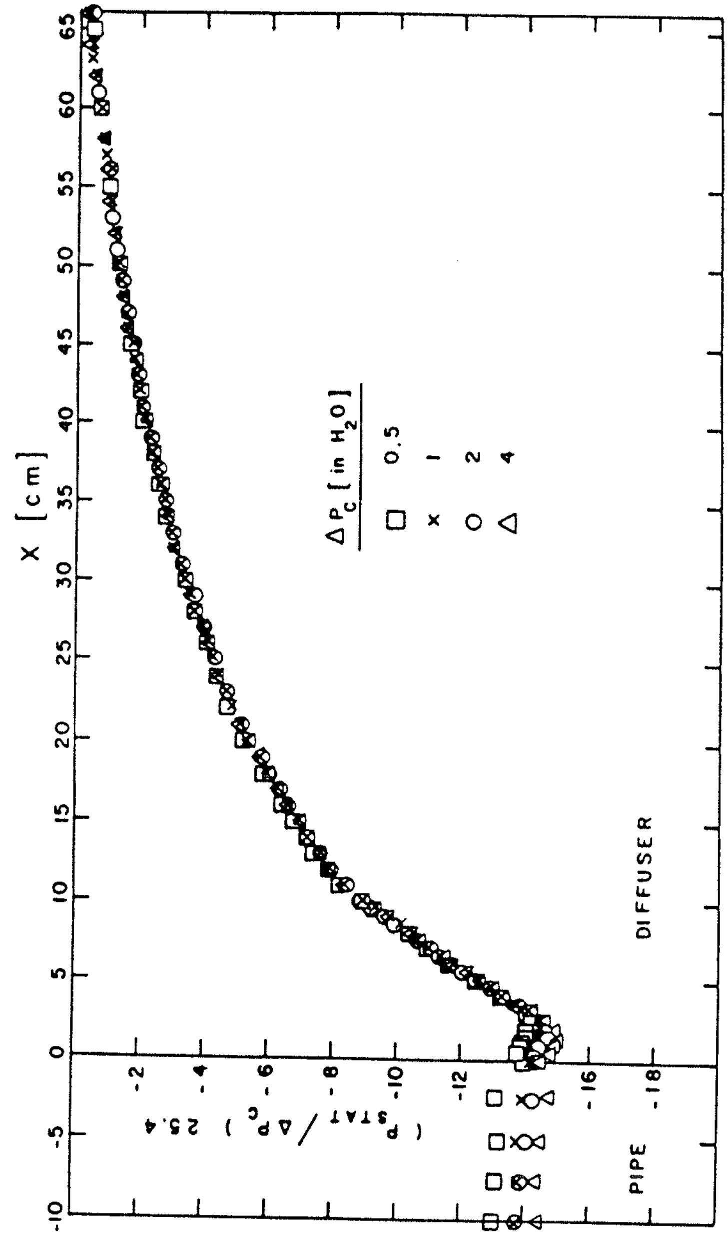

Figure 4.5: Static Pressure Distribution in the Diffuser

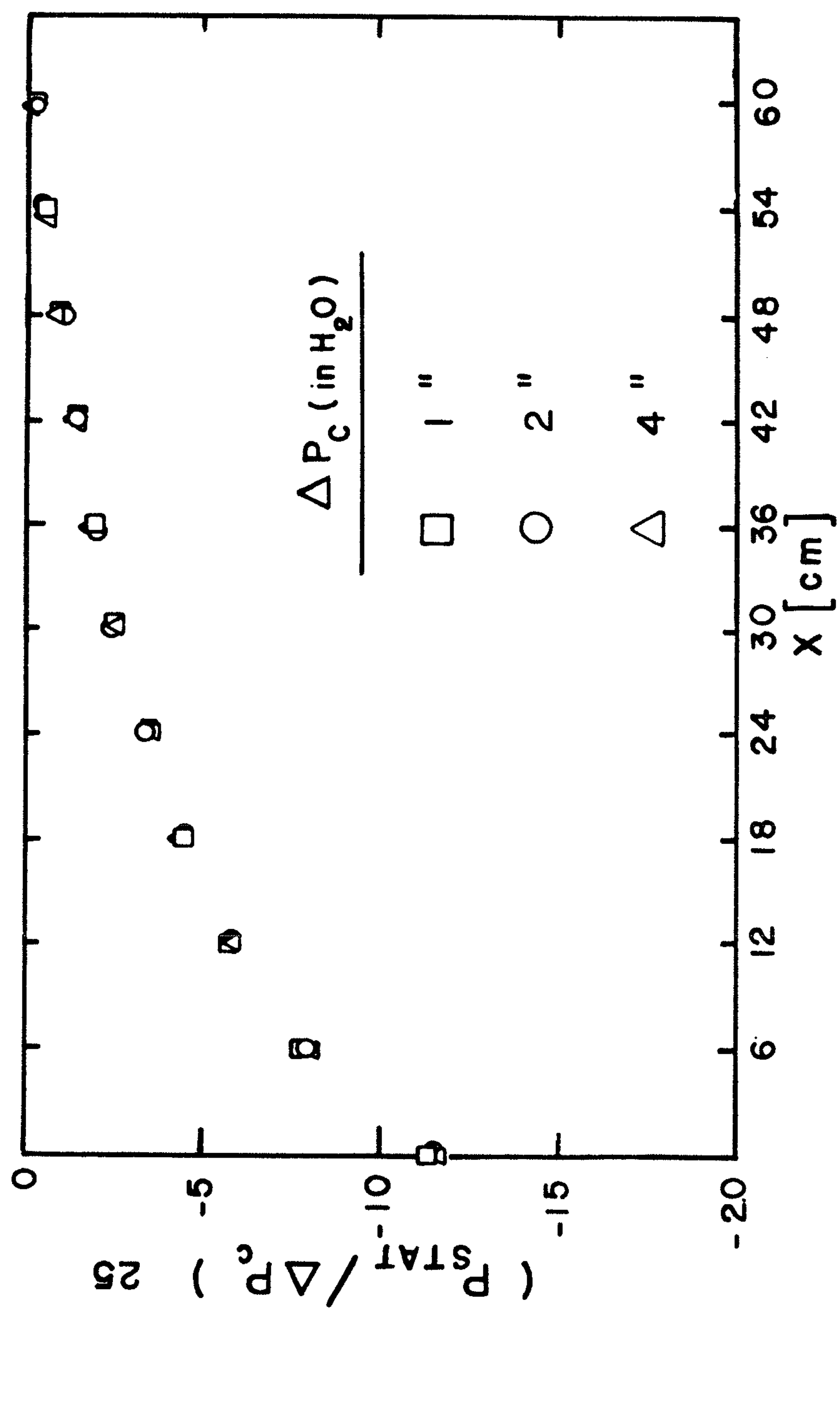

Figure 4.6: Static Pressure from Wall taps

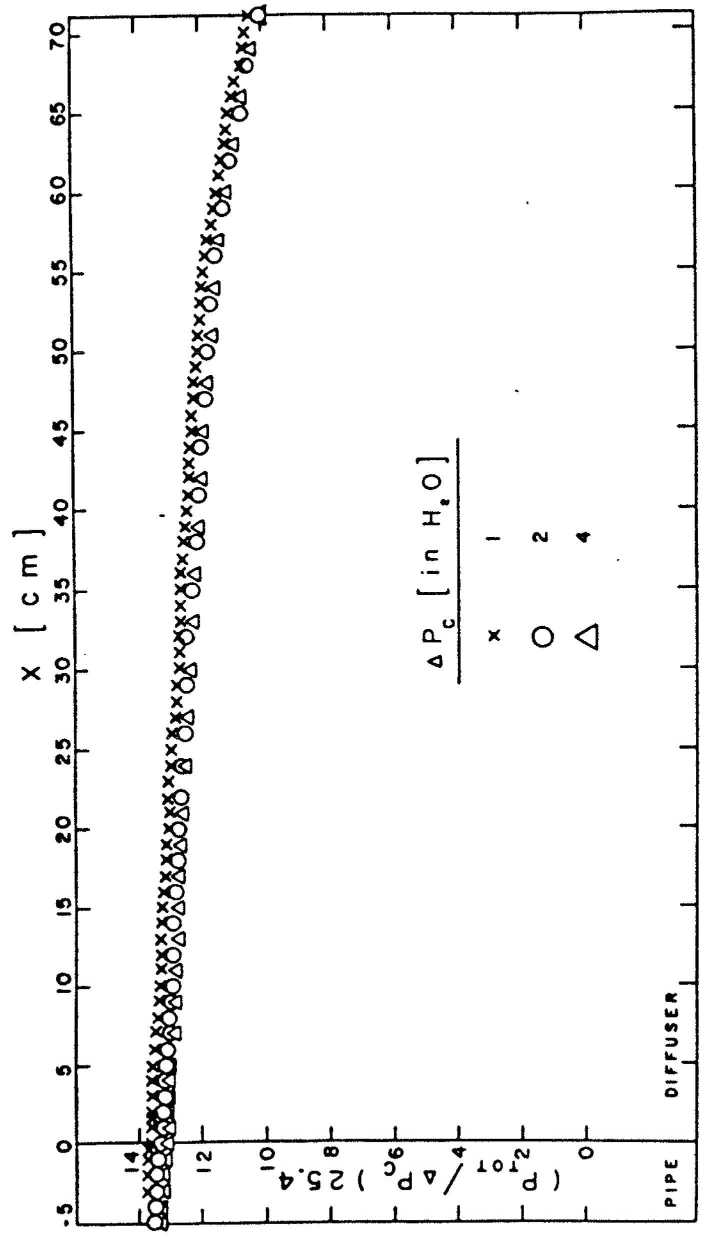

Figure 4.7: Axial total pressure in the Diffuser

4.2.2 Friction Velocities - Preston Pressure Method

Methods for determining the friction velocity in a negative or favourable pressure gradient flow such as pipe flow are well known. The simplest method would be to determine the pressure drop over a length of pipe. However, in the case of an adverse pressure gradient flow, such as diffuser flow, these methods are not as well established. Okwuobi [1972] in his study of diffuser flow, considered three methods for obtaining values of friction velocity. These were by the law of the wall, the Ludweig and Tillman equation, and the total shear stress extrapolation to the wall.

In this study, Preston pressures were measured to determine the friction velocity, u*, along the diffuser wall. A Preston tube is basically a round Pitot tube resting upon a solid surface. Preston [1954] based the measurement of skin friction on the concept of universality of the wall region in turbulent wall shear layers where

$$u / u^* = f\,(y\,u^* / \nu)$$

is the nondimensional form of the law of the wall. If instead of the mean velocity, the pressure difference recorded by a pitot tube resting against the wall and the local static pressure is used, then the above relation may be written as :

$$\tau_0\, D^2/4\rho\nu^2 = h(\Delta p\; D^2/4\rho\nu^2)$$

where D is the outer diameter of the round pitot. This relation provides a convenient way for determining skin friction since the shear stress is now uniquely related to the Preston and local static pressures.

Patel [1965] later confirmed Preston's work and went on to establish a calibration curve. The calibration curve has been divided into three regions:

1. Fully developed region

   $$55 < u^* D / 2\nu < 800$$

   or $3.5 < y^* < 5.3$ and $5.6 < x^* < 7.6$, where the calibration curve is given by :

   $$x^* = y^* + 2 \log(1.95\, y^* + 4.10) \quad ,$$

2. Transition region

   $$5.6 < u^* D / 2\nu < 55$$

   or $1.5 < y^* < 3.5$ and $2.9 < x^* < 5.6$, where the calibration curve is given by :

   $$y^* = 0.8287 - 0.1381\, x^* + 0.1437\, x^{*2} - 0.0060\, x^{*3} \ ,$$

3. Sublayer

   $$u^* D / 2\nu < 5.6$$

   or $0 < y^* < 1.5$ and $0 < x^* < 2.9$, and the calibration curve is given by the linear relation :

   $$y^* = {}^1/_2\, x^* + 0.037 \quad ,$$

where $x^* = \log(\Delta p\, D^2 / 4\rho\nu^2)$ and $y^* = \log(\tau_0\, D^2 / 4\rho\nu^2)$ are the nondimensional argument and function respectively.

Patel reported that the Preston tube overestimates the skin friction in both favourable and adverse pressure gradients, with increased errors occuring with increasing Preston tube diameter. Patel was able to suggest limits in terms of an inner pressure gradient parameter, $\Delta = (\nu/\rho u^{*3})(dp/dx)$.

1. adverse pressure gradients:

   maximum error 3%: $0 < \Delta < 0.01$, $u^*D/\nu \leq 200$,

   maximum error 6%: $0 < \Delta < 0.015$, $u^*D/\nu \leq 250$.

2. favourable pressure gradients:

   maximum error 3%: $0 < -\Delta < 0.005$,

   $u^*D/\nu \leq 200$, $d\Delta/dx < 0$,

   maximum error 6%: $0 < -\Delta < 0.007$,

   $u^*D/\nu \leq 200$, $d\Delta/dx < 0$.

Frei and Thomann [1980] conducted exhaustive studies for Preston pressures in strong adverse pressure gradients. Their findings showed the Preston tube error to depend on both u^*D/ν and on Δ, the inner pressure gradient parameter. Frei and Thomann developed a set of look-up tables used to estimate the error from the uncorrected measurements.

The friction velocities, u^*, determined via Patel's calibration and Frei and Thomann corrections, are shown in Figure 4.8. The friction velocity decreases from 82 cm/sec at the diffuser inlet to 17 cm/sec close to the diffuser outlet. The greatest rate of change in the decreasing friction velocity occurs in the first 20 cm into the diffuser.

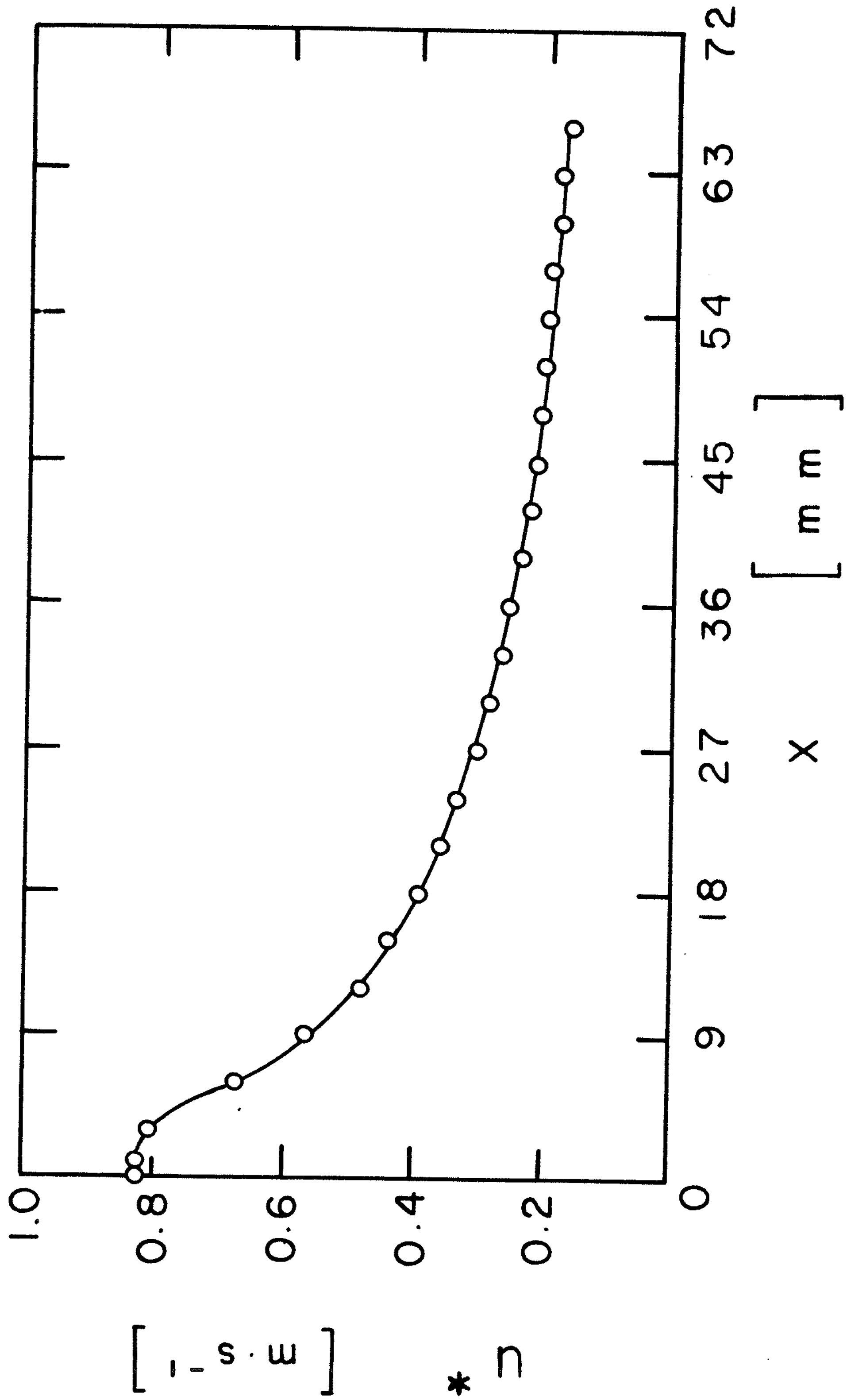

Figure 4.8: Friction Velocity Distribution in the Diffuser

4.2.3 Velocity Distributions

Due to the presence of the strong, continuous, and smoothly varying adverse pressure gradient, it was expected that the flow adjustment in the diffuser would also be continuous and smooth. The mean longitudinal velocity distributions were determined at 3 cm intervals. The twenty-three velocity profiles were taken at right angles to the diffuser wall rather than, as with previous studies, perpendicular to the diffuser axis. As expected from flow continuity, the increased cross-sectional area results in a decreased mean longitudinal velocity in the axial direction which coincides with a simultaneous pressure increase.

The velocity distributions near the diffuser entry are similar to that of pipe flow velocity profiles. This is true for approximately the first third of the diffuser length. Gradually, as the distance from the diffuser entry increases, the profiles appear to develop two regions: a central core with a high degree of curvature, and an approximately linear region near the diffuser wall. This inflectional type profile is most clearly seen in the final third length of the diffuser, and is indicative of adverse pressure gradient flow. The point of inflection in the velocity profiles occurs at a radial position approximately 5 cm from the diffuser axis. This distance, 5 cm, is the magnitude of the diffuser inlet radius. The decrease in slope and magnitude of the velocity profiles is due to the retardation of the fluid layers relative to each other caused by rising pressure in the downstream direction. This is especially true for the region near the wall.

Previous studies by Hummel [1978] and Derksen [1986] seem to suggest the flow in the latter third of the diffuser display characteristics of a jet in the core, a boundary layer near the wall, and a mixing layer between the two regions. However, when considering the distribution of the third order moment of the diffuser flow, positive in the wall region and negative in the core region, a much more complex flow structure seems to be indicated.

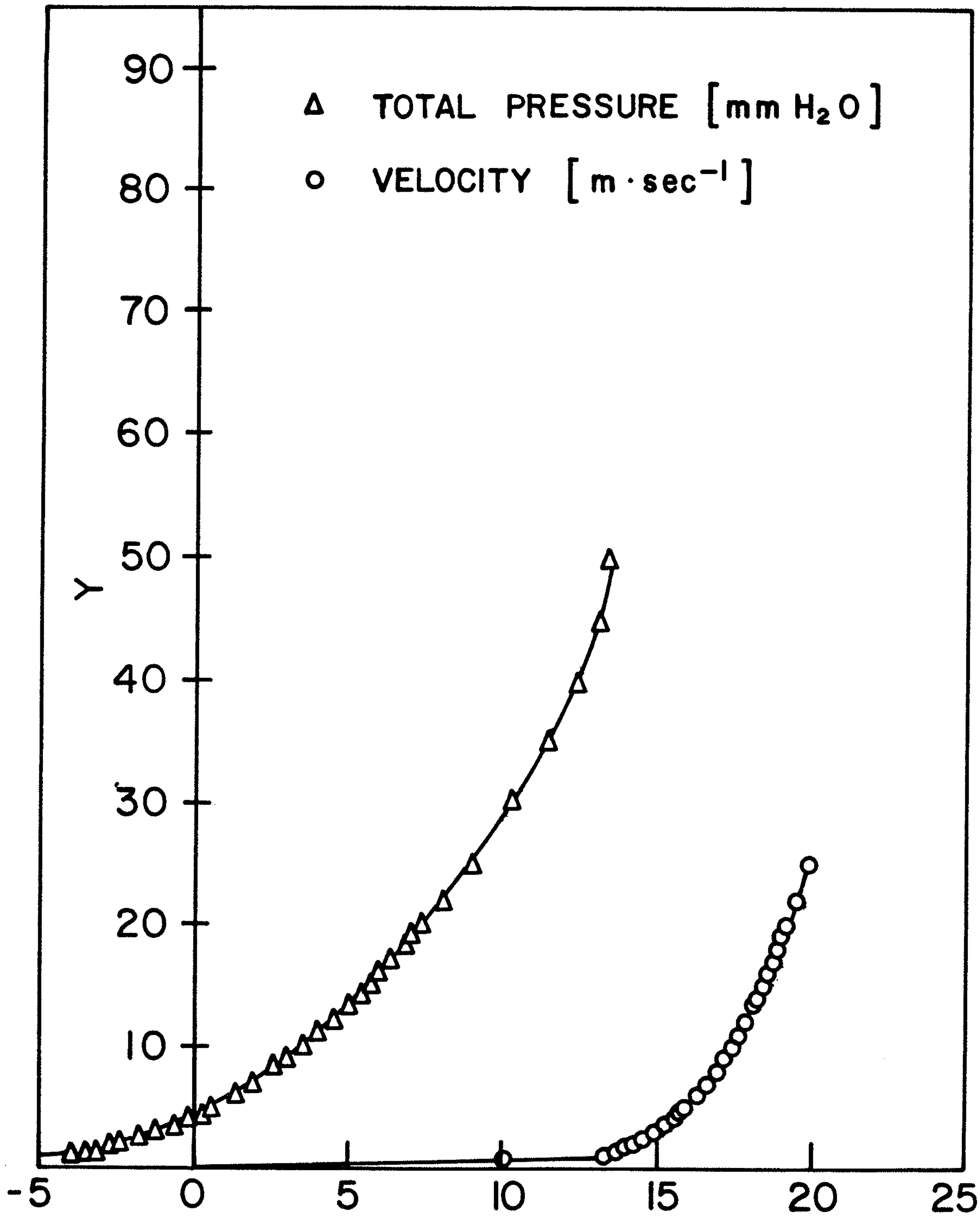

Figure 4.9: Velocity Distribution at x = 3 cm

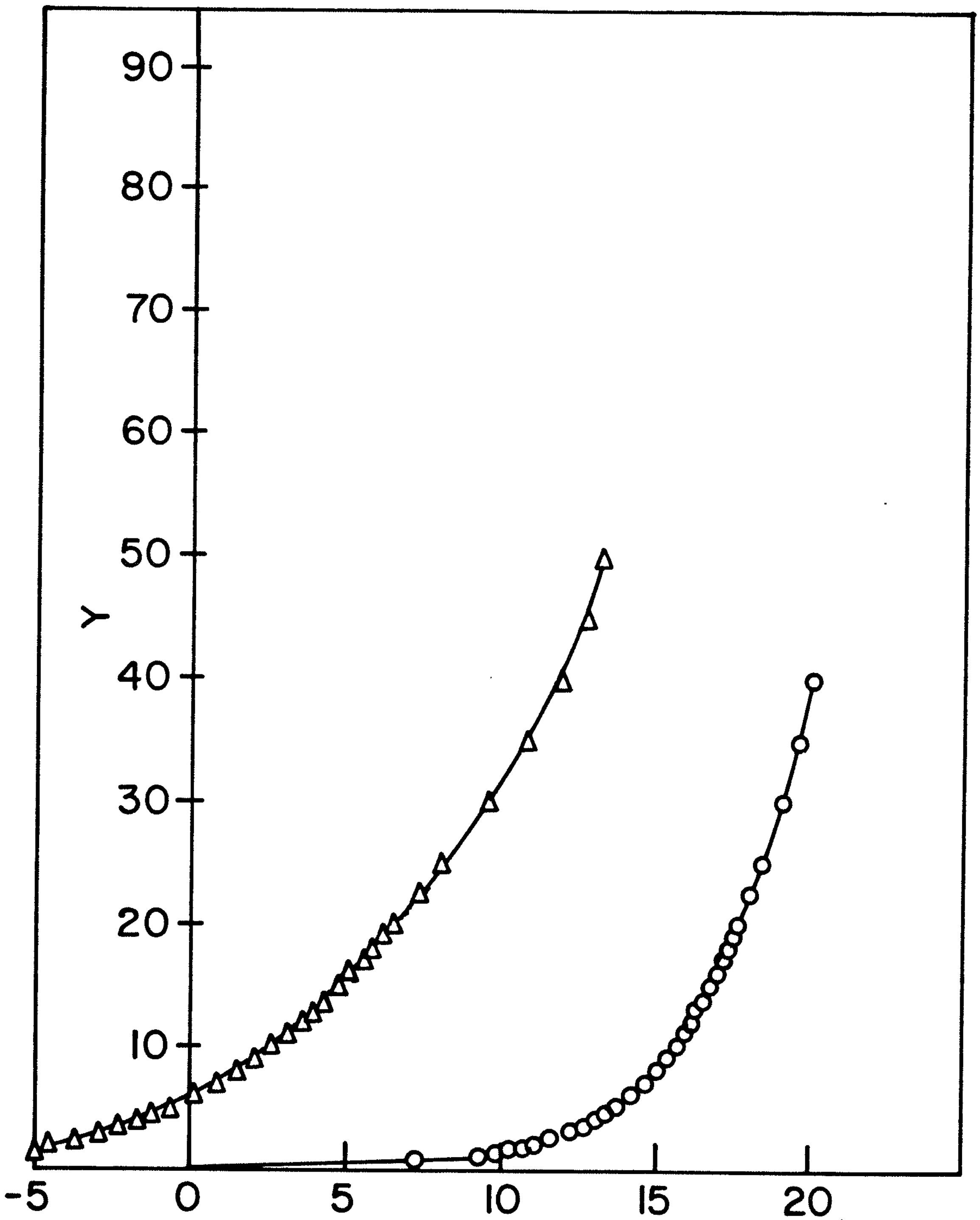

Figure 4.10: Velocity Distribution at x = 6 cm

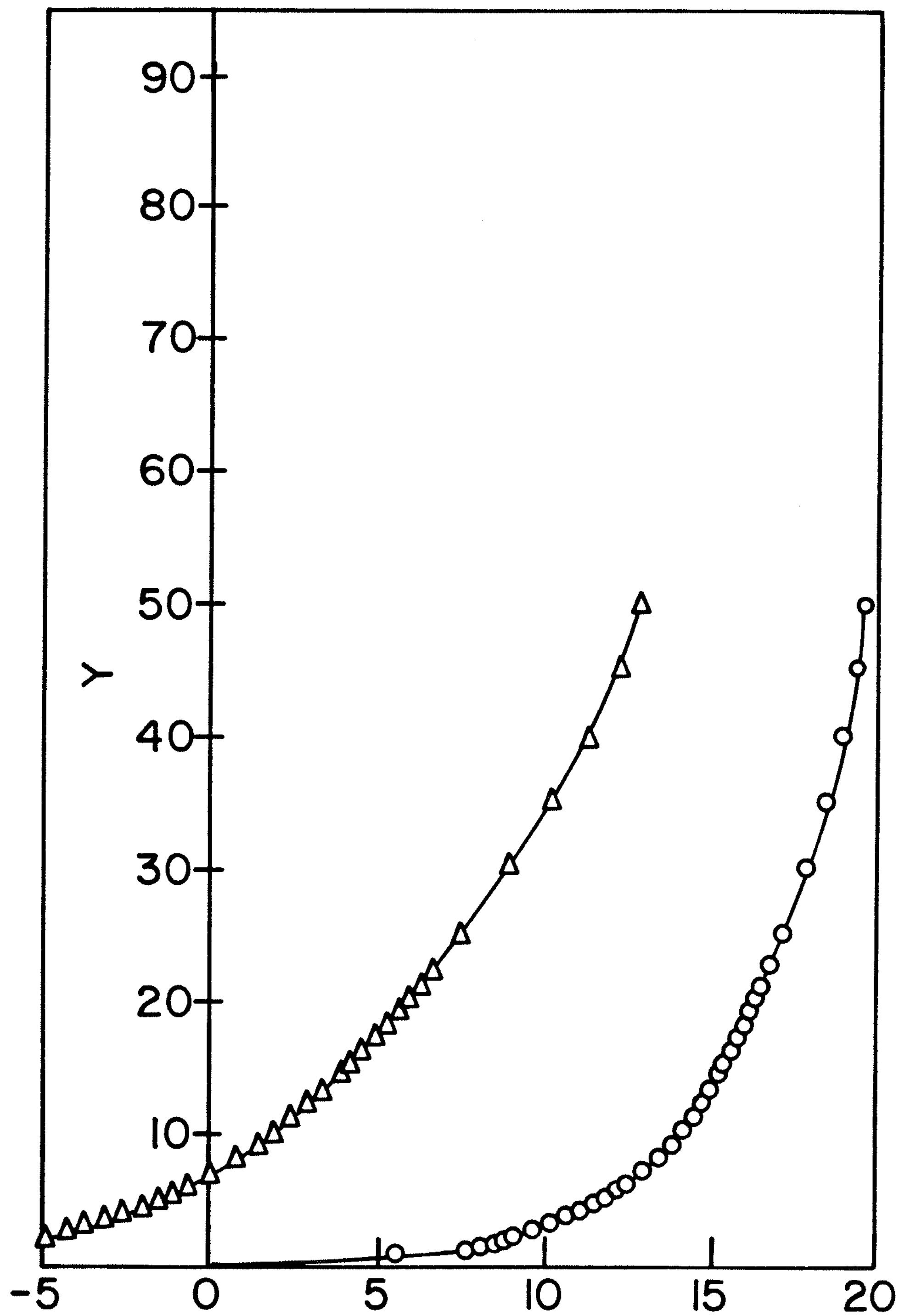

Figure 4.11: Velocity distribution at x = 9 cm

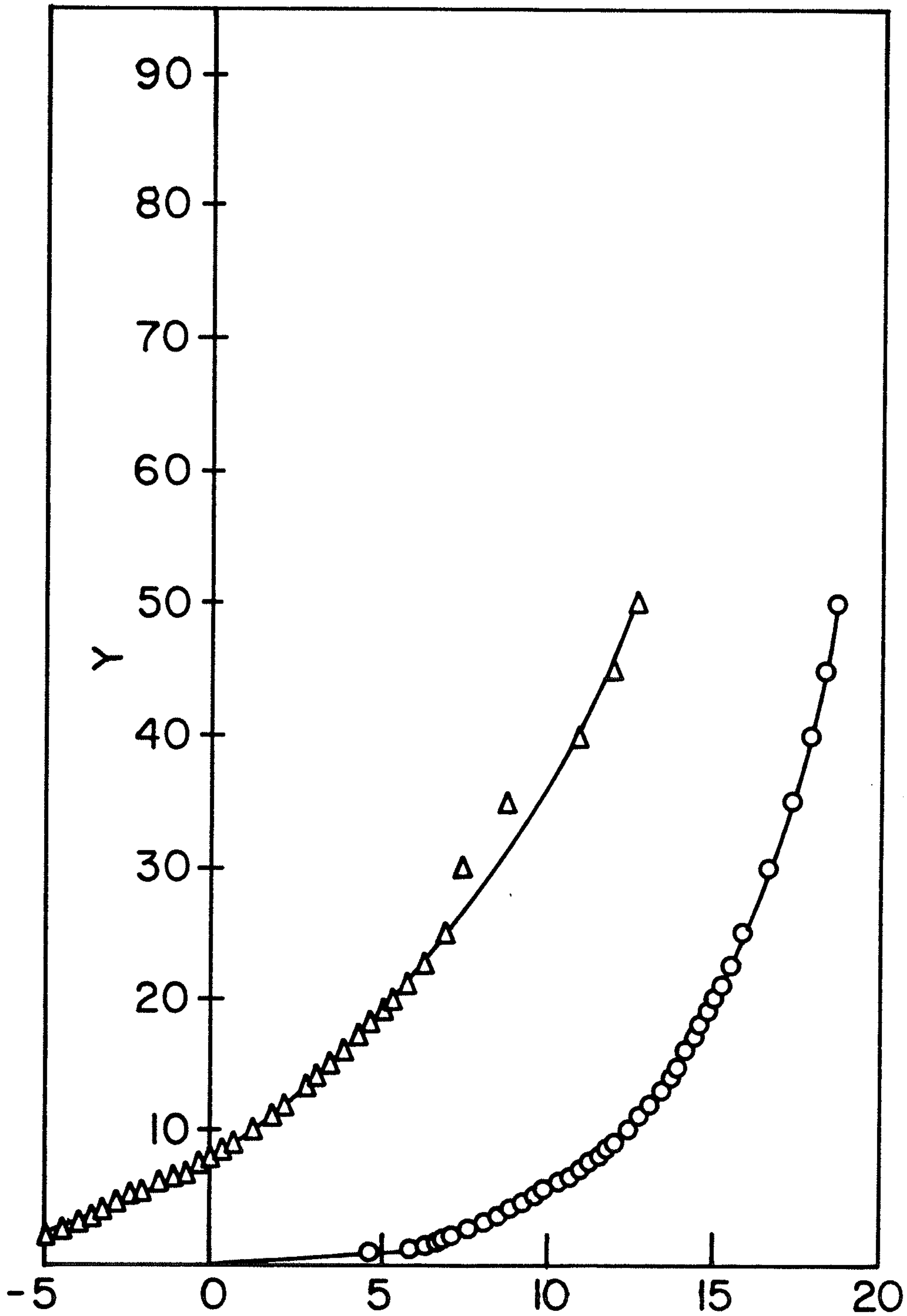

Figure 4.12: Velocity distribution at x = 12 cm

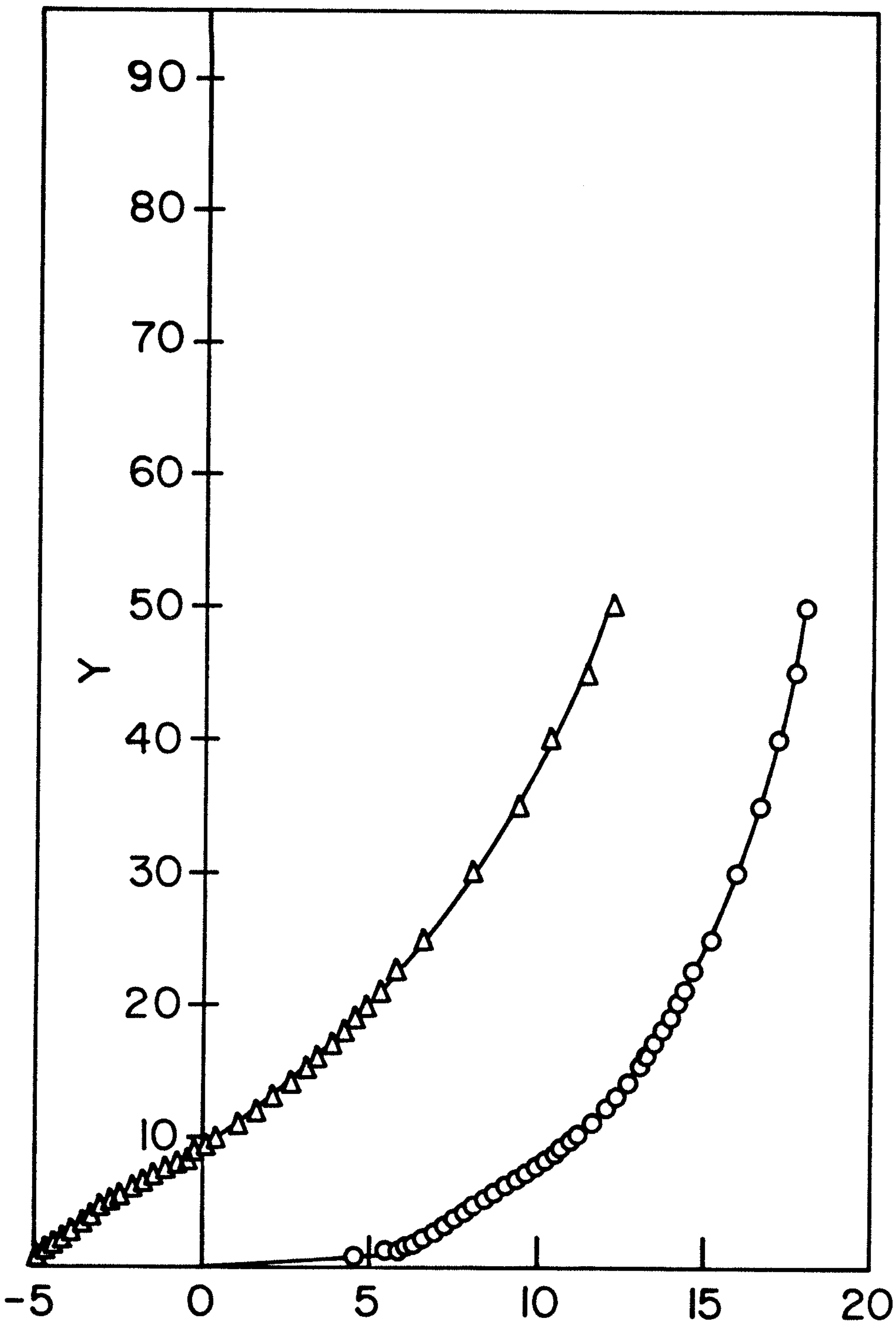

Figure 4.13: Velocity distribution at x = 15 cm

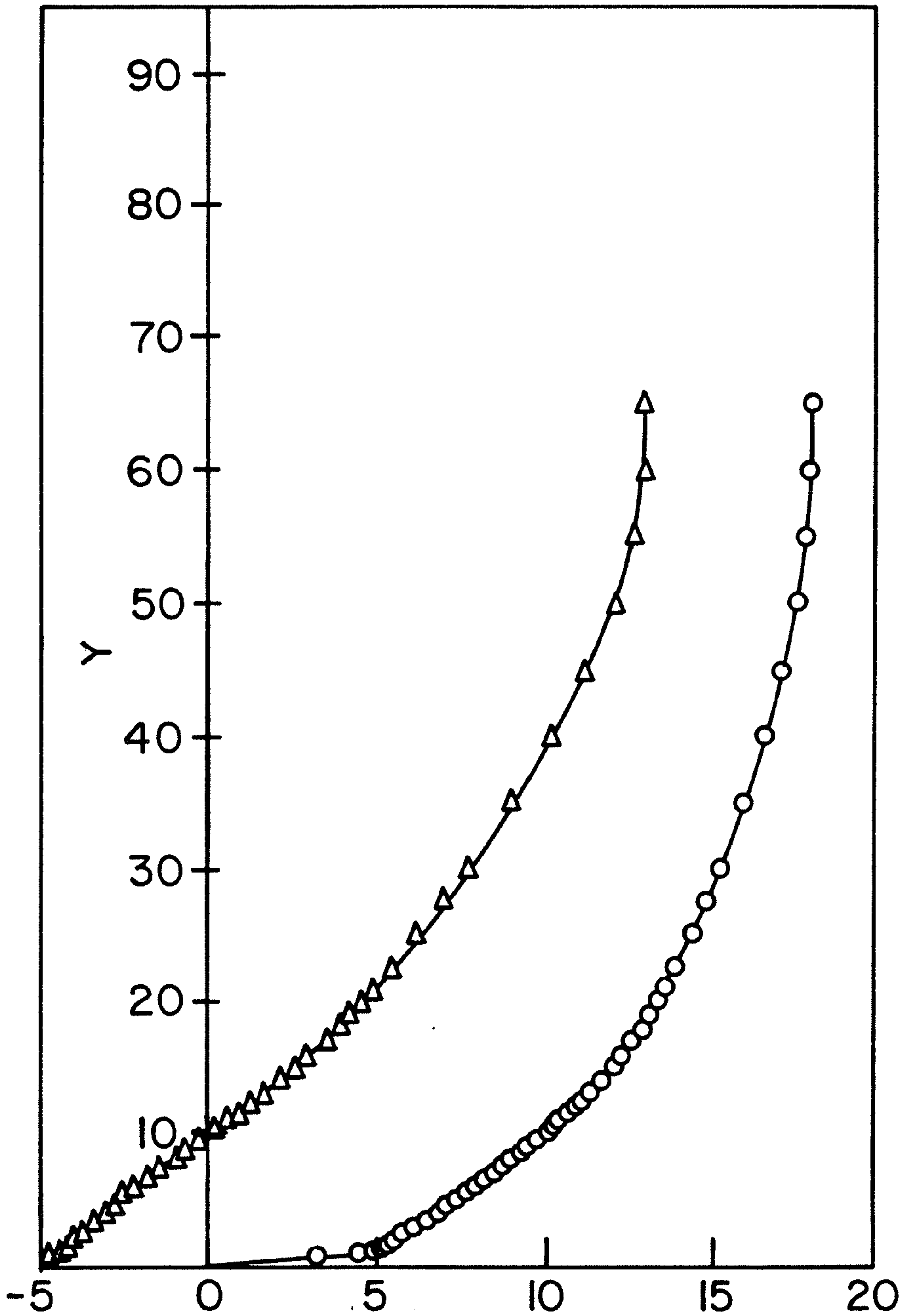

Figure 4.14: Velocity distribution at x = 18 cm

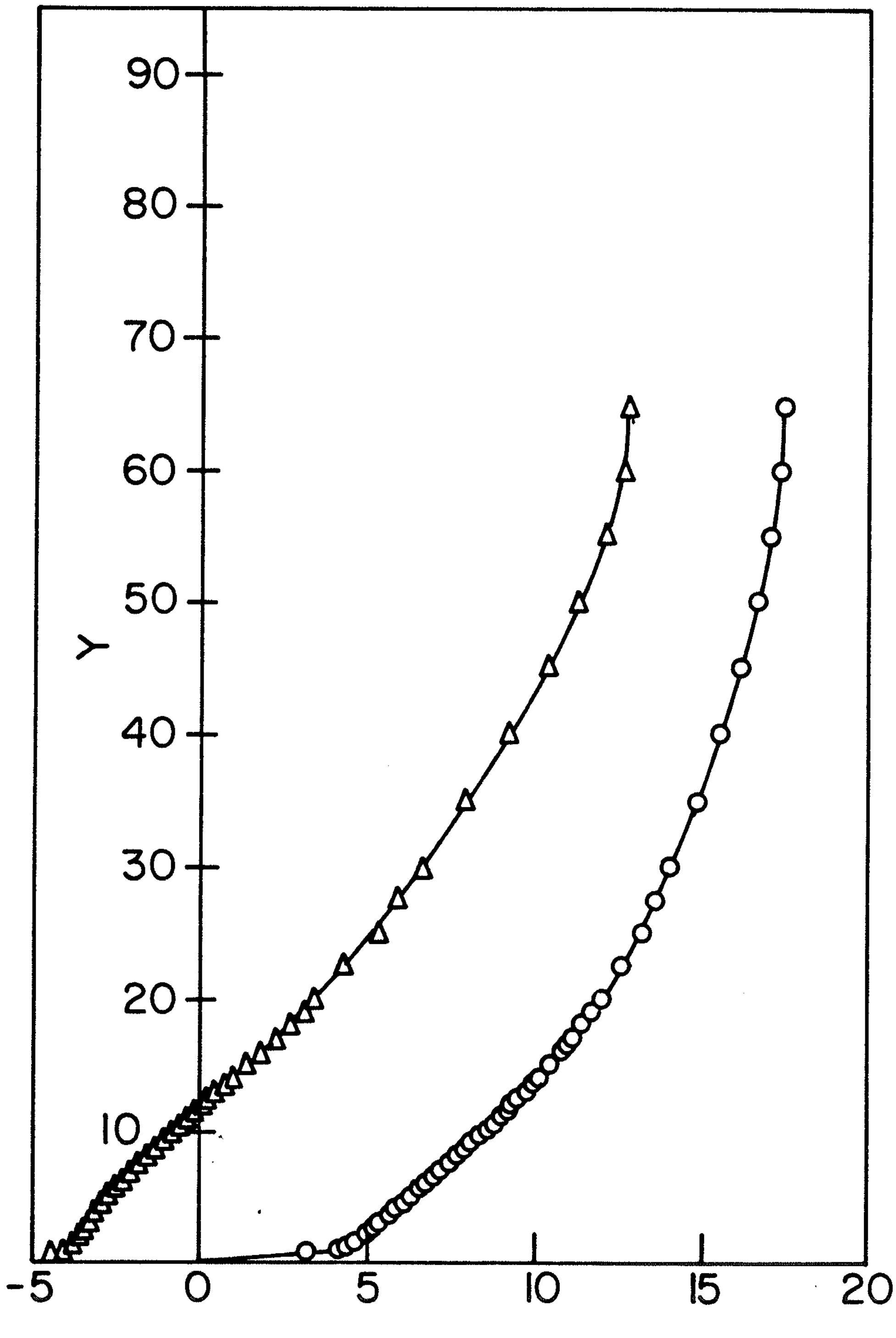

Figure 4.15: Velocity distribution at x = 21 cm

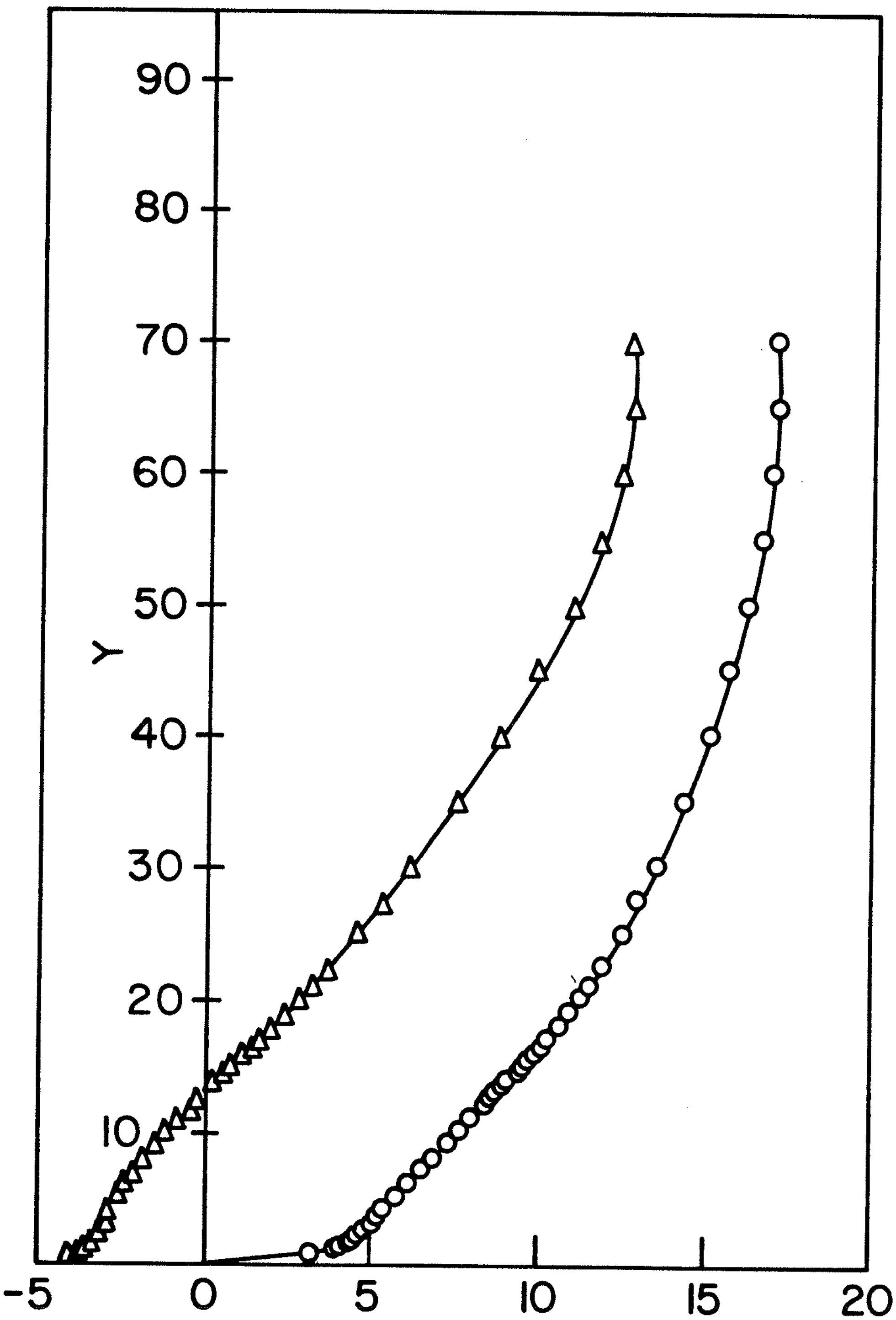

Figure 4.16: Velocity distribution at x = 24 cm

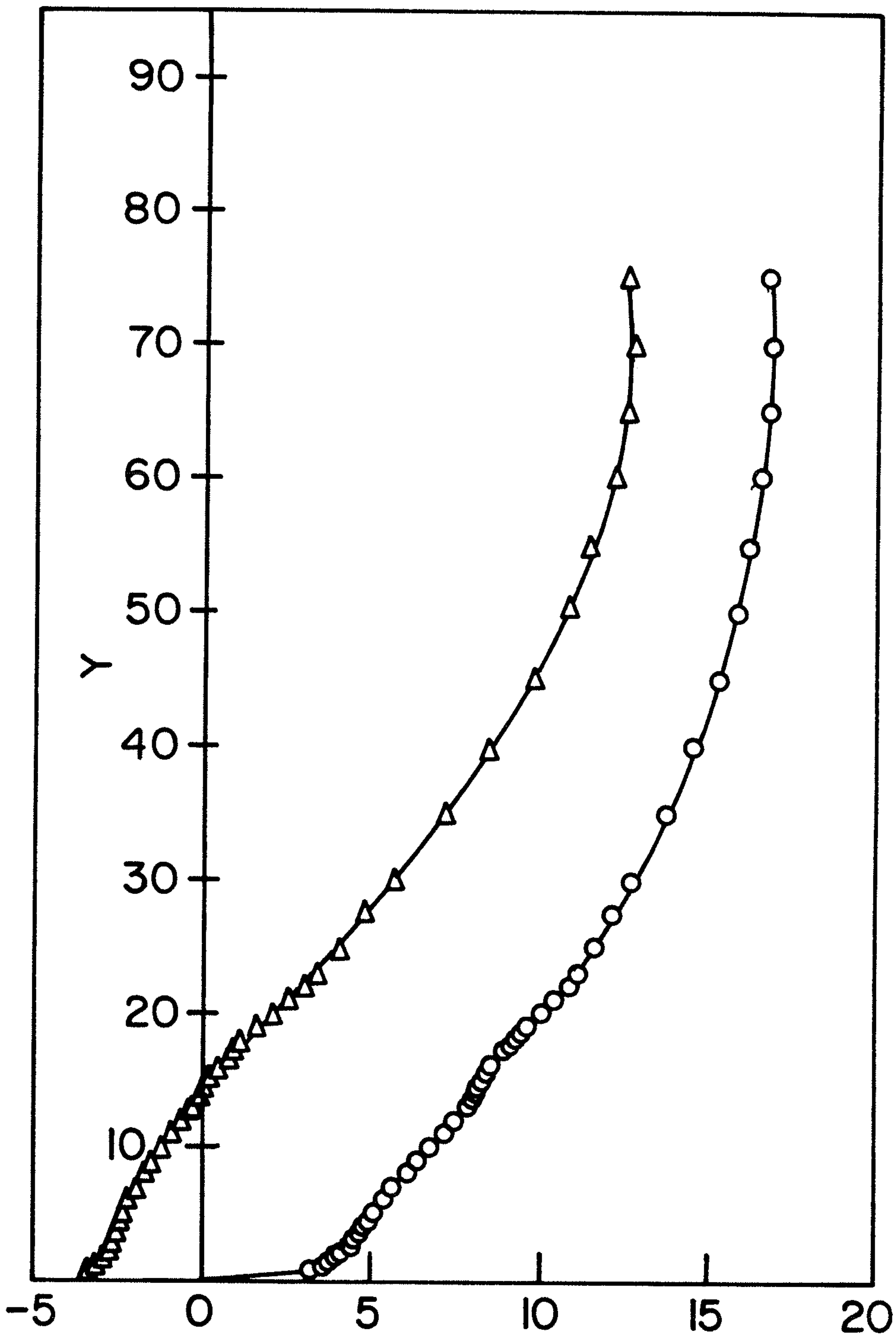

Figure 4.17: Velocity distribution at x = 27 cm

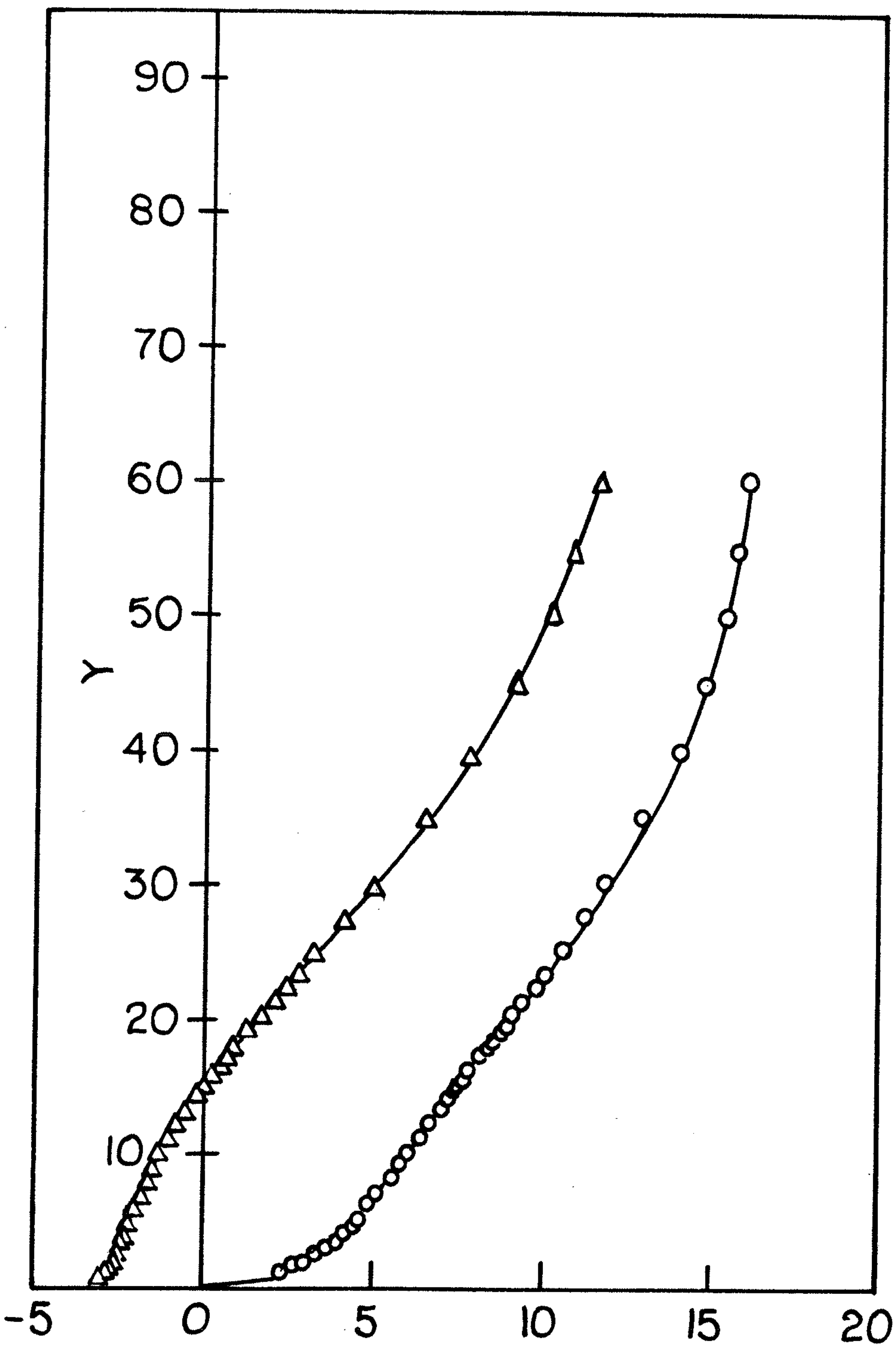

Figure 4.18: Velocity distribution at x = 30 cm

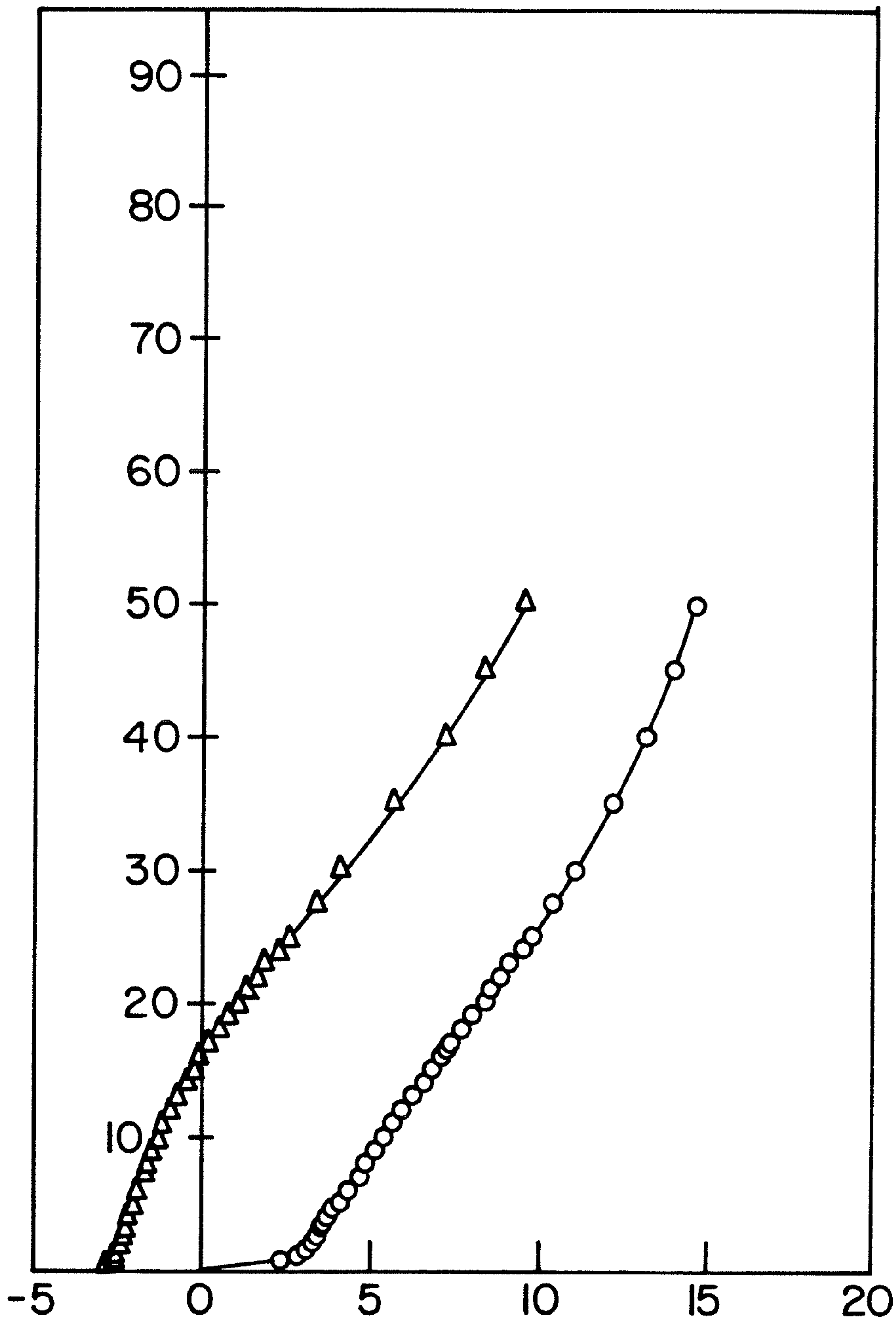

Figure 4.19: Velocity distribution at x = 33 cm

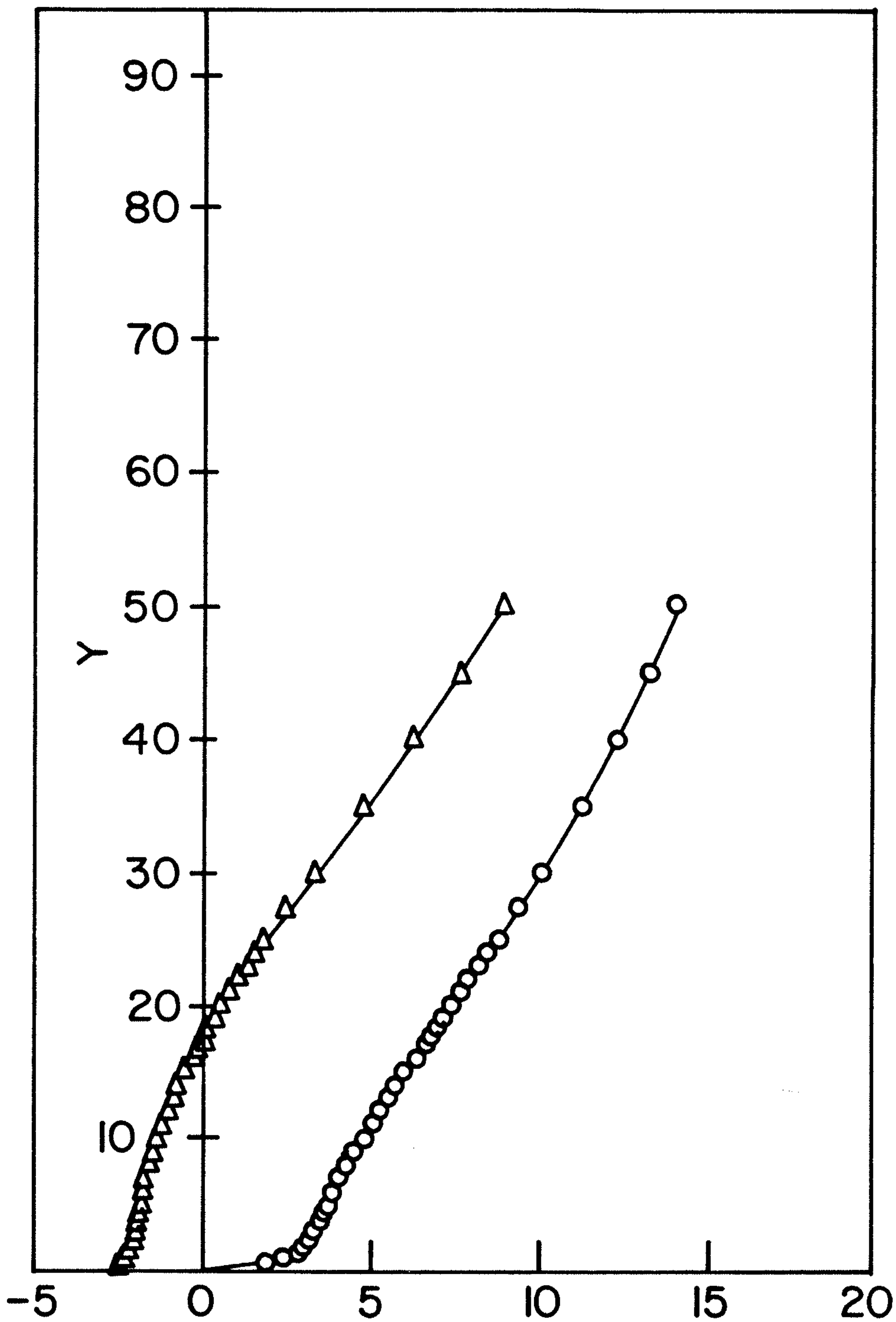

Figure 4.20: Velocity distribution at x = 36 cm

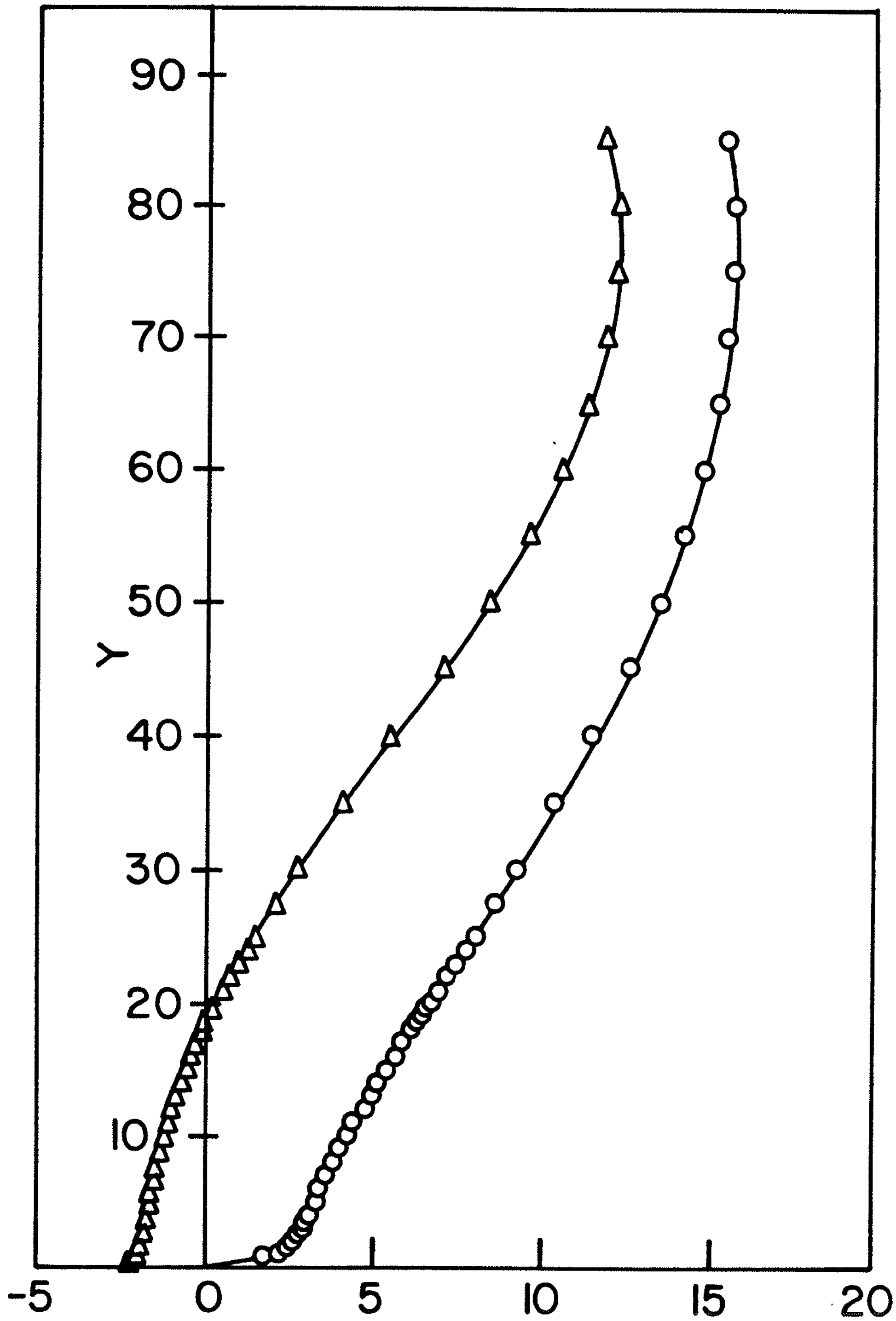

Figure 4.21: Velocity distribution at x = 39 cm

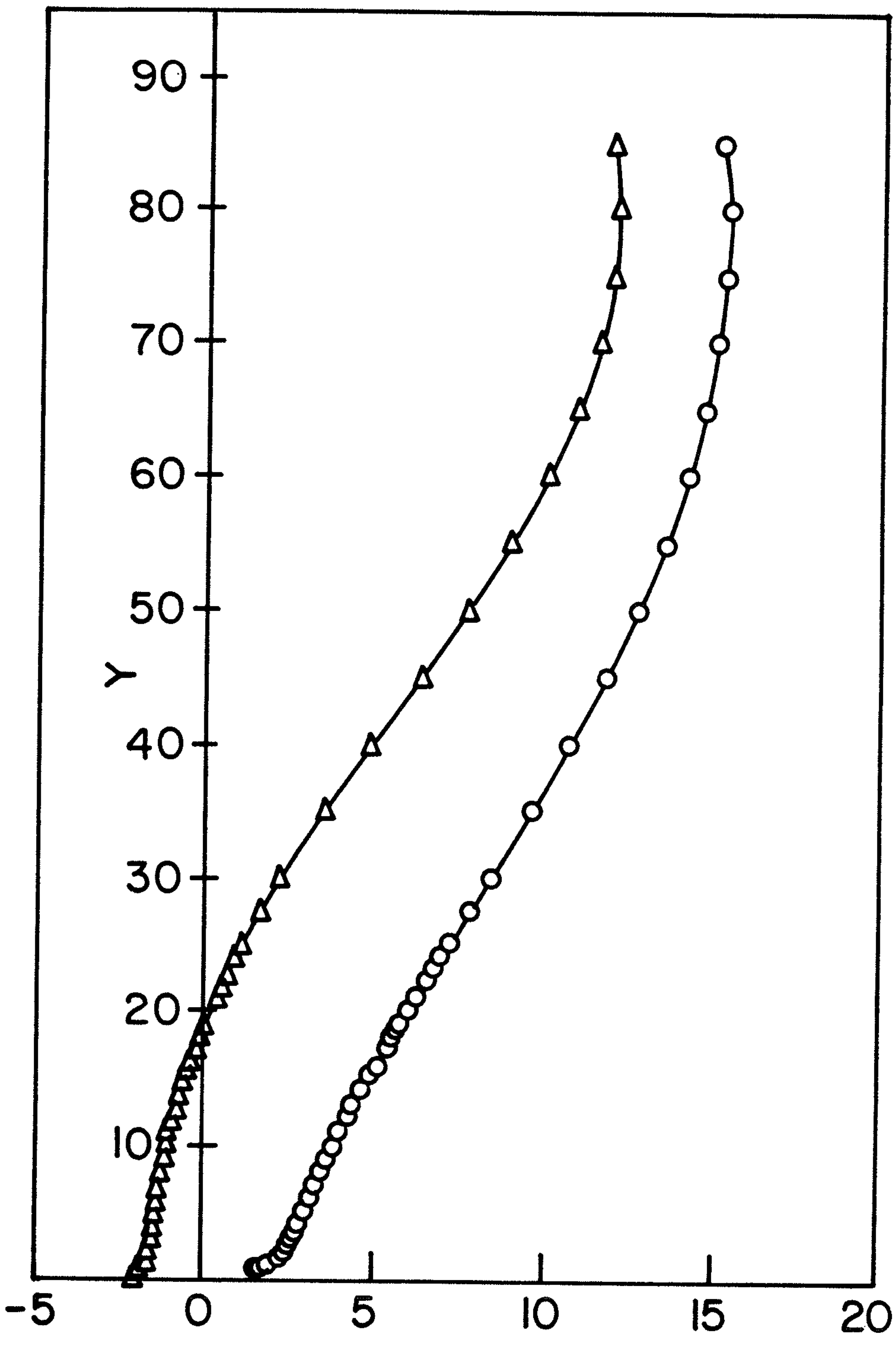

Figure 4.22: Velocity distribution at x = 42 cm

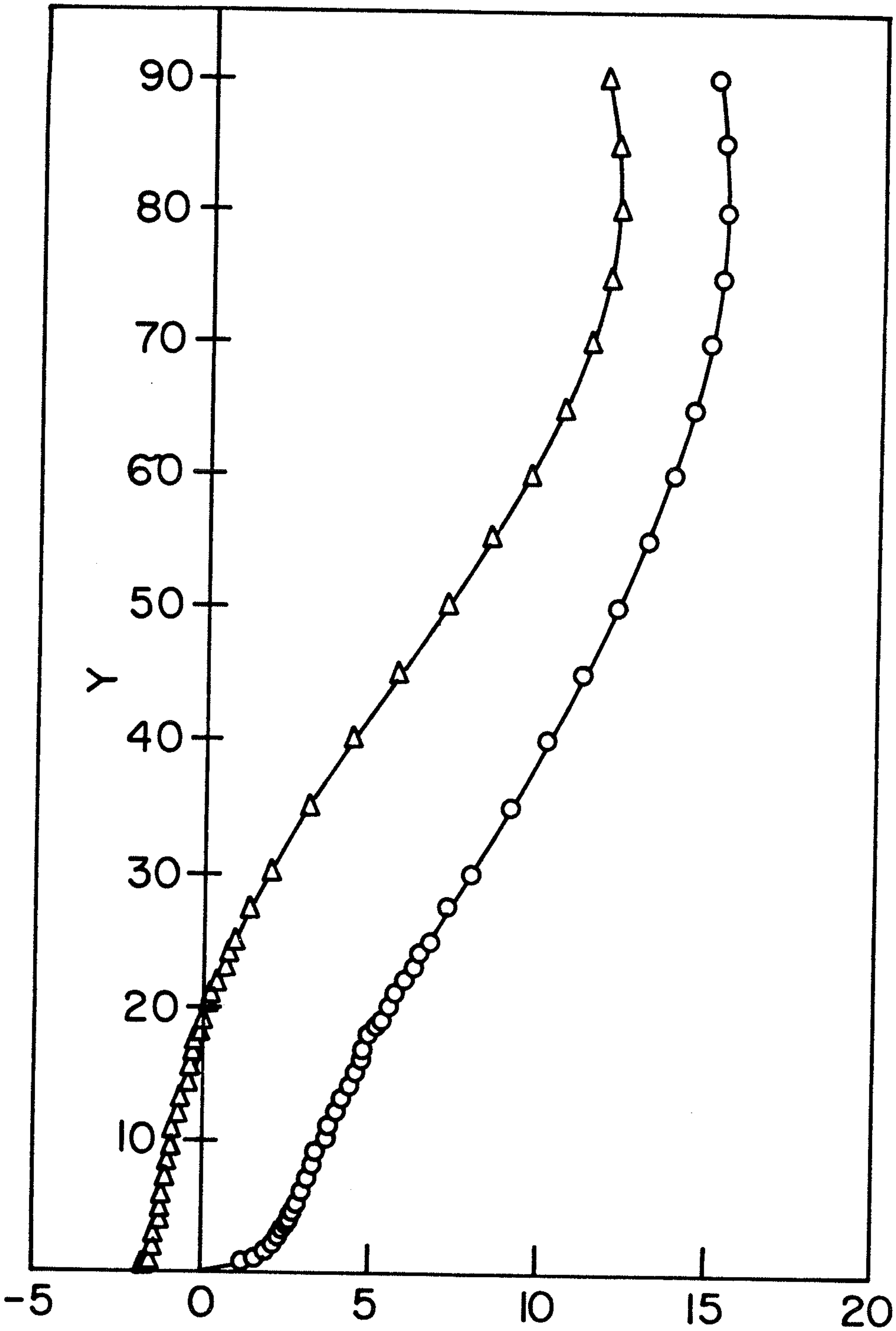

Figure 4.23: Velocity distribution at x = 45 cm

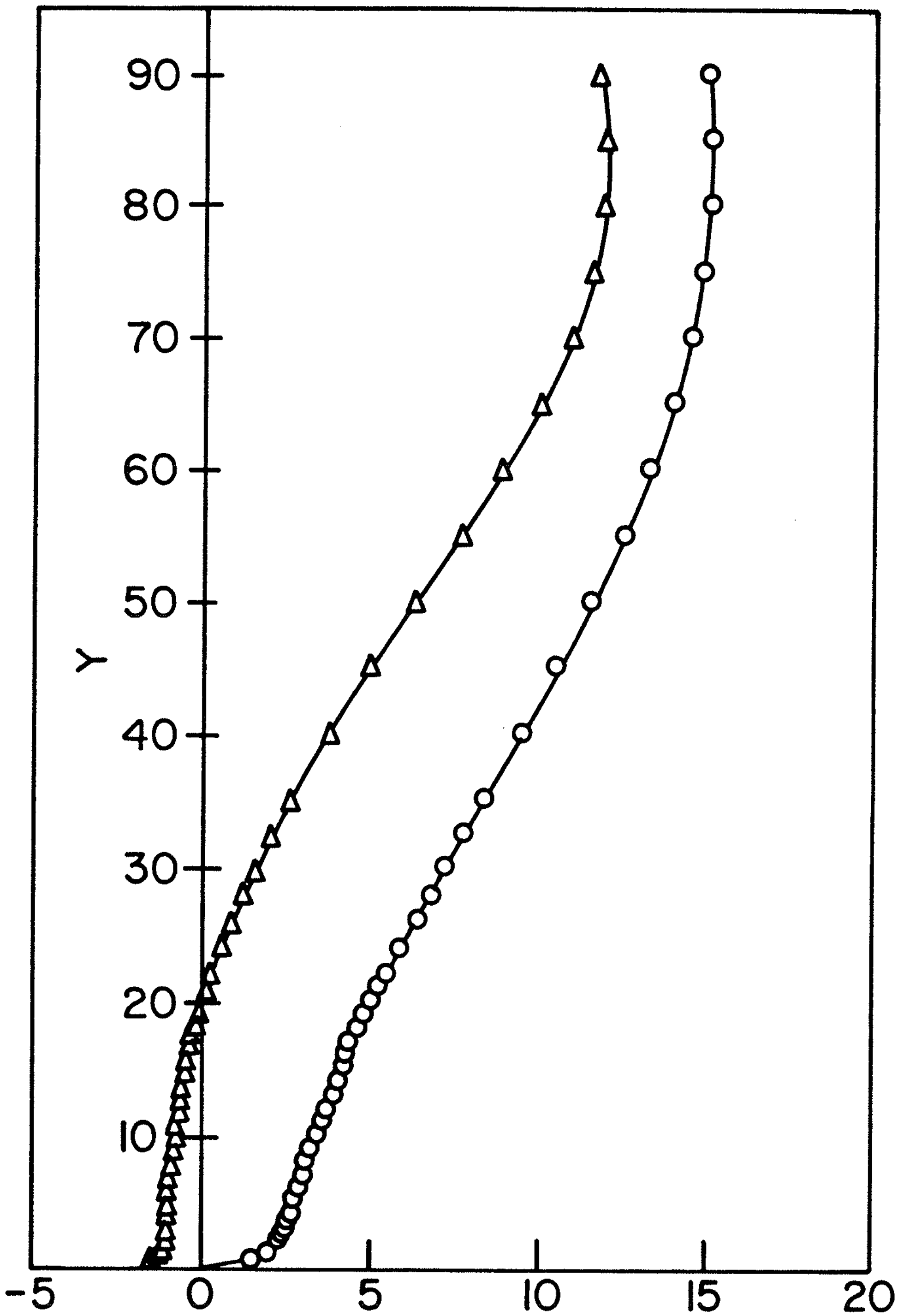

Figure 4.24: Velocity distribution at x = 48 cm

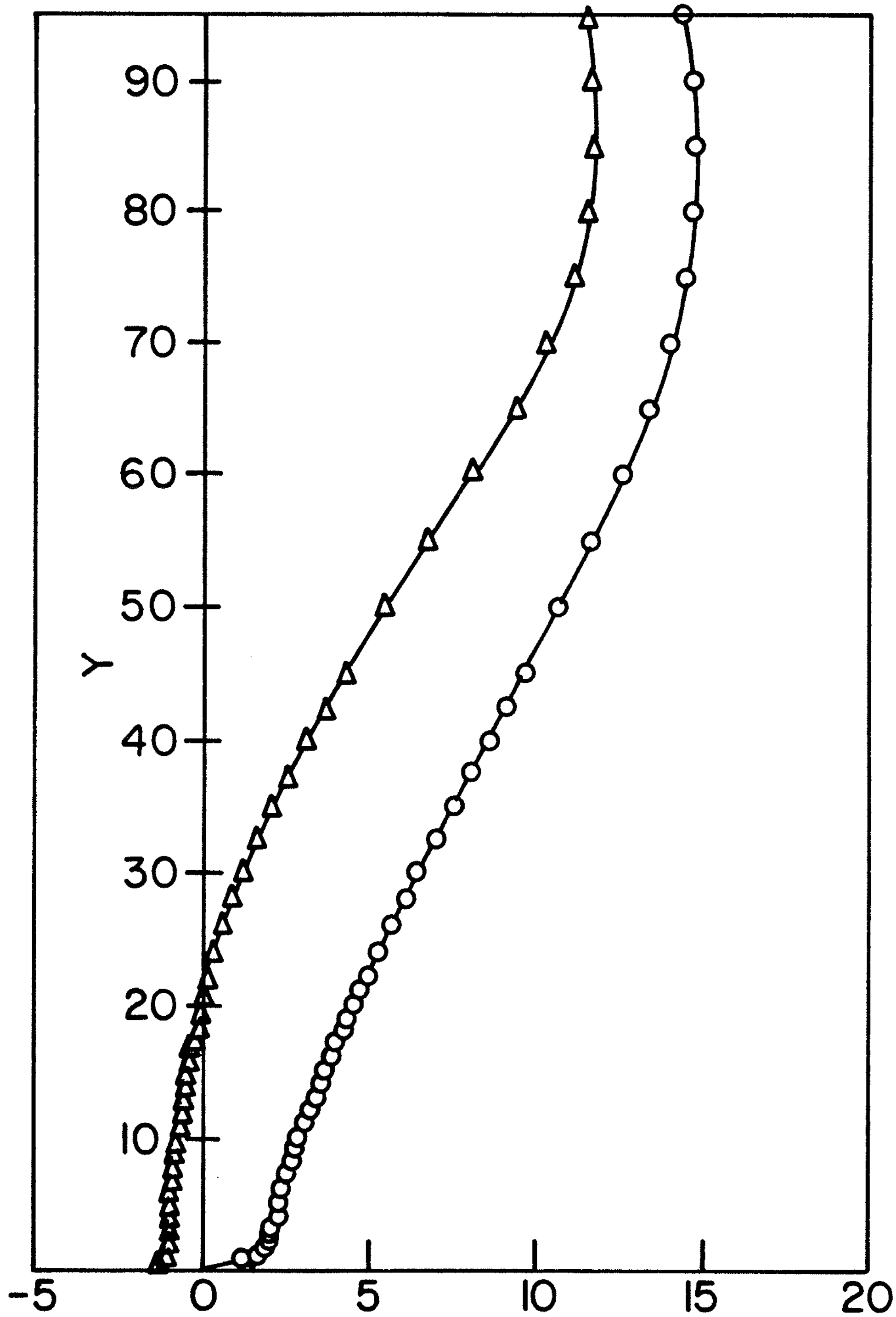

Figure 4.25: Velocity distribution at x = 51 cm

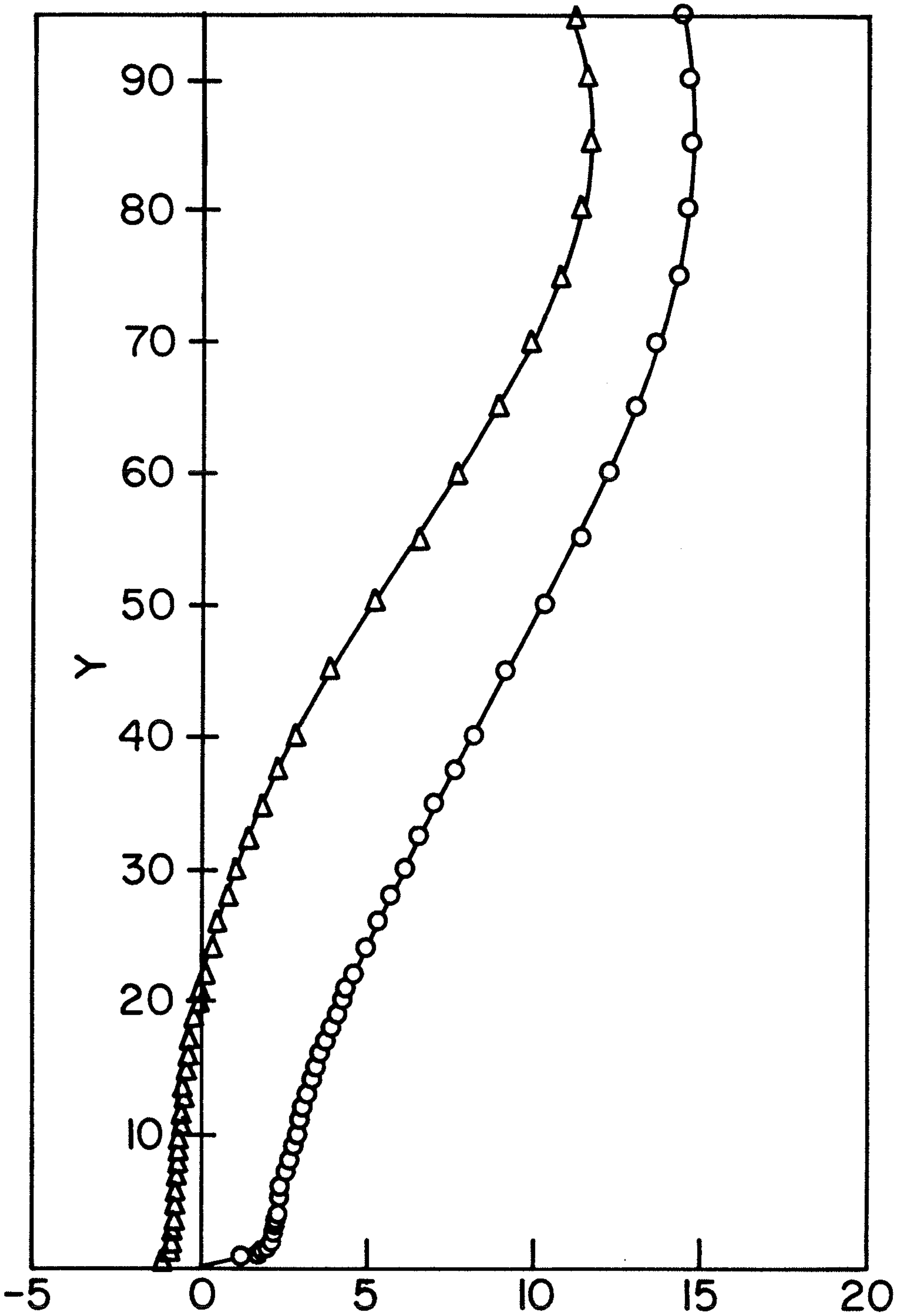

Figure 4.26: Velocity distribution at x = 54 cm

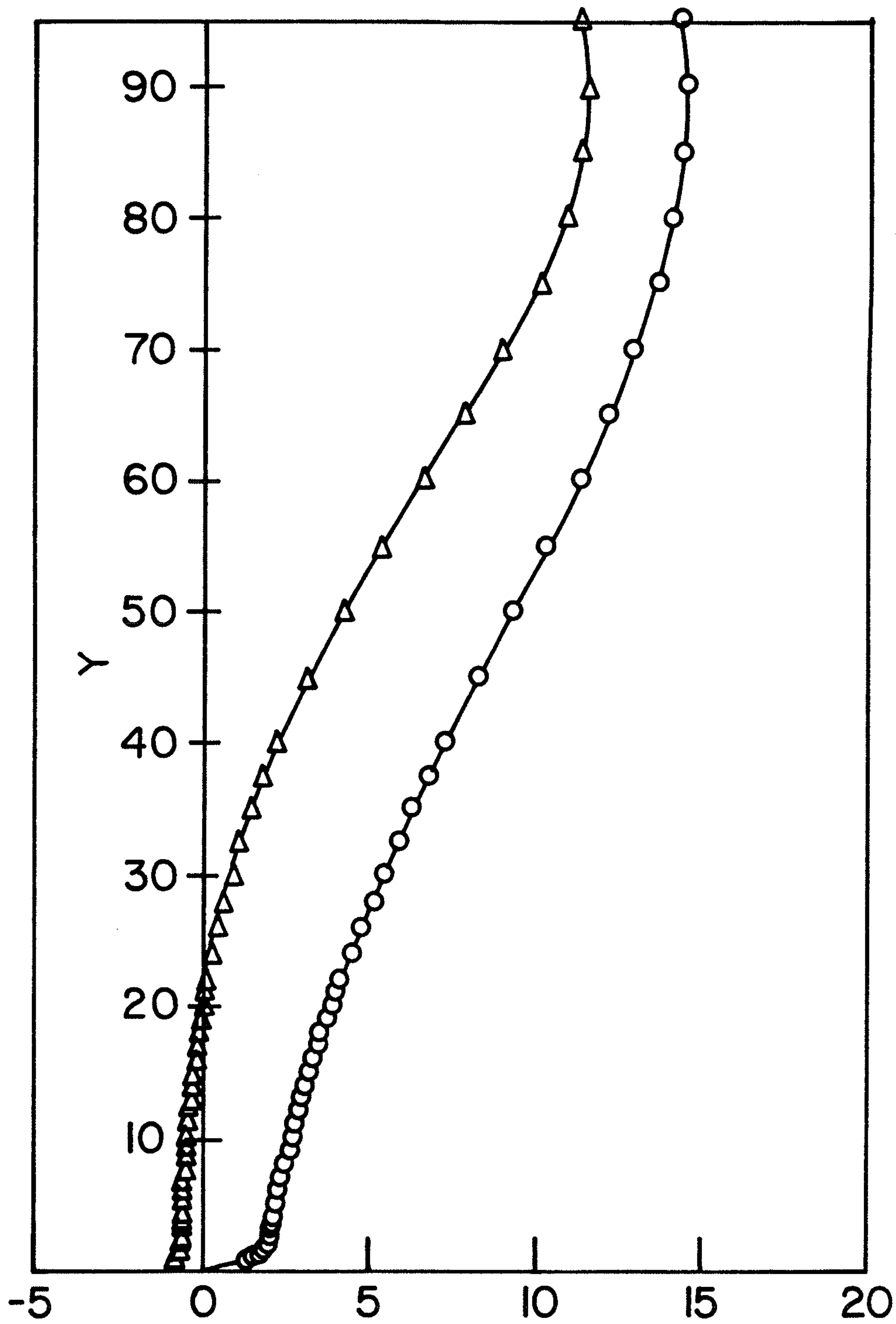

Figure 4.27: Velocity distribution at x = 57 cm

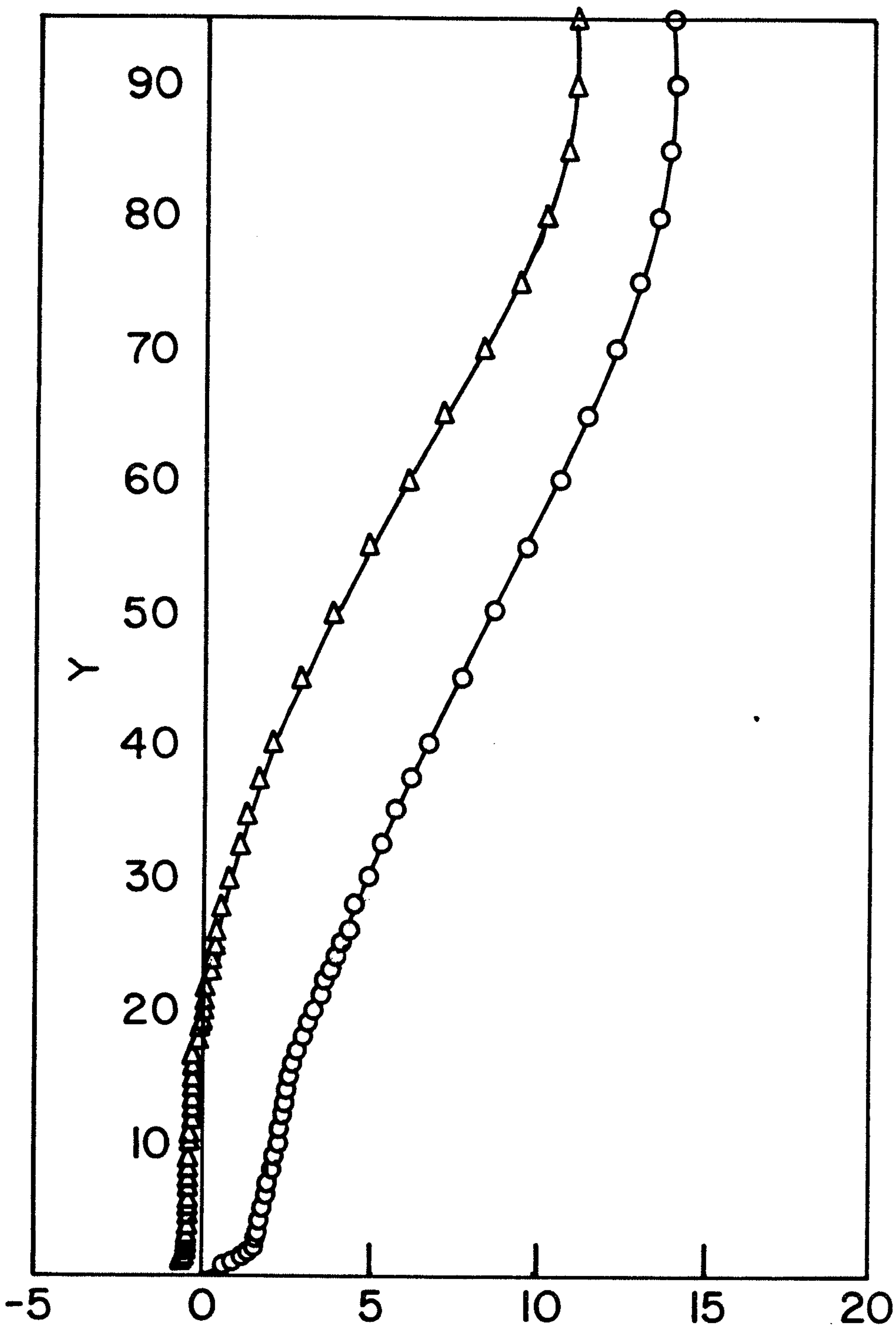

Figure 4.28: Velocity distribution at x = 60 cm

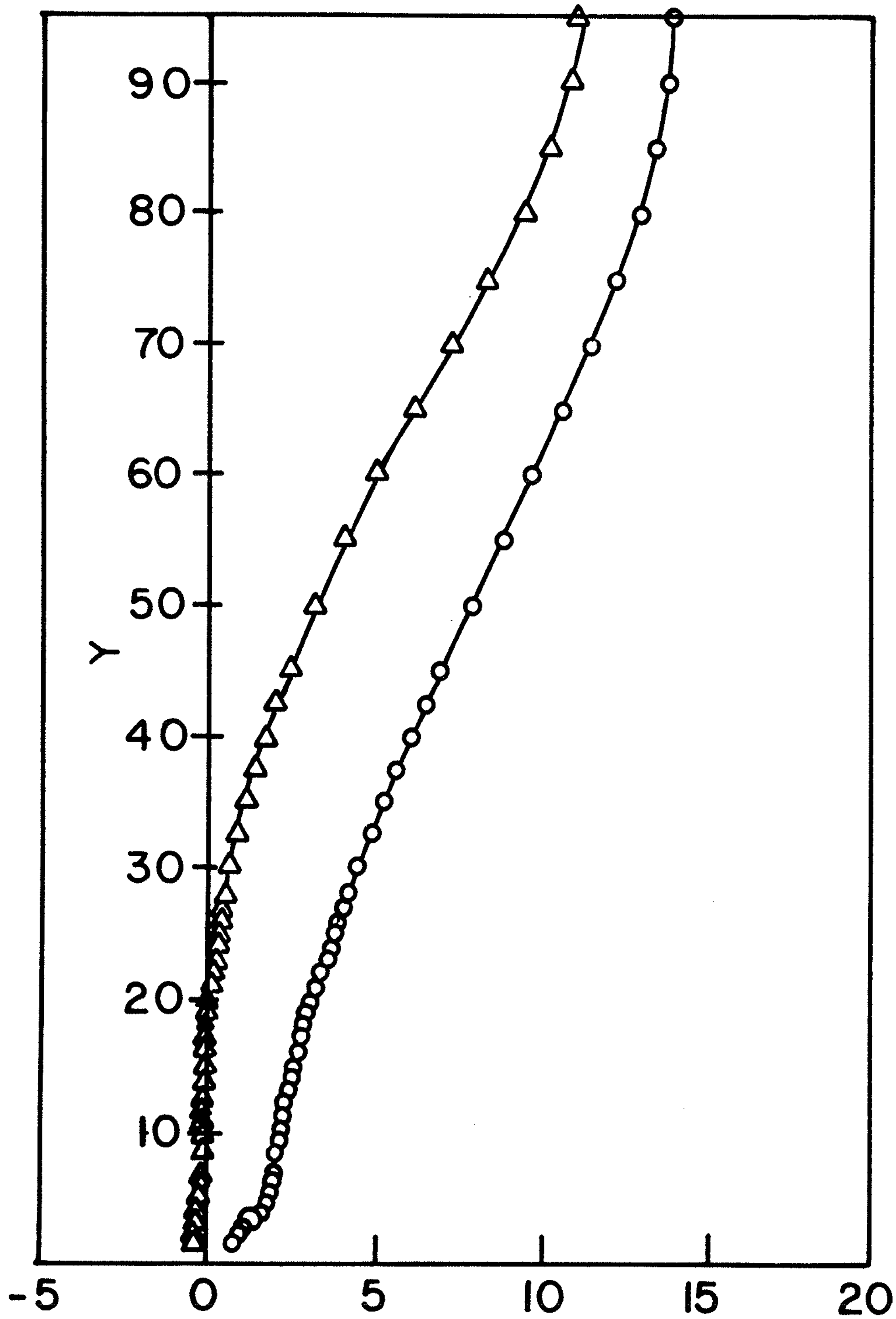

Figure 4.29: Velocity distribution at x = 63 cm

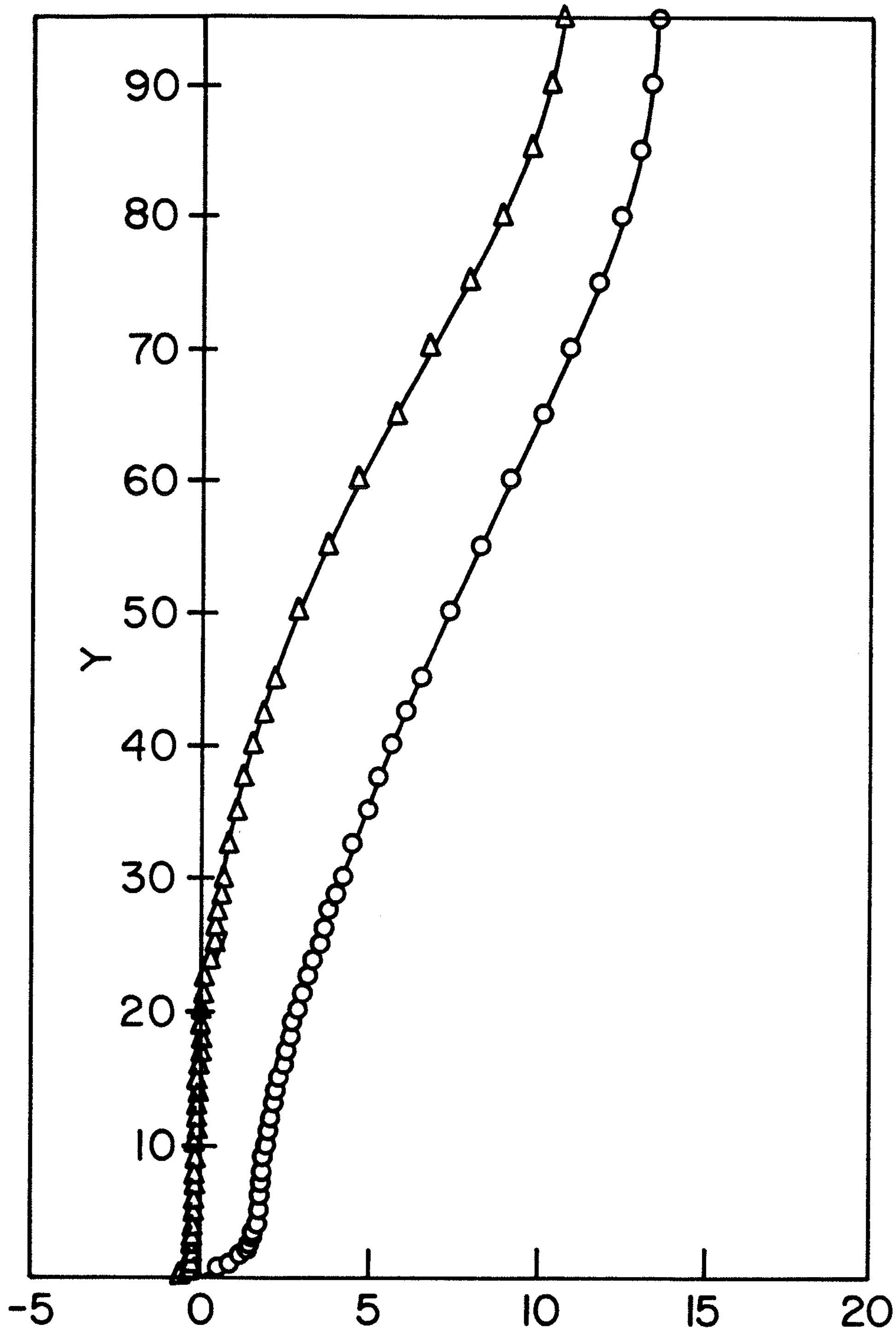

Figure 4.30: Velocity distribution at x = 66 cm

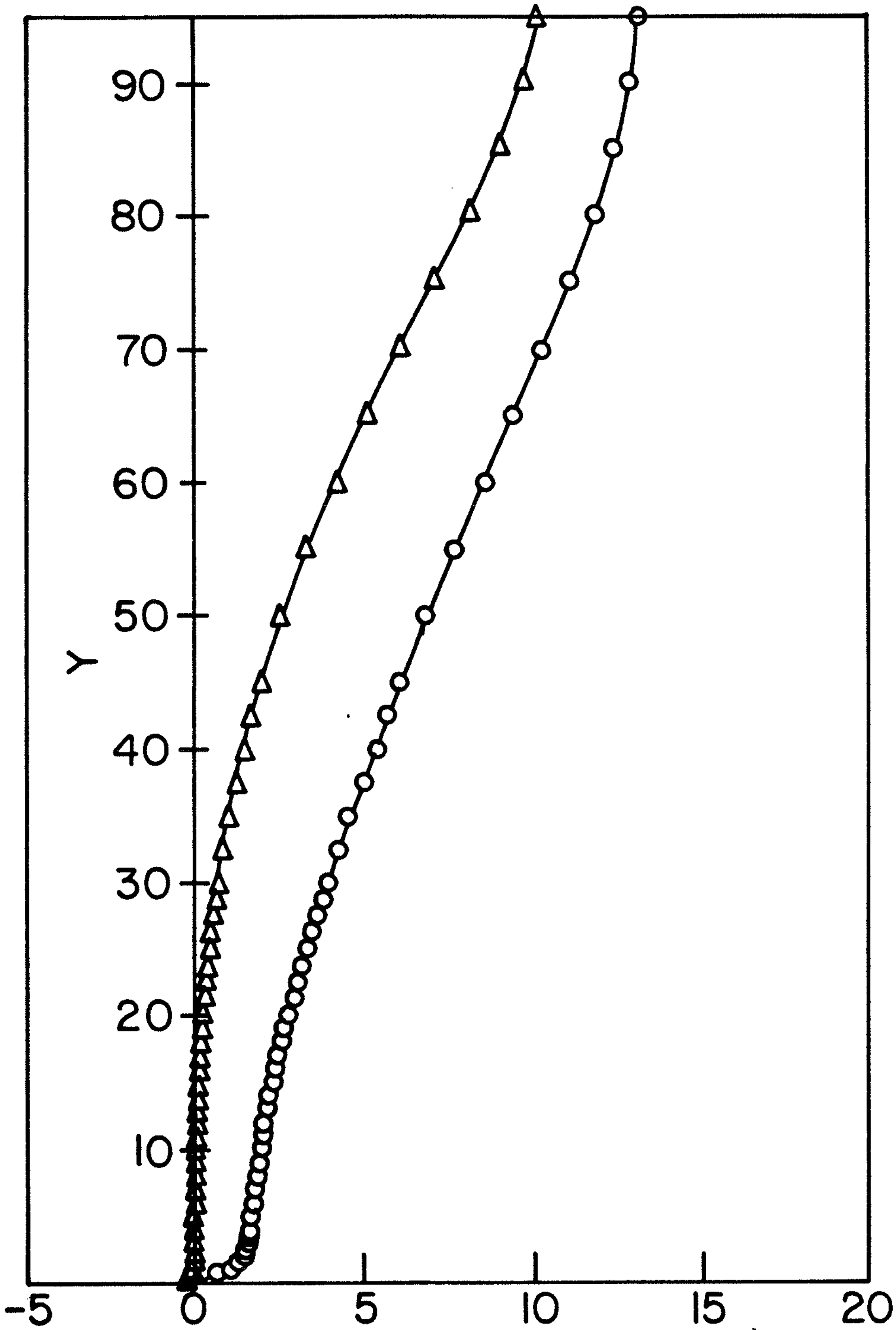

Figure 4.31: Velocity distribution at x = 69 cm

Chapter V

HOT-WIRE MEASUREMENTS - RESULTS AND DISCUSSION

The velocity distributions obtained through pressure measurements served as calibration standards for the hot-wire measurements in boundary layer and diffuser flow. The turbulence parameters from the hot-wire measurements were obtained by both analog and digital means. The results from the two methods were then compared.

The computer programs used for data acquisition and analysis employing the PDP-11 computer were developed by Derksen [1986]. Descriptions of the hardware and listings and explanations of the code used may be found in his Appendices C and D.

5.1 BOUNDARY LAYER TUNNEL

A turbulent boundary layer was grown on the inside of a pipe wall. There is a small positive velocity gradient in this flow and hence a slightly favourable pressure gradient. Analog and digital results obtained from measurements taken by boundary layer hot wire probes placed normal to the flow are compared. In the digital measurements, 200 data buffers were filled at a rate of $3x10^3$ samples/second.

5.1.1 Mean Velocity Field

Analog procedures were used to obtain a mean velocity distribution across the horizontal radius, 15 cm from the pipe exit. Figure 5.1 shows the velocity profile taken for a free stream velocity of 8 m/sec. The boundary layer thickness, defined as the point in the flow where the mean velocity becomes 0.99 of the free stream velocity, is nearly 4.5 cm.

The mean velocity data were used in a cross plot method to obtain the friction velocity, u*. The friction velocity obtained through the cross plot method is based on the log law:

$$U_+ = A \ln Y_+ + B \ , \qquad 30 < Y_+ < 300$$

where A = 2.44 is the reciprocal of the Karman constant $k = 0.41$, $Y_+ = y\, u^*/\nu$ and $u^* = u(\text{internal})/U_+$, and B is a constant dependant on the wall roughness. Here for a smooth wall, B = 5.0.

The internal velocity of the flow can be found from the point of intersection between the velocity profile obtained from the experimental data and the relation $uy = U_+ Y_+ \nu = c\nu$ where c is a constant determined from Y_+ in the range $30 < Y_+ < 300$ and the corresponding U_+ from the log law. Based on the cross plot method, the friction velocity was found to be 0.32 m/sec for a free stream velocity of 8 m/sec and 0.18 m/sec for a free stream velocity of 4 m/sec.

Figure 5.2 shows a plot of U_+ versus Y_+ using the values of the friction velocities estimated from the cross plot method. The logarithmic profile may be broken into four regions: the viscous sublayer, the buffer layer, the logarithmic layer, and the outer layer or wake region. Before data could be gathered in the region of the viscous sublayer ($Y_+ < 6$), the free stream velocity was reduced from the original 8 m/sec to 4 m/sec. The viscous sublayer may be described by the linear relation $U_+ = Y_+$ in the range $Y_+ < 6$ and the logarithmic layer may be described by the relation $U_+ = A \ln Y_+ + B$ in the range $30 < Y_+ < 300$. The buffer layer is found in the range $6 < Y_+ < 30$ and the wake region, which is highly dependent on Reynolds number, in the range $y/\delta = 0.2$ (here, $Y_+ > 300$) to $y/\delta = 1$ where δ is the boundary layer thickness. An empirical equation based on the logarithmic equation plus a function of the boundary layer thickness was proposed by Coles [1956] in order to describe the wake or outer region:

$$U_+ = A \ln Y_+ + B + (\Pi/k)\, W(y/\delta)$$

where Π is a pressure gradient parameter, $k = 0.41$ is the Karman constant, and $W(y/\delta)$ is the wake function.

The longitudinal turbulence intensity u'/U for a free stream velocity of 8 m/sec is shown in Figure 5.3. The first point on the plot is in the neighbourhood of $Y_+ = 15$ where the rms fluctuating velocity, u', is at a maximum.

The local mean velocity, U, gradually increases to reach the free stream velocity while the rms fluctuating velocity, u', asymptotically approaches zero.

5.1.2 Third and Fourth Order Moments

Values of the third and fourth order moments obtained by analog and digital means are shown in Figures 5.4, 5.5, and 5.6. Analog values were obtained from Derksen [1981] and Kassab [198_]. Digital values were obtained from a linearized hot wire signal fed into and processed by the PDP-11 computer.

The probability distribution of the mean longitudinal velocity, U , falls into three groups: positively skewed, negatively skewed, and symmetric about the mean velocity. Figure 5.4 shows the distribution of skewness values in the first 1 $^{1}/_{2}$ mm from the tunnel wall for a free stream velocity of 4 m/sec to be positively skewed in the viscous sublayer. Figure 5.5 shows the skewness distribution in the boundary layer tunnel for a free stream velocity of 8 m/sec in the logarithmic and wake regions of the flow to be predominately negatively skewed. Basically, the probability distribution of the mean velocity, U , for values of $Y_+ < 15$ is positively skewed, Y_+ in the neighbourhood of 15 is symmetric about the mean velocity, and $Y_+ > 15$ is negatively skewed. The minimum skewness value occurs at approximately 45 mm, the boundary layer thickness.

A trace of the flatness factor or kurtosis for a free stream velocity of 8 m/sec is shown in Figure 5.6. The flatness factor has a nearly constant value of 2.8, just below the Gaussian value of 3, for the first 20 mm from the tunnel wall or $y/\delta < 0.4$ where δ is the boundary layer thickness. The increase in value of the flatness factor occurs in the wake region of the flow and approaches a maximum at the boundary layer thickness before decreasing in magnitude.

When examining the flatness factor in the range $y/\delta < 0.4$, the boundary layer flow can be said to simultaneously display both organized and random features. This is possible as the value of the flatness factor in the first 20 mm from the tunnel wall, $K(u) = 2.8$, falls between the Gaussian value of three for a completely random phenomenon and the sine wave value of 1.5 for a well organized structure.

A comparison of the plotted analog and digital results shows good agreement between both methods of data analysis. Discrepancies in proximity to the wall may be attributed to effects of imperfect spatial resolution of the hot wire and small fluctuations in the Reynolds number. Discrepancies further from the wall may be attributed to the intermittent nature of the flow. In addition, in both analog and digital techniques, the input signal may have been under amplified resulting in poor resolution of the signal or the input signal may have been over amplified, saturating the electrical instrumentation, and resulting in a clipped signal. Both under amplification and over amplification of the turbulent signal result in inaccurate values of the processed signal.

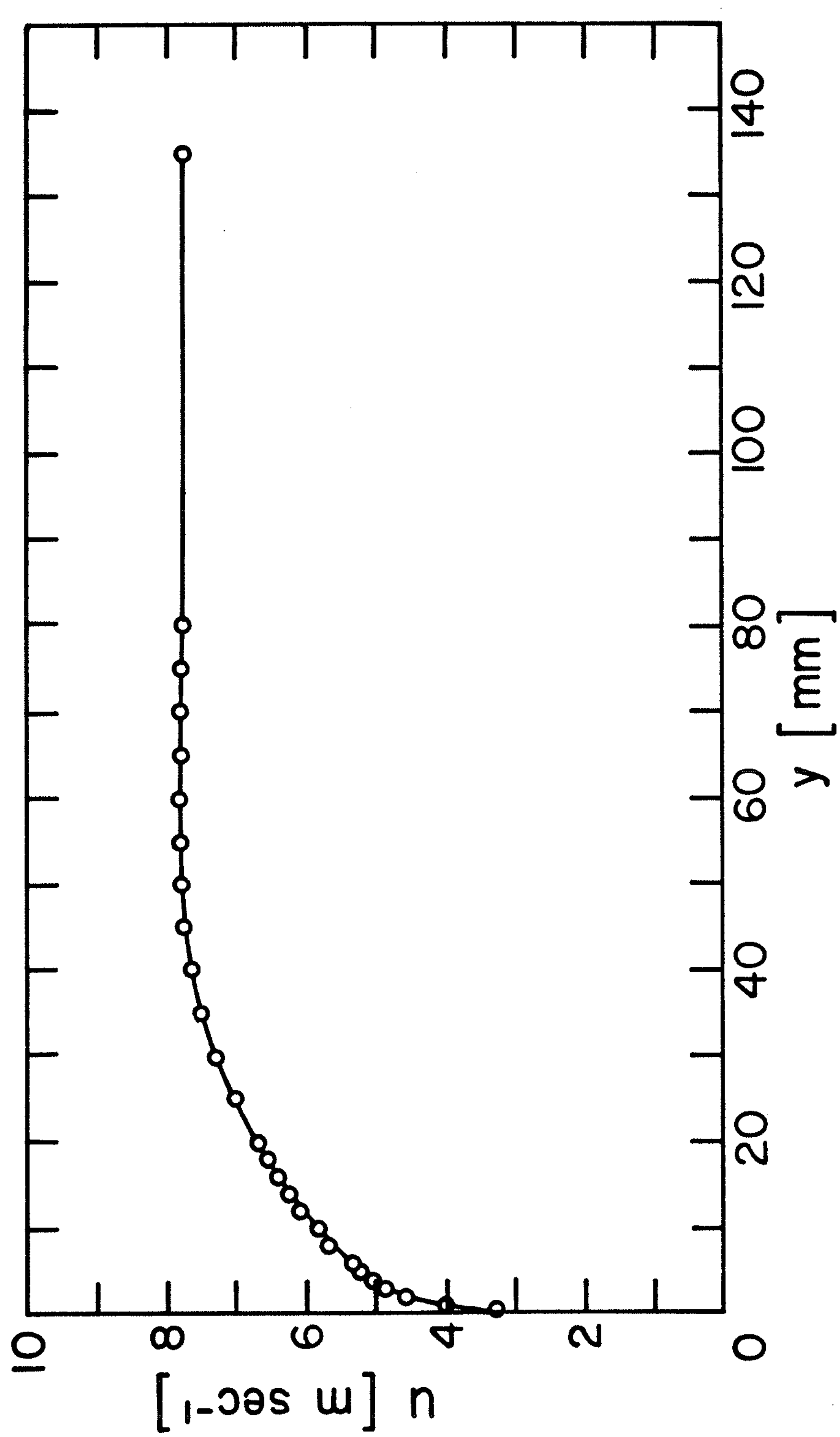

Figure 5.1: Velocity profile for $U_\infty = 8$ m/sec

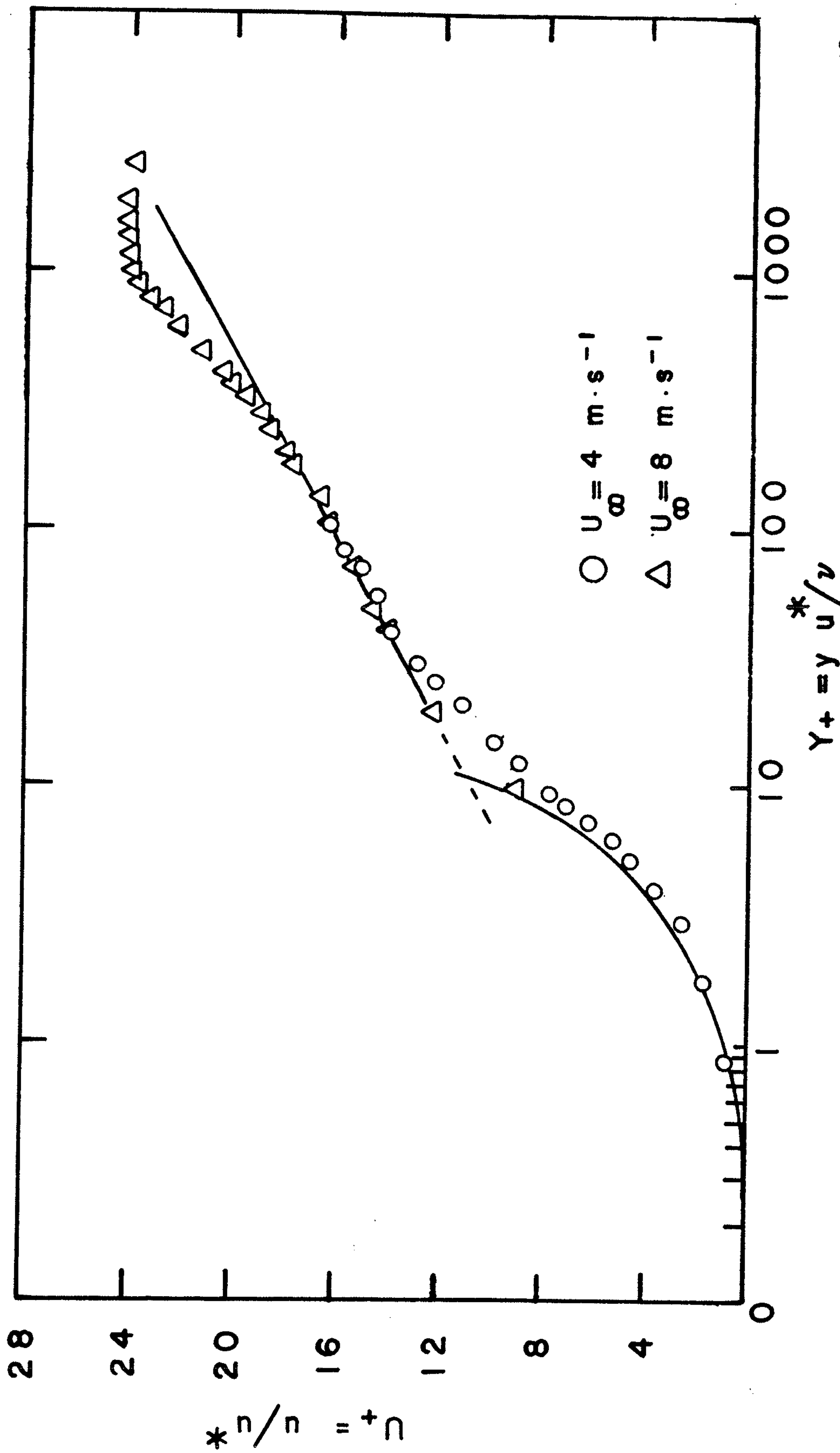

Figure 5.2: U+ versus Y+ for U_{∞} = 8 m/sec

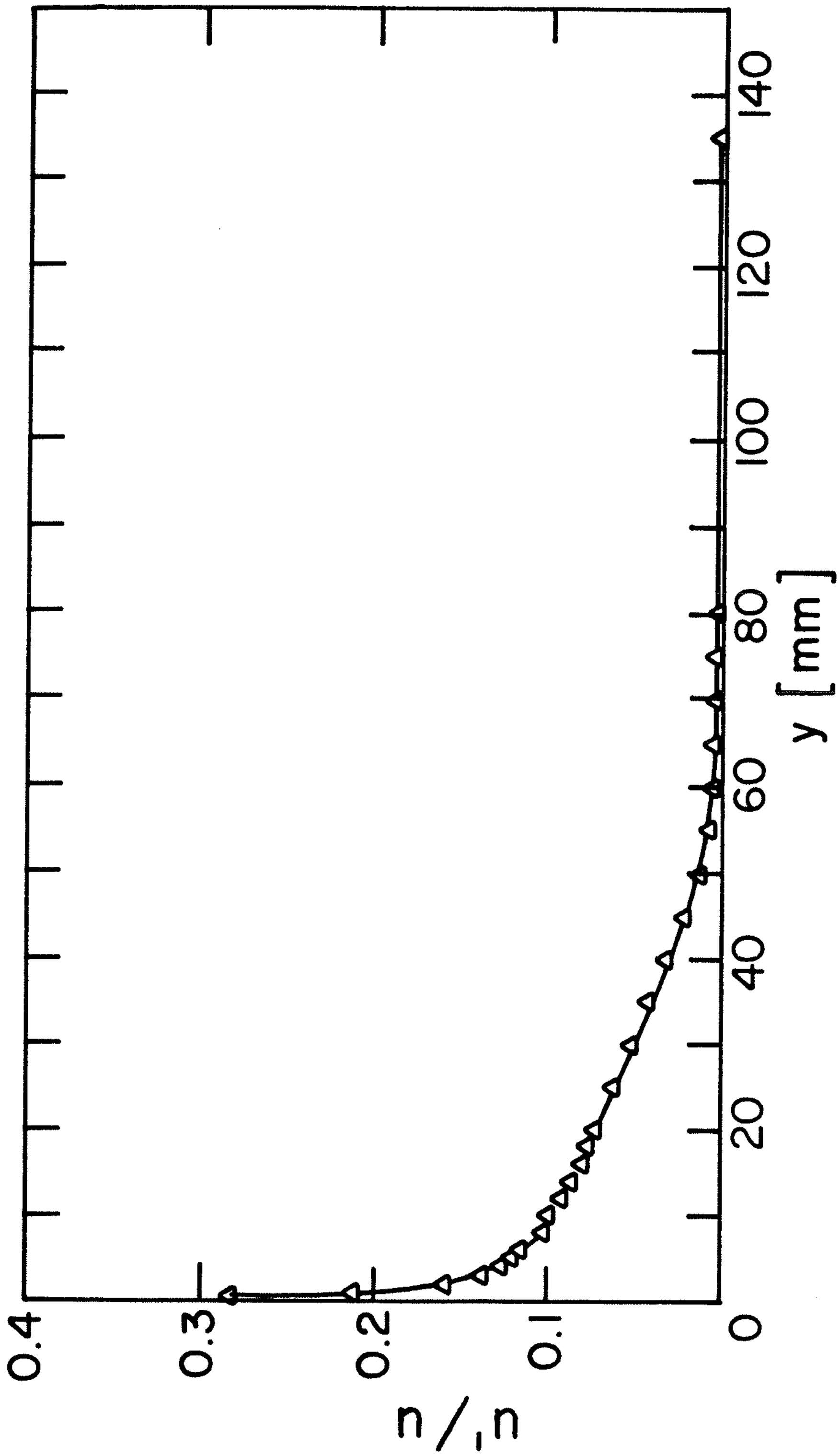

Figure 5.3: Distribution of turbulence intensity, u'/U

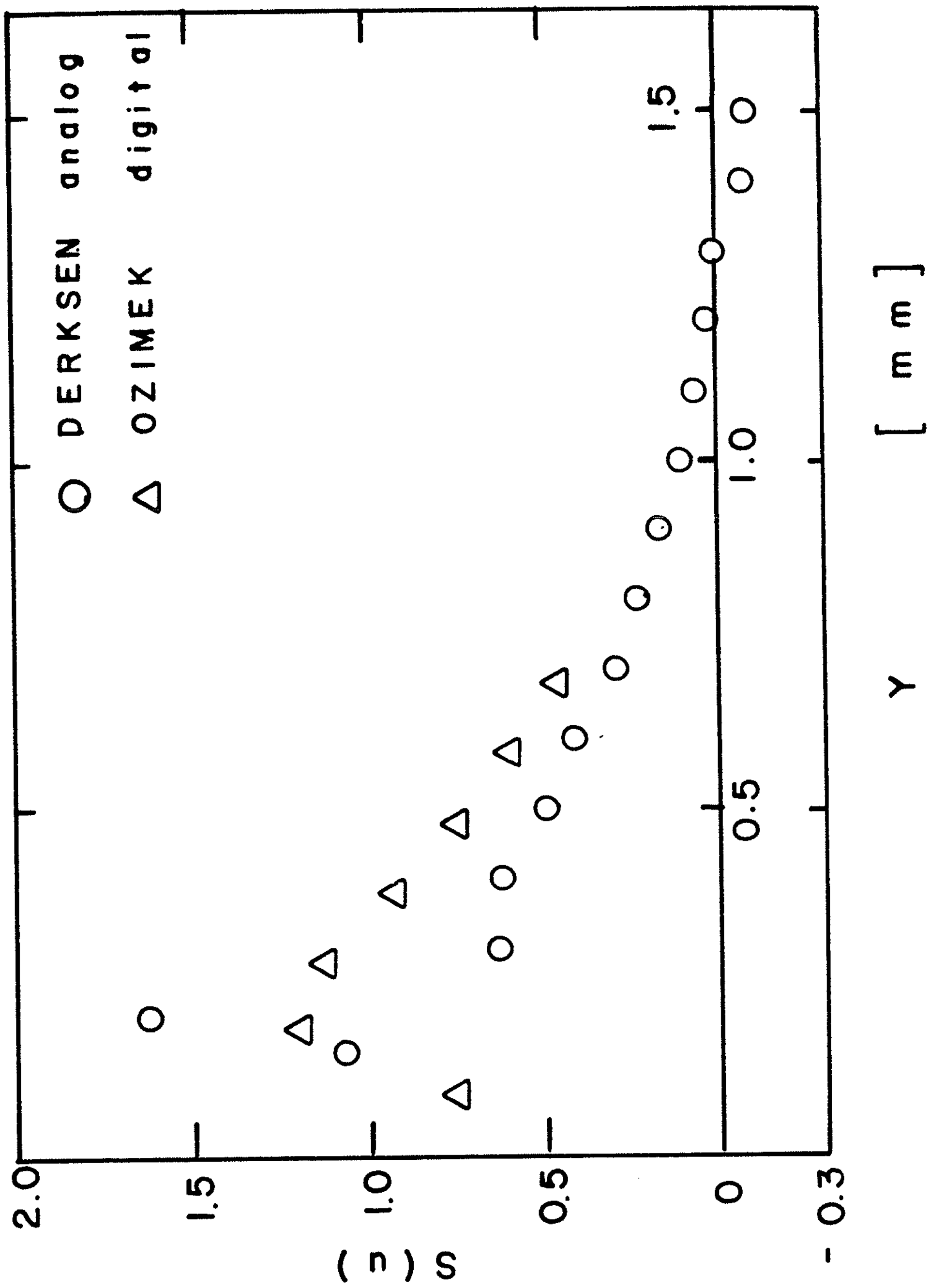

Figure 5.4: Skewness distribution in sublayer, U_∞ = 4 m/sec

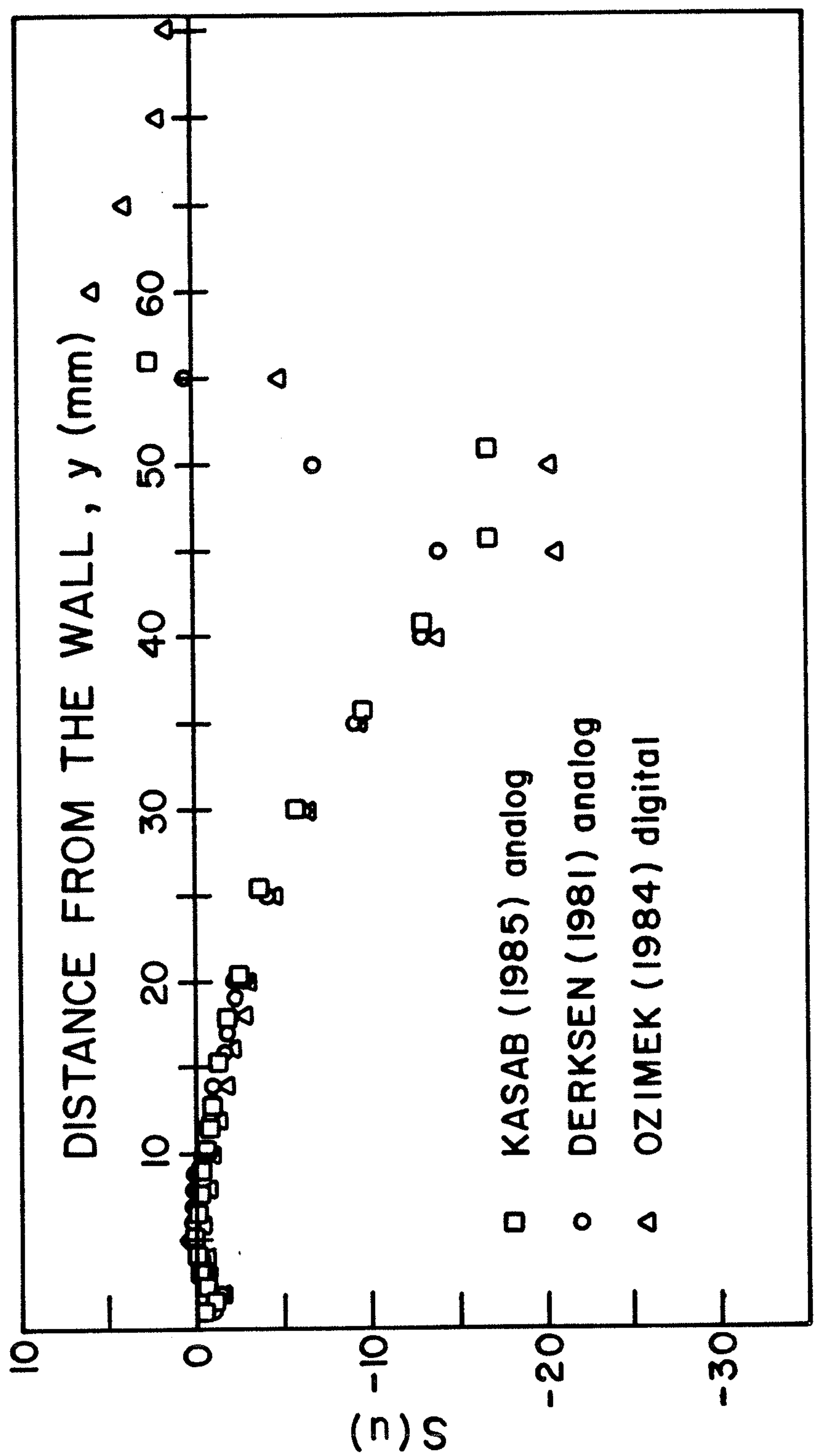

Figure 5.5: Skewness distribution for U_{∞} = 8 m/sec

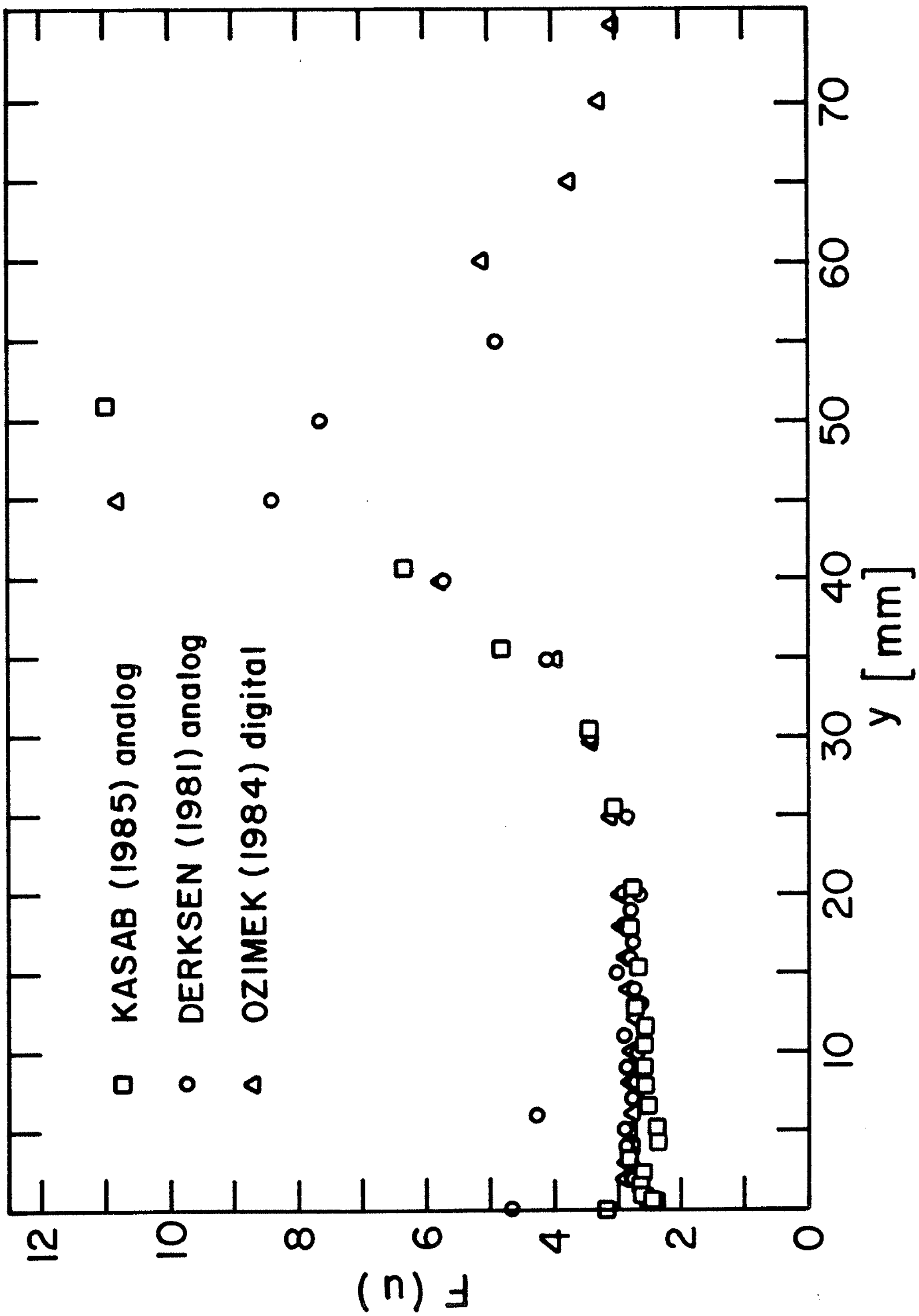

Figure 5.6: Kurtosis for $U_{\infty} = 8$ m/sec

5.1.3 Probability Density Measurements

The probability densities of the axial velocity in the boundary layer tunnel were measured using a boundary layer probe placed in the air flow and the PDP-11 computer. Probability distributions and density functions were computed with FORTRAN subroutines described in Derksen [1986]. After the data was collected and processed by the computer, the probability density results were plotted by the Hewlett·Packard plotter.

The probability distributions and density functions of u are shown in Figures 5.7 to 5.15 inclusive. The positively skewed PDF, Figure 5.7, was obtained in the viscous sublayer for a flow of 4 m/sec free stream velocity. It was possible to obtain this PDF due to a thicker sublayer at lower velocities. The remaining results show that for a free stream velocity of 8 m/sec, the probability densities are negatively skewed towards the centerline as was the case with the previous analog and digital skewness measurements. The skewness of the PDF curves is displayed most prominently in the semilog plots of the PDF's. The probability density functions are bounded to within -4 standard deviations to 5 standard deviations. The peak value of the PDF's are approximately 0.4, similar to that of the Gaussian distribution.

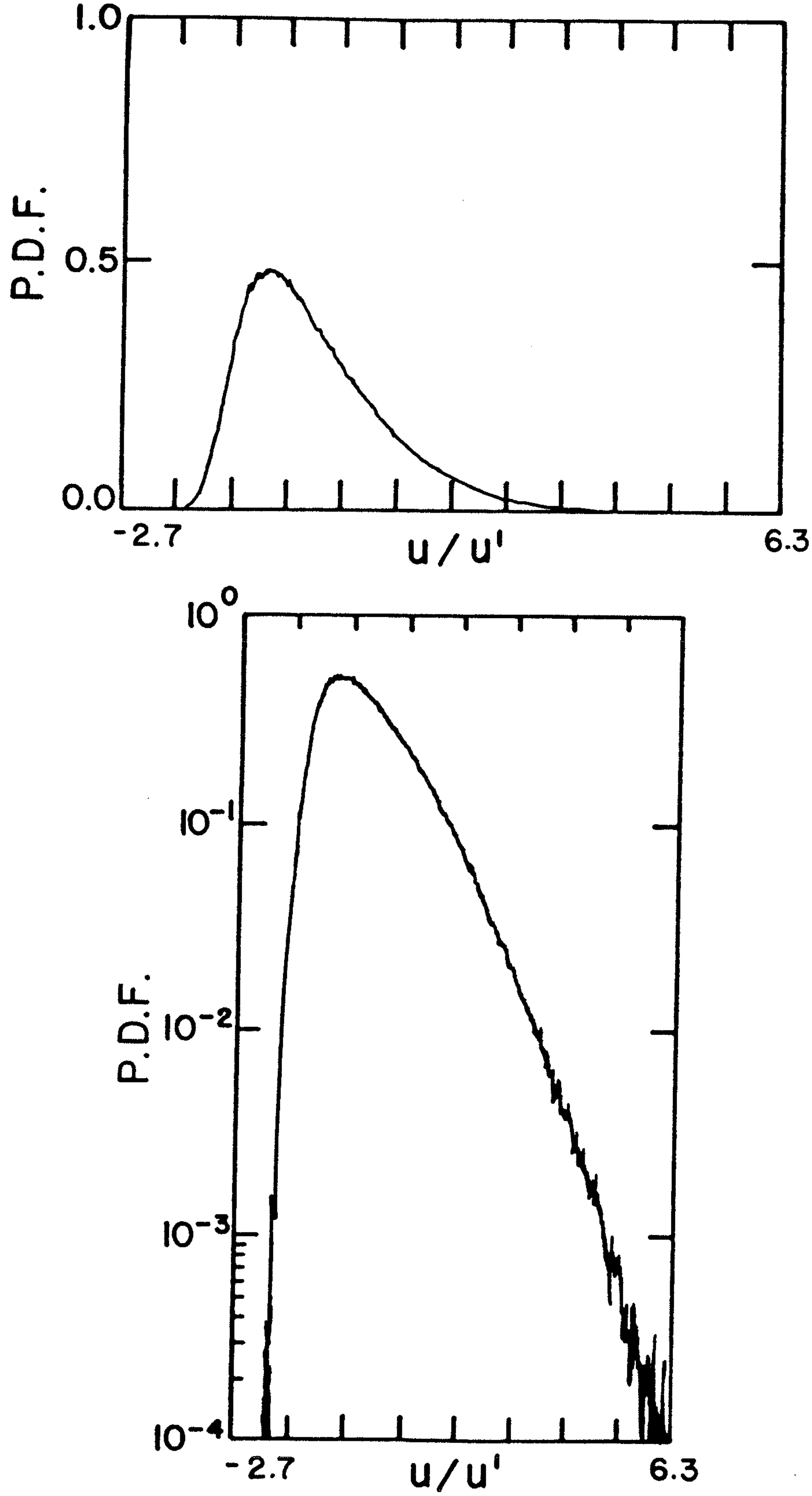

Figure 5.7: PDF(u/u') in the sublayer
S(u)=1.123 F(u)=4.642

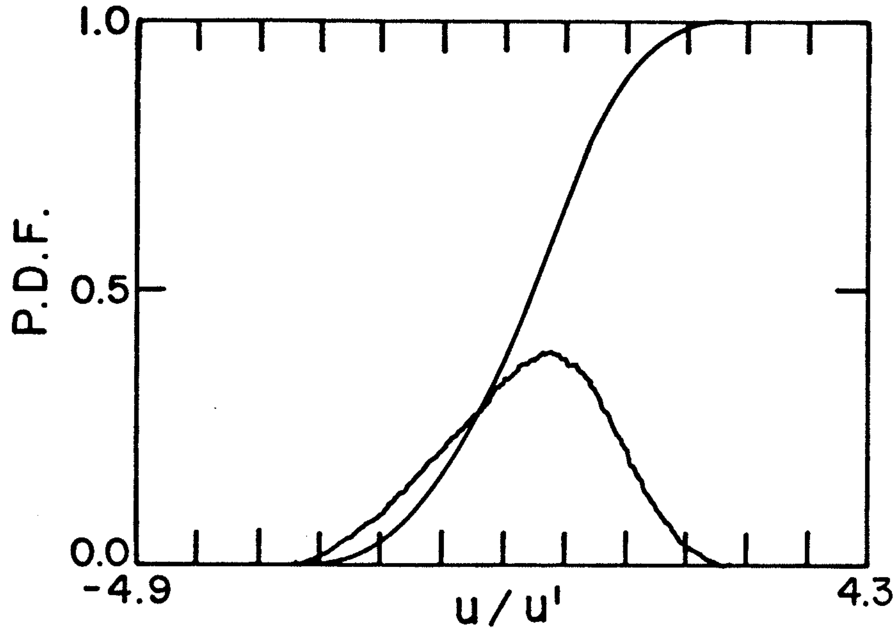

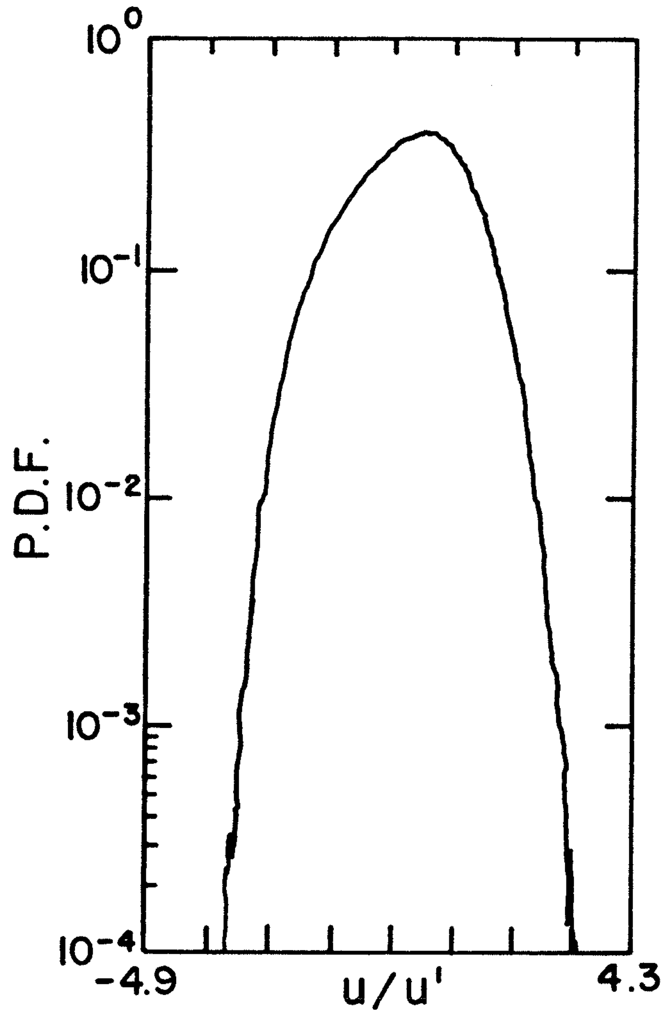

Figure 5.8: PDF(u/u') at y = 1 mm
S(u)=-0.216 F(u)=2.639

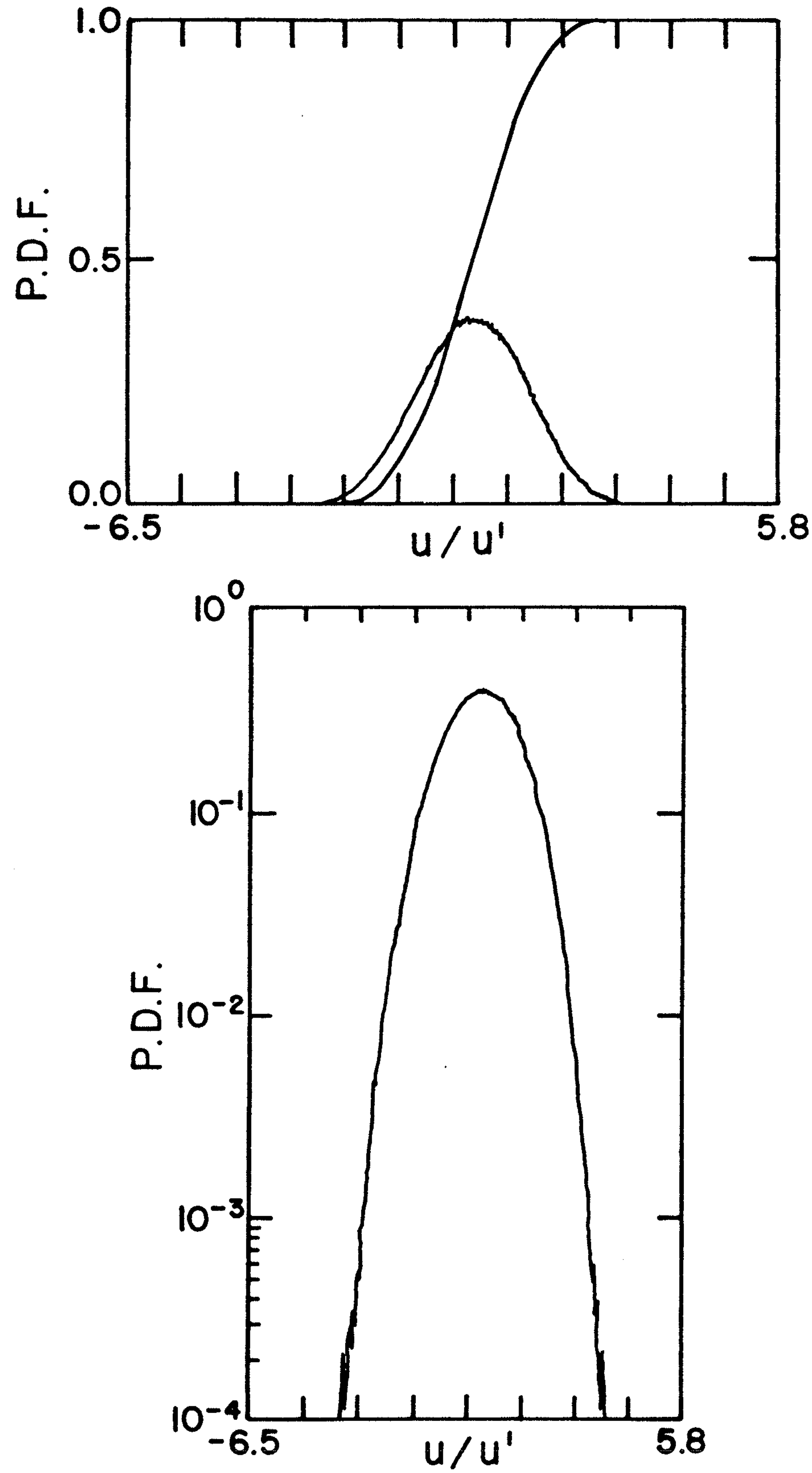

Figure 5.9: PDF(u/u') at y = 5 mm
S(u)=-0.040 F(u)=2.755

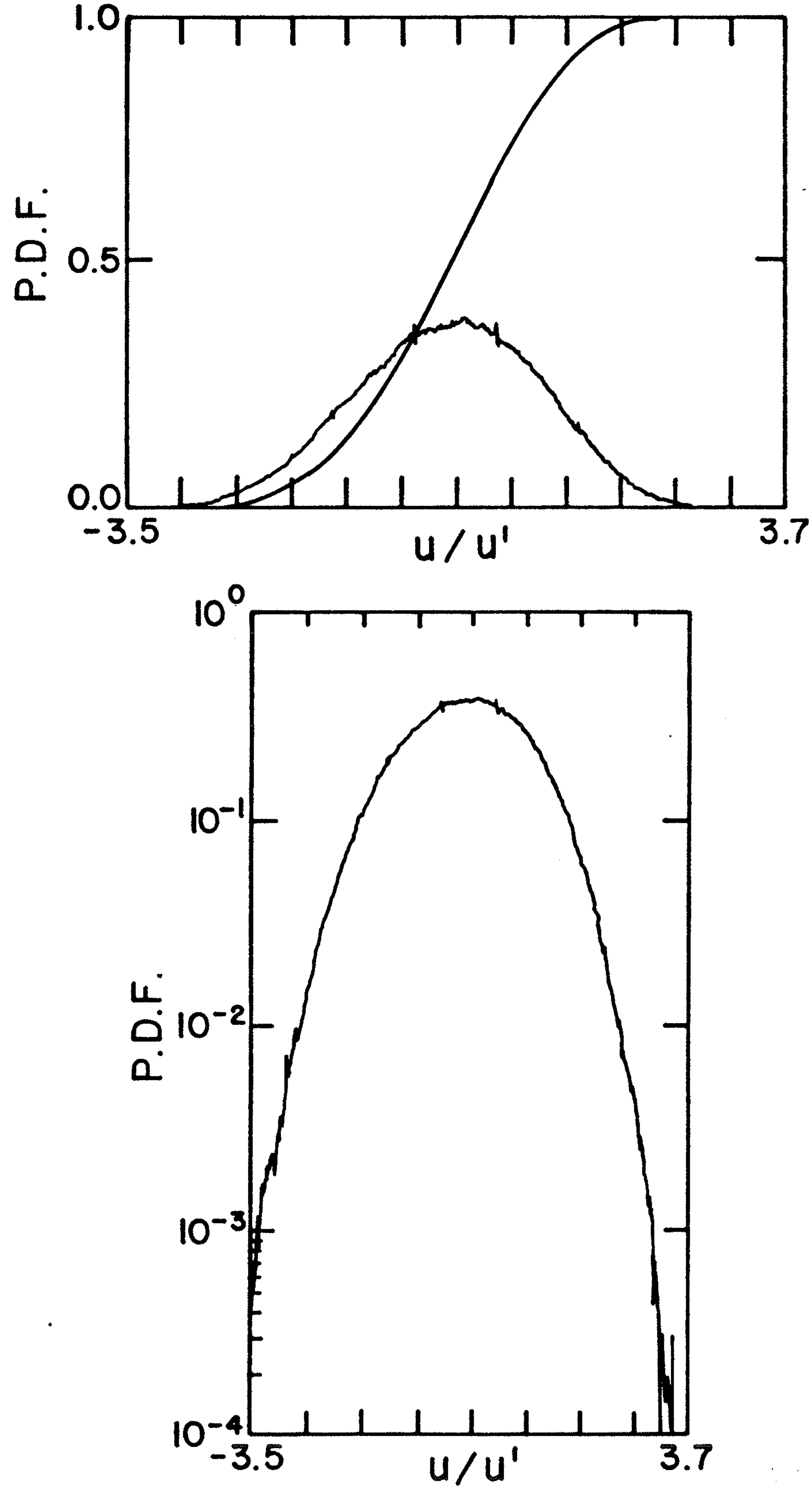

Figure 5.10: PDF(u/u') at y = 10 mm
S(u)=-0.106 F(u)=2.715

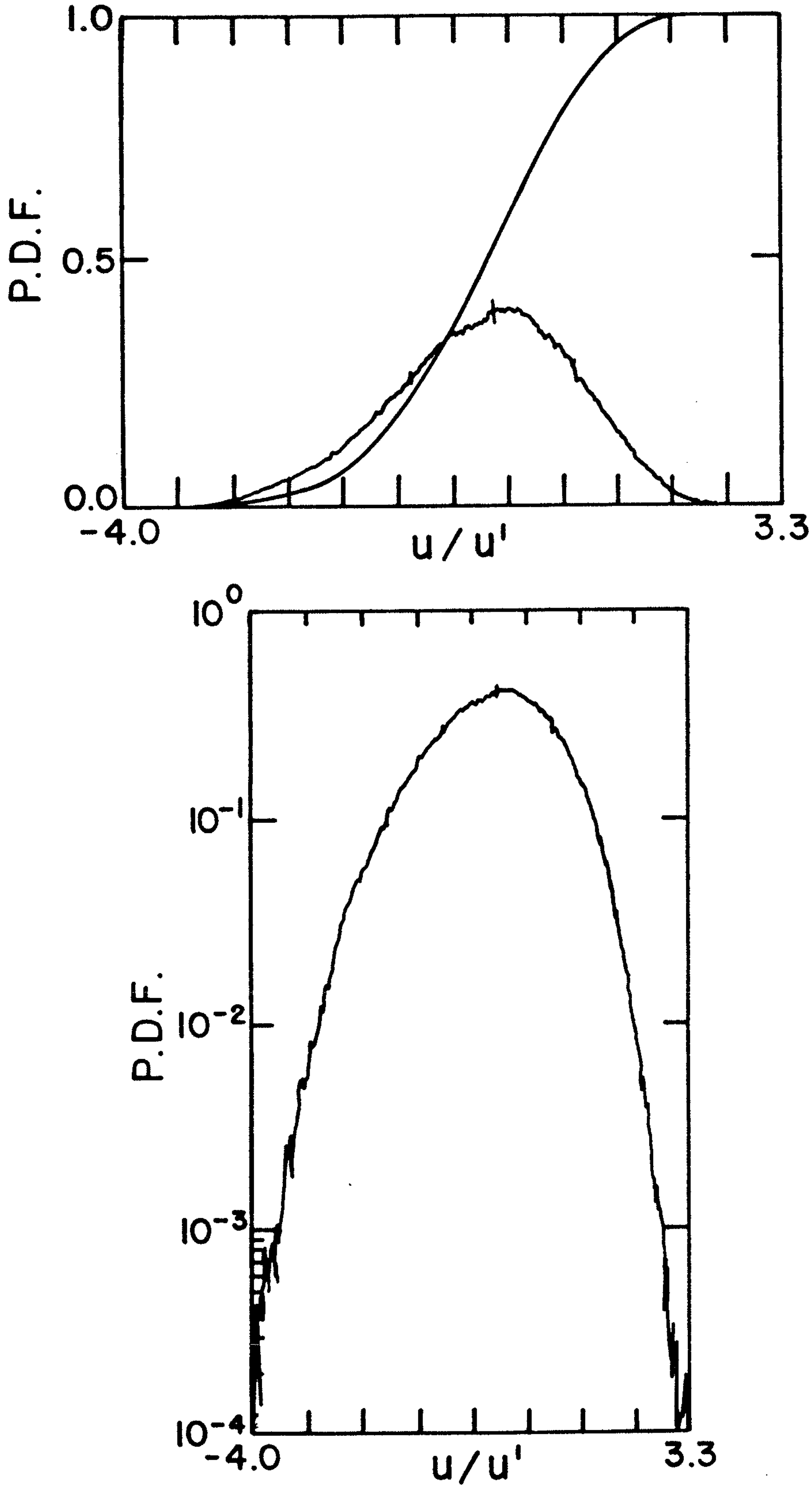

Figure 5.11: PDF(u/u') at y = 20 mm
S(u)=-0.312 F(u)=2.852

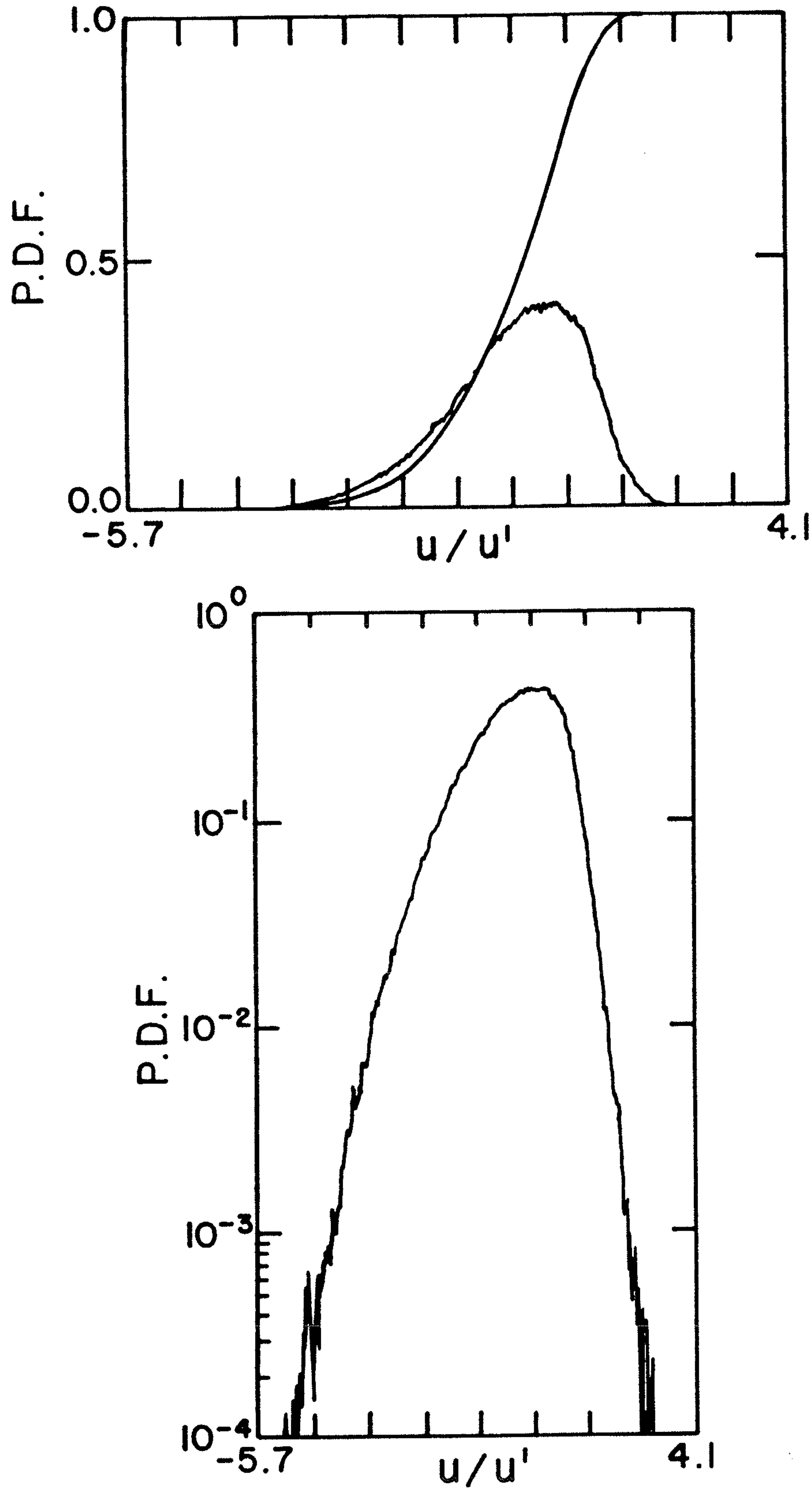

Figure 5.12: PDF(u/u') at y = 30 mm
S(u)=-0.672 F(u)=3.384

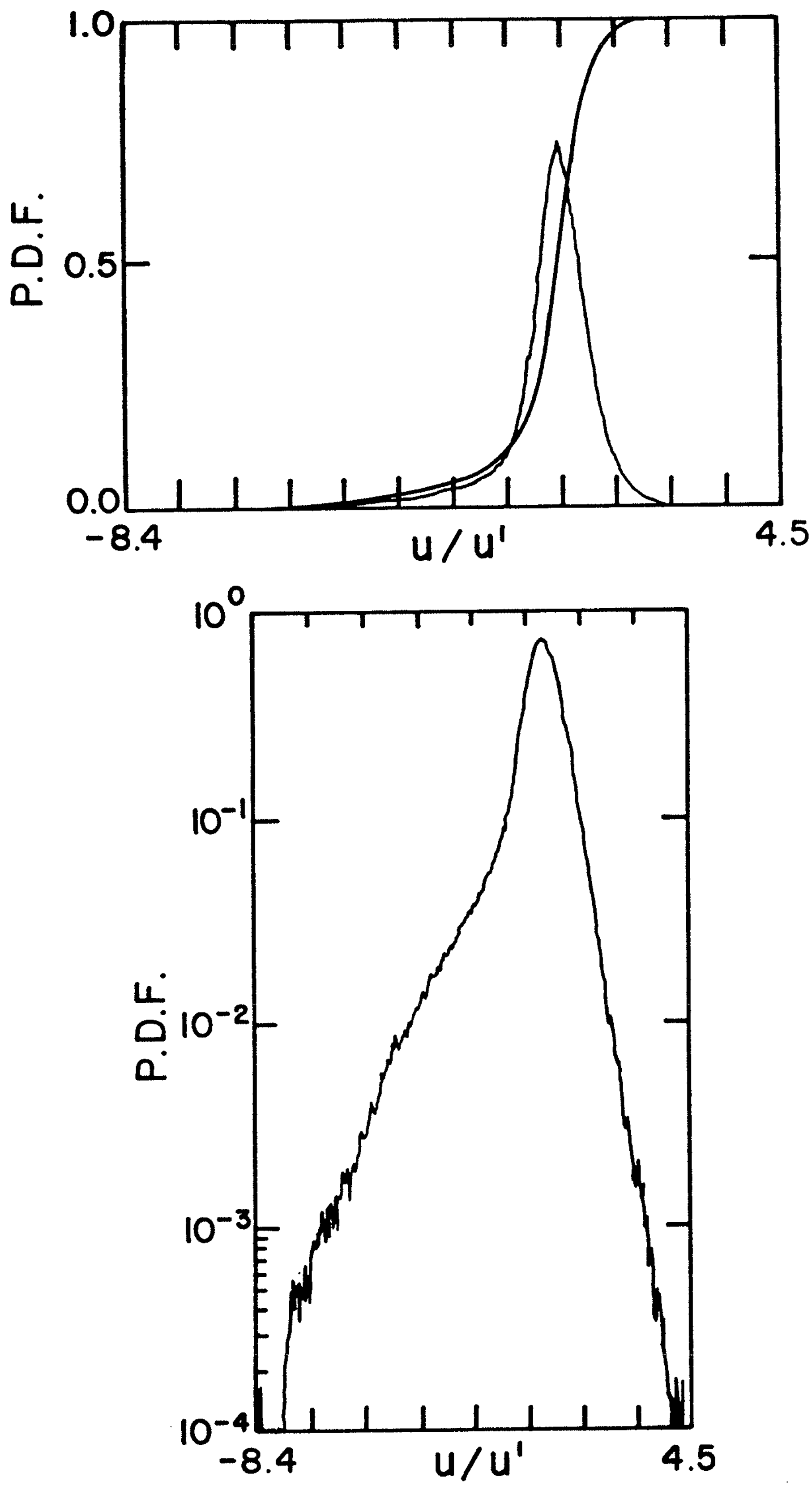

Figure 5.13: PDF(u/u') at y = 45 mm
S(u)=-2.074 F(u)=10.764

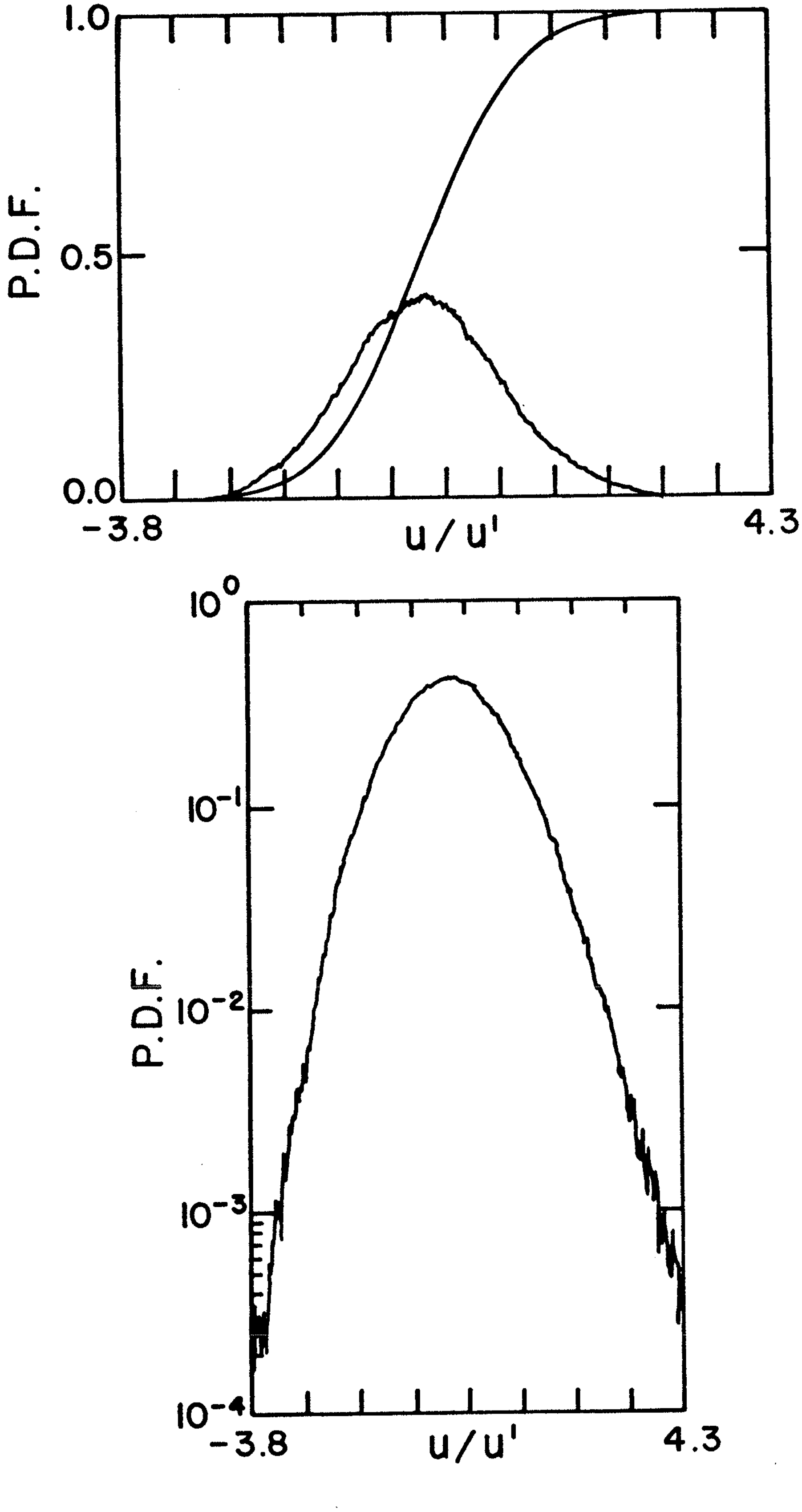

Figure 5.14: PDF(u/u') at y = 70 mm
S(u)=0.193 F(u)=3.247

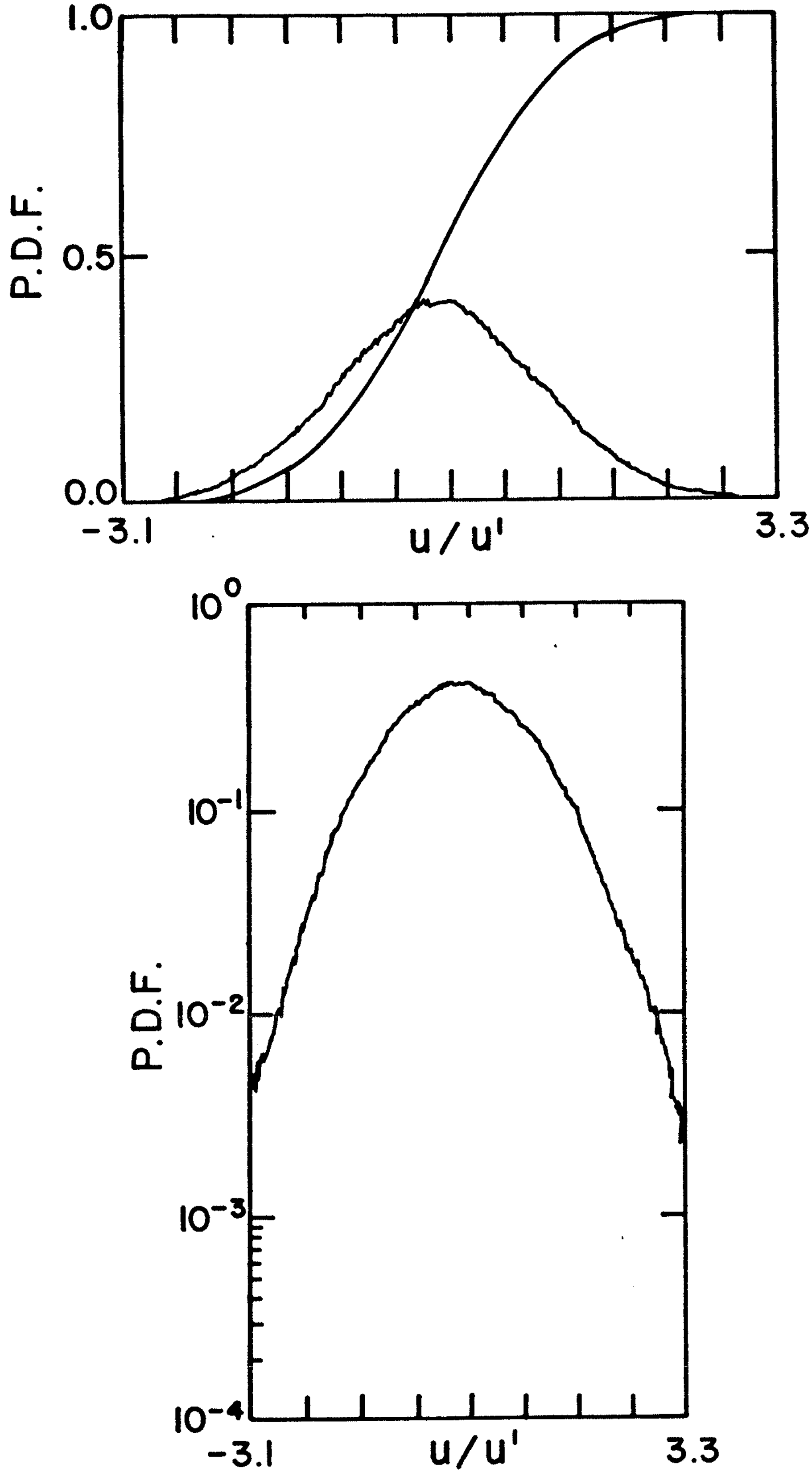

Figure 5.15: PDF(u/u') at y = 135 mm
S(u)=0.033 F(u)=3.026

5.1.4 Spectra of the Longitudinal Velocity

The data for the analog/digital comparisons of u-spectra in the boundary layer tunnel were collected by different experimenters at different times. The hot wire signal for the digital results was filtered at the Kolmogorov frequency $f(K) = U / 2\pi\eta$ where η is the Kolmogorov length, by means of the signal conditioner. The dc component of the signal was subtracted, leaving the fluctuating component to be amplified to within the ±5 volts limit accepted by the computer.

The analog results obtained by Kassab [198_] were collected for frequency values between 2 Hz and 12 kHz after the u^2 signal was low passed at the Kolmogorov frequency $f(K) = U / 2\pi\eta$.

The digital spectral results were calculated using the fast Fourier transform and spectra subroutines supplied by DEC. The spectra was calculated by two passes of the data: a 'high frequency' spectra calculated from the data as is and a 'low frequency' spectra calculated from the data stream filtered using a second order Butterworth infinite-inpulse-response filter or IIR filter. The 'low frequency' data was then sampled at $^1/_{64}$ of the sampling rate, the spectra calculated, and multiplied by a factor of 64 to account for the shift in bandwidth. The spectra was then plotted by the H·P plotter.

The analog/digital comparison of the dimensional velocity spectra in the boundary layer tunnel for an airflow of 8 m/sec free stream velocity is shown in Figures 5.16 to 5.25. The energy containing range of the u-spectra is at the low frequencies, mostly below 100 Hz, and displays a nearly constant value before dropping in energy at the higher frequencies. The energy content at the different radial positions gradually decreases further and further from the tunnel wall.

A comparison of the analog and digital data shows firstly some scatter at the low frequency end of the spectra and secondly a wider analog bandwidth before the onset of 'digital noise', seen in the digital data at approximately 10 kHz. Noise in the analog data occurs at a much higher frequency. Some of the 'scatter' in the low frequency end of the digitally obtained spectra could be attributed to the poorer averaging and reduced sample size found from the second pass of the data stream.

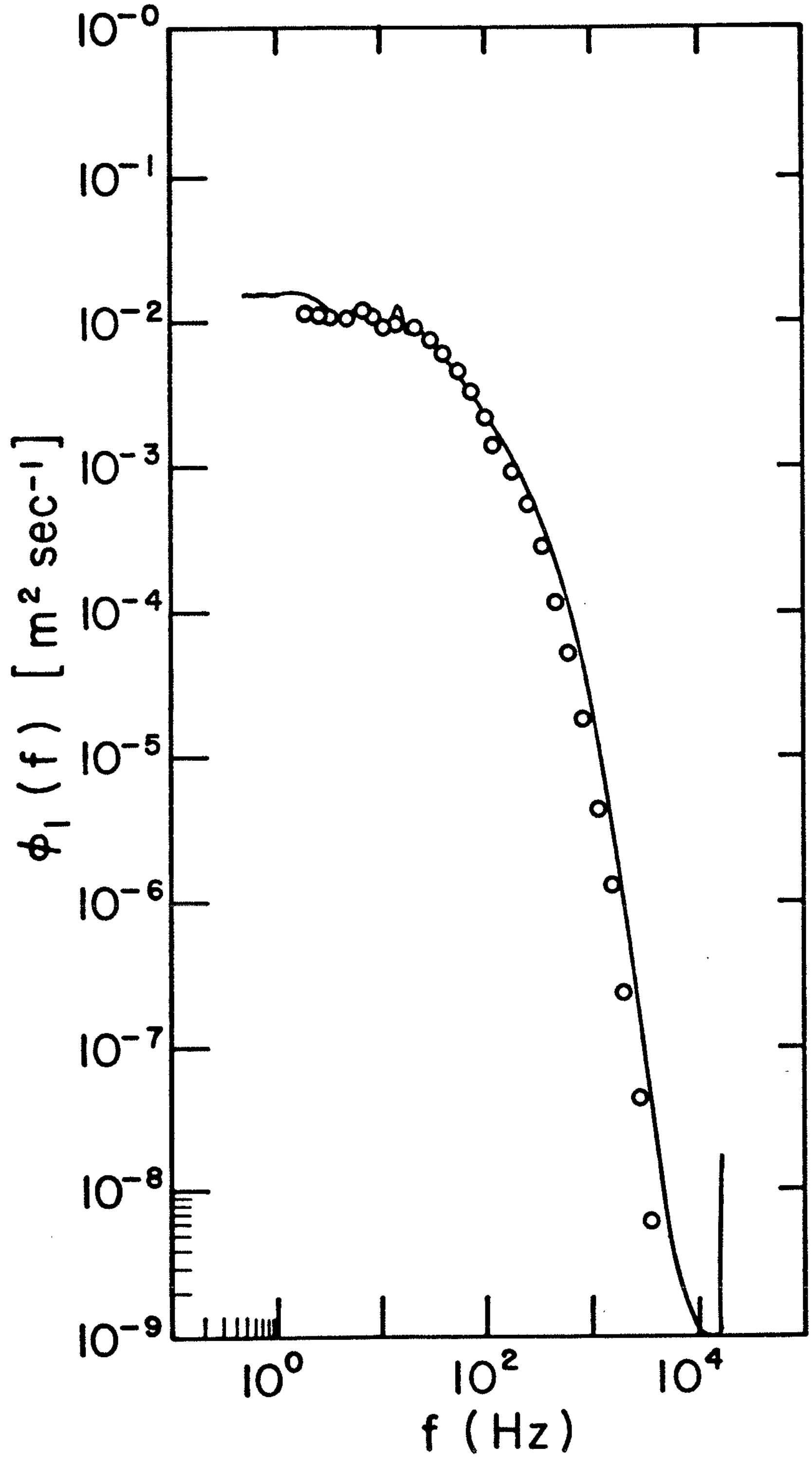

Figure 5.16: Spectra at y = 0.5 mm

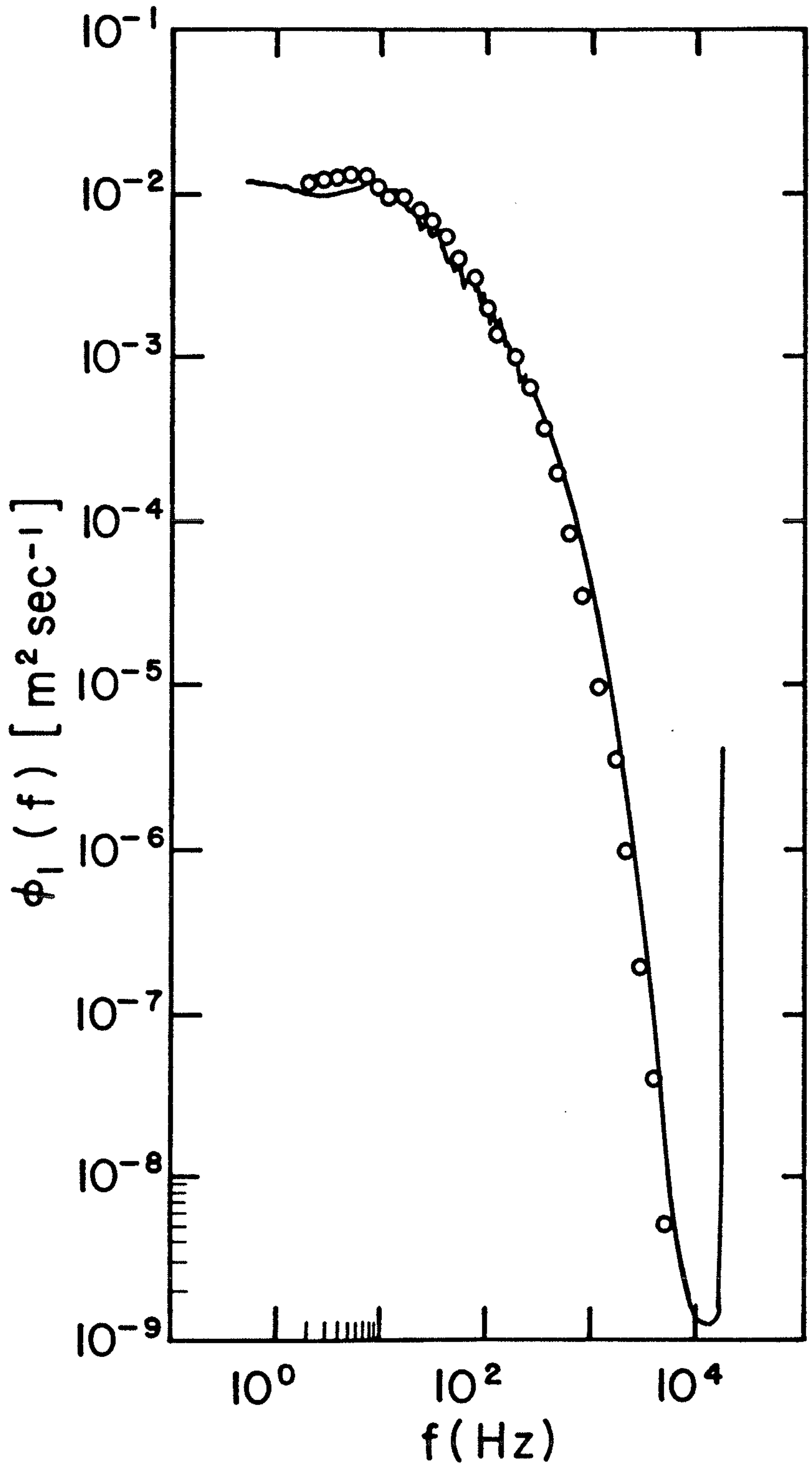

Figure 5.17: Spectra at y = 1.0 mm

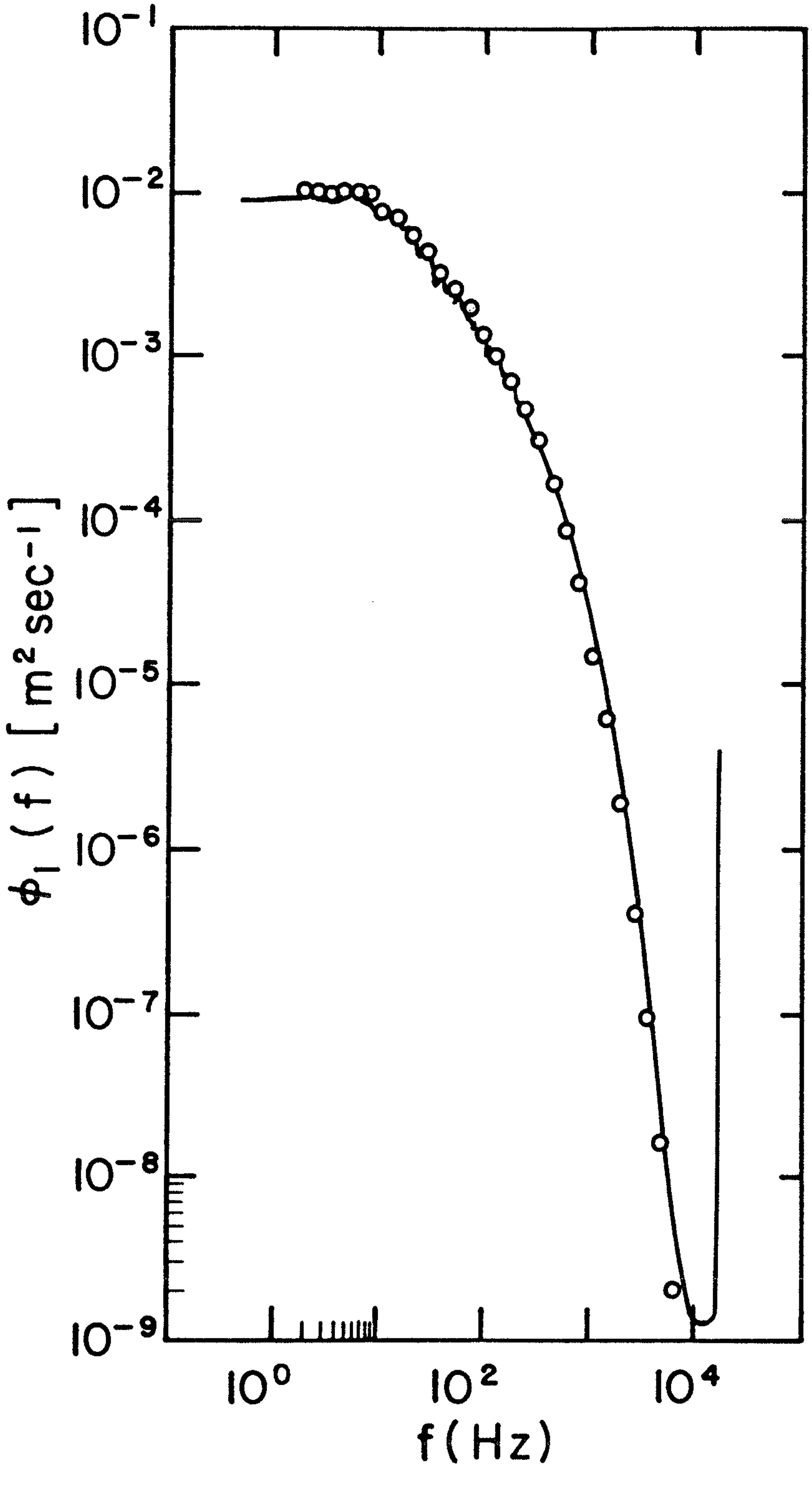

Figure 5.18: Spectra at y = 2 mm

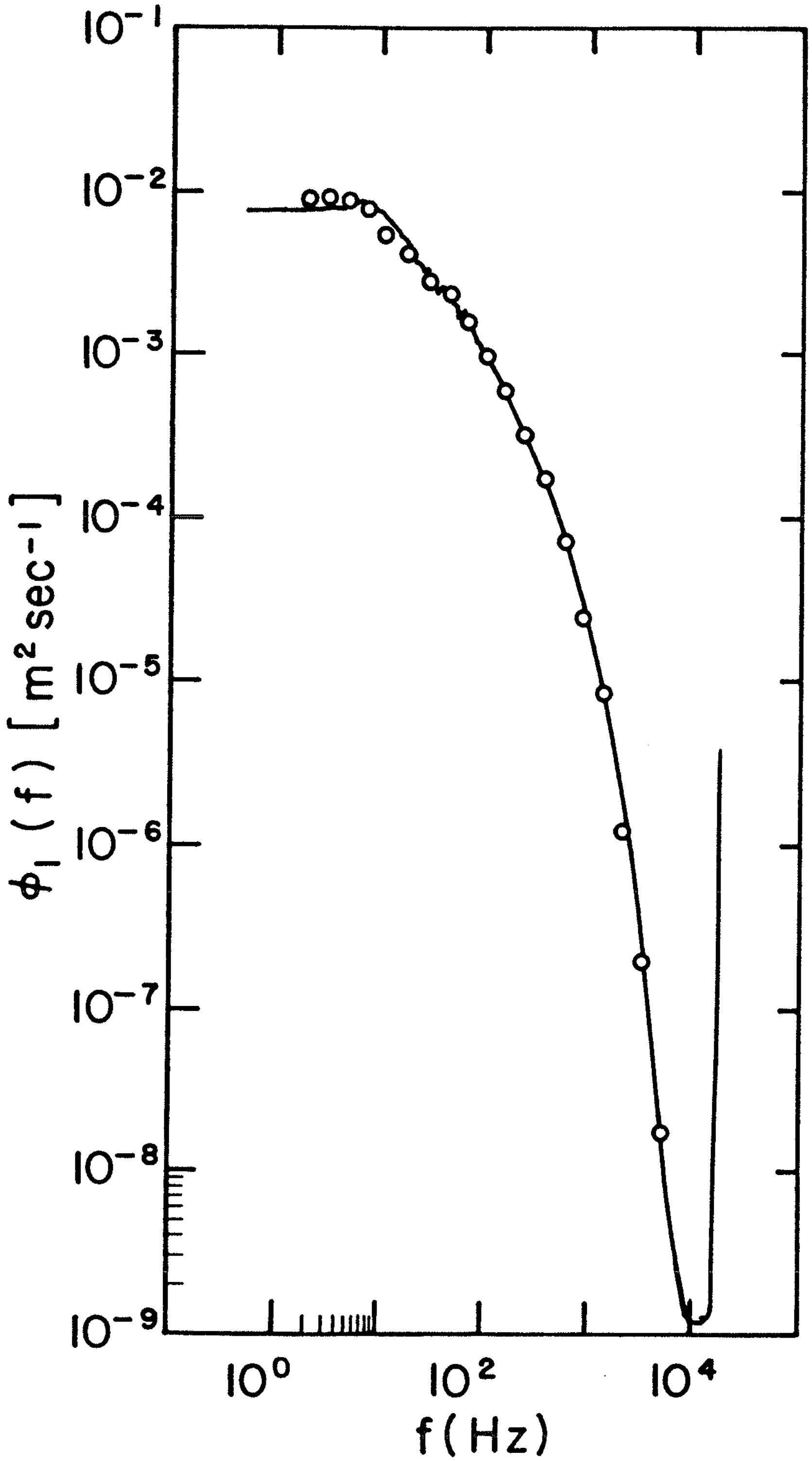

Figure 5.19: Spectra at y = 5 mm

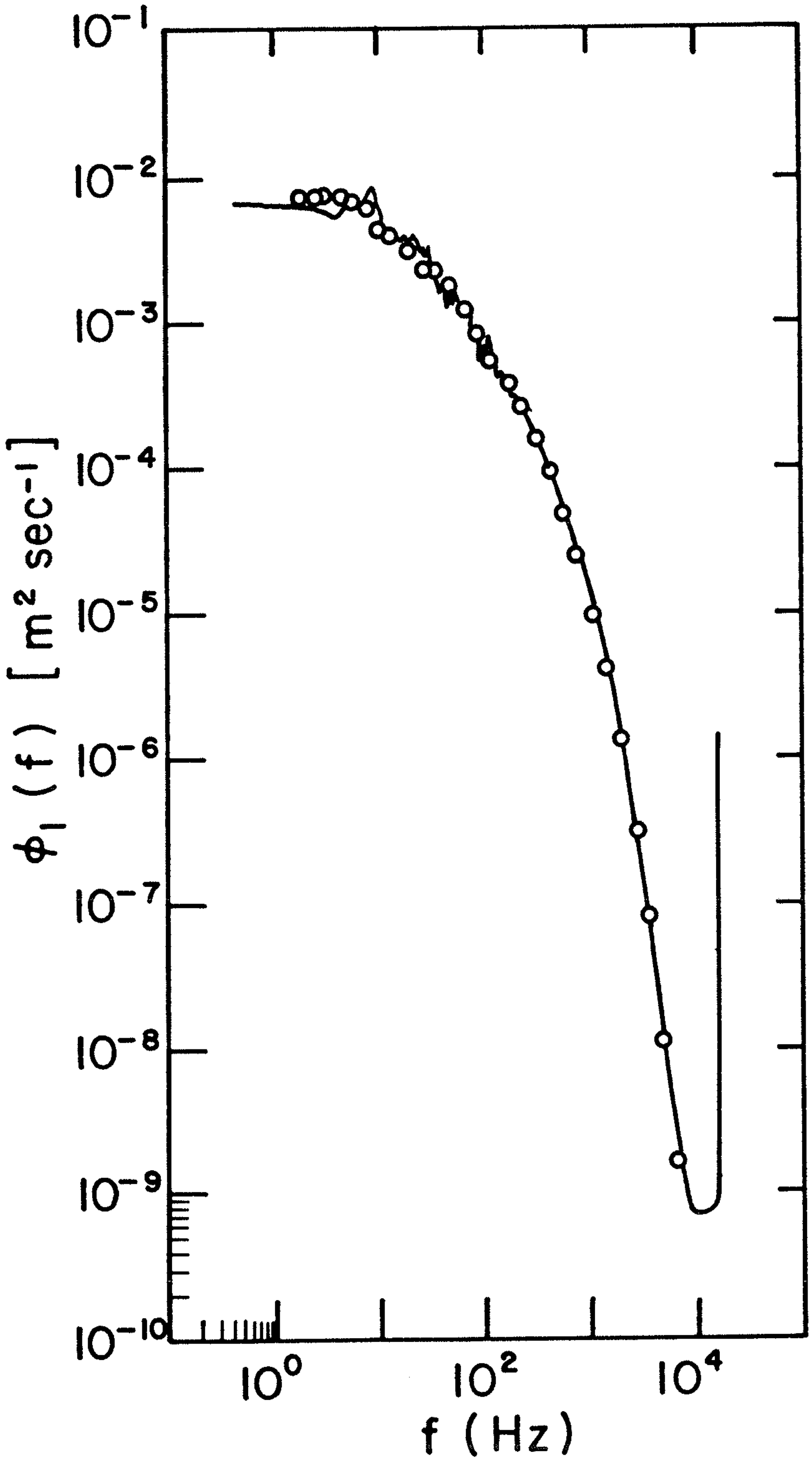

Figure 5.20: Spectra at y = 10 mm

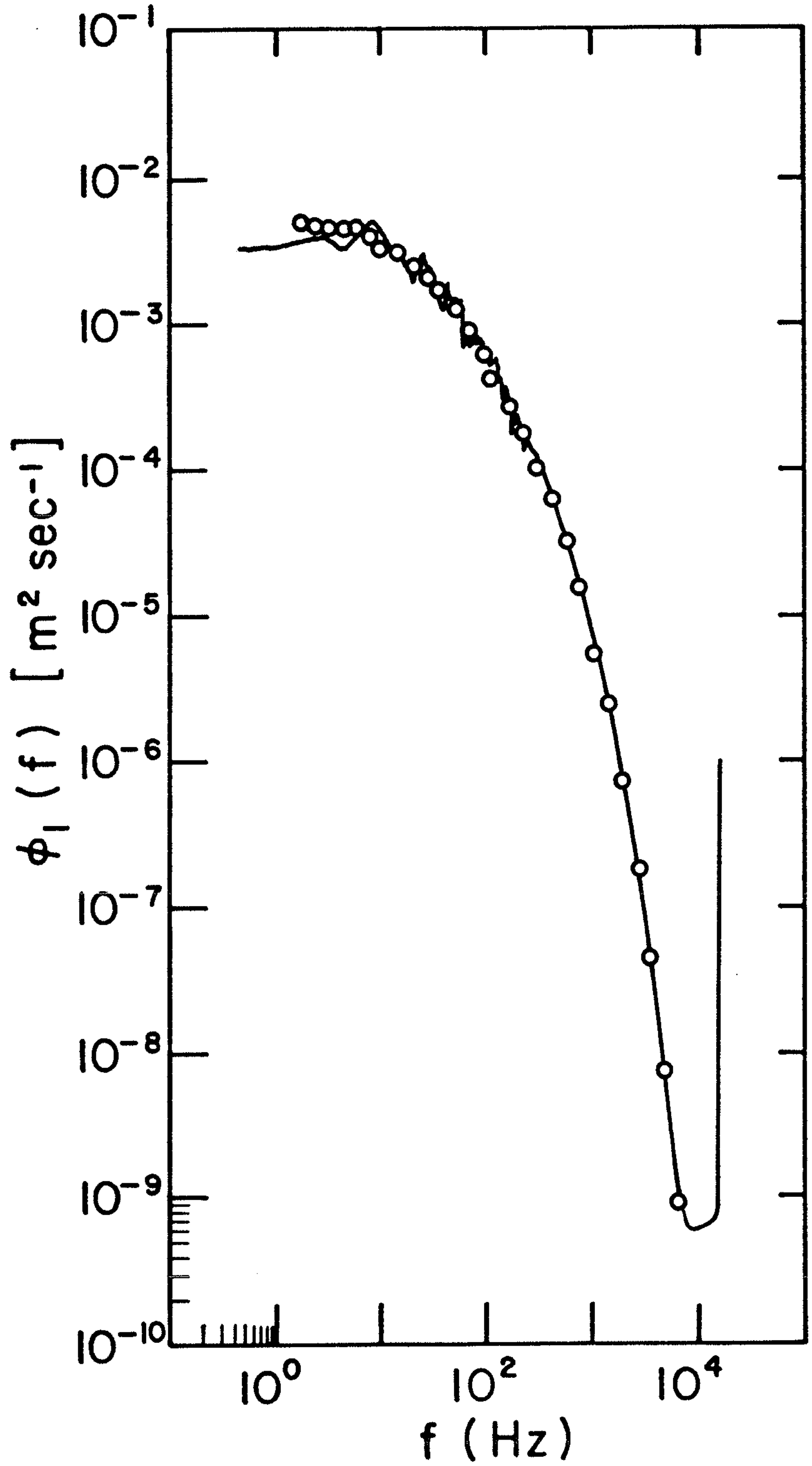

Figure 5.21: Spectra at y = 20 mm

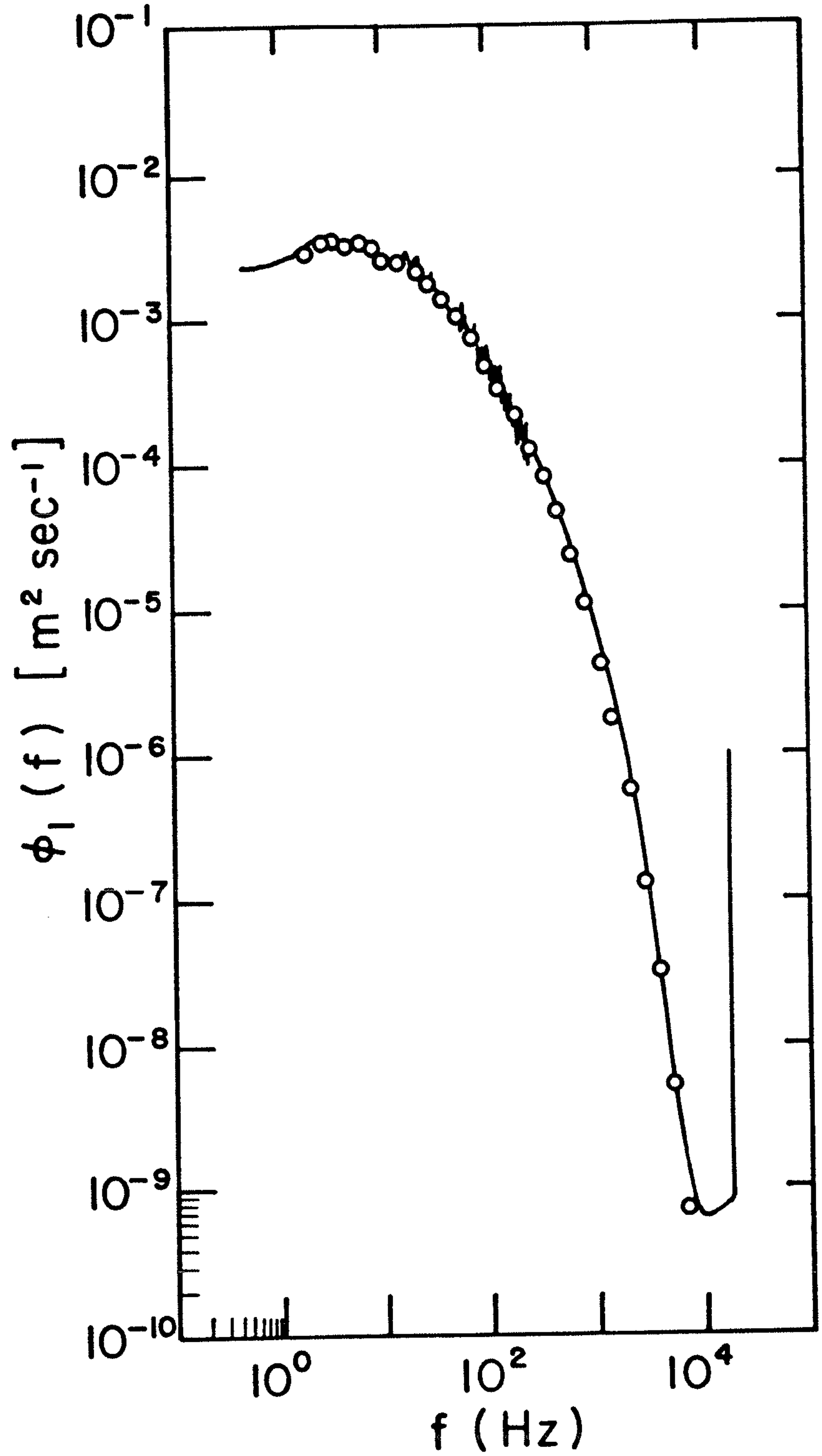

Figure 5.22: Spectra at y = 25 mm

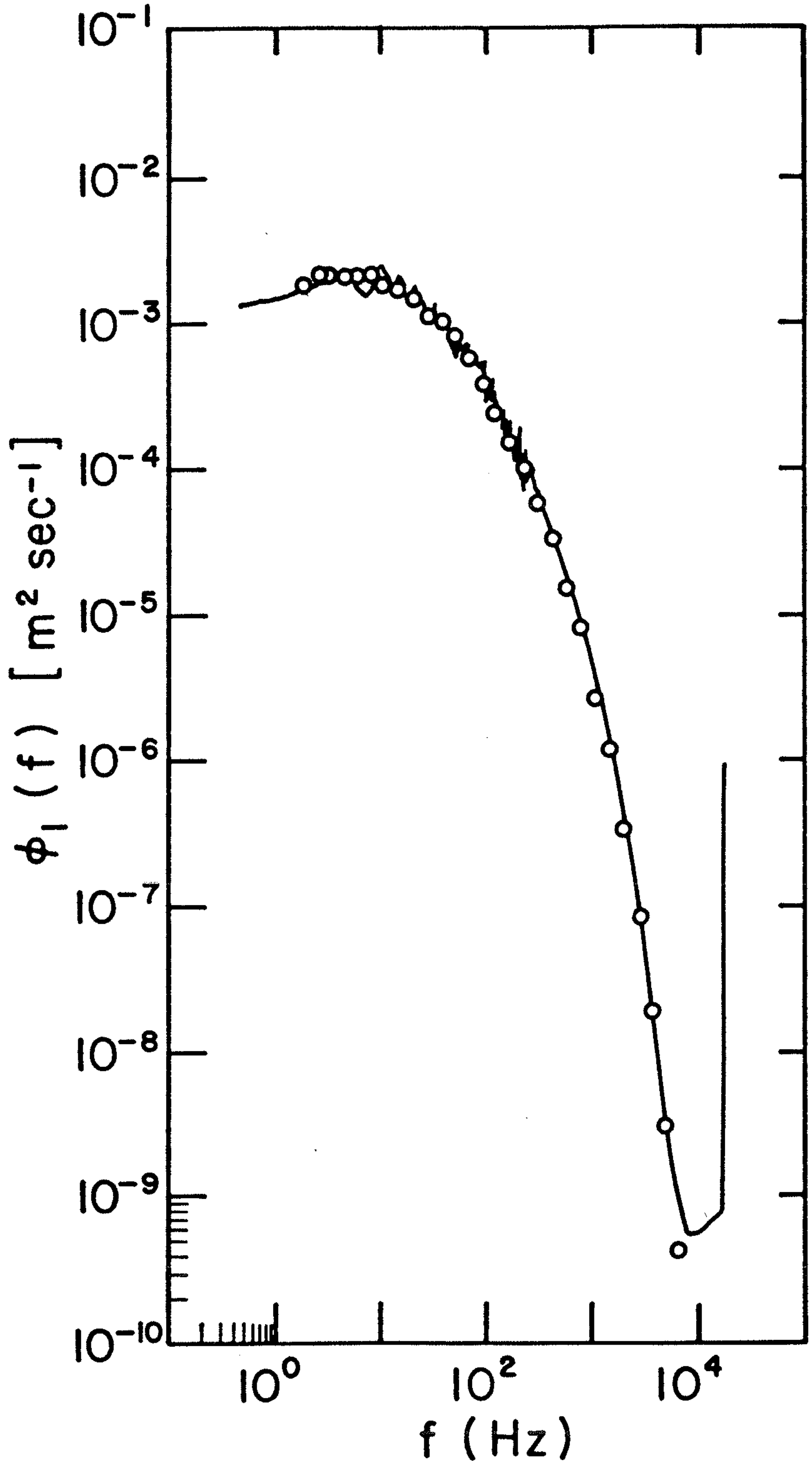

Figure 5.23: Spectra at y = 30 mm

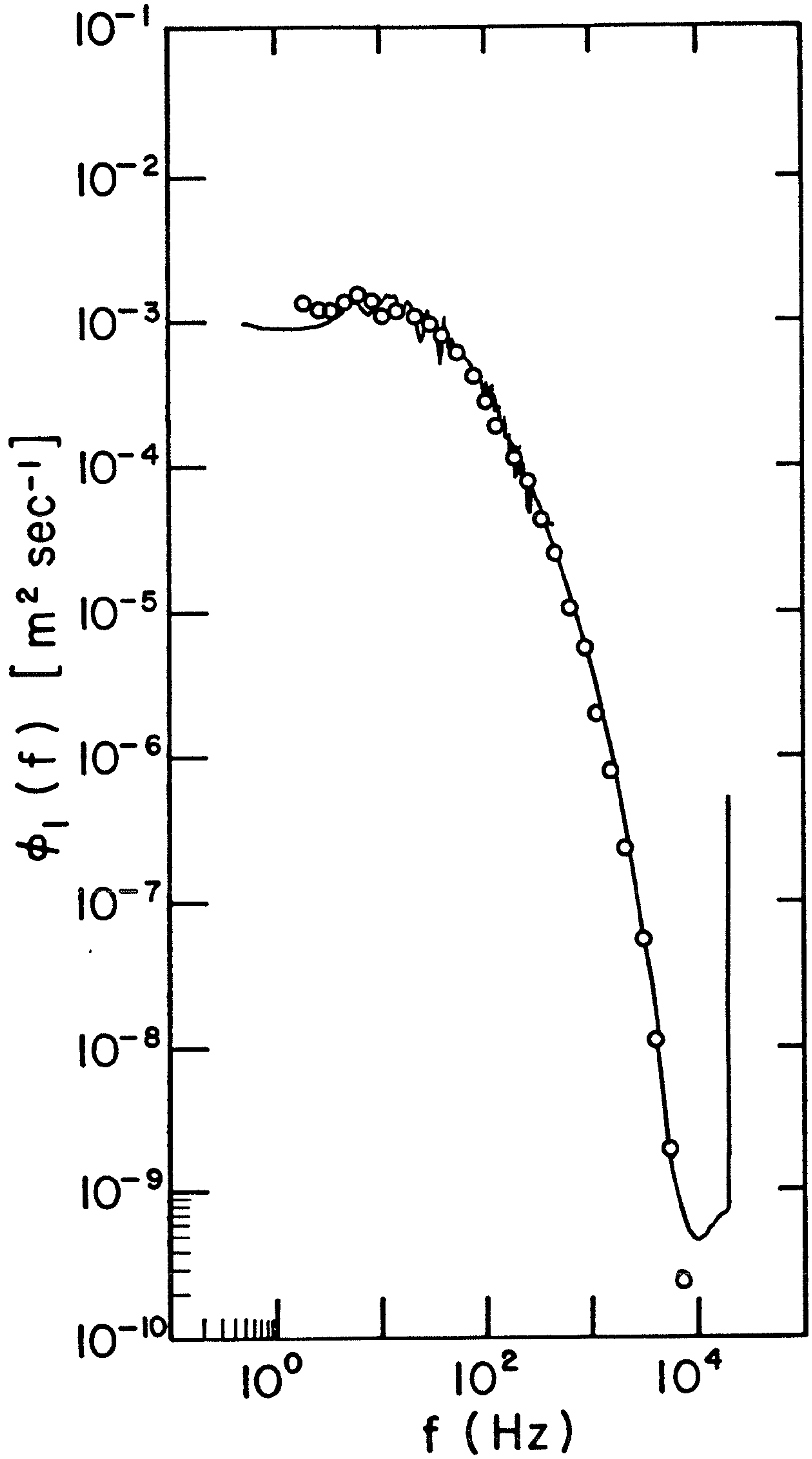

Figure 5.24: Spectra at y = 35 mm

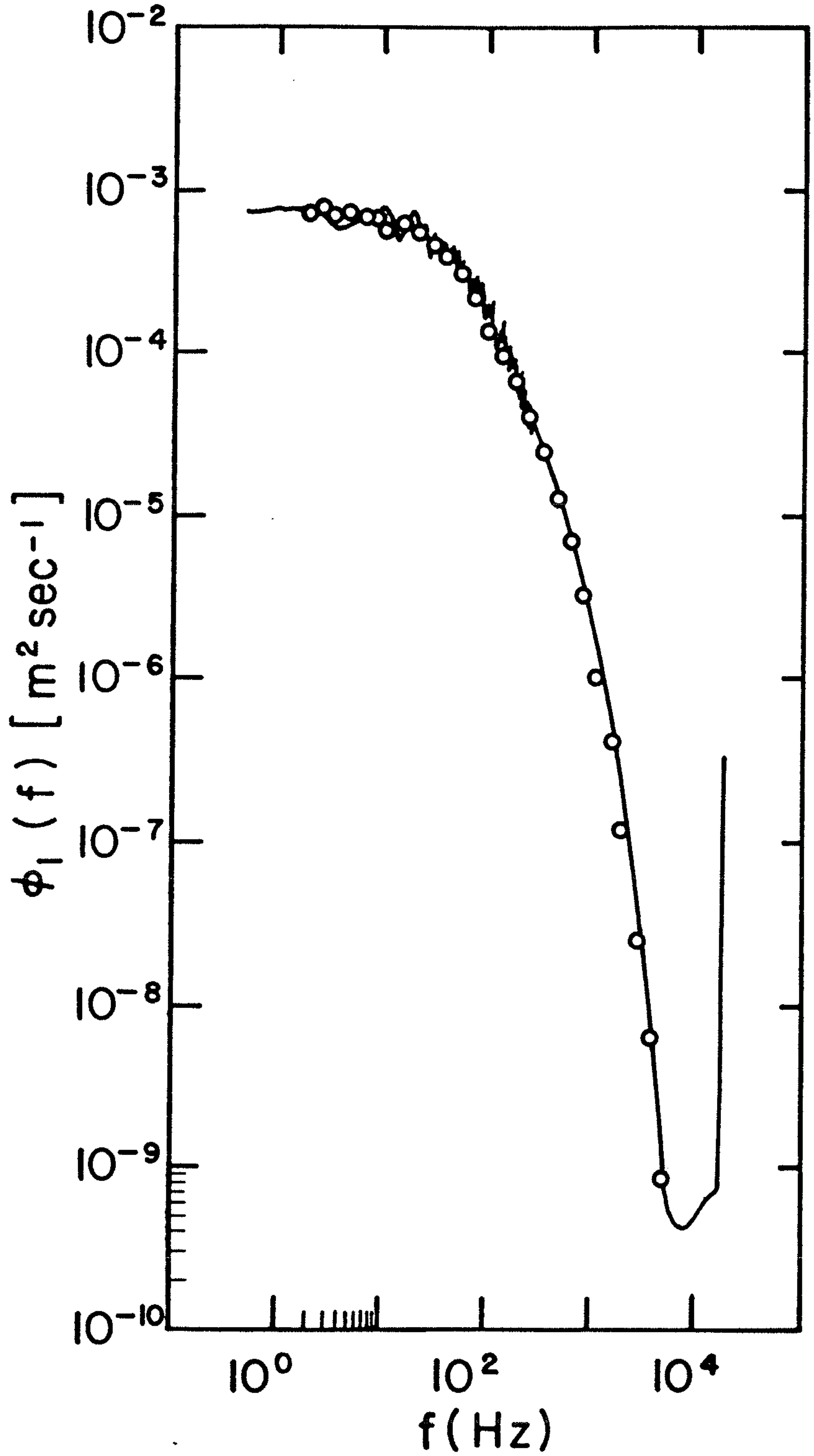

Figure 5.25: Spectra at y = 40 mm

5.2 THE DIFFUSER

An 8° conical diffuser of 4:1 area ratio was fed by fully developed pipe flow at a Reynolds number of 130,000 based on the entry pipe diameter and pipe bulk velocity. Analog and digital measurements in the adverse pressure gradient flow were taken simultaneously, first for a single wire boundary layer probe and later for a cross wire probe. Measurements were taken perpendicular to the diffuser wall at a location 63 cm from the diffuser inlet or 9 cm from the diffuser outlet. This position was chosen firstly because at a distance of approximately half the diffuser outlet diameter, the location was thought to be free of exit effects, and secondly for its convenience for experimentation.

Linearization of the hot wire anemometer was performed in situ in the same orientation and measuring station as was used for data collection. The velocity profile obtained through the pressure measurements was used as the calibration standard. Special care was taken in matching the frequency response and sensitivity of each wire in the X-array probe to reduce contamination of one component by the other. The digital data was collected into 2000 buffers at a rate of 2×10^4 samples/sec for a total of 2053120 data points at each probe position.

5.2.1 Points of Consideration

Unlike the boundary layer results obtained in addition to those of Derksen [1981] and Kassab [198_], the Tri-Met turbulence processor was used to measure flow parameters in the 8° conical diffuser. As already demonstrated by Derksen [1981], no significant difference exists in results obtained through use of the DISA or Tri-Met processors. However, unlike the single wire signal, when using the cross wire probe with the Tri-Met processor, it is necessary to remember that it is the negative of both the "u" and the "v" flow components from the cross wire signal that is available from the Tri-Met processor output. These output signals are then fed into the signal conditioner before being fed into and processed by the PDP-11 computer. These negative values of the flow components processed by the computer have no effect on spectral results since the spectra is determined using a squared signal, nor on even order moments such as kurtosis, but does produce PDF's the mirror image of those obtained with the single wire boundary layer probe and also produces odd order moments such as skewness equal in magnitude but opposite in sign of those obtained with the boundary layer probe and analog results. In addition, the digitally obtained $\overline{u^m v^n}$ mixed correlations of odd valued m or n exponents are equal in magnitude but opposite in sign from those obtained by the Tri-Met analog processor. Hence, where appropriate, the digital results presented, due to the signal inversion prior to processing, have been multiplied by a factor of -1 in order to retain the correct phase information.

An additional point to remember is the effect of tangential cooling with the cross wire probe. Directional sensitivity of the cross wire probe is explained in greater detail in Appendix A. As a result of the effect of tangential cooling, the measured rms component v' has been multiplied by a yaw correction factor of 1.1117, and the measured $\overline{u^m v^n}$ mixed correlations have been multiplied by a correction factor of 1.1117^n. The central moments however are obtained from the ratio of the correlations to the appropriate powers of the rms values, thereby negating the effect of the yaw correction terms.

5.2.2 Velocity Measurements

The velocity distribution at the location 63 cm from the diffuser inlet as determined from the pressure measurements is shown in Figure 4.29. This velocity distribution was used as a calibration standard for the analog velocity measurements. The local velocity from single and cross wire measurements, in Figure 5.26, show the same inflectional profile as that obtained from the pressure measurements. The point of inflection in the these velocity profiles occurs at a position 50 mm perpendicular to the diffuser wall.

The rms fluctuating 'axial' or longitudinal and 'radial' or transverse velocities, u' and v', are shown in Figure 5.27 and 5.28. The maximum u' and v' values occur at a position 45-50 mm from the diffuser wall. This location is in a line level with the leading edge of the diffuser inlet or entry radius. The value of the u' component is approximately twice that of the v' component throughout most of the flow. A relative minima for both the u' and v' components occur at the diffuser centerline, a position 95 mm from the diffuser wall. The effect of the yaw correction term on the v' component is shown in Figure 5.28.

The rms fluctuating longitudinal velocity normalized by the local mean longitudinal velocity, shown in Figure 5.29, shows a relative turbulence intensity in excess of 60% in the first 20 mm from the wall. The relative turbulence intensity, u'/U , decreases from over 100% at the wall to approximately 10% at the diffuser axis. The v'/U ratio increases to 30% relative intensity in the first 10 mm from the wall and remains approximately constant over the next 15 mm before decreasing to approximately 7% relative intensity at the centerline.

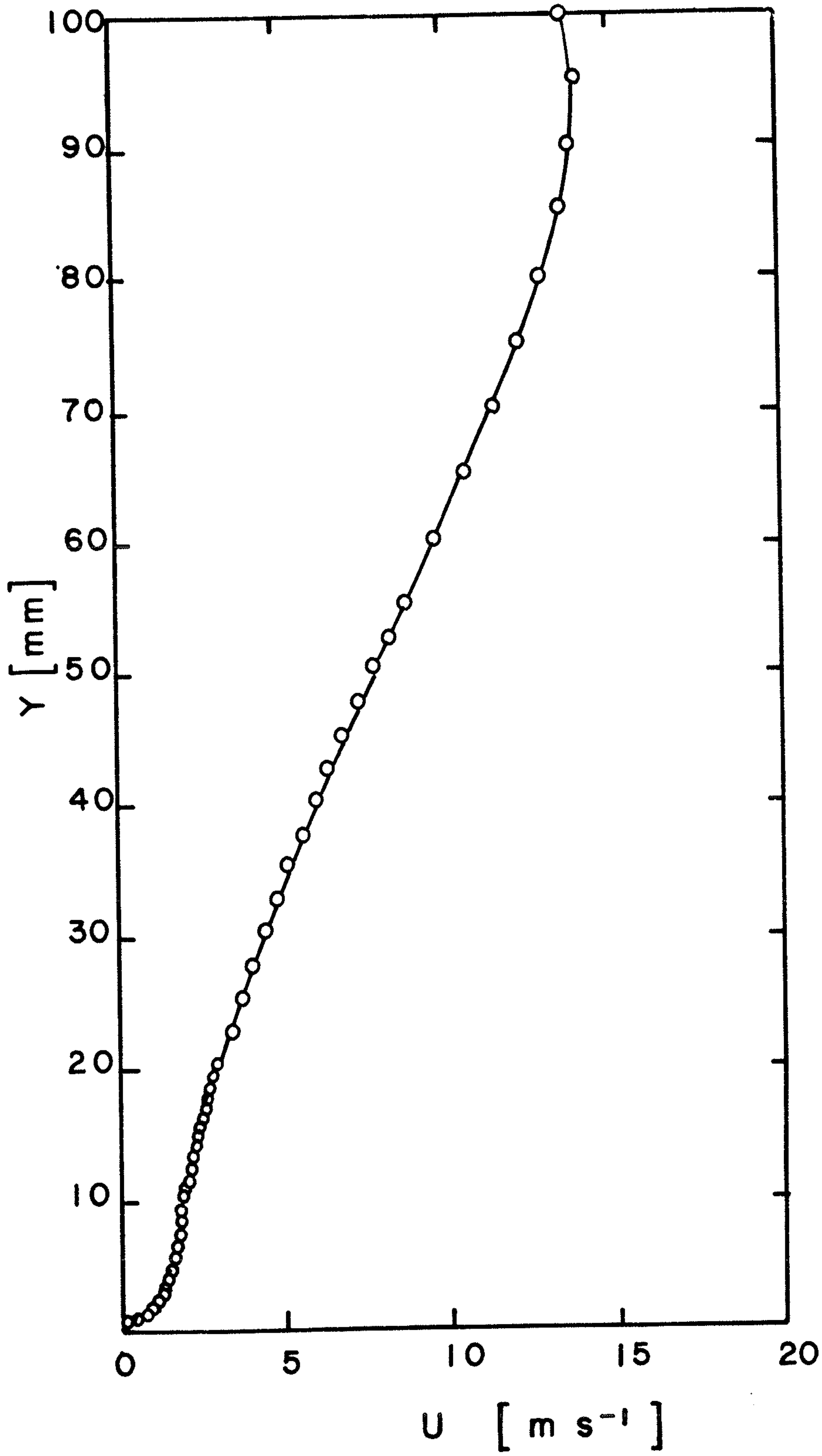

Figure 5.26: Hot Wire Velocity Profile at x = 63 cm

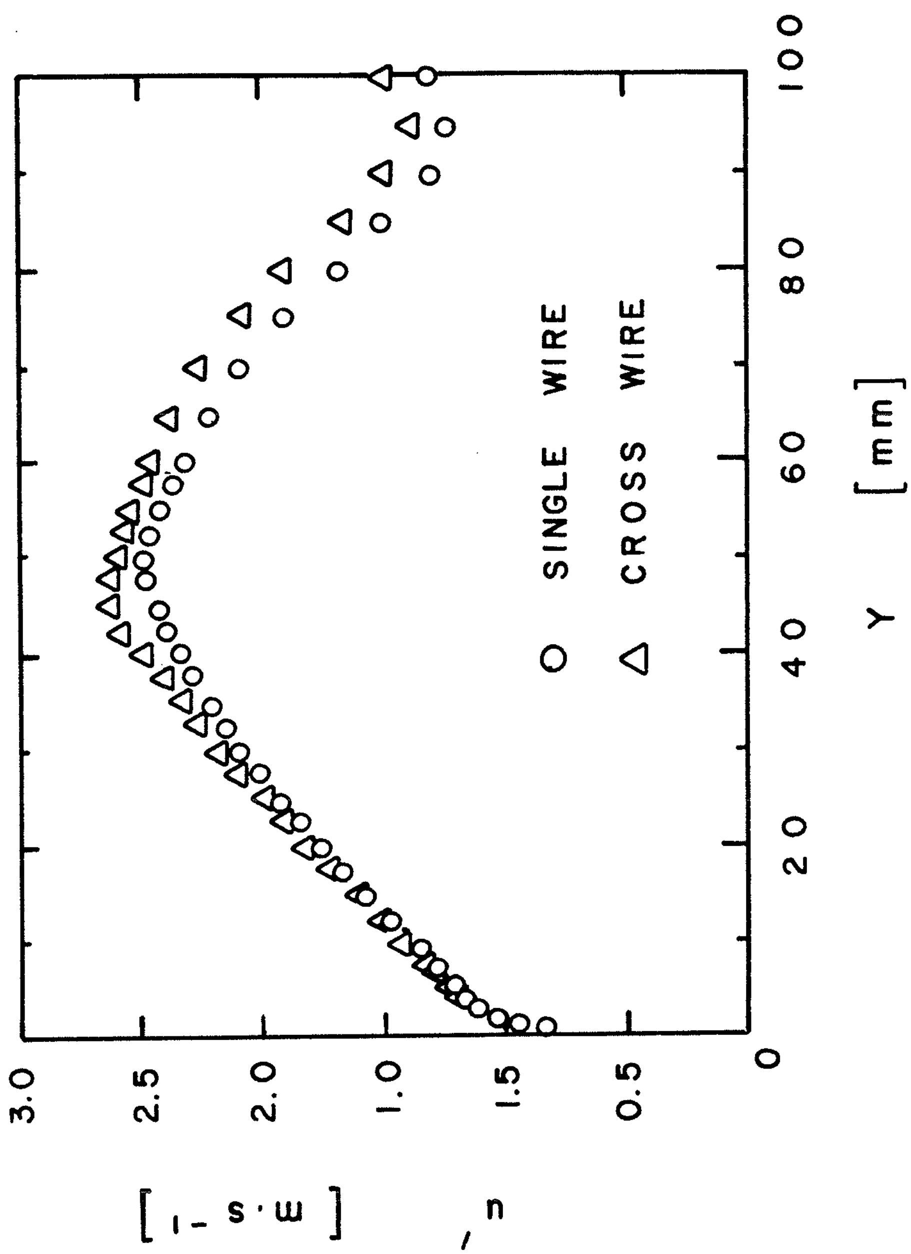

Figure 5.27: The rms fluctuating component, u'

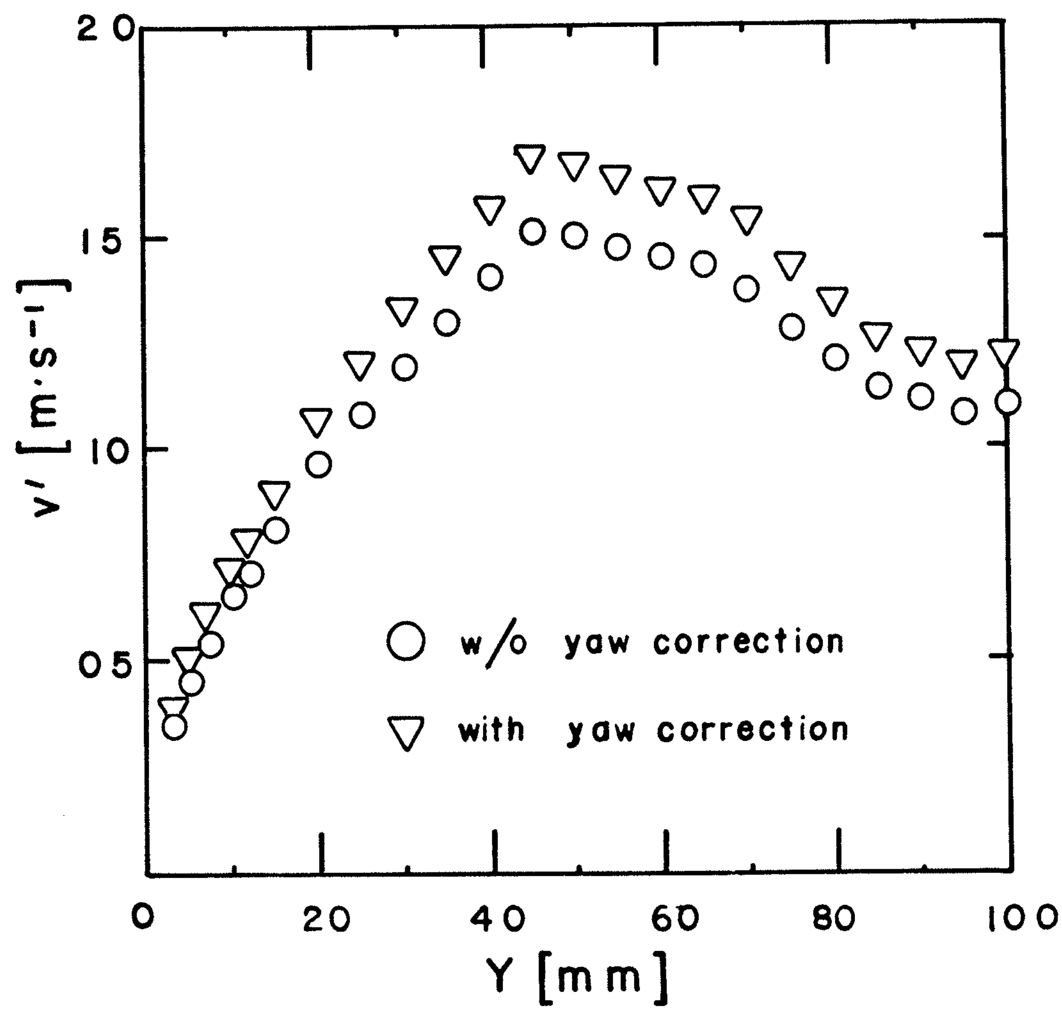

Figure 5.28: Effect of yaw correction on v'

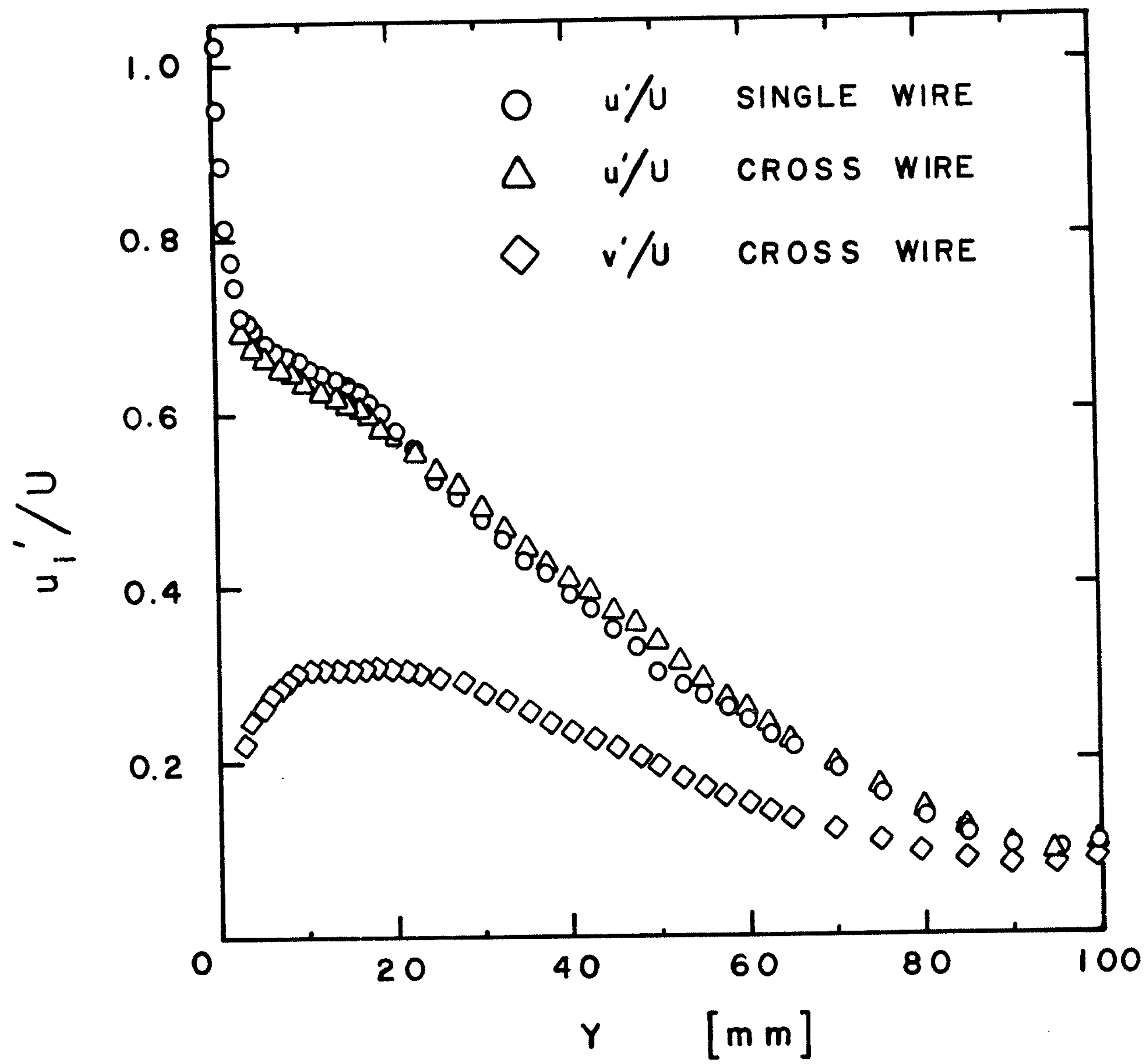

Figure 5.29: The relative turbulence intensities

5.2.3 Third and Fourth Order Moments

The first set of values for skewness and flatness of the turbulence signal were obtained using the single wire boundary layer probe. Later, skewness and flatness values of 'axial' and 'radial' velocity components were obtained using a cross wire probe.

5.2.3.1 The Longitudinal Velocity Component

The skewness and flatness factors obtained by both analog and digital means via boundary layer and cross wire probes are shown in Figure 5.30 and Figure 5.31. The skewness of the axial velocity component is highly positive and hence asymmetric in the first few millimeters from the wall and gradually approaches zero or symmetry about the mean velocity at a position in line with the entry radius. The skewness values continue to increase in the negative direction until a minimum is reached at the diffuser axis, then due to symmetry about the axis, the skewness values begin to increase.

The flatness factors of the 'axial' or longitudinal velocity component, K(u), are positive. The fourth order moments decrease in value from the wall to a minimum value below that of the Gaussian value of three at a position approximately in line with the entry radius before increasing in value. The increasing values of the flatness factors reach a relative maximum at the diffuser axis.

Just as skewness is used as a measure of symmetry, the flatness factor is used as a measure of the extent of the 'skirts' of the probability curve. A large value of kurtosis as observed in proximity to the diffuser wall indicates that fluctuations vary greatly from the mean.

As with the boundary layer flow, the diffuser flow exhibits areas of simultaneously random and organized features. Values of kurtosis fall between the Gaussian value of three for a random phenomenon and the sine wave value of 1.5 for an ordered structure in a 40 mm range between 30 mm and 70 mm perpendicular from the wall. The minimum value of the flatness factor, approximately 2.5, occurs at a point 50 mm from the wall, midway through the simultaneously random/ordered range, at a position approximately in line with the entry radius of the diffuser. The minimum value of the fourth order moment, 2.5, falls below that of the nearly constant value of 2.8 in the range y/δ in the boundary layer flow, and hence the diffuser flow at that point exhibits a larger degree of ordered randomness than the boundary layer flow.

5.2.3.2 Defining the Blue Line

From the behaviour of the rms fluctuating longitudinal velocity, and the skewness and kurtosis of the longitudinal mean velocity, a special point in the diffuser flow may be defined. The 'blue line' is defined as that point in the flow where the rms longitudinal fluctuating velocity, u', reaches a maximum, the skewness, S(u), is zero, and the flatness factor or kurtosis, K(u), reaches a minimum. Previous studies by Okwuobi [1972], Hummel [1978], and Arora [1978] have shown that for measurements taken perpendicular to the diffuser axis, the 'blue line' falls on a line approximated by the radius of the diffuser inlet, that is at a distance 5 cm away from the diffuser axis. The velocity profiles in Chapter 4 show, that in the latter third of the diffuser flow, a point of inflection also falls in the same region.

Studies by Hummel [1978] show that in approximately the last 15 cm of the diffuser, approaching the venting end of the diffuser, the 'blue line' bends toward the diffuser axis. A bending of the axial total pressure curve, shown in Figure 4.7, occurs at approximately the same location in the flow. Preliminary exploratory measurements in the latter half of the diffuser taken at right angles to diffuser wall showed the same trends as found by Hummel [1978]:

1. maximum u' values, zero skewness and minimum values of kurtosis at the same point in the flow - a position roughly in line with the entry radius.
2. a 'bending' of the 'blue line' towards the diffuser axis in the last few measuring stations approaching the venting end of the diffuser.

At the measuring station 63 cm from the diffuser inlet or 9 cm from the diffuser outlet, the diffuser axis is 9.5 cm from the wall measured at right angles to the wall. The blue line crossed a point 50 mm from the wall, just inside the region of the entry radius.

A few similarities can be drawn between the diffuser flow in the vicinity of the blue line and boundary layer flow in the vicinity of $Y_{+} = 15$. In both flows, skewness is positive and decreasing in magnitude from the wall to those points, u' values reach a maximum and the flatness factors reach a minimum value below that of the Gaussian value of 3 and skewness becomes negative beyond those points.

5.2.3.3 The Transverse Velocity Component

Skewness and flatness measurements of the 'radial' or transverse velocity component were determined using the cross wire probe. Due to the configuration of the cross wire probe and its relatively larger size, the cross wire probe could only be positioned a distance no closer than 3 mm from the diffuser wall. The trace of the skewness values cross the zero value twice: once at a position approximately 60 mm from the diffuser wall just beyond the blue line and again at the diffuser axis. The skewness of the 'radial' velocity component is negative in the first two-thirds of the flow and reaches a positive valued peak just before the centerline before dropping to zero at the diffuser axis.

The flatness factors of the 'radial' velocity component are larger in value than corresponding 'axial' values between the wall and the 'blue line'. The flatness values decrease in magnitude, approaching the Gaussian value of three in the region of the entry pipe radius before increasing in value and peaking at the diffuser axis. The flatness values of the 'radial' component in the core region of the diffuser flow are lower in magnitude than corresponding 'axial' component flatness values.

A comparison between skewness and flatness of the axial velocity measurements taken with the single wire boundary layer probe and the cross wire probe shows the cross wire results to be slightly larger than corresponding single wire results. The digitally obtained skewness results, $S(u)$ and $S(v)$, cross the zero value ahead of the corresponding analog results, otherwise no significant difference between analog and digital results can be determined.

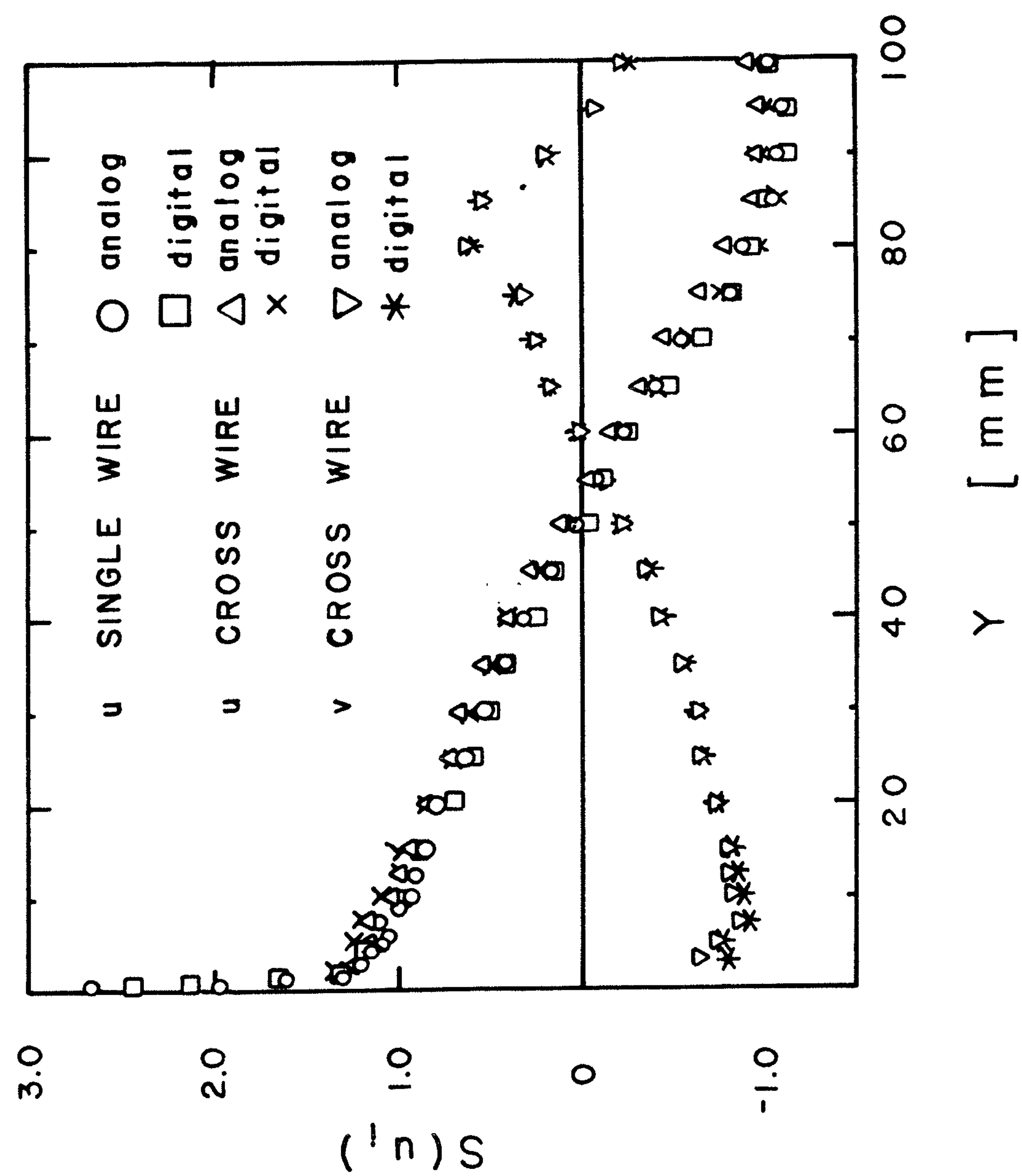

Figure 5.30: Skewness of u and v velocity components

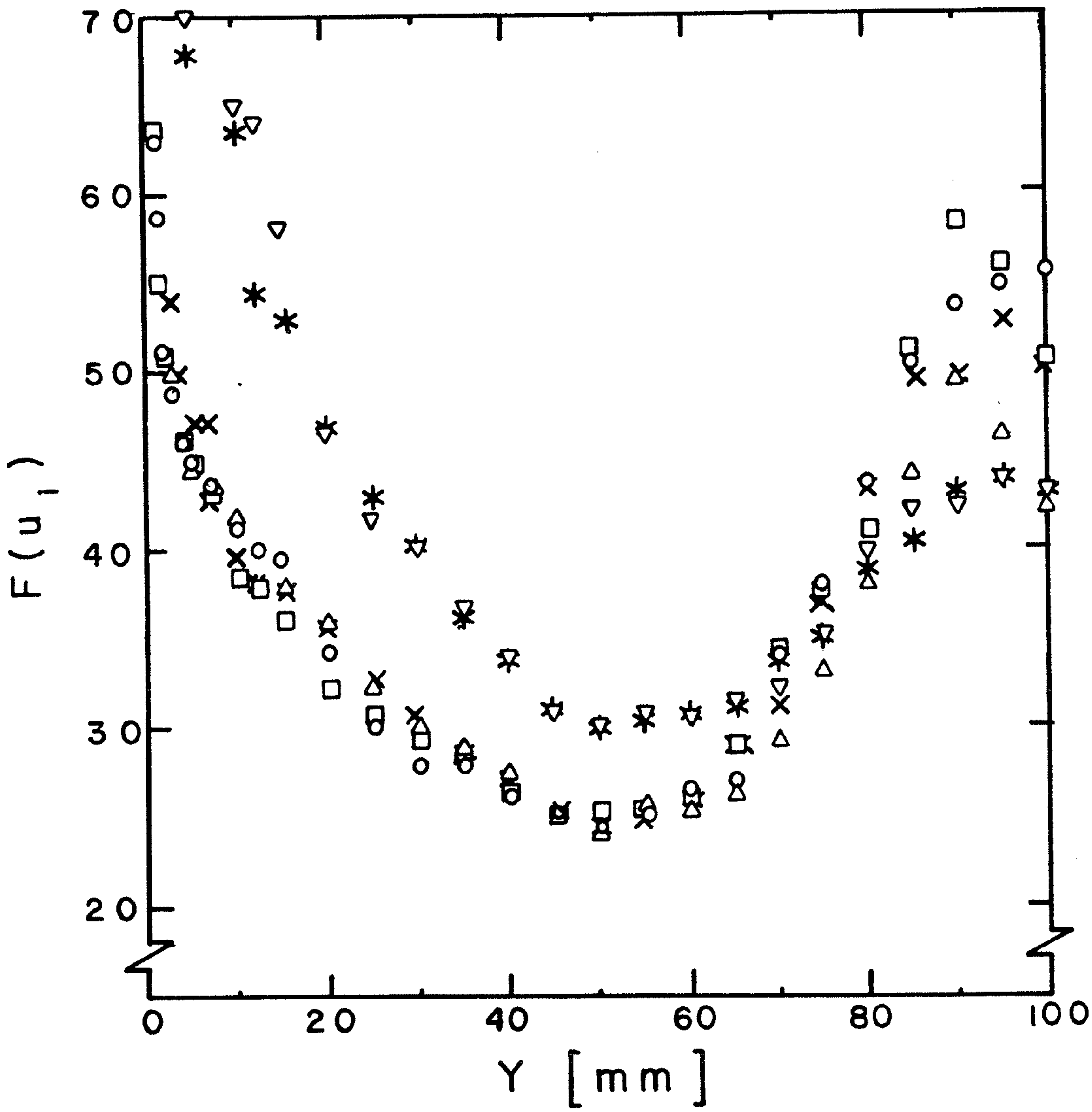

Figure 5.31: Flatness of u and v velocity components

5.2.4 Fifth and Sixth Order Moments

The higher order moments were digitally obtained through the single wire boundary layer probe. No circuit was available with which to determine and compare values obtained by analog means. The results are plotted in Figure 5.32. The fifth order moment, super skewness, is highly positive close to the diffuser wall, drops rapidly in the first 5 mm gradually approaching and crossing zero at the blue line before dropping to its minimum value in the region of the diffuser axis.

The plot of the sixth order moment, super flatness, follows the same pattern as the plot for kurtosis. A relative minimum is once again seen in the region of the entry pipe radius, Y = 50. The super flatness, $K_6(u)$, drops in value from 400 at Y = 0.5 to the Gaussian value of fifteen in the first third of the flow, continues to drop below 10 at Y = 50, and increases to 240 at the diffuser axis, Y = 95, before decreasing in value.

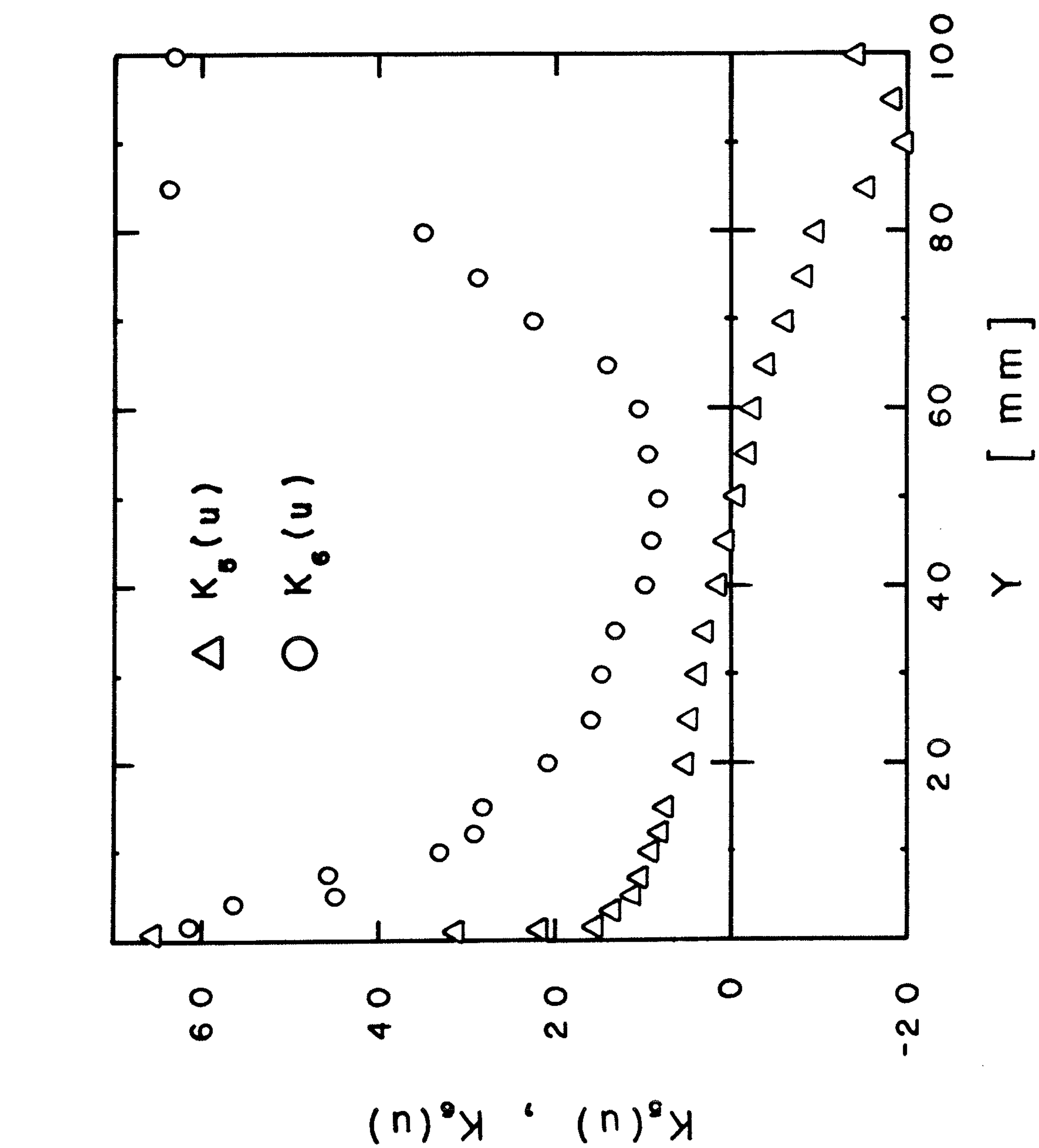

Figure 5.32: Super skewness and super flatness of u

5.2.5 Mixed moments

Simultaneous analog and digital third and fourth order correlations and their central moments were determined using a cross wire probe. The digital results were computed as central moments. The appropriate yaw corrections were applied to the correlation terms.

5.2.5.1 Correlation coefficient and Reynolds shear stress

The correlation coefficient $\overline{uv}/u'v'$ shown in Figure 5.33 vary in the 'radial' direction. They increase in value from the wall and reach a region of approximately constant value beginning at the blue line and extending approximately 20 mm before decreasing in value. Due to flow symmetry, the correlation coefficient has a value of zero at the diffuser axis and a sign change beyond. The region of constant coefficients has a value of approximately 0.5. Arora [1978], who took his measurements at right angles to the diffuser axis, reported a constant valued region of 0.4, slightly less than that found here for measurements taken at right angles to the diffuser wall.

The behaviour of the $\overline{uv}$ shear stresses taken in the diffuser and plotted both dimensionally and nondimensionally display a different character than those of similar plots for pipe flow or boundary layer flow.

The curve of the Reynolds shear stress $\overline{uv}$ shown in Figure 5.34 exhibits a linear region in the first 20 mm from the wall before increasing in slope and reaching a maximum value at the blue line. Two distinct linear regions are observed from the blue line to the diffuser axis. The first extends for approximately the following 20 mm and has a slightly negative slope. The second has a large negative slope and extends beyond the diffuser axis. The Reynolds shear stress, $\overline{uv}$, in the pipe are linear in nature between the wall and the central axis.

When comparing the analog and digital results, no significant difference is apparent.

5.2.5.2 Third Order Moments

Third order mixed moments are important as momentum transport terms. Triple correlations $\overline{uv^2}$ and $\overline{u^2v}$ were taken at right angles to the diffuser wall. Their central moments displayed distributions similar to that of other third order moments, the u and v skewness distributions.

The central moment of the $\overline{uv^2}$ correlation, although smaller in magnitude, is of the same sign as the skewness of the longitudinal velocity component: positive in the wall region and negative in the core region of the flow with the phase change occuring at the blue line and relative minimum, due to symmetry, occuring at the diffuser axis. As with the

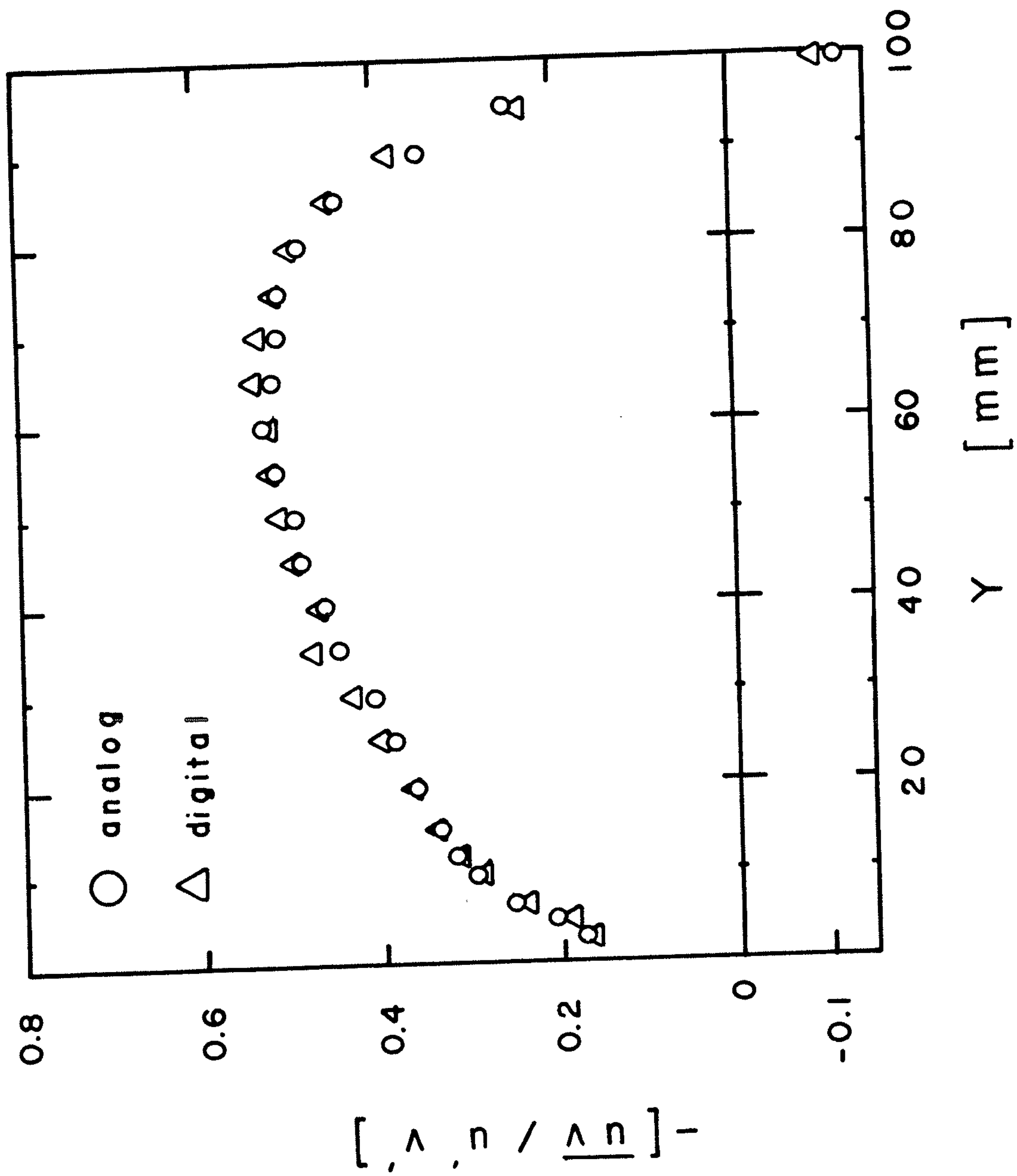

Figure 5.33: Correlation coefficient, $\overline{uv}/u'v'$

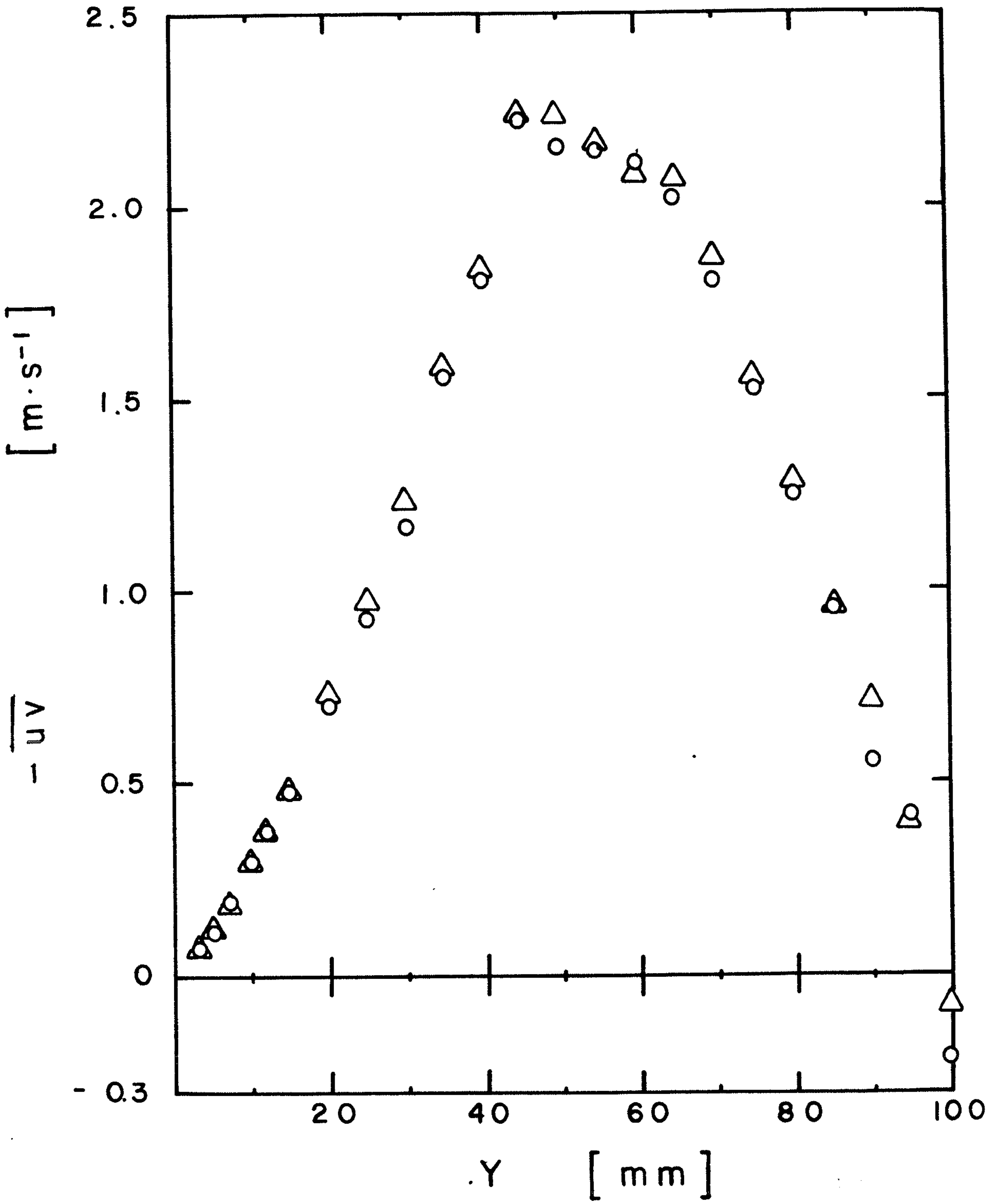

Figure 5.34: Reynolds shear stress, $\overline{uv}$

$\overline{uv}$ correlation, the corrected $\overline{uv^2}$ correlation displays a linear relationship in the first 20 mm from the diffuser wall before increasing in slope. The $\overline{uv^2}$ correlation has an absolute maximum just before the blue line and a minimum midway between the blue line and diffuser axis.

The central moment of the $\overline{u^2v}$ correlation is smaller in magnitude but of the same sign as the skewness of the 'radial' velocity component. As with the S(v) distribution, the $\overline{u^2v}/u'^2v'$ distribution changes sign twice: first just after the blue line and second at the diffuser axis. Similar to the $\overline{uv^2}$ distribution, the plot of the $-(\ \overline{u^2v}\ )$ distribution approaches zero at the wall, and reaches maximum and minimum values just before the blue line and midway between the blue line and diffuser axis respectively.

No significant difference is seen between the analog and digital measurements although the $\overline{u^2v}$ correlations and central moments display more scatter in the vicinity of the wall and diffuser axis.

The triple velocity correlations taken in the diffuser behave differently from those in fully developed pipe flow or boundary layer flow. From looking at the local velocity profile, the main mean strain rate in this flow is also different than that of fully developed pipe flow and boundary layer type flow. This implies that the process of producing turbulence, or extracting energy from the mean flow, has a different mechanism in the diffuser flow than in pipe flow or boundary layer flow.

5.2.5.3 Fourth Order Moments

Simultaneous analog and digital quadruple correlations $\overline{uv^3}$, $\overline{u^2v^2}$, and $\overline{u^3v}$ and their central moments were taken at right angles to the diffuser wall. Unlike the mixed third order moments, the mixed fourth order moments do not exhibit the same trends in distributions as the u and v flatness factors although all three plots of the central moments show minimum values occuring at the blue line. The magnitudes of these central moments are lower than either flatness factors of the u or v velocity components everywhere in the field. All three central moments exhibit a complex wave-like distribution of points while the correlations increase in magnitude from the wall forming a sharp peak at the blue line before decreasing in magnitude towards the diffuser axis.

The mixed fourth order velocity correlations can be divided into two groups. The first grouping consists of the even powered components $\overline{u^2v^2}$, and the second grouping consists of the odd powered components $\overline{uv^3}$ and $\overline{u^3v}$. Both groups exhibit different behaviours.

The $\overline{u^2v^2}/u'^2v'^2$ wave-like distribution fluctuates between values of one and three. The distribution approaches the upper limit of three in proximity of the wall and the lower

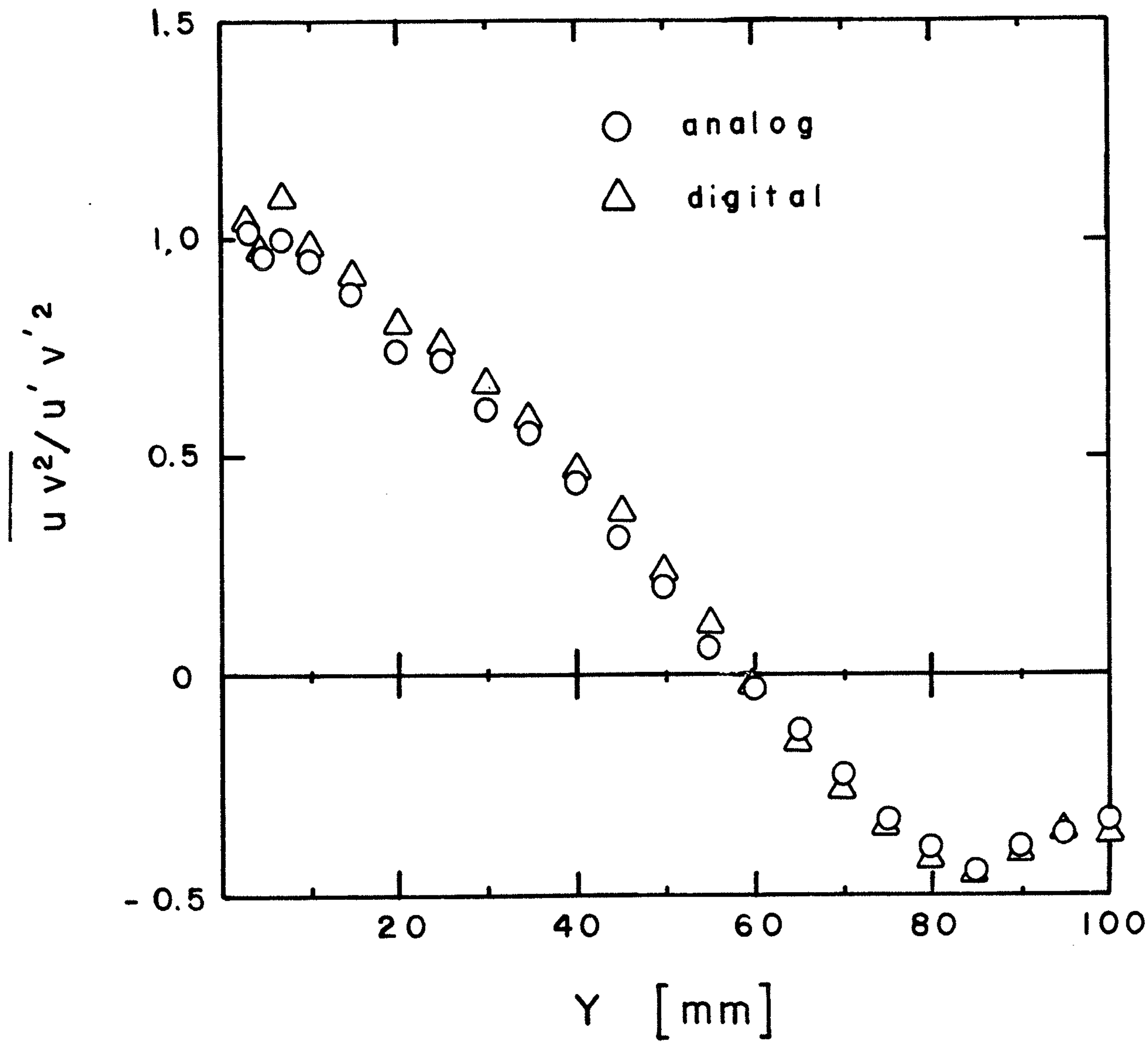

Figure 5.35: $\overline{uv^2}$ central moment

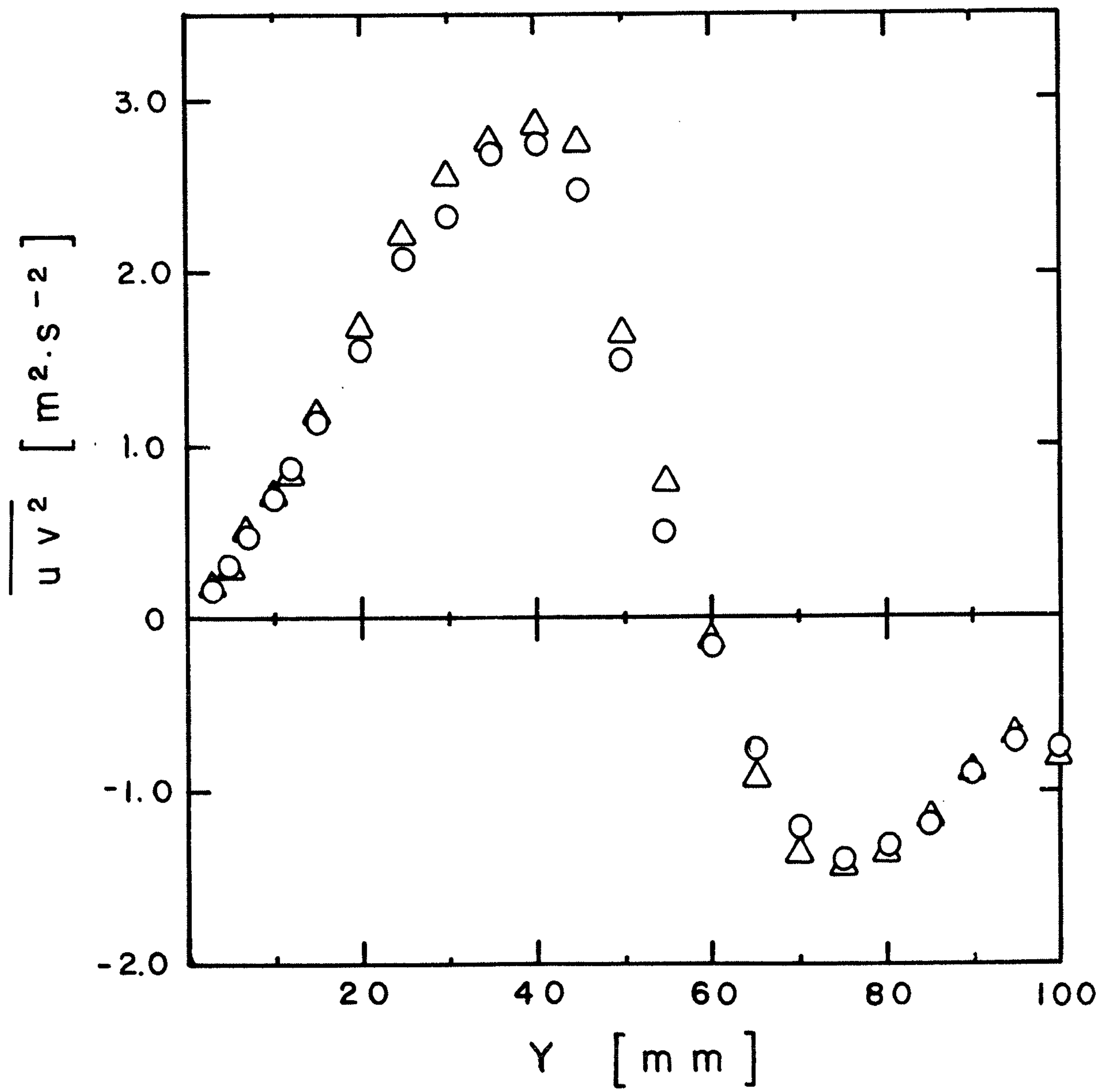

Figure 5.36: $\overline{uv^2}$ correlation

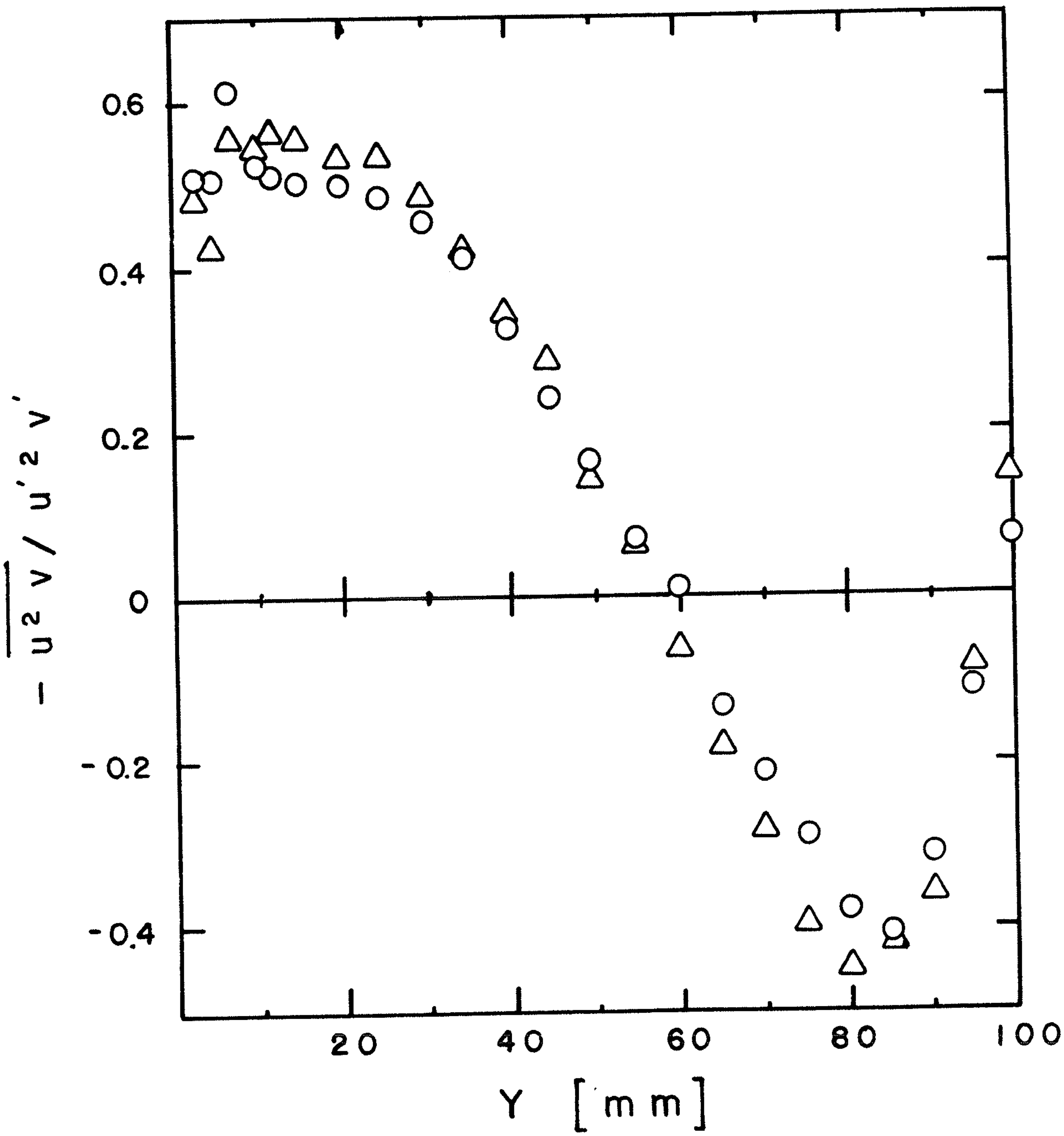

Figure 5.37: $\overline{u^2v}$ central moment

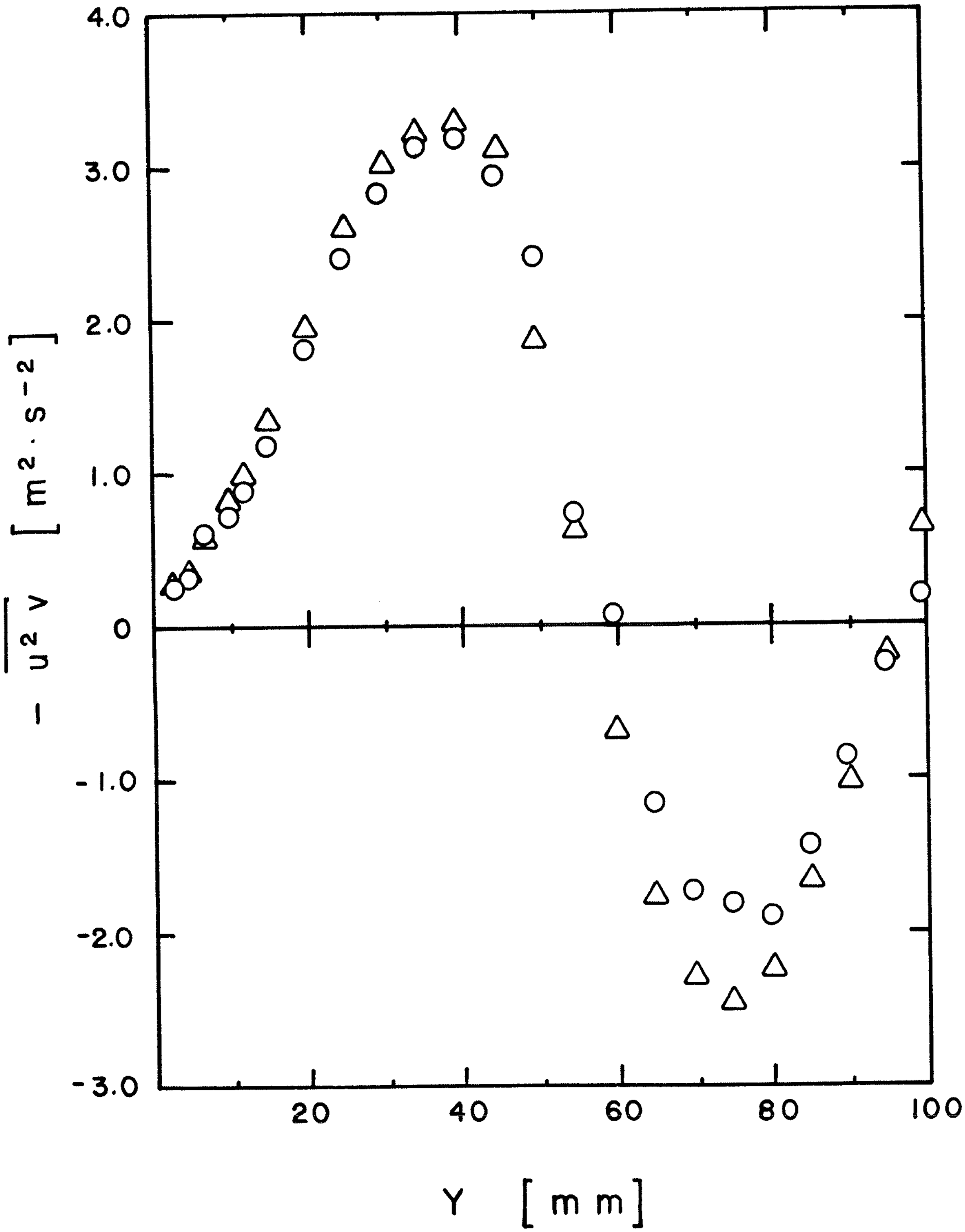

Figure 5.38: $\overline{u^2 v}$ correlation

limit of one at the blue line. Since both components are even powered, the $\overline{u^2v^2}$ correlations and central moments are positive and have a definite value at the axis. A relative minimum occurs in the core region approaching the diffuser axis. Except in close proximity to the wall, little scatter is observed between the analog and digital data points.

The fourth order moments with odd powered components have the same sign as the Reynolds shear stress $\overline{uv}$, and as such have a zero crossing at the diffuser axis. Both central moments, $\overline{uv^3}/u'v'^3$ and $\overline{u^3v}/u'^3v'$, as with results from Arora [1978], collapse onto the same curve in the core region of the flow. The $\overline{u^3v}/u'^3v'$ central moment was lower in value than the $\overline{uv^3}/u'v'^3$ central moment in the wall region of the flow. In both distributions, the values of the central moments approached a value of one at the blue line. Again, no significant difference between the analog and digital data exists.

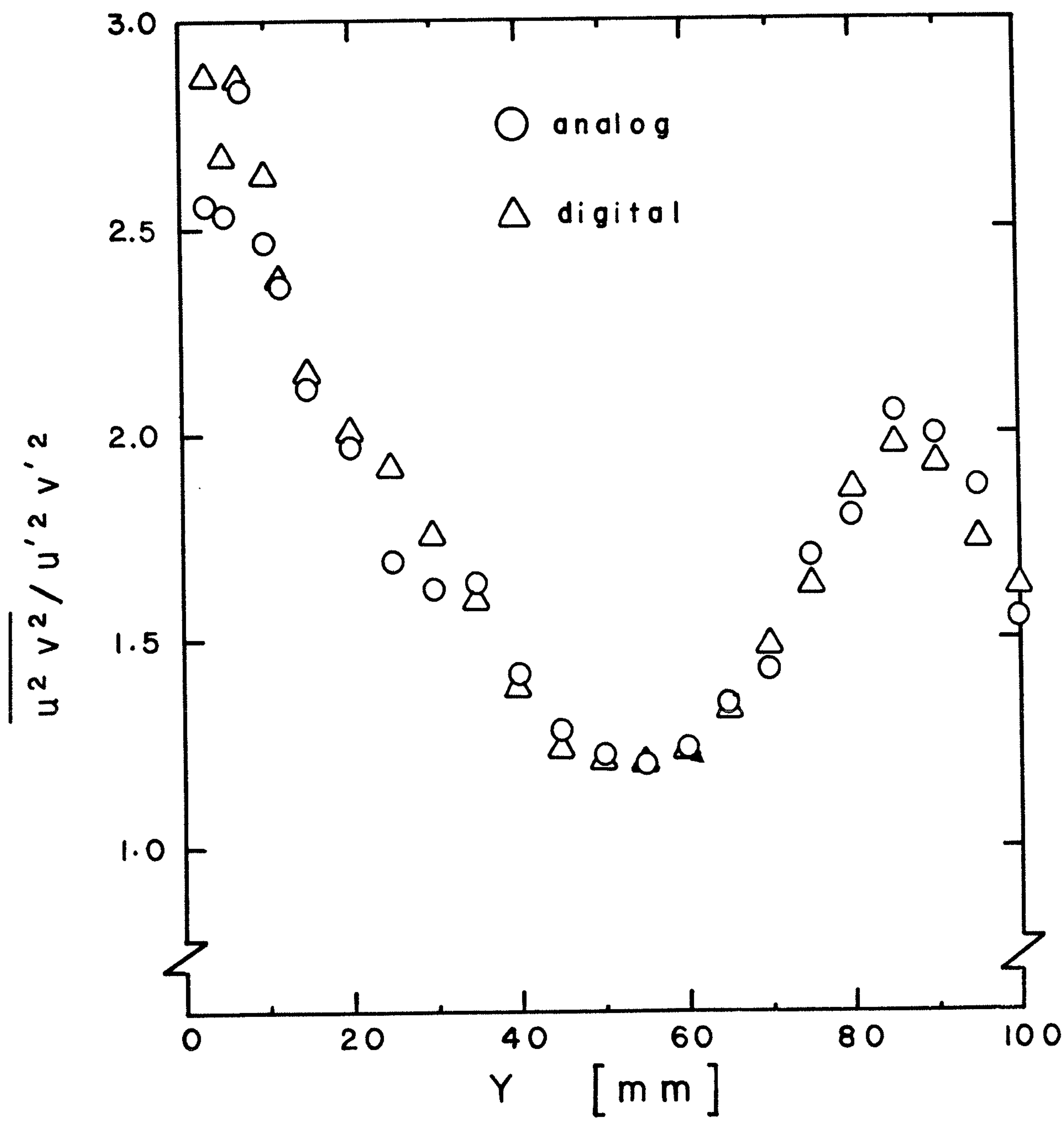

Figure 5.39: $\overline{u^2v^2}$ central moment

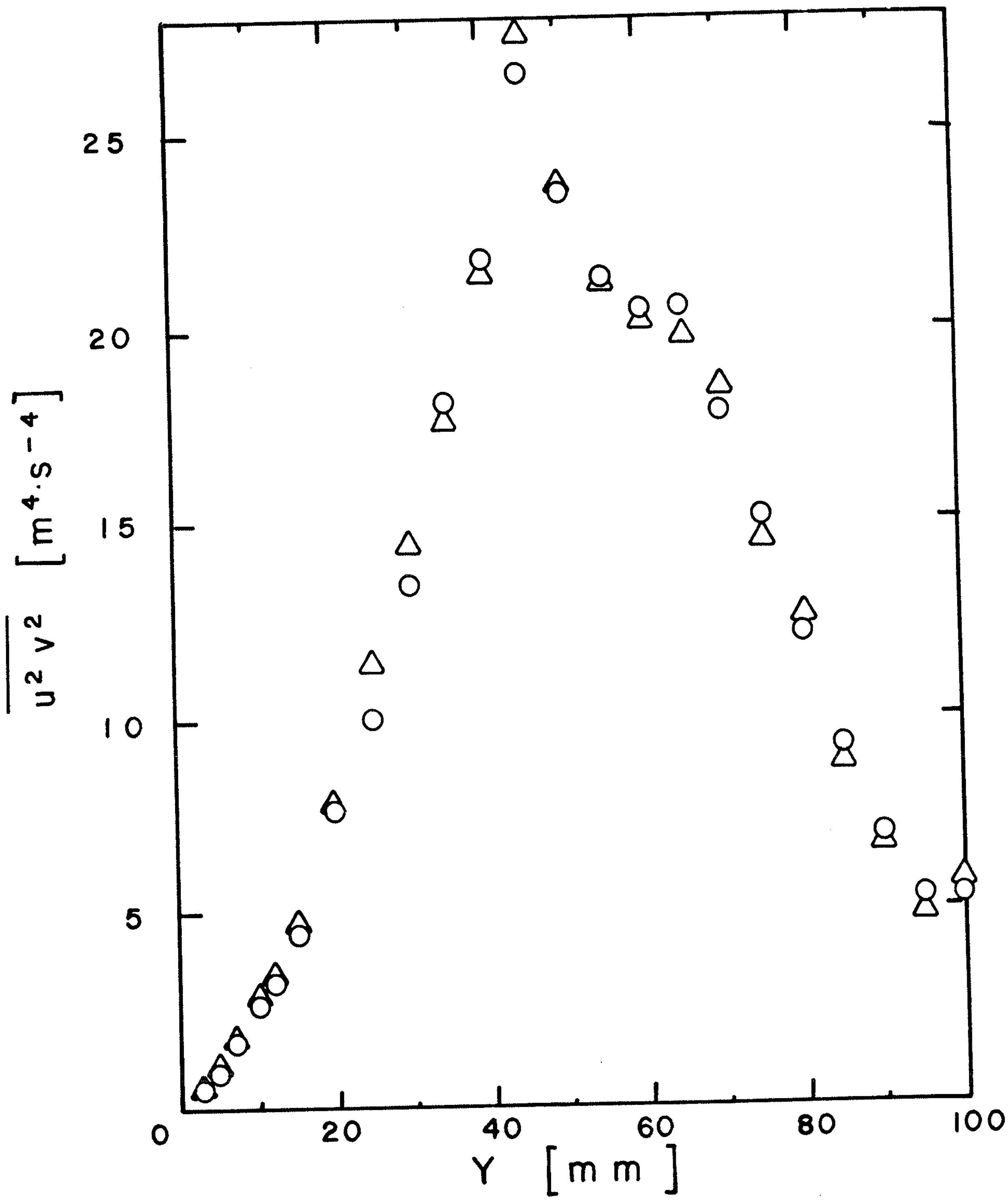

Figure 5.40: $\overline{u^2v^2}$ correlation

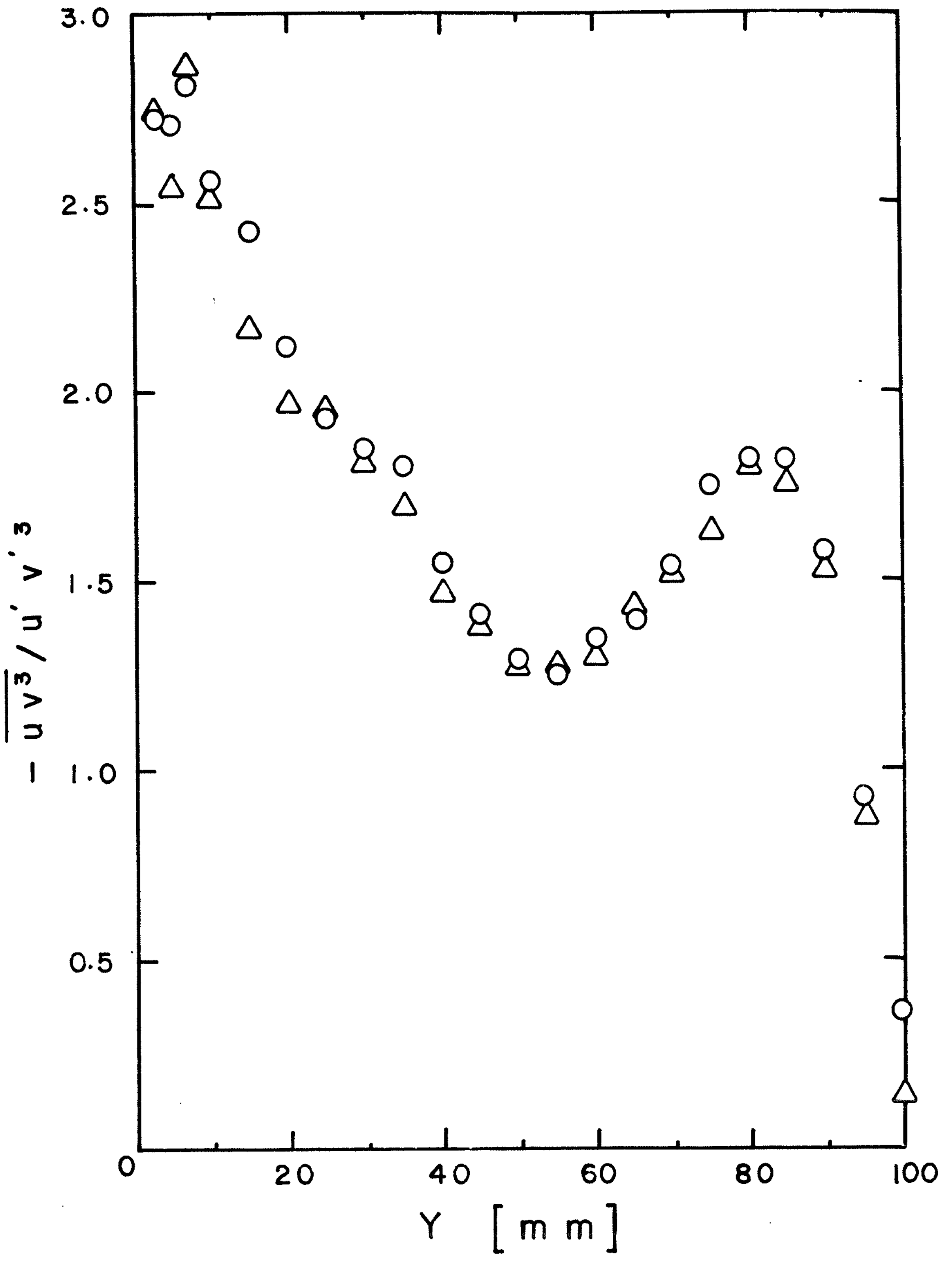

Figure 5.41: $\overline{uv^3}$ central moment

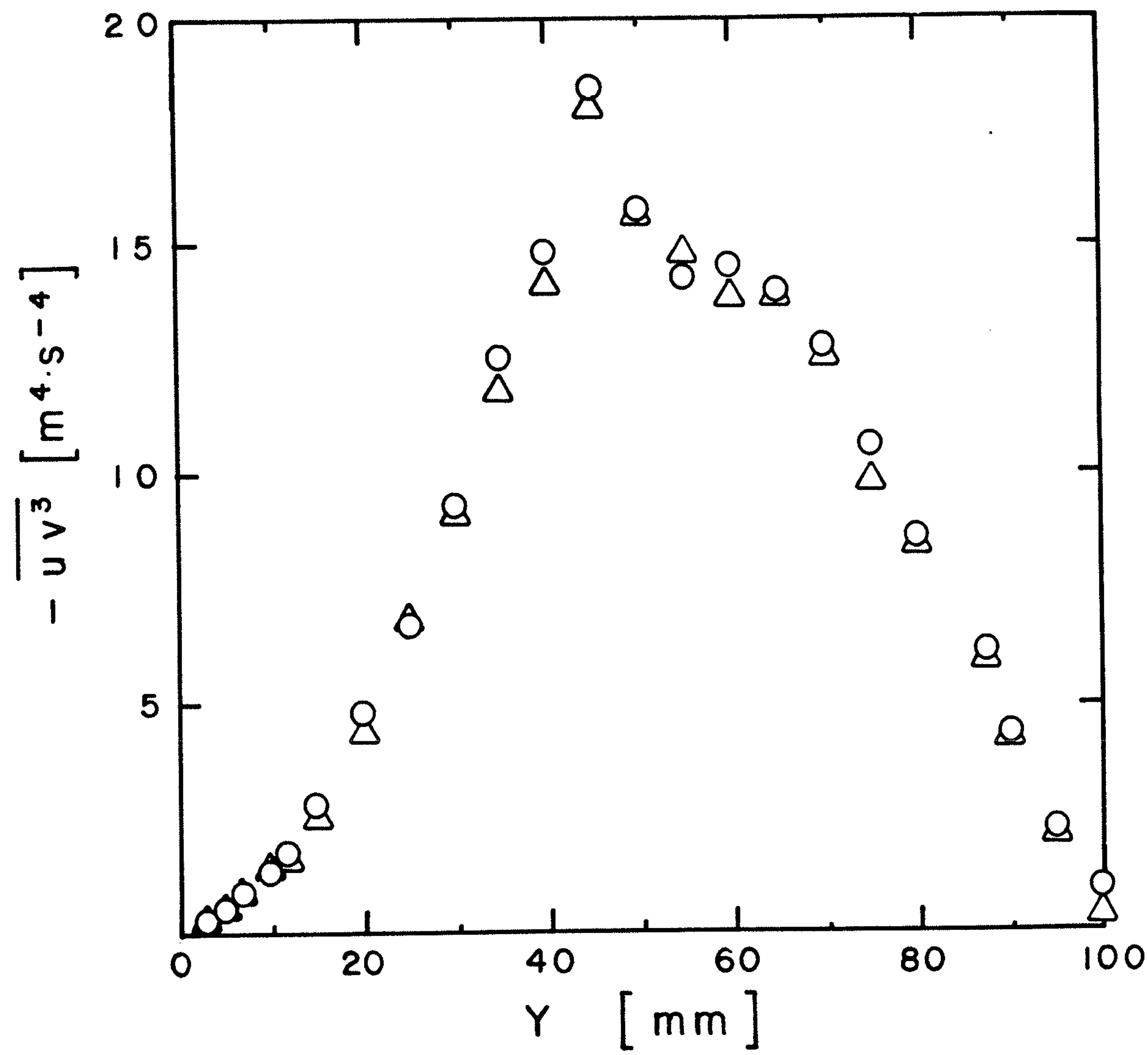

Figure 5.42: $\overline{uv^3}$ correlation

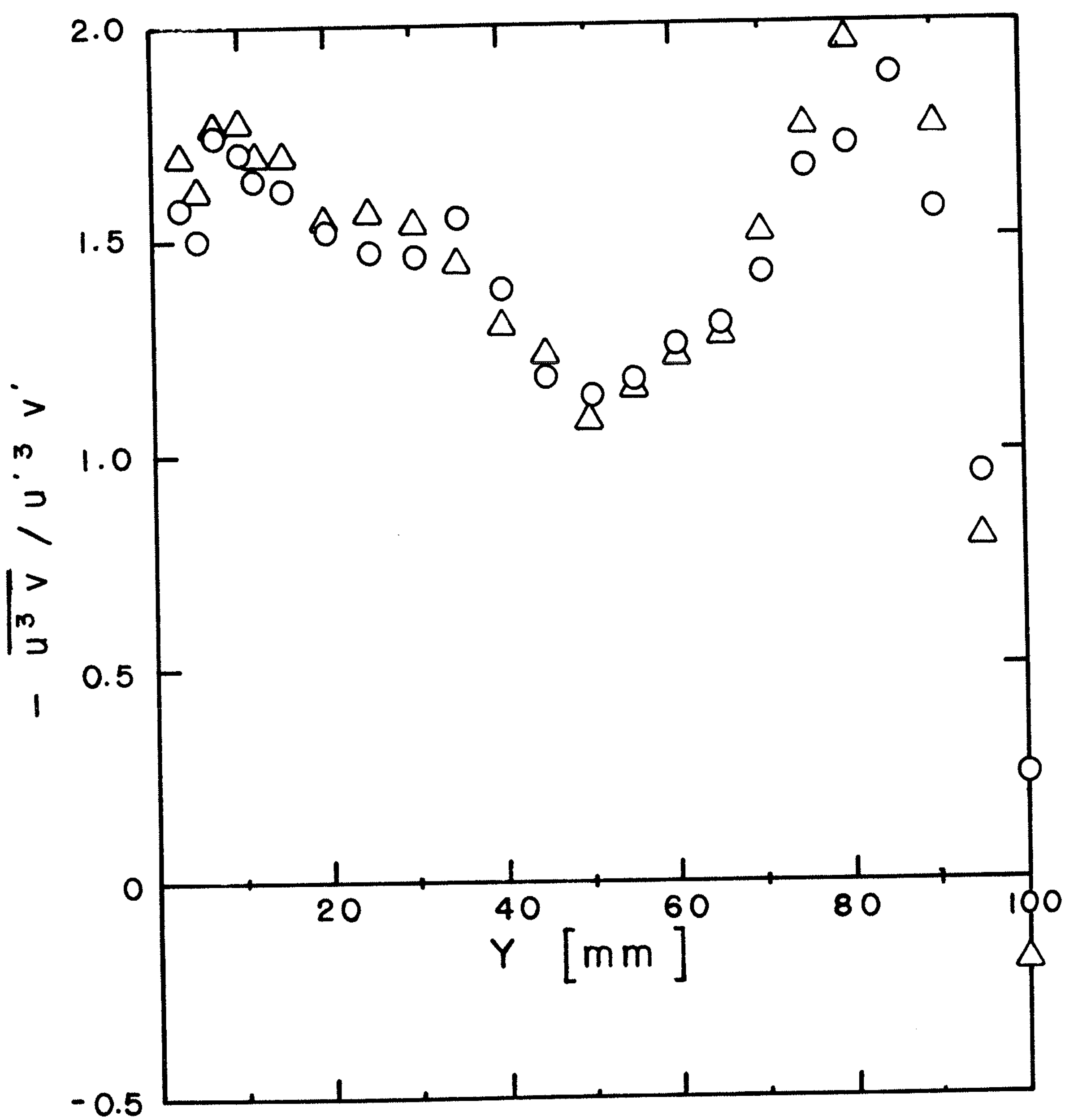

Figure 5.43: $\overline{u^3 v}$ central moment

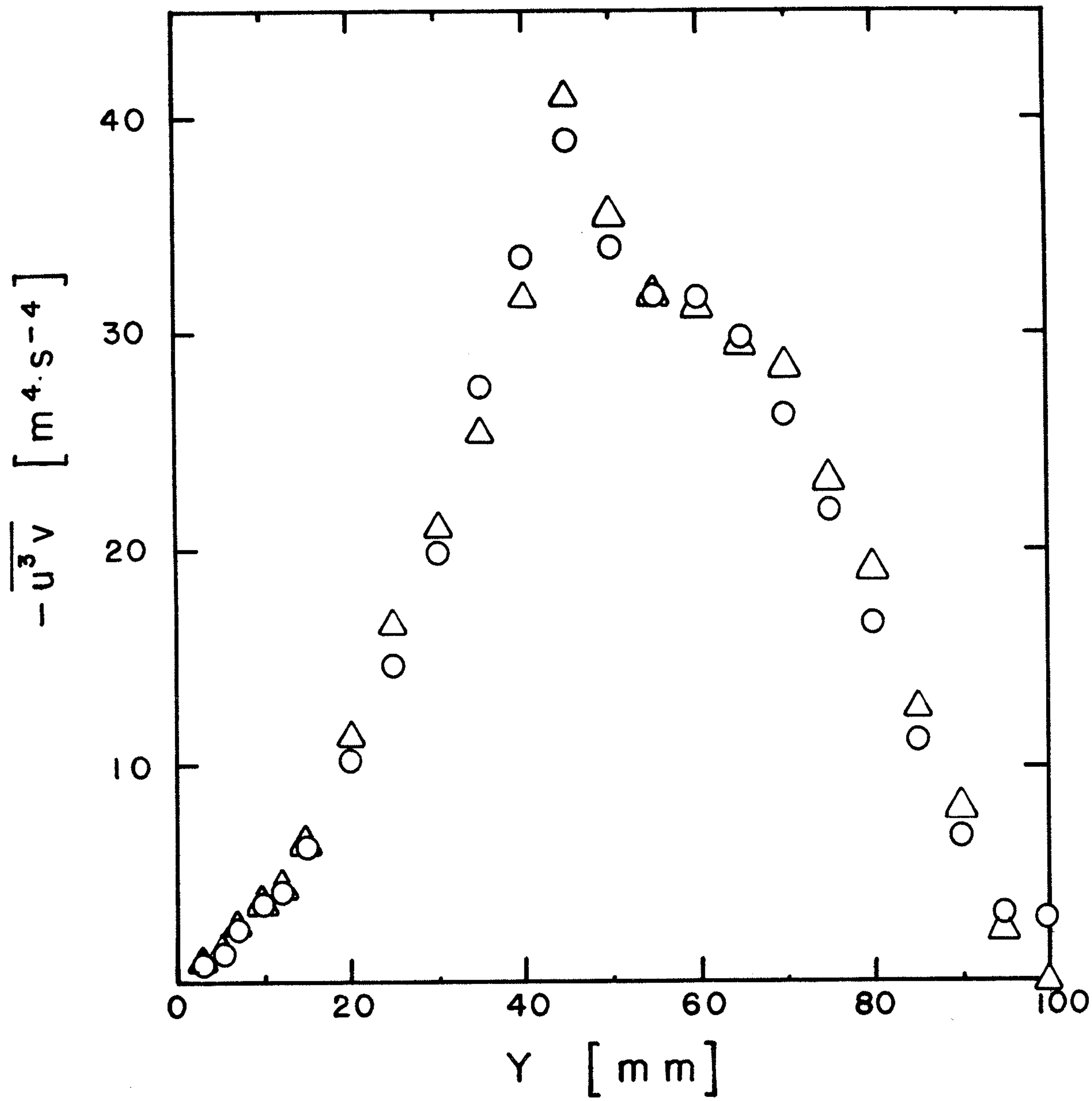

Figure 5.44: $\overline{u^3v}$ correlation

5.3 MOMENTS OF THE LONGITUDINAL VELOCITY DERIVATIVE

The central moments of the longitudinal velocity derivative $\partial u/\partial t$ were taken at right angles to the diffuser wall with a single wire boundary layer probe. The linearized hot wire signal was filtered at the Kolmogorov frequency f(K), differentiated and again filtered at the Kolmogorov frequency f(K) before analog and digital processing to determine the central moments of the differentiated velocity signal. The results are shown in Figures 5.45 to 5.48 inclusive.

The skewness of $\partial u/\partial t$ show two levels, one on each side of the blue line. The wall layer has a nearly constant value of 0.58 gradually decreasing to a nearly constant value of 0.42 in the core. Measurements taken very close to the wall indicate negative values of skewness in the first $^3/_4$ mm from the wall. A fair bit of scatter (10% to 16%) is seen between the analog and digital measurements taken in the wall layer. The digital measurements show a consistently higher value than the corresponding analog measurements.

The values of the flatness factors $K(\partial u/\partial t)$ are high in proximity to the wall. As distance from the wall is increased the values of $K(\partial u/\partial t)$ are decreased, approaching a lower limit of six in the region of the blue line. The values of the flatness factors in the core region increase to a relative maximum, approaching nine, at the diffuser axis. Then due to symmetry, they begin to decrease in value. The velocity derivative displays none of the ordered randomness seen in the fourth order moment of the longitudinal velocity in the boundary layer and diffuser flows. No significant difference between the analog and digital results is apparent in the flatness factors of the velocity derivative.

Azad and Hummel [1971] have shown that from the wall to the blue line, the fine structure of the flow is highly intermittent. Intermittency is characterized by high values of kurtosis although high values of kurtosis does not prove intermittency. Once intermittency is established, it can be estimated from the flatness factor and the relationship $\gamma = 3/K(\partial u/\partial t)$ where γ is the intermittency factor. For a very intermittent signal $K(\partial u/\partial t)$ is large and γ is therefore small. Here, the large values of the flatness factor indicate the wall layer to be very intermittent ($\gamma < 0.5$). The highly intermittent nature of the flow would help account for some of the fluctuations in the collective results.

Although no analog results are available, the digital results of the fifth and sixth central moments of the velocity derivative are shown to be highly positive in proximity to the wall. They decrease in value towards the blue line and remain relatively constant from the blue line to a point approximately midway between the blue line and the diffuser axis before rising and peaking in value in the vicinity of the diffuser axis.

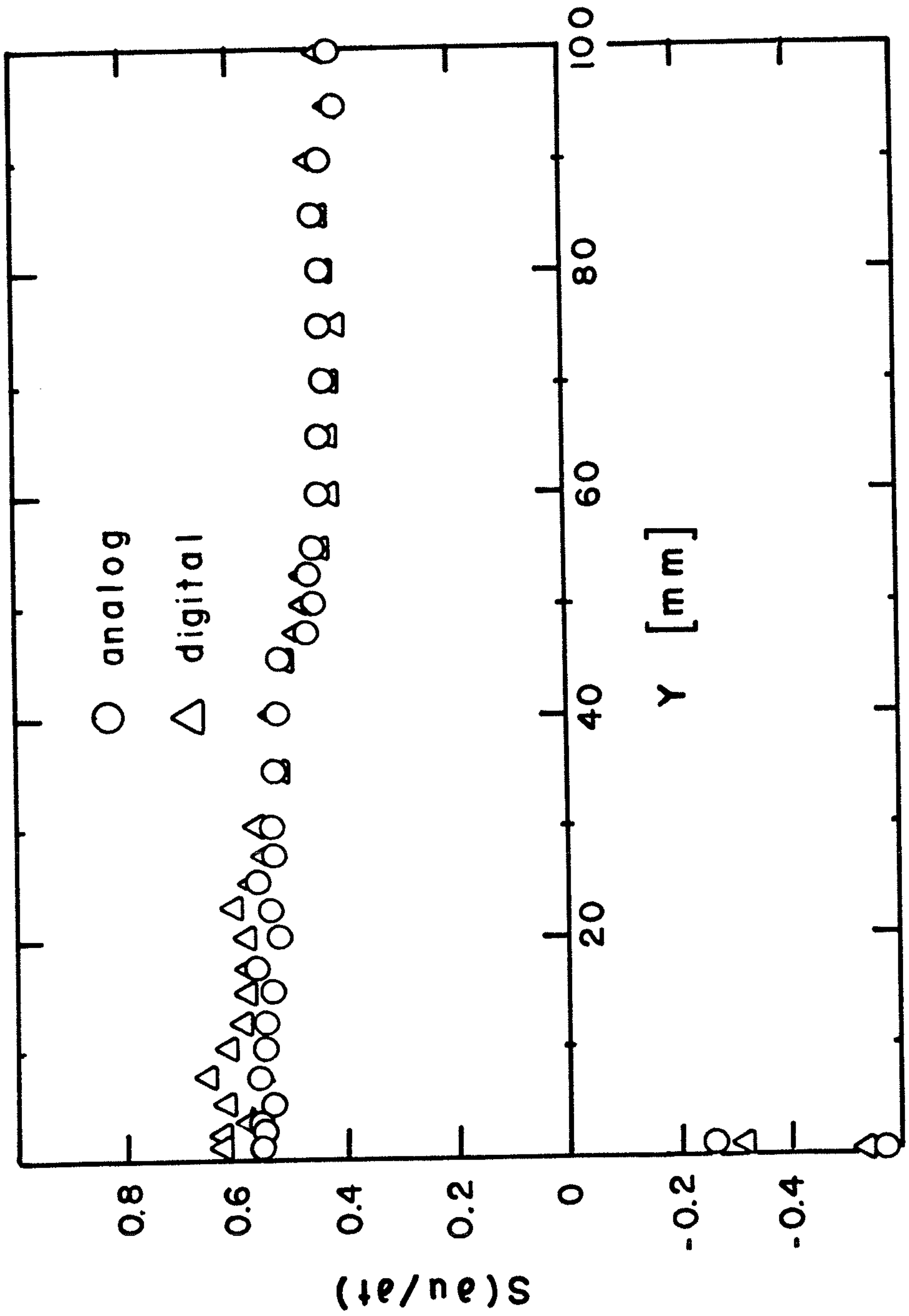

Figure 5.45: Skewness of the velocity derivative

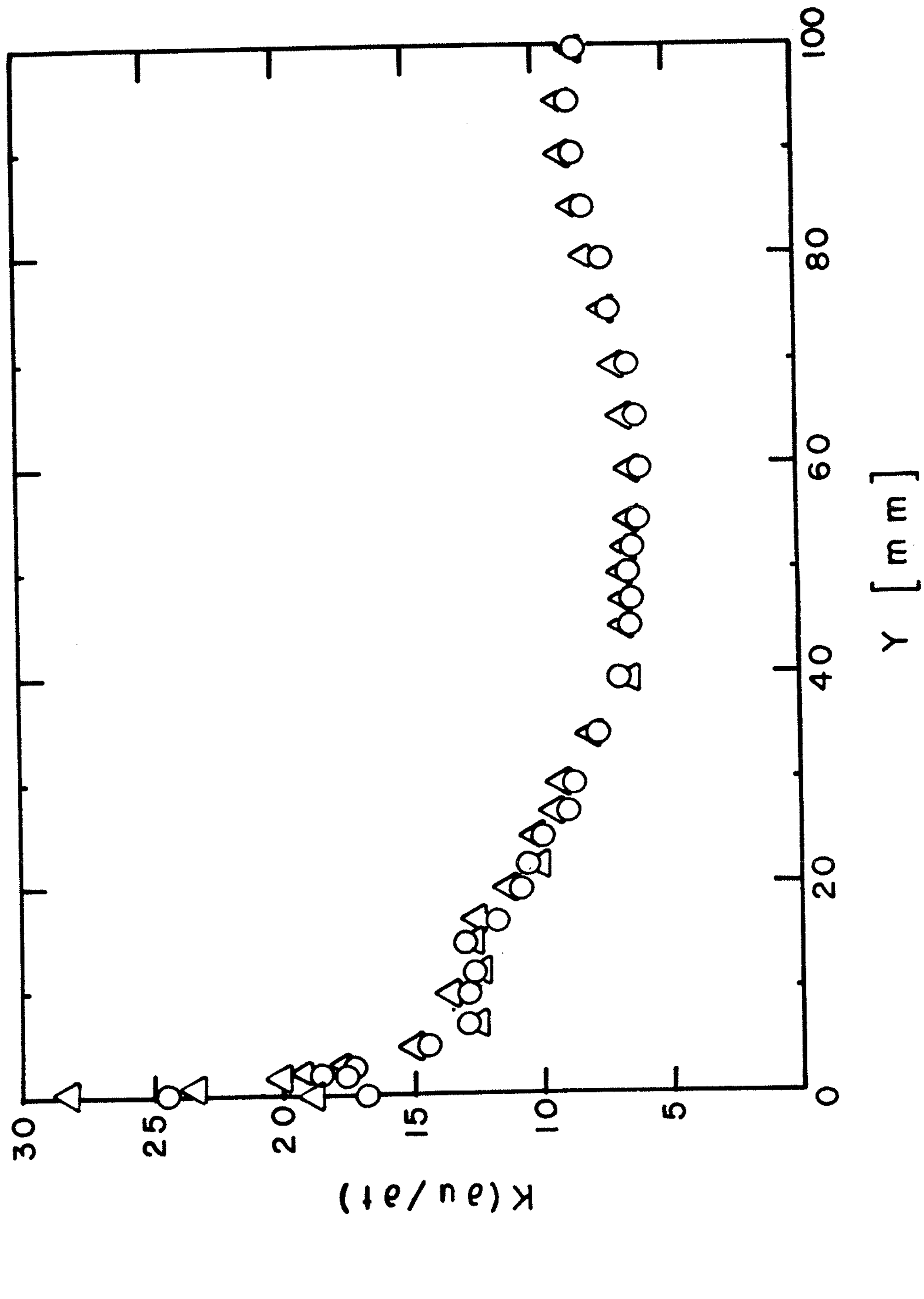

Figure 5.46: Flatness of the velocity derivative

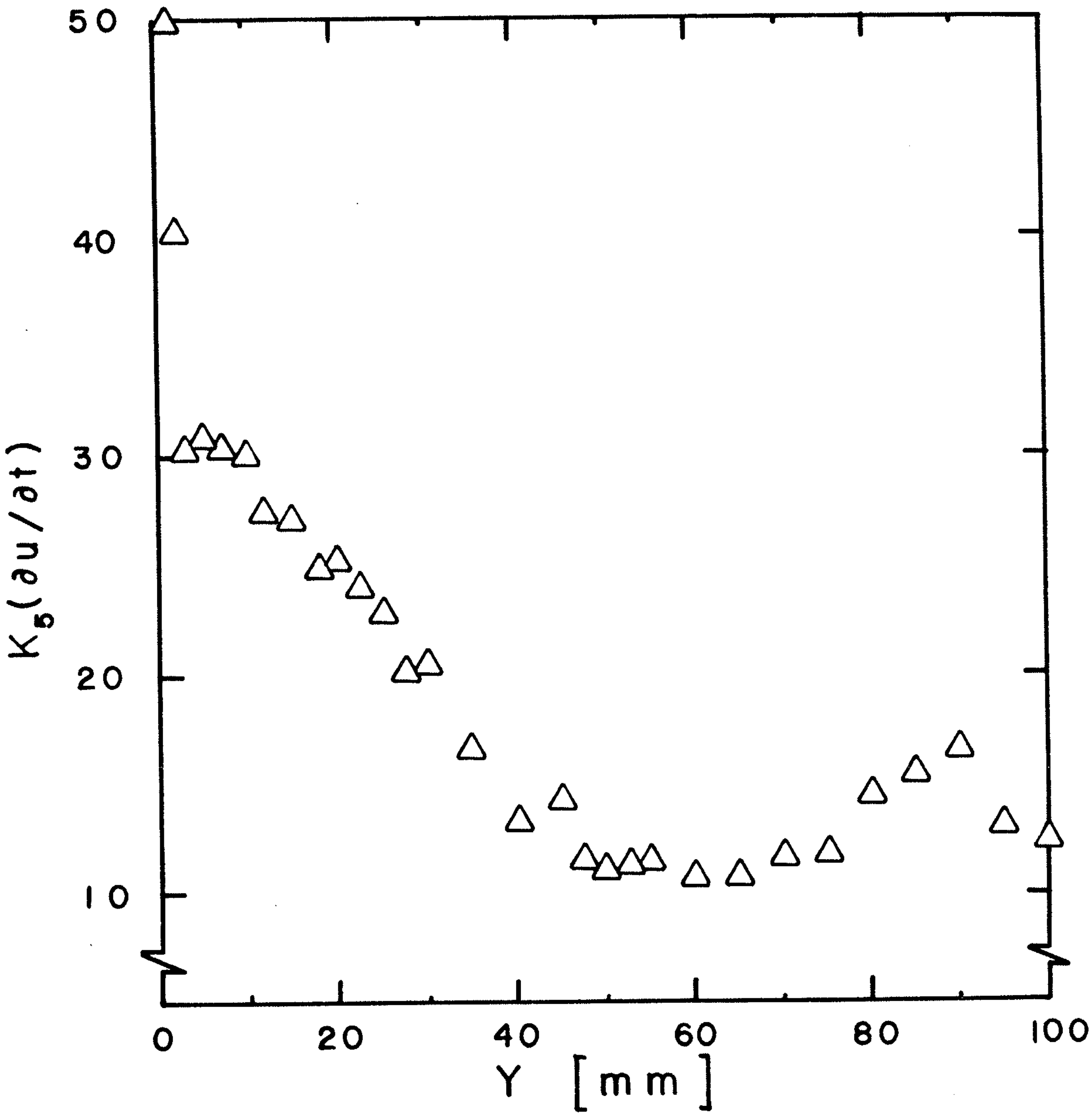

Figure 5.47: Super skewness of the velocoity derivative

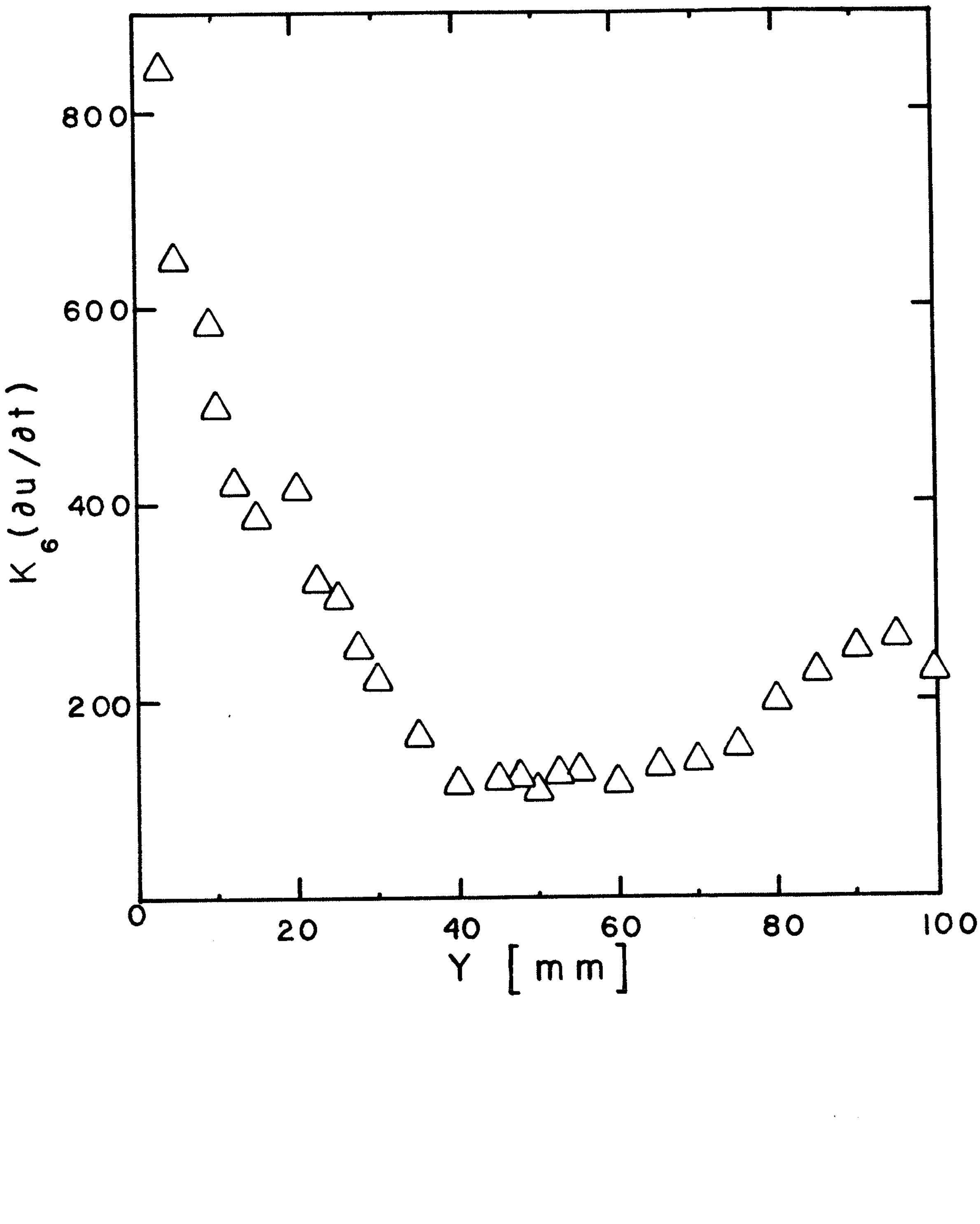

Figure 5.48: Super flatness of the velocity derivative

5.4 PROBABILITY DENSITY MEASUREMENTS

The probability densities of the longitudinal and transverse velocities in the diffuser were measured using a single wire boundary layer probe and a cross wire probe placed at right angles to the diffuser wall. The hot wire signal was collected and processed by the PDP-11 computer using programs developed by Derksen [1986]. The probability density results were plotted by the Hewlett·Packard plotter after processing. The results from the cross wire probe, due to signal inversion prior to processing, are the mirror image of the true PDF's, shown by the single wire results.

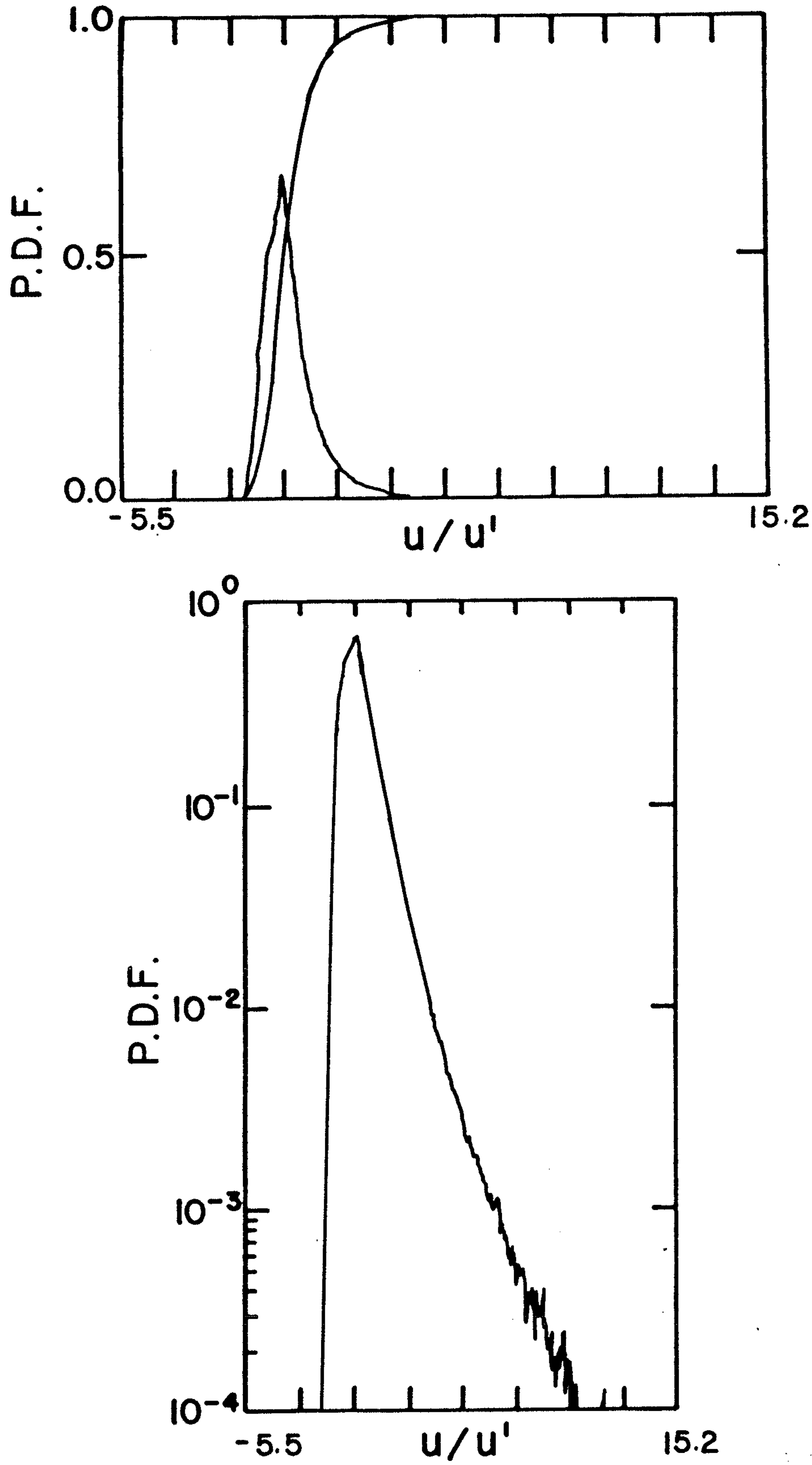

Figure 5.49: Single wire PDF(u/u') at y = 0.5 mm

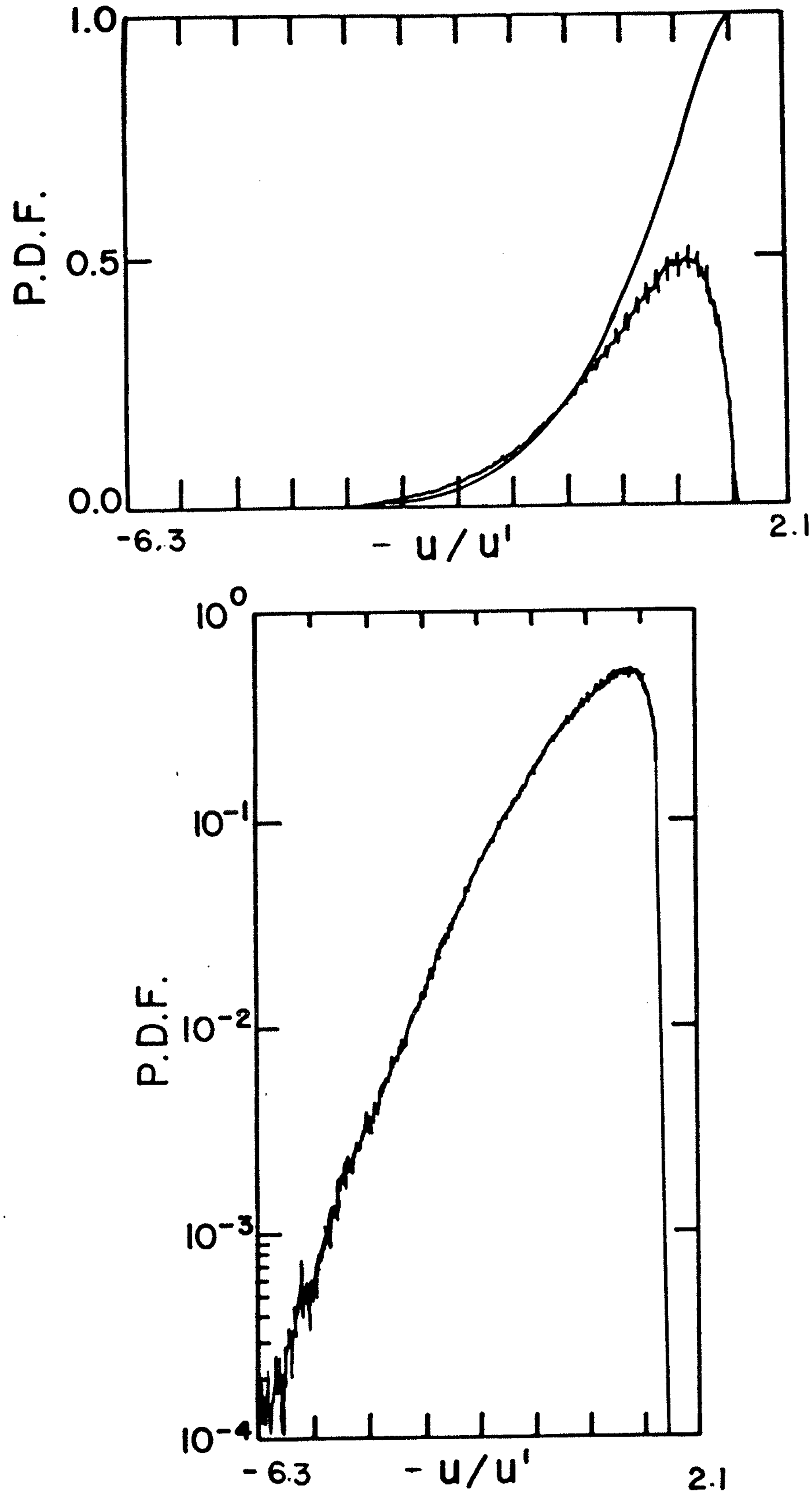

Figure 5.50: Cross wire PDF(u/u') at y = 3 mm
S(u)=1.193 F(u)=4.743

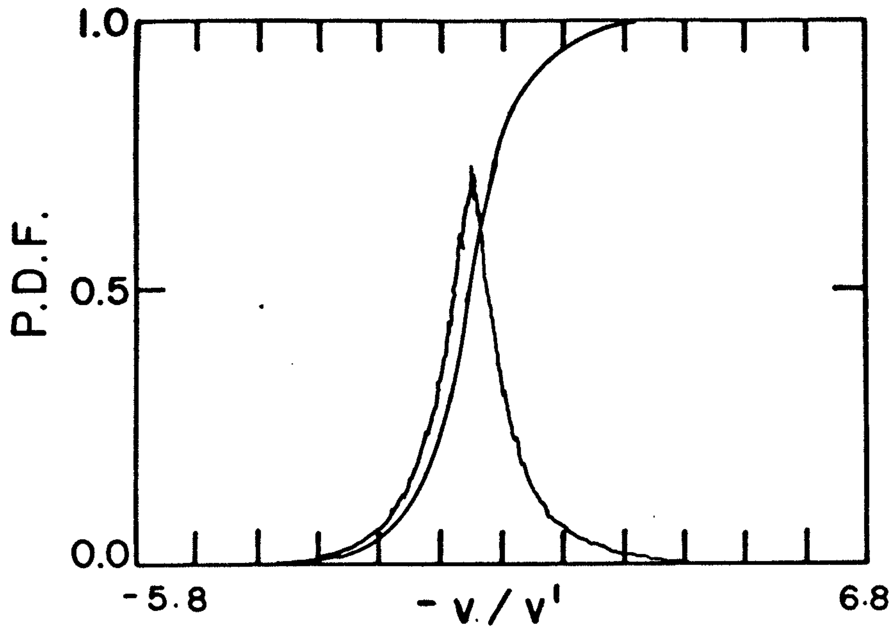

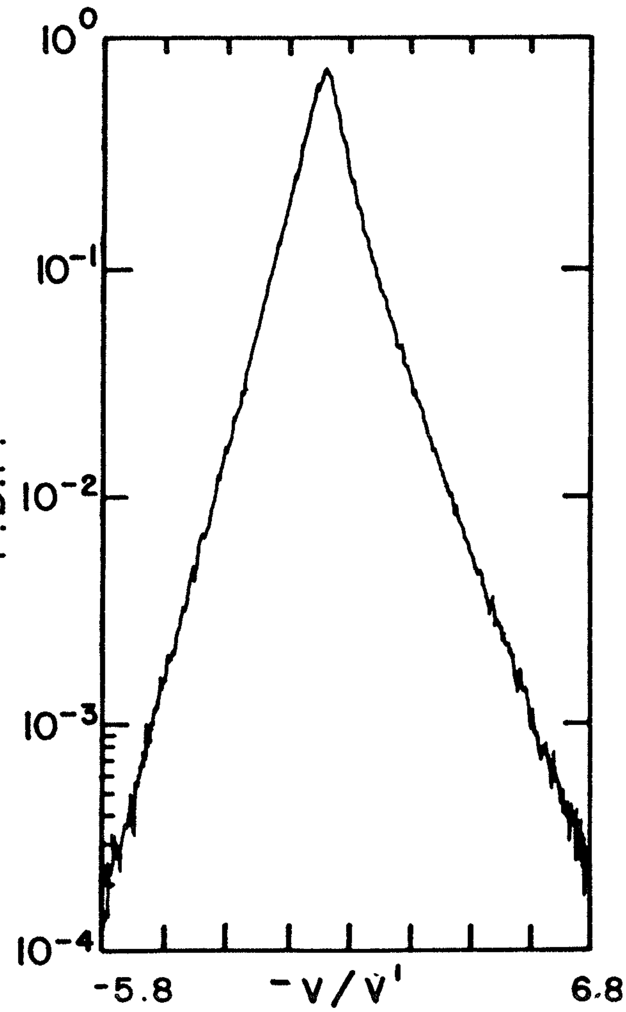

Figure 5.51: Cross wire PDF(v/v') at y = 3 mm
S(v)=-0.529 F(v)=7.370

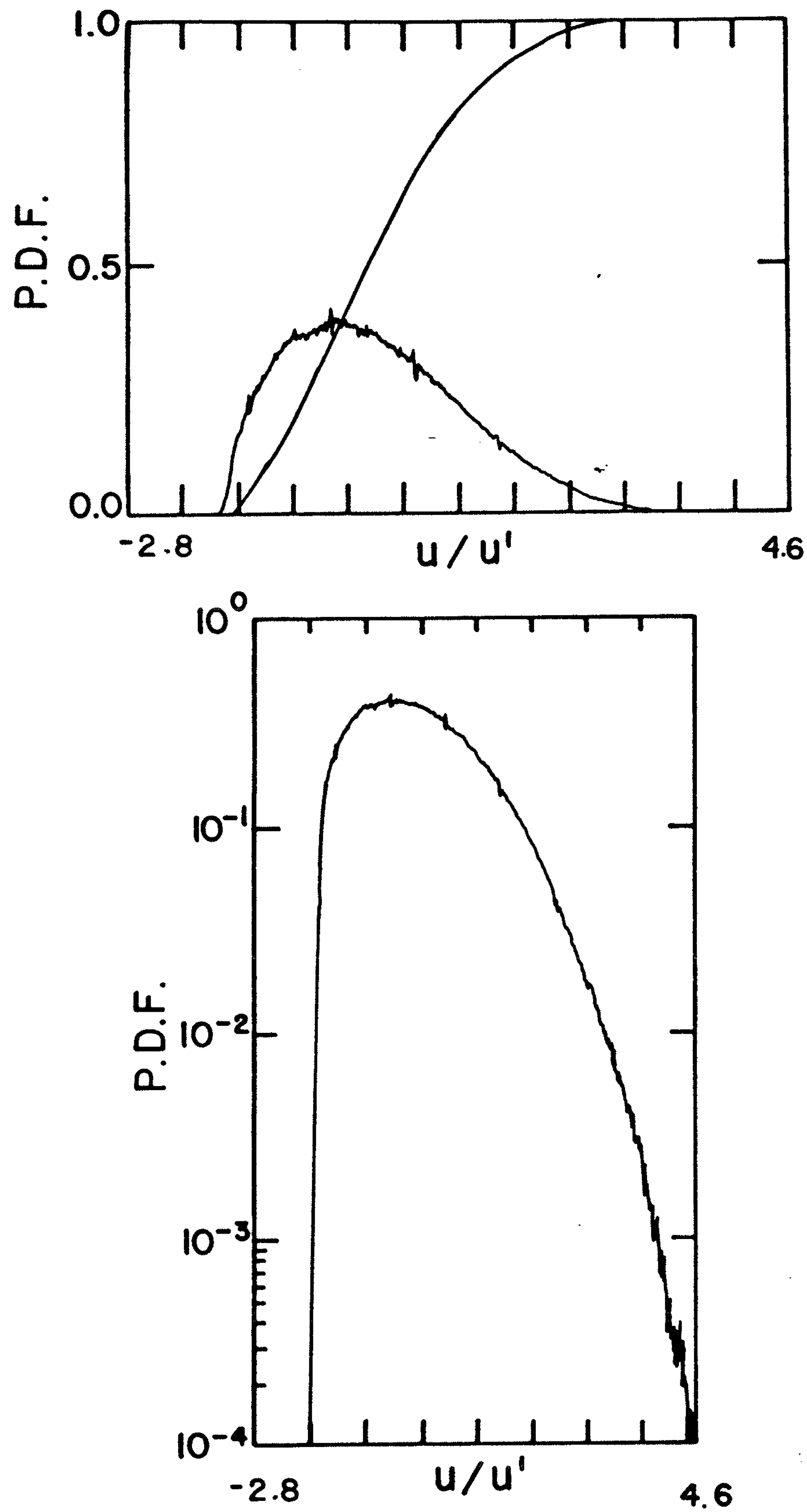

Figure 5.52: Single wire PDF(u/u') at y = 25 mm

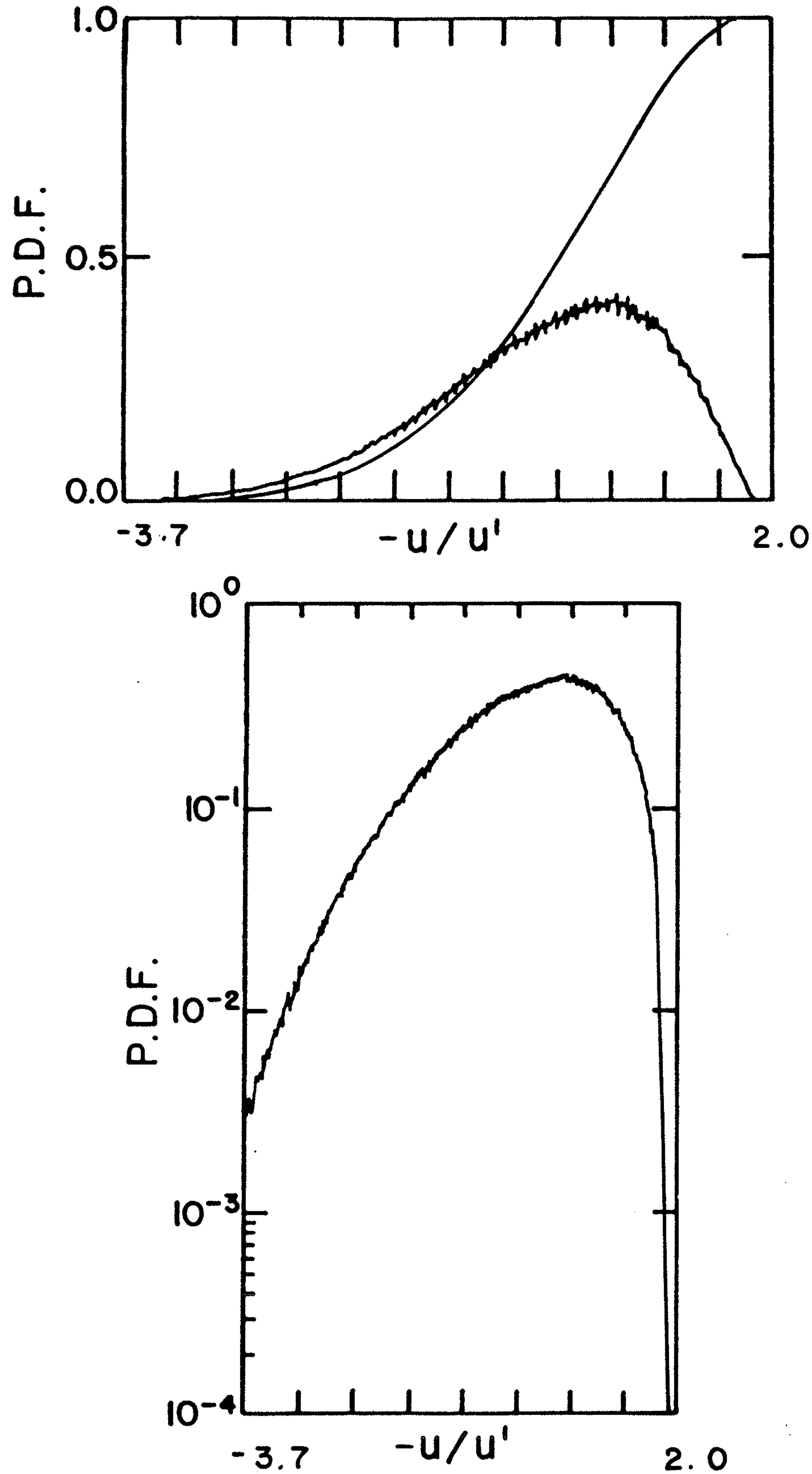

Figure 5.53: Cross wire PDF(u/u') at y = 25 mm
S(u)=0.634 F(u)=4.222

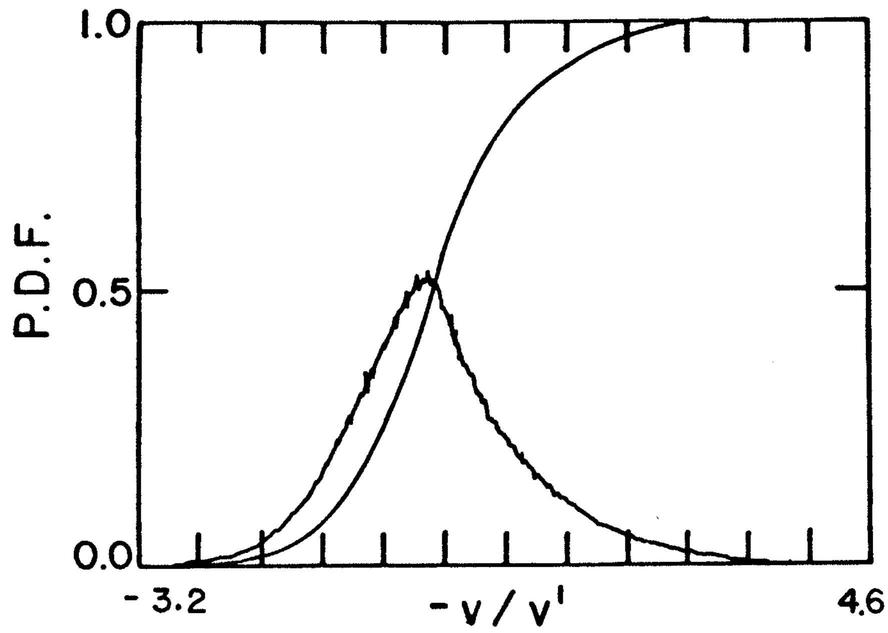

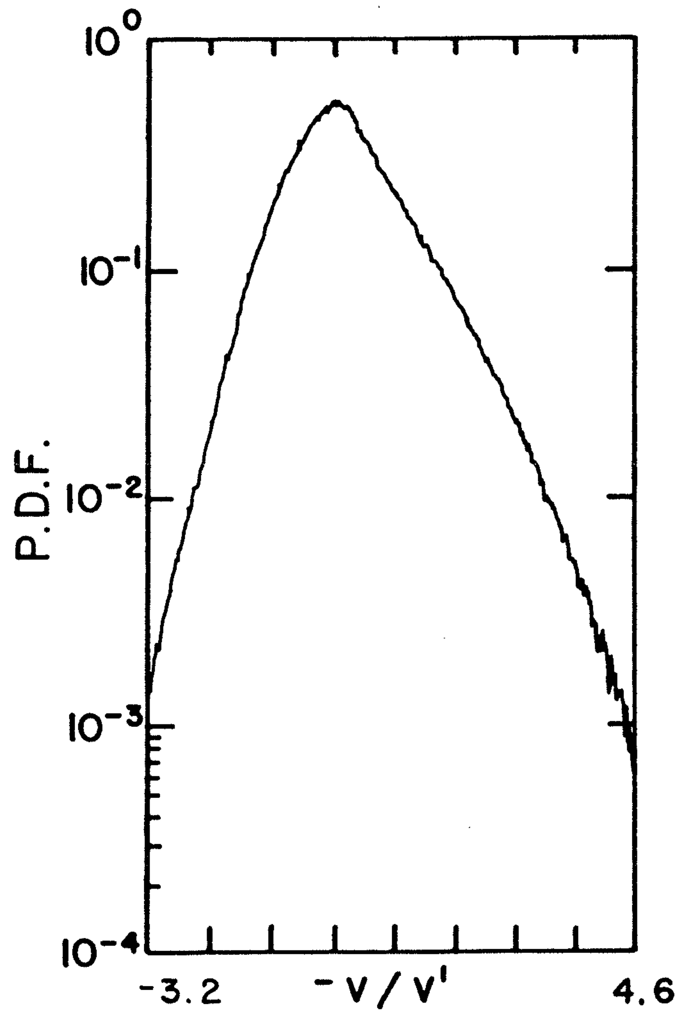

Figure 5.54: Cross wire PDF(v/v') at y = 25 mm
S(v)=-0.676 F(v)=3.141

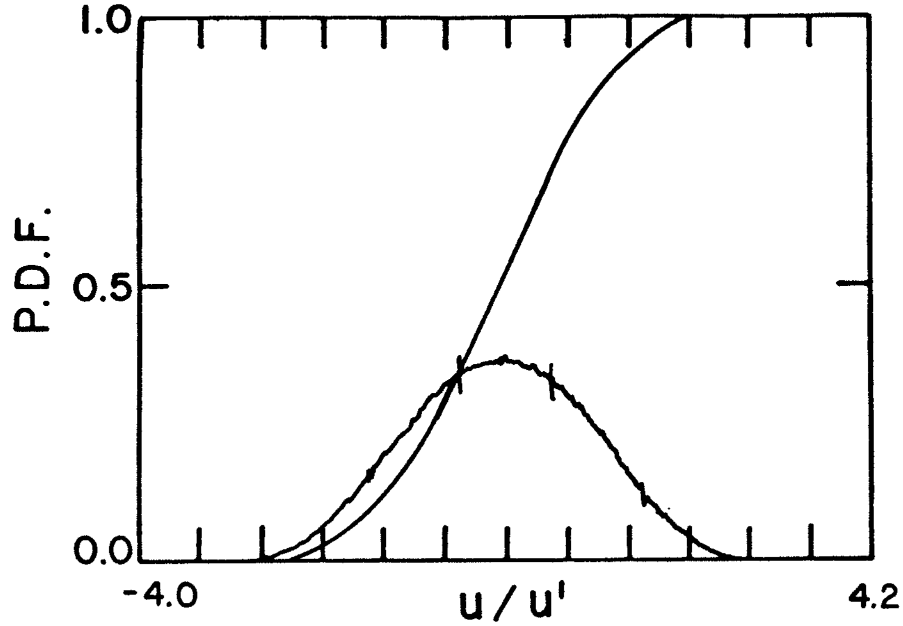

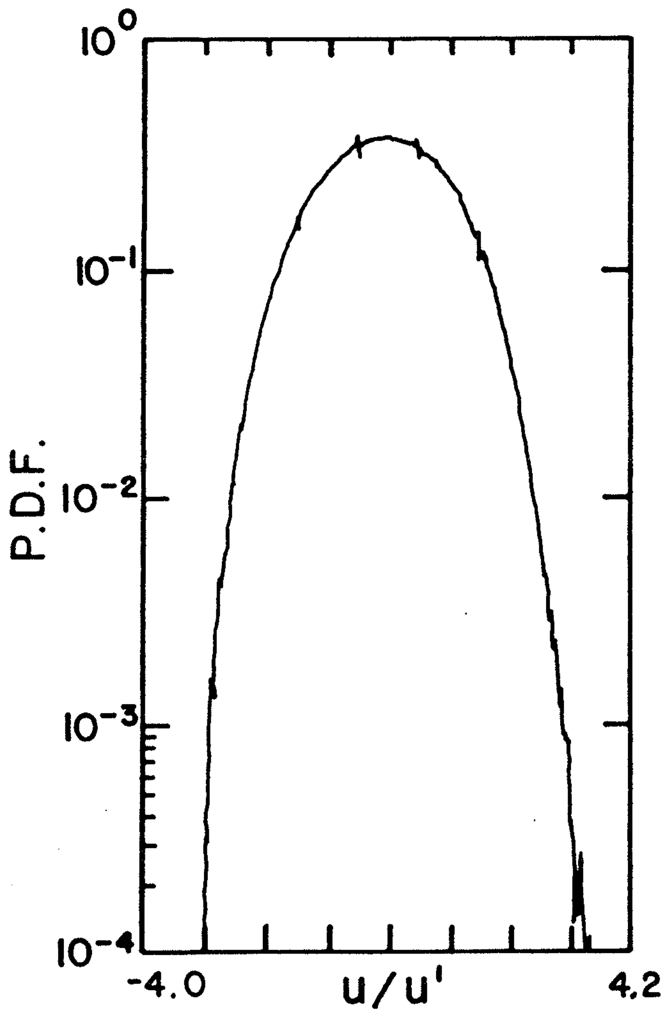

Figure 5.55: Single wire PDF(u/u') at y = 50 mm

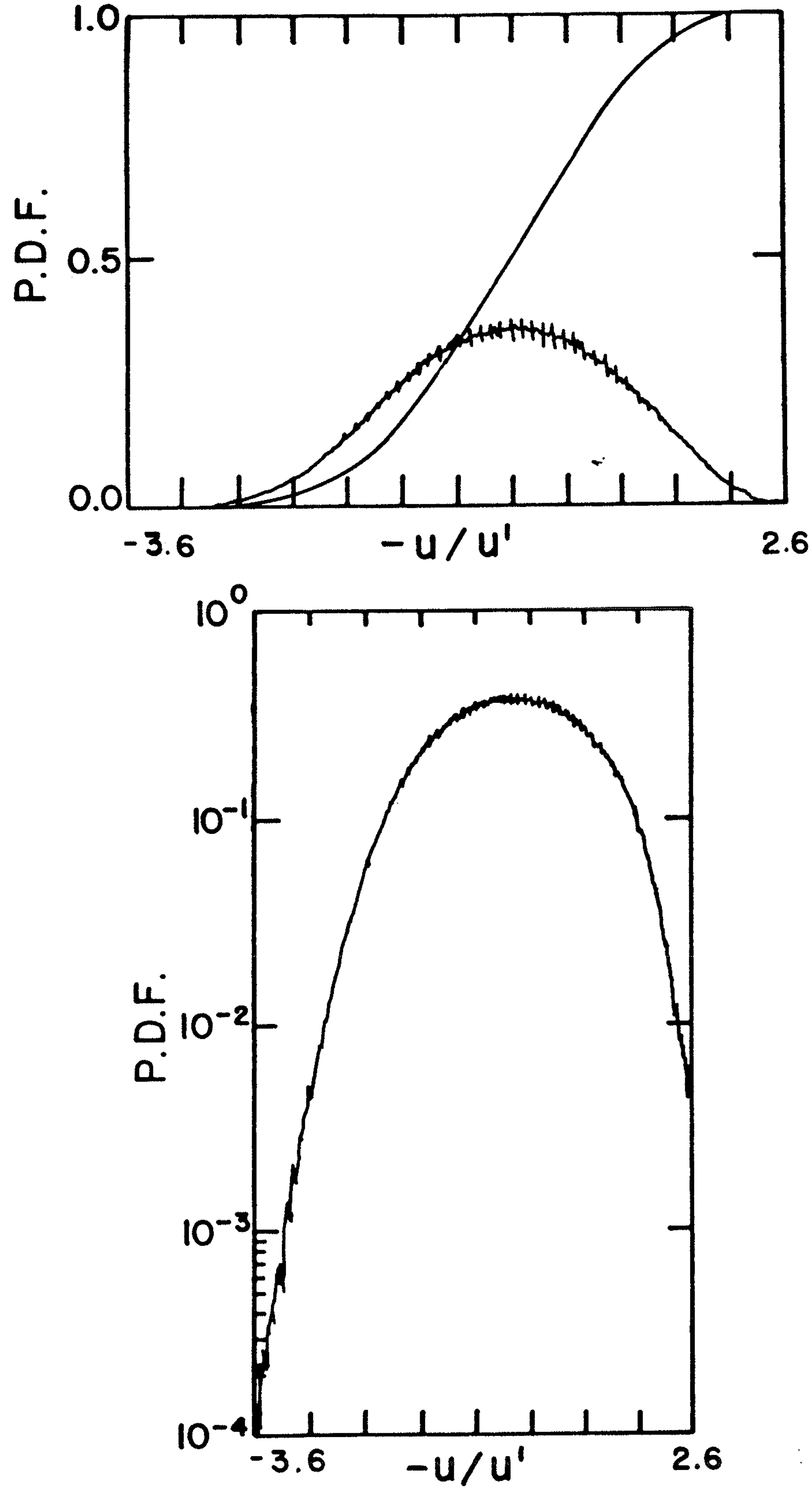

Figure 5.56: Cross wire PDF(u/u') at y = 50 mm
S(u)=0.114 F(u)=2.497

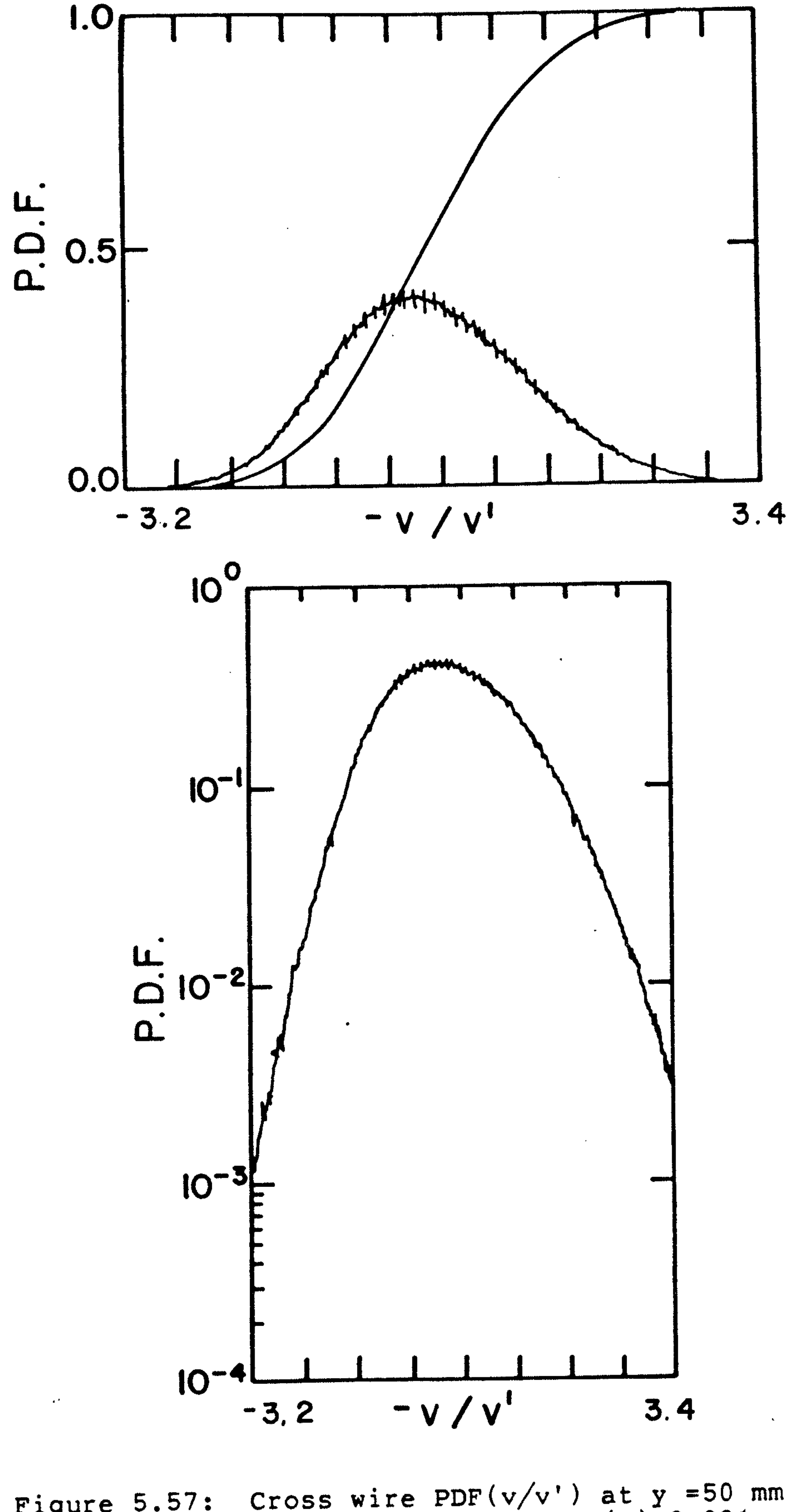

Figure 5.57: Cross wire PDF(v/v') at y =50 mm
S(v)=-0.256 F(v)=3.021

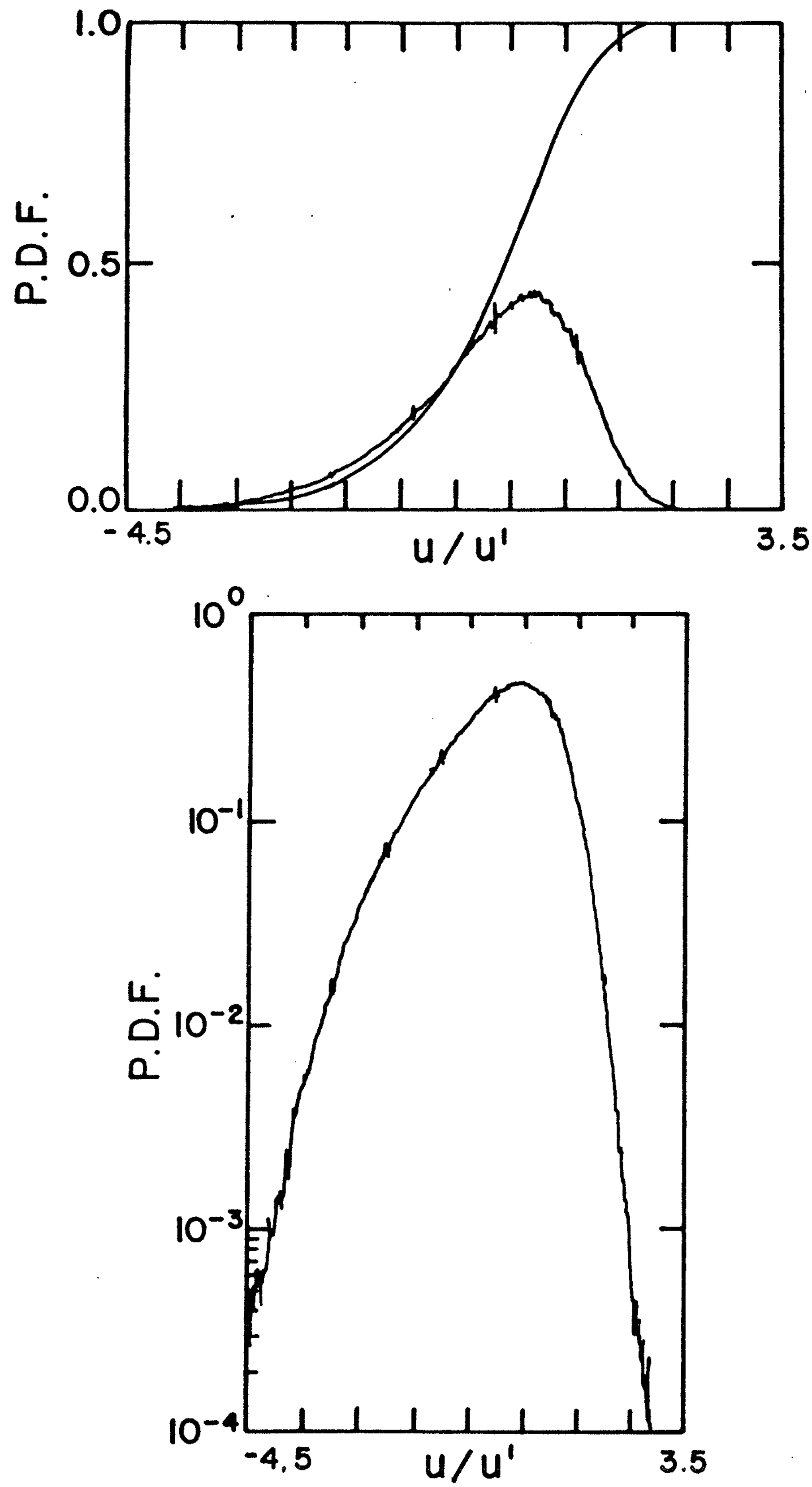

Figure 5.58: Single wire PDF(u/u') at y = 70 mm

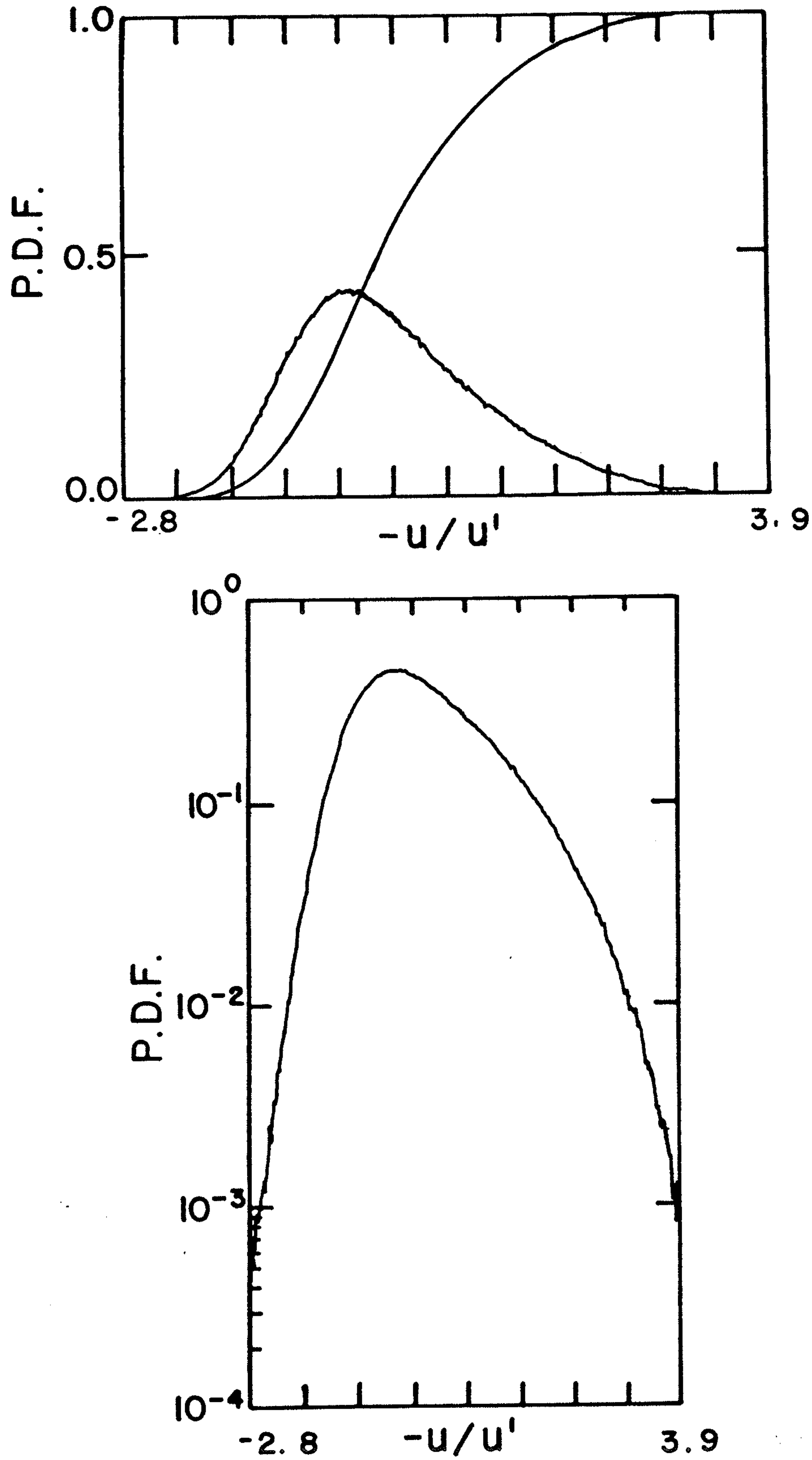

Figure 5.59: Cross wire PDF(u/u') at y = 70 mm
S(u)=0.605 F(u)=3.155

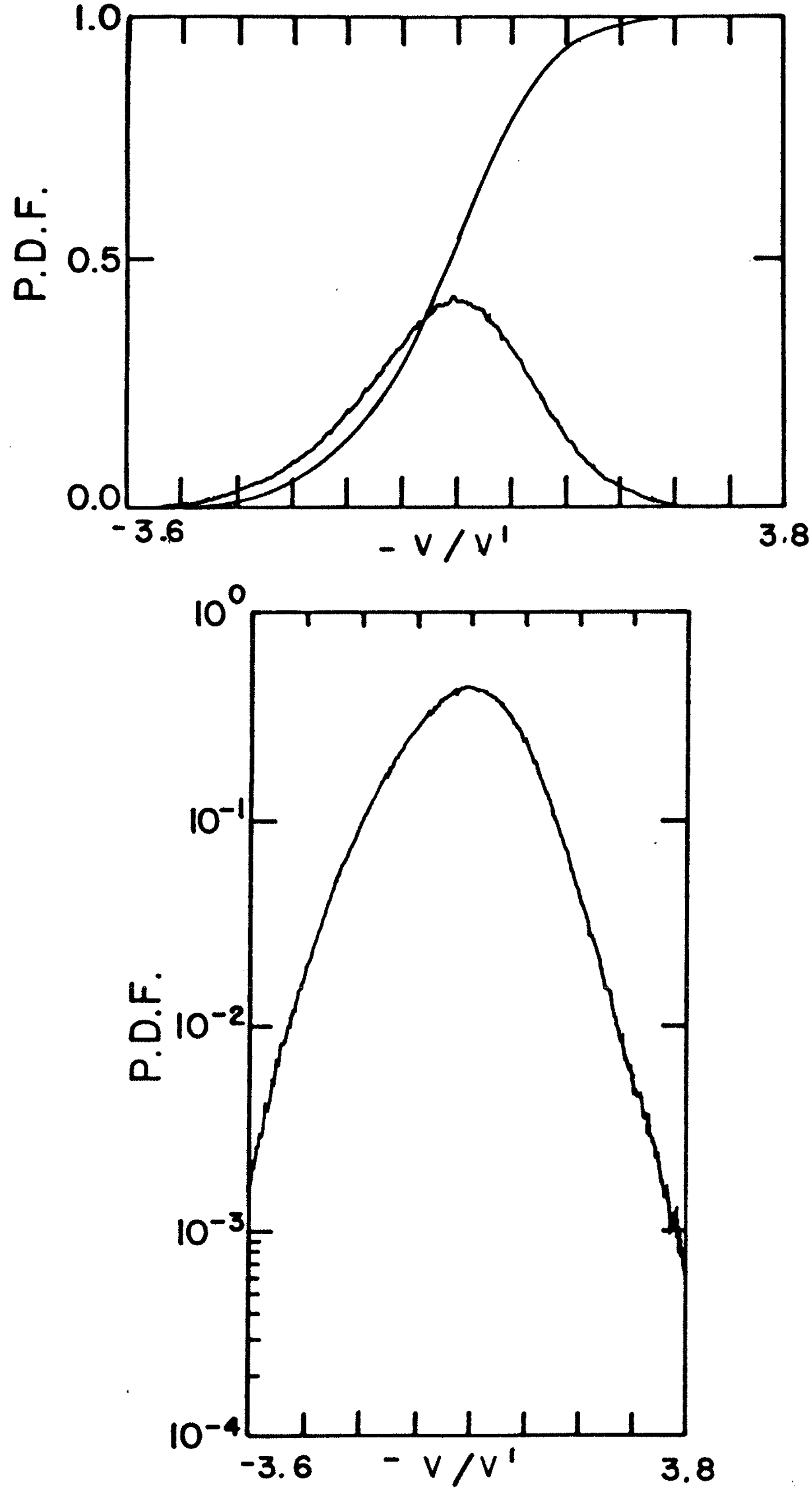

Figure 5.60: Cross wire PDF(v/v') at y = 70 mm
S(v)=-0.195 F(v)=3.302

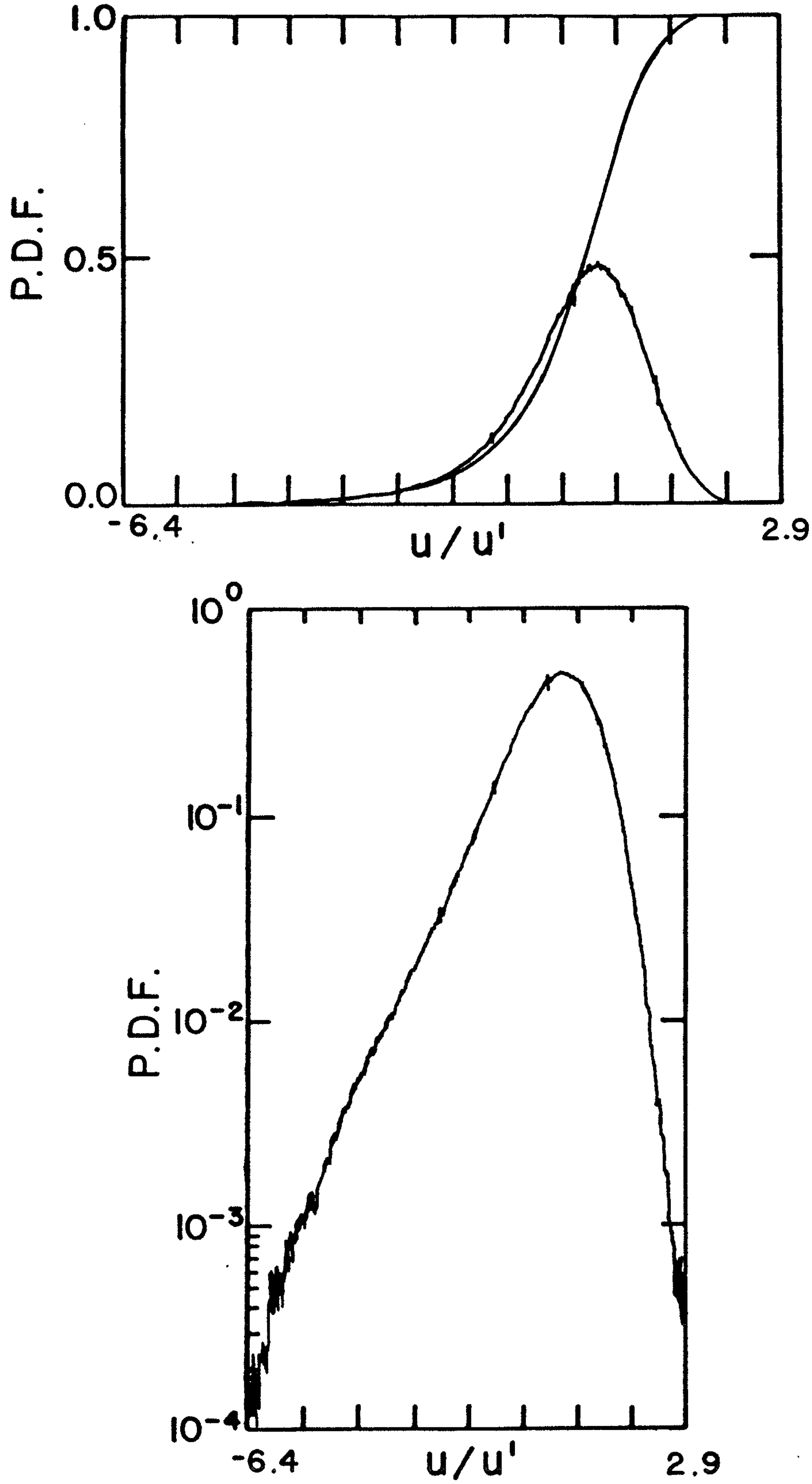

Figure 5.61: Single wire PDF(u/u') at y = 95 mm

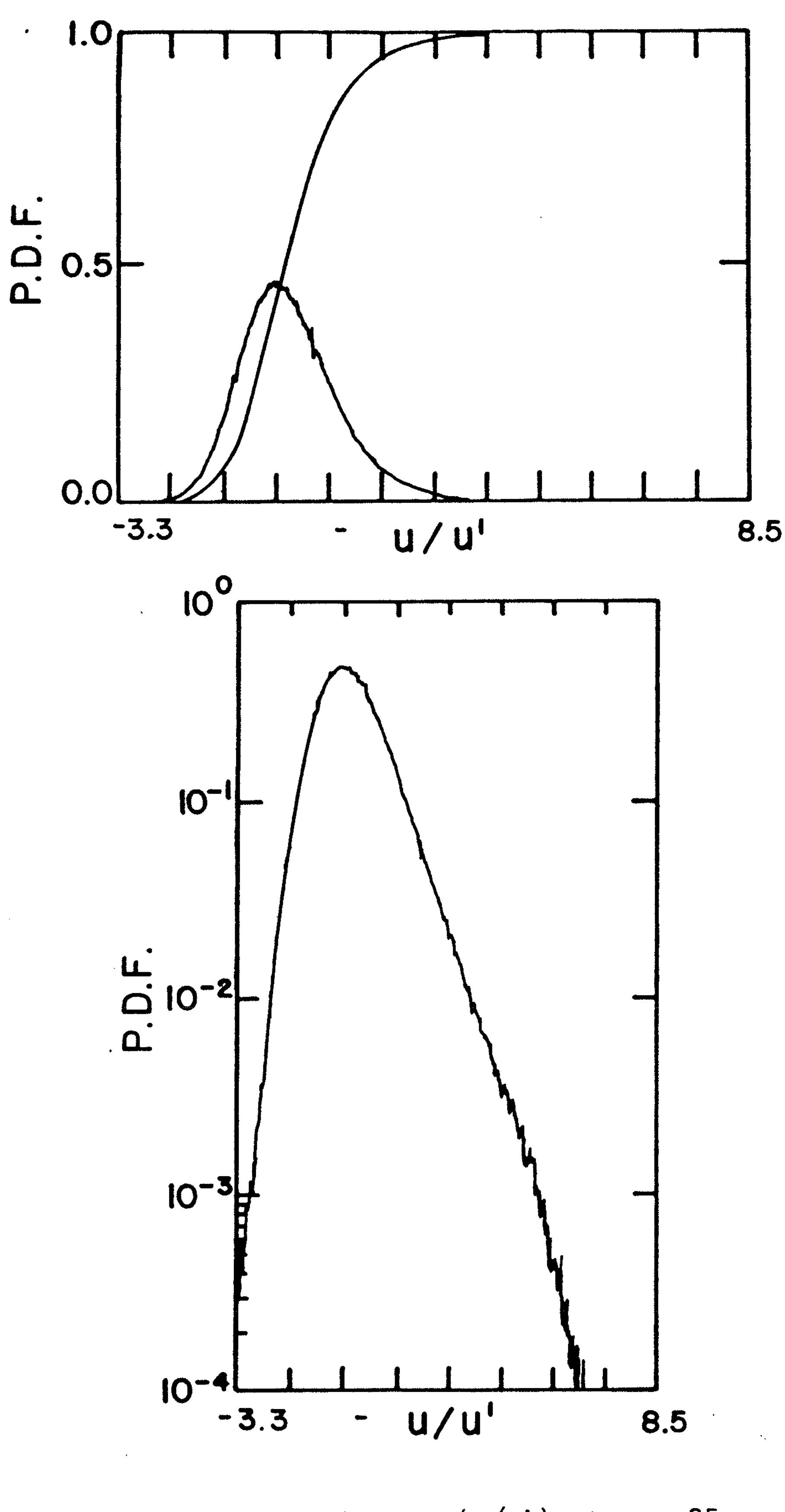

Figure 5.62: Cross wire PDF(u/u') at y = 95 mm
S(u)=0.937 F(u)=5.085

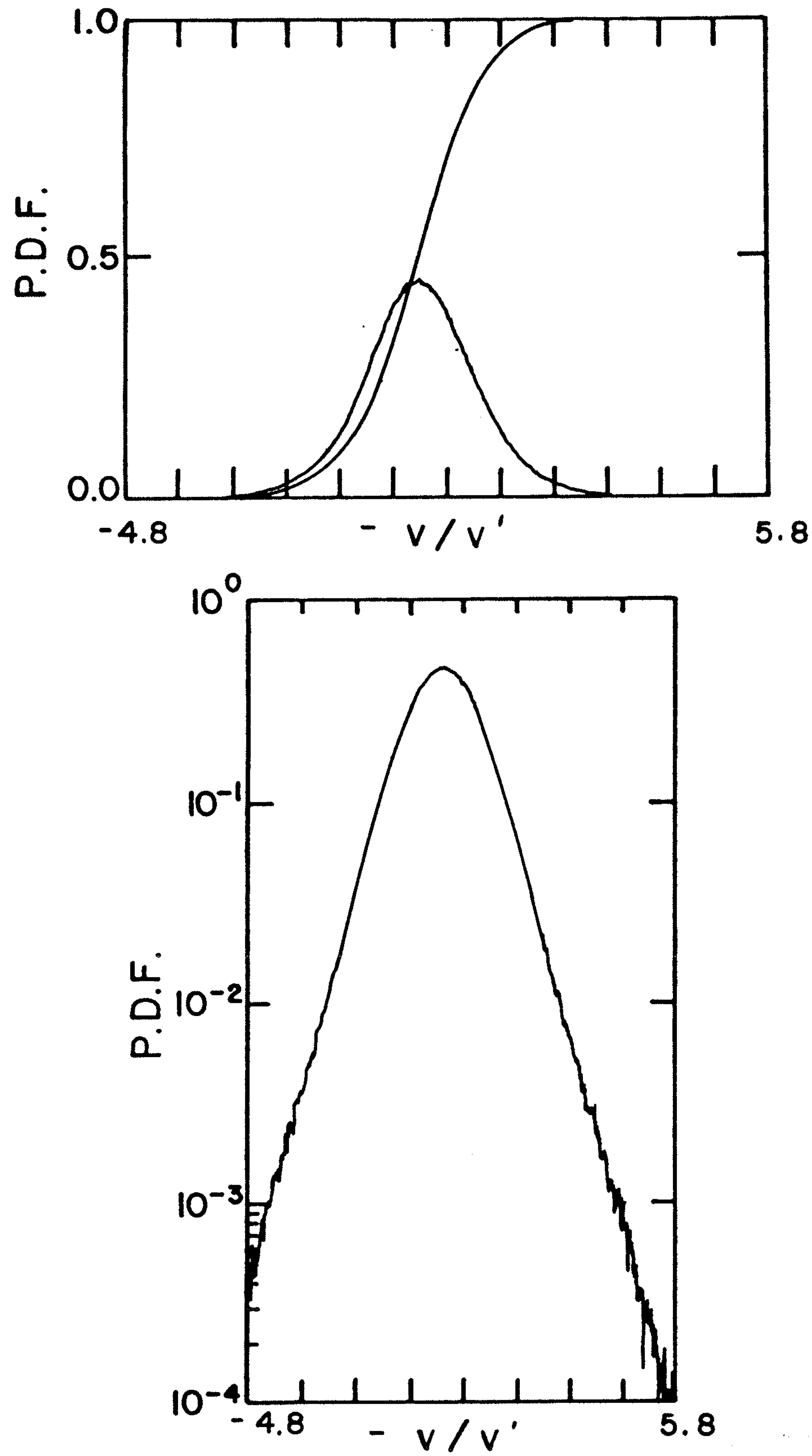

Figure 5.63: Cross wire PDF(v/v') at y = 95 mm
S(v)=0.057 F(v)=4.339

5.5 VELOCITY SPECTRA

The analog and digital data for the comparison of the diffuser velocity spectra were collected and processed at different times. As the spectra was collected for u_2 and v_2 signals, there was no concern about signal inversion as there was with some of the moment and probability measurements.

The signal used for the digital spectral results was filtered at approximately the Kolmogorov frequency $f(K) = U/2\pi\eta$ where η is the Kolmogorov length, with the signal conditioner. The dc component of the signal was removed before the fluctuating component was amplified to within the allowable ±5 volt limits and sent to the computer for collection and processing. The digital spectral results were calculated using the fast Fourier transform and spectra subroutines supplied by DEC. The spectra was calculated, following the same procedure used for the boundary layer spectral calculations, from the 'high frequency' and 'low frequency' passes of the data stream and then plotted by the H·P plotter.

The analog spectral results were collected by low pass filtering the signal at the Kolmogorov frequency and then band pass filtering the signal for frequencies between 2Hz and 35 kHz. Eight measurements per decade were taken.

The spectral results of the u-velocity component taken with the single wire and cross wire probes were the same. Little difference was observed between the analog and digital results. As the with the boundary layer results, the high energy range of the u-spectra is at the low frequencies, mostly below 10 Hz, and drops at the higher frequencies. The energy content of the spectra rise in value from the wall, peak at the blue line and decrease towards the diffuser axis.

The spectra of the v-velocity component follow the same trend as the spectra of the u-velocity component: rising in the wall layer, peaking at the blue line and decreasing in the core region. The energy content of the v-spectra is approximatly one decade lower than that of the u-spectra. The high energy content of the v-spectra remain mostly constant below 100 Hz and fall at the higher frequencies.

As with the boundary layer spectra, the velocity spectra display the same trends: some scatter in low frequency range, and 'digital noise' occuring at approximately 10 kHz with analog noise occuring at higher frequencies. No significant difference is seen between the plotted analog and digital spectral results.

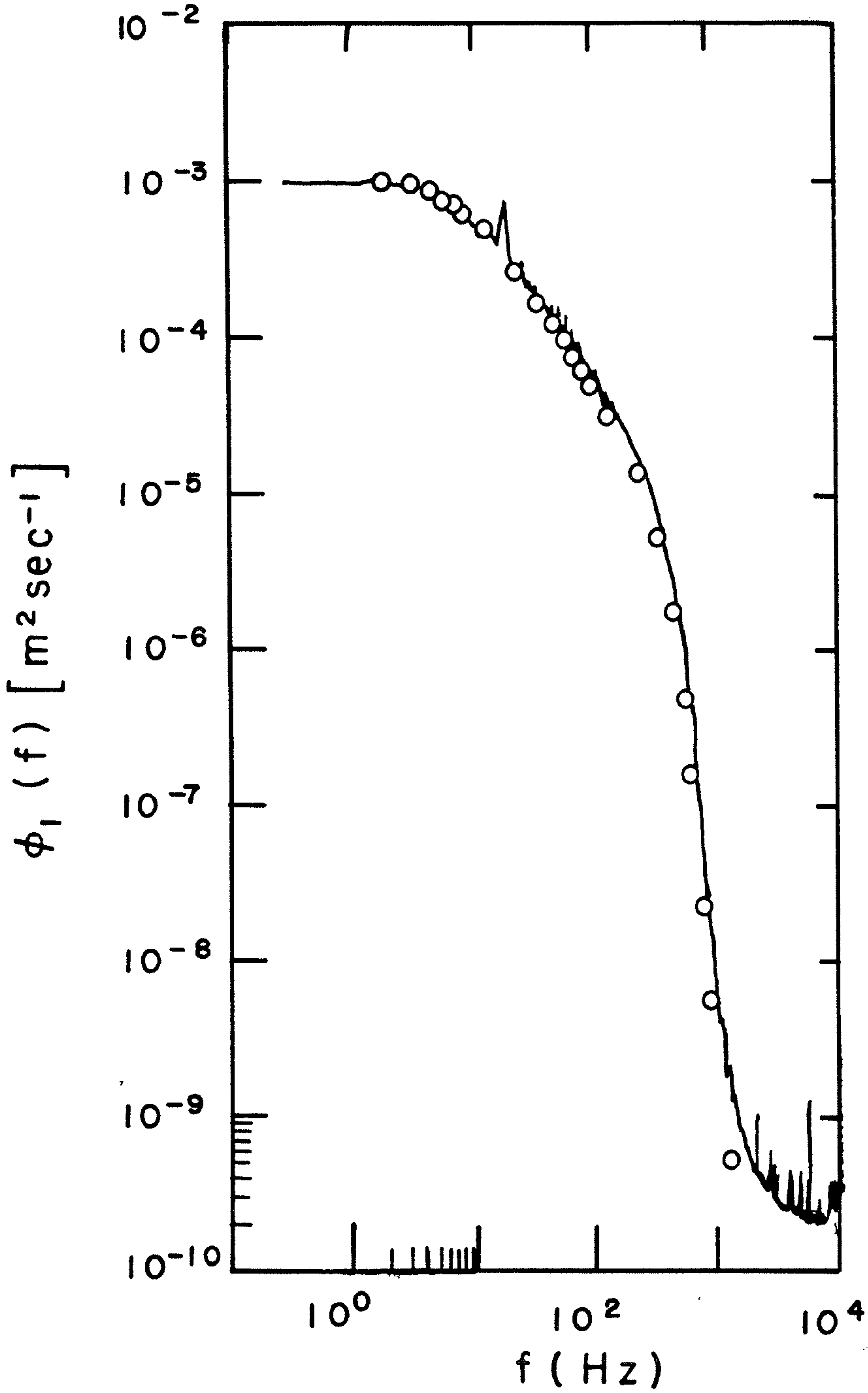

Figure 5.64: Single wire u-spectra at y = 0.5 mm

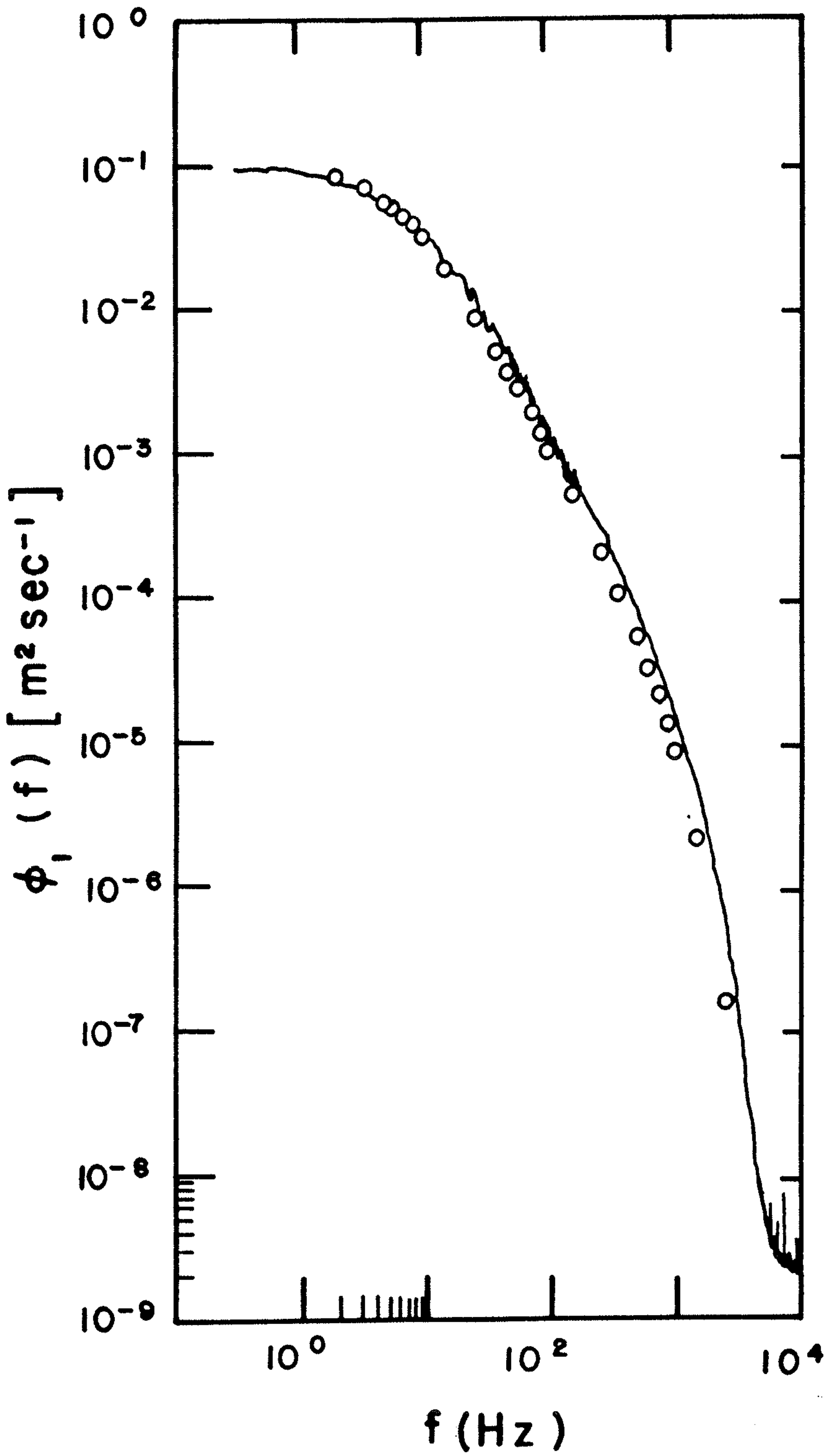

Figure 5.65: Cross wire u-spectra at y = 3 mm

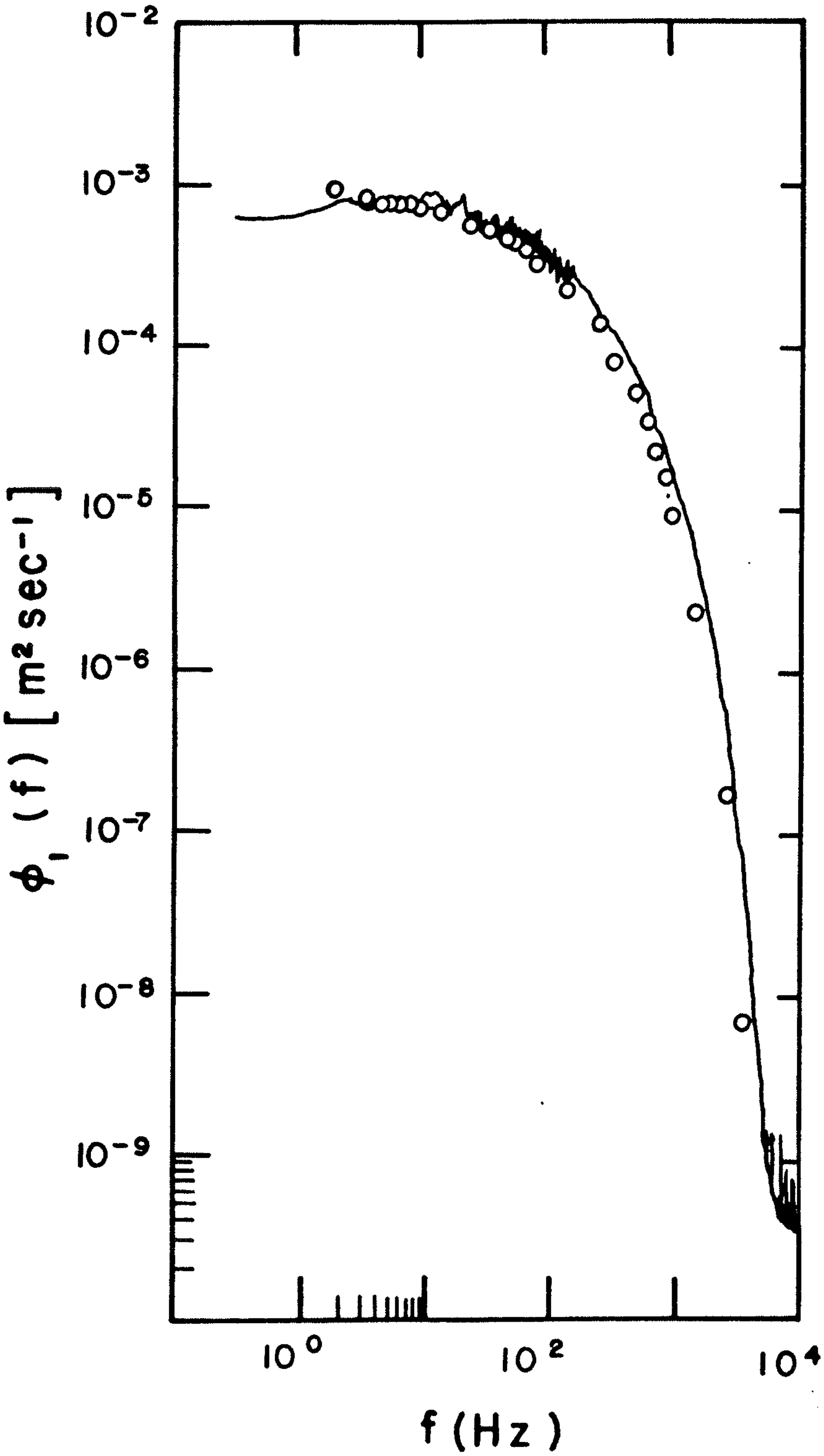

Figure 5.66: Cross wire v-spectra at y = 3 mm

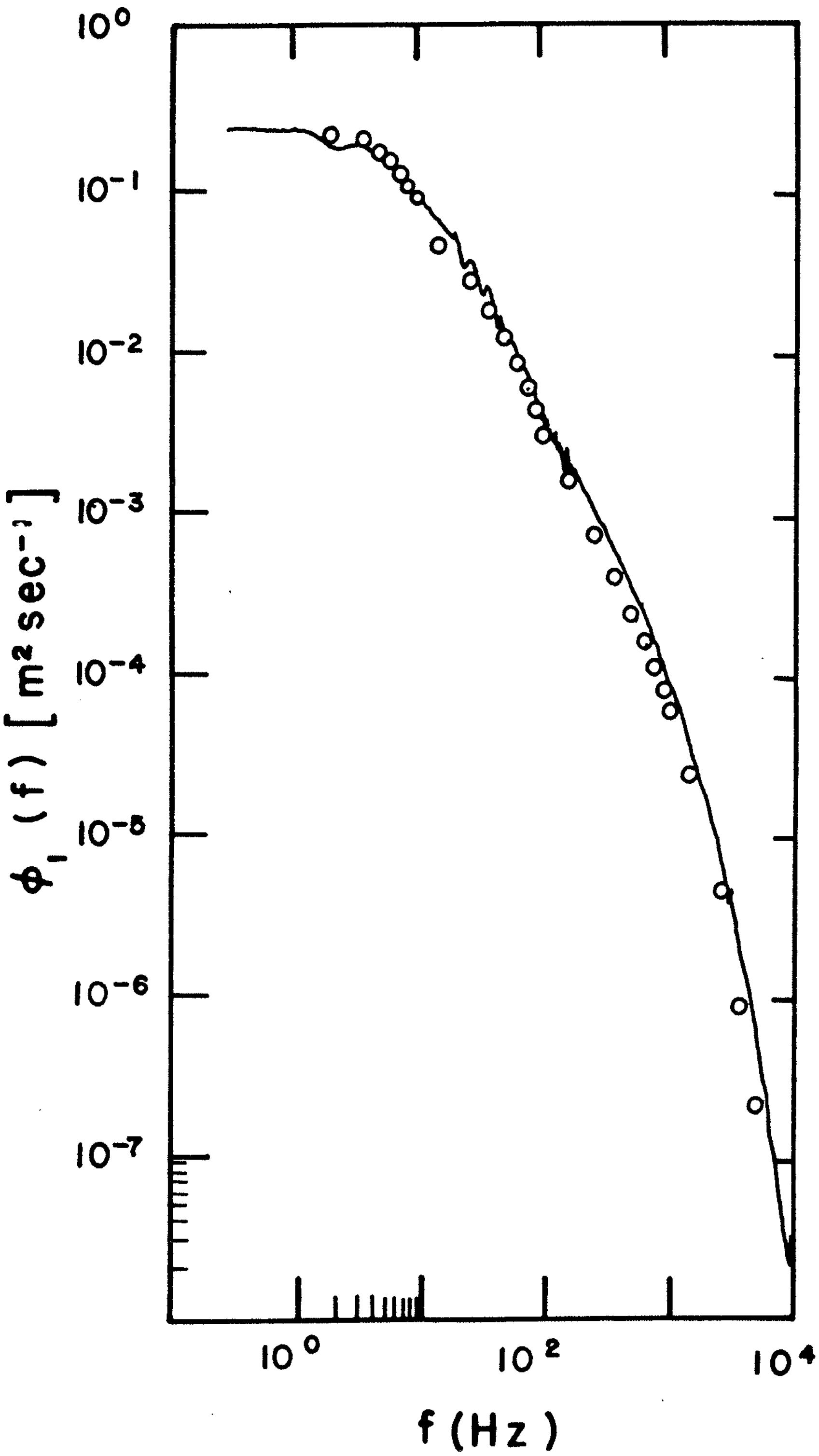

Figure 5.67: Single wire u-spectra at y = 25 mm

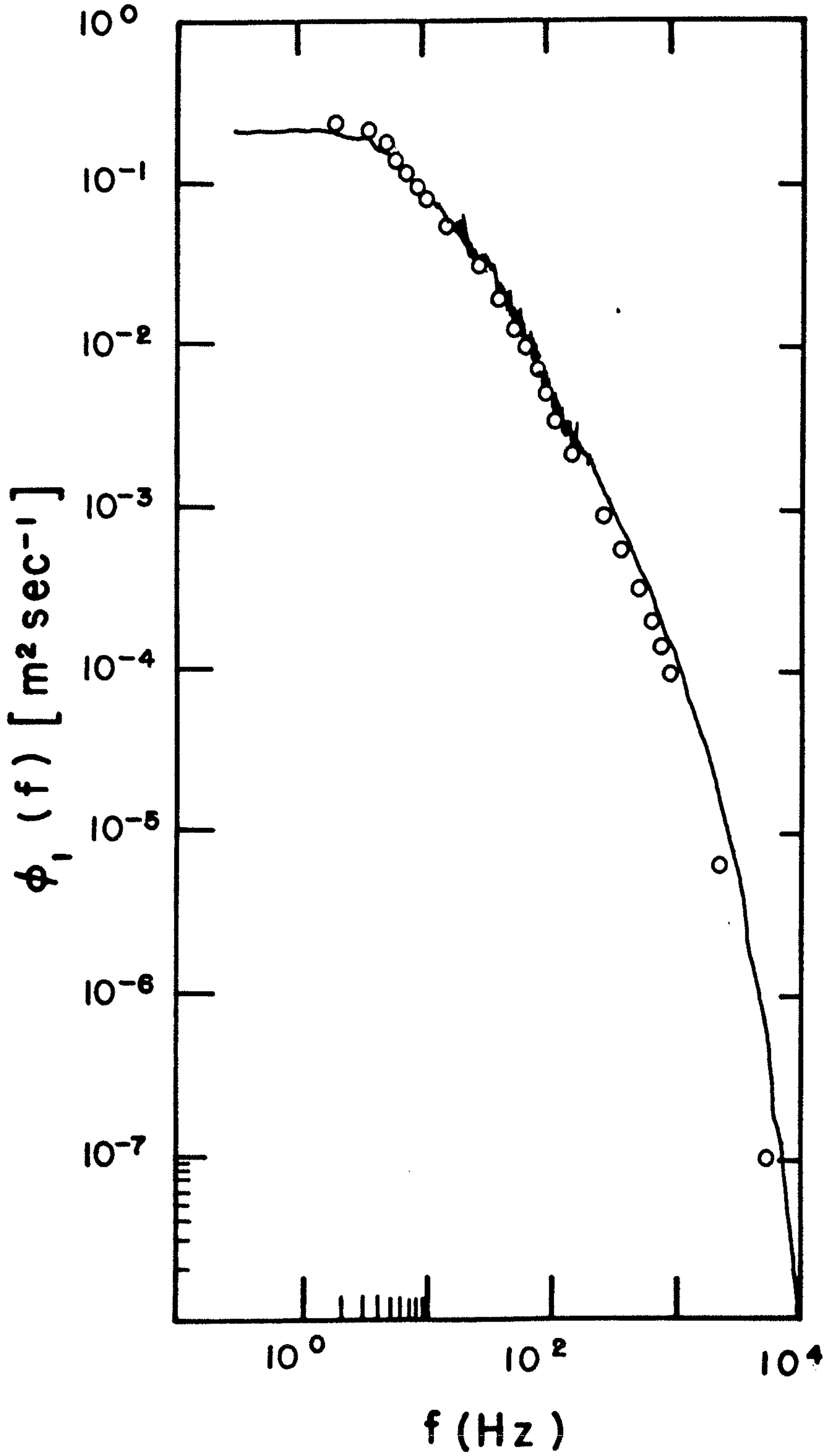

Figure 5.68: Cross wire u-spectra at y = 25 mm

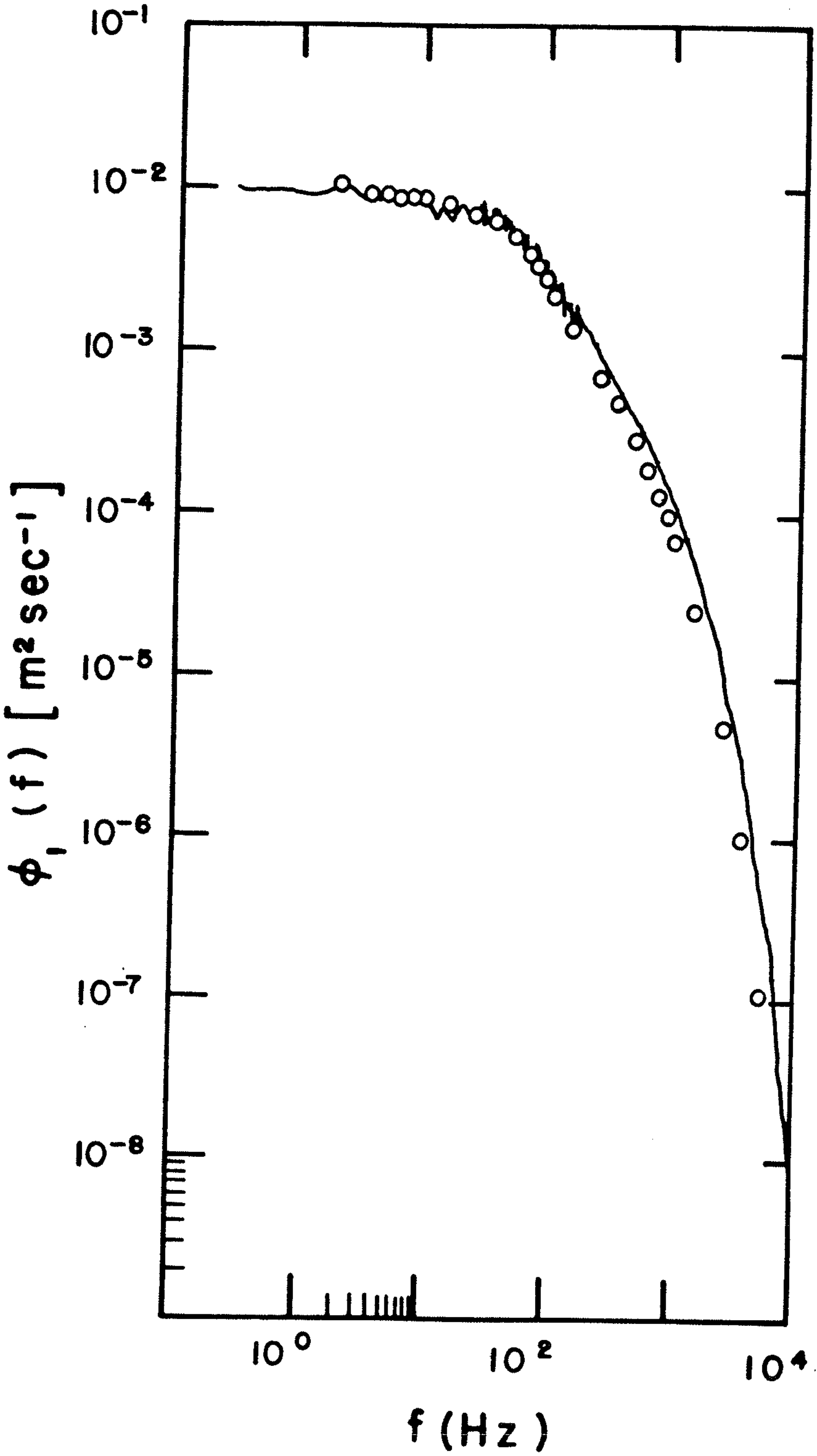

Figure 5.69: Cross wire v-spectra at y = 25 mm

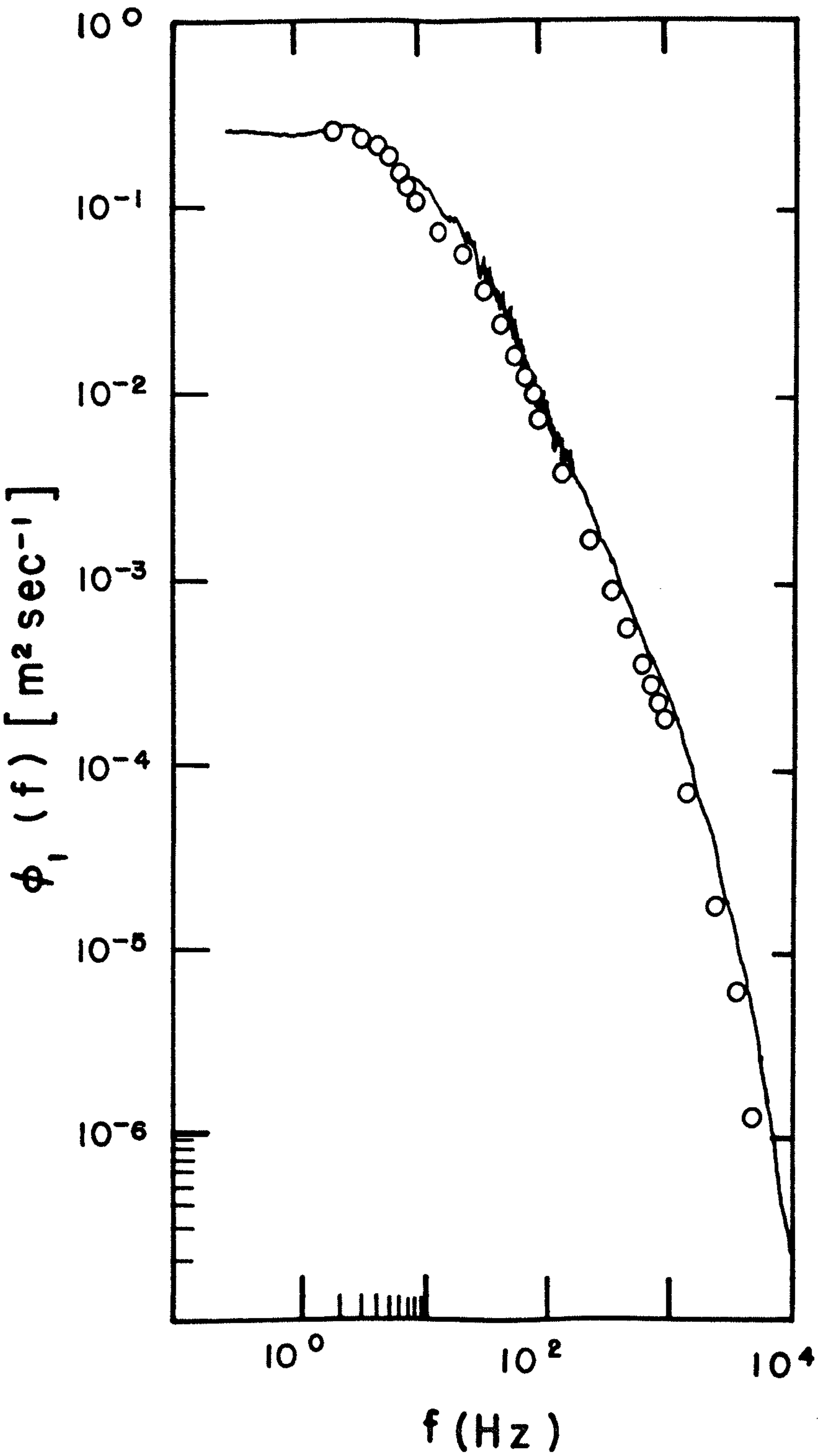

Figure 5.70: Single wire u-spectra at y = 50 mm

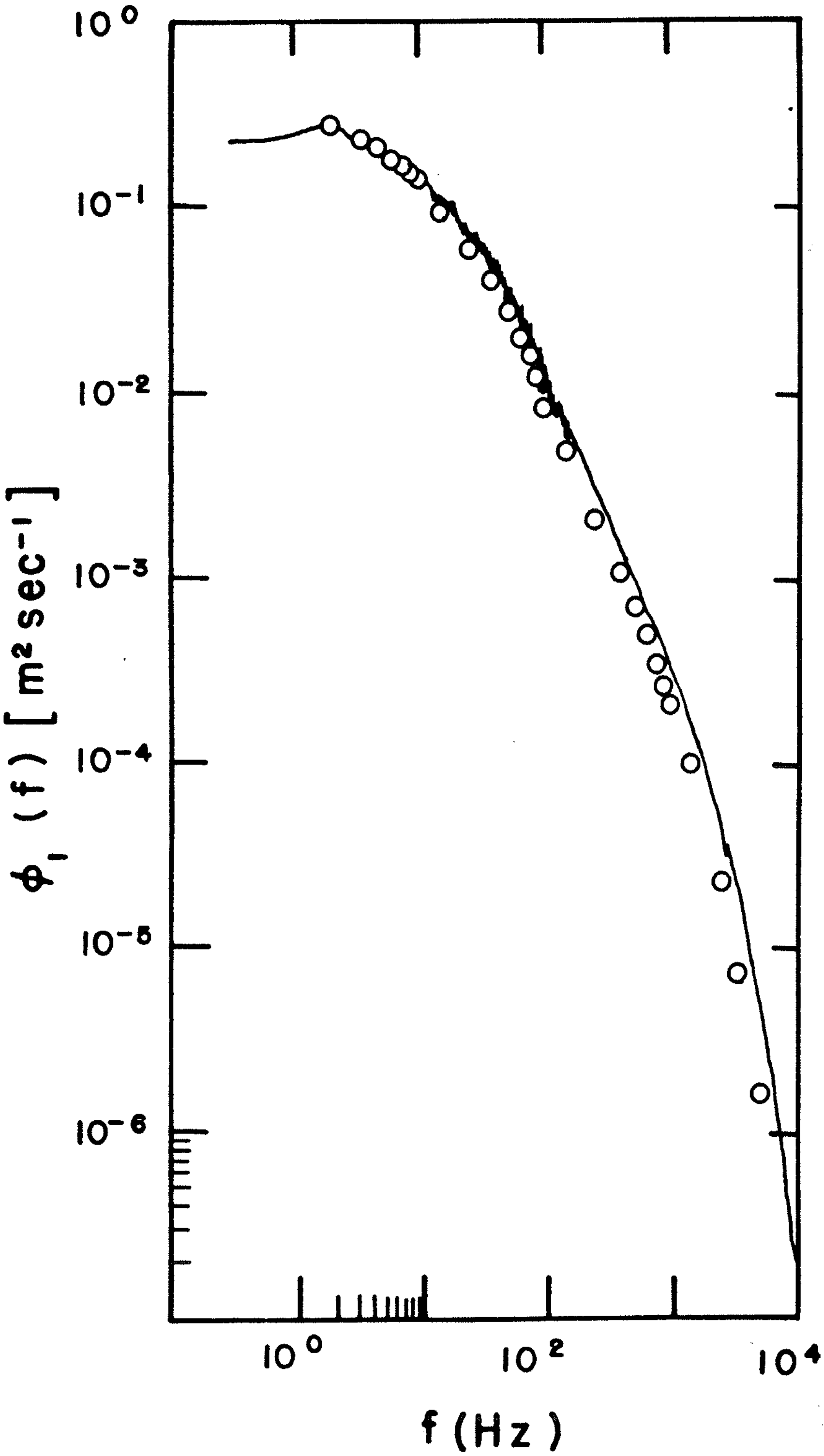

Figure 5.71: Cross wire u-spectra at y = 50 mm

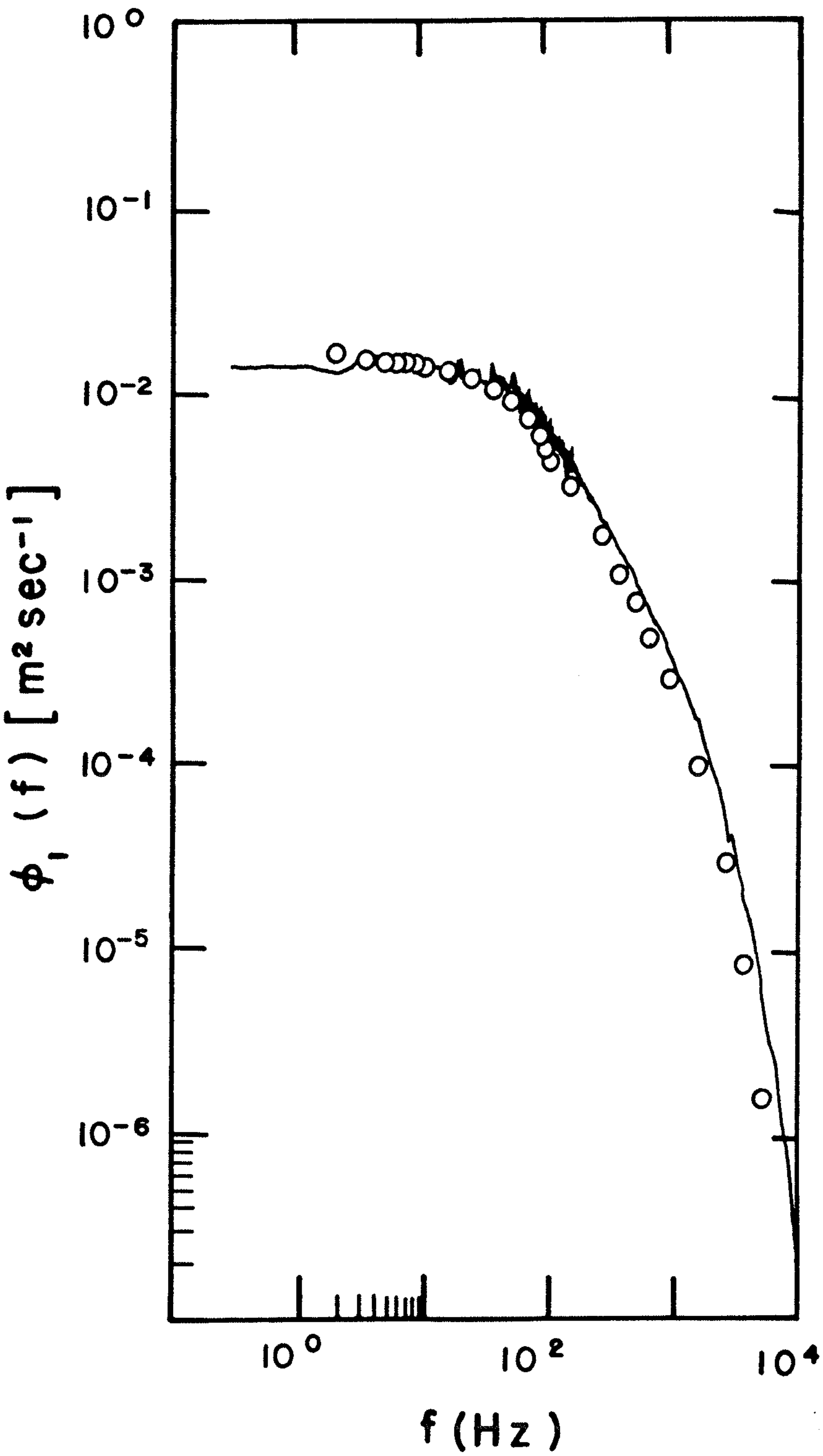

Figure 5.72: Cross wire v-spectra at y = 50 mm

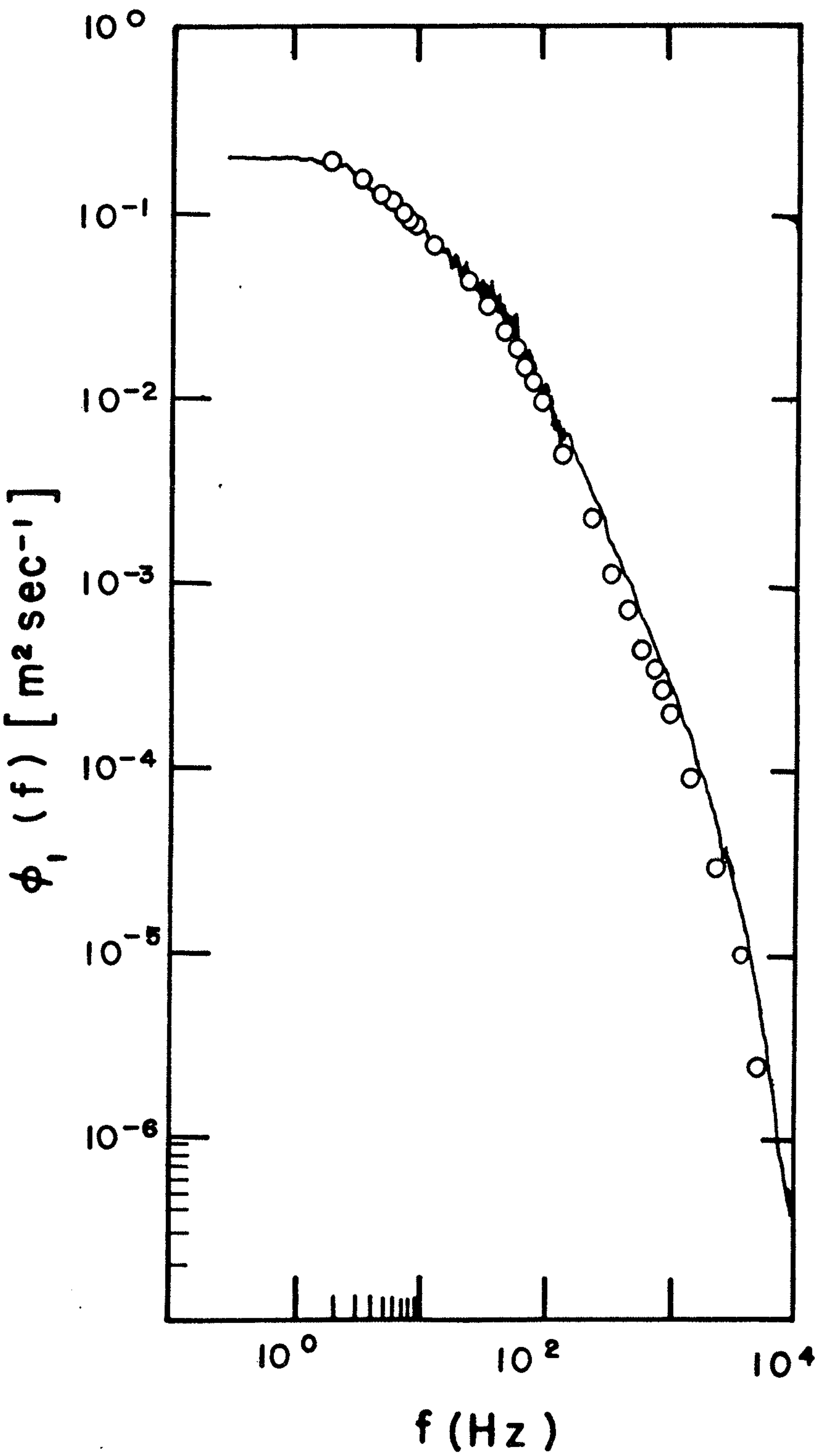

Figure 5.73: Single wire u-spectra at y = 70 mm

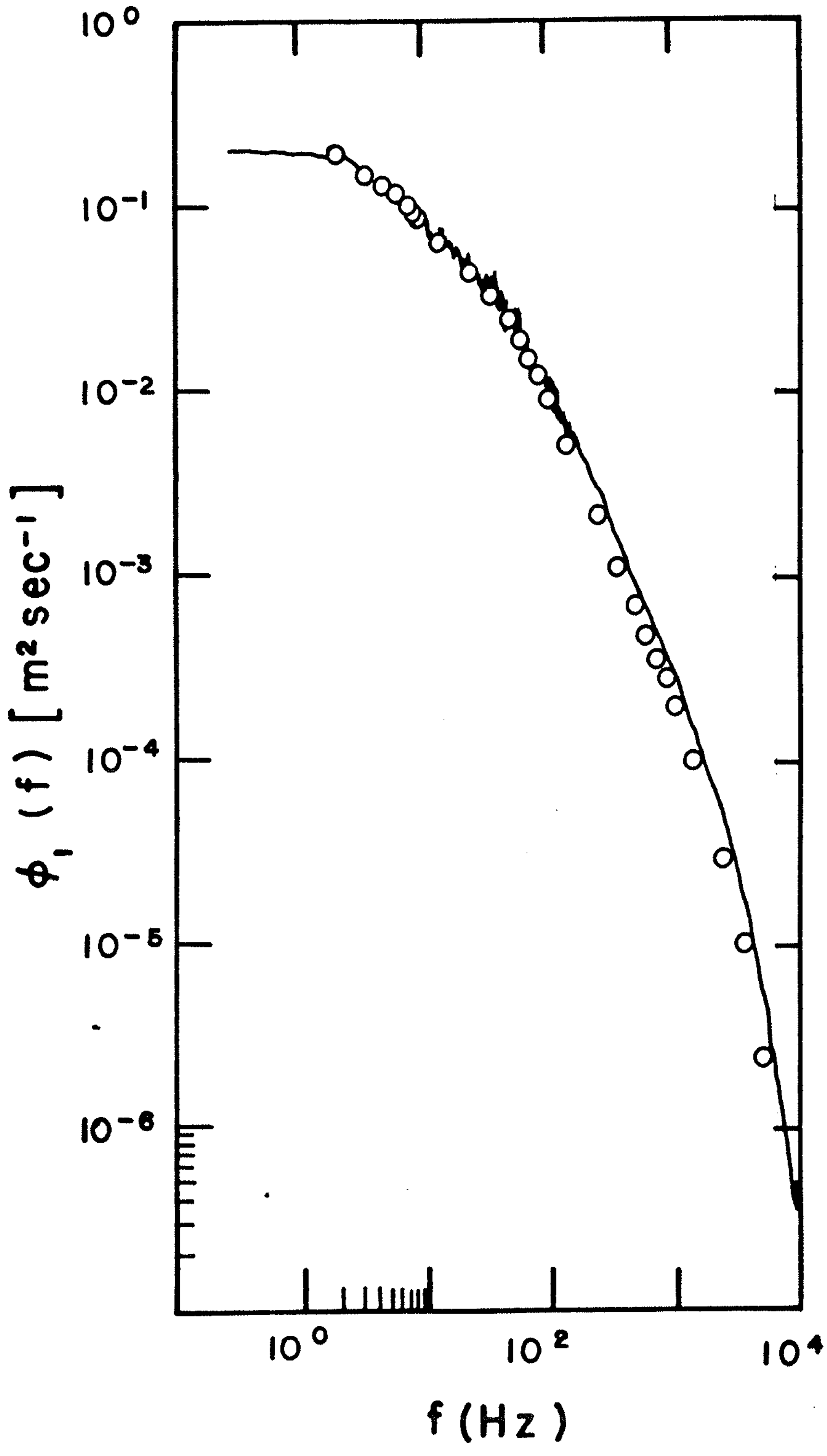

Figure 5.74: Cross wire u-spectra at y = 70 mm

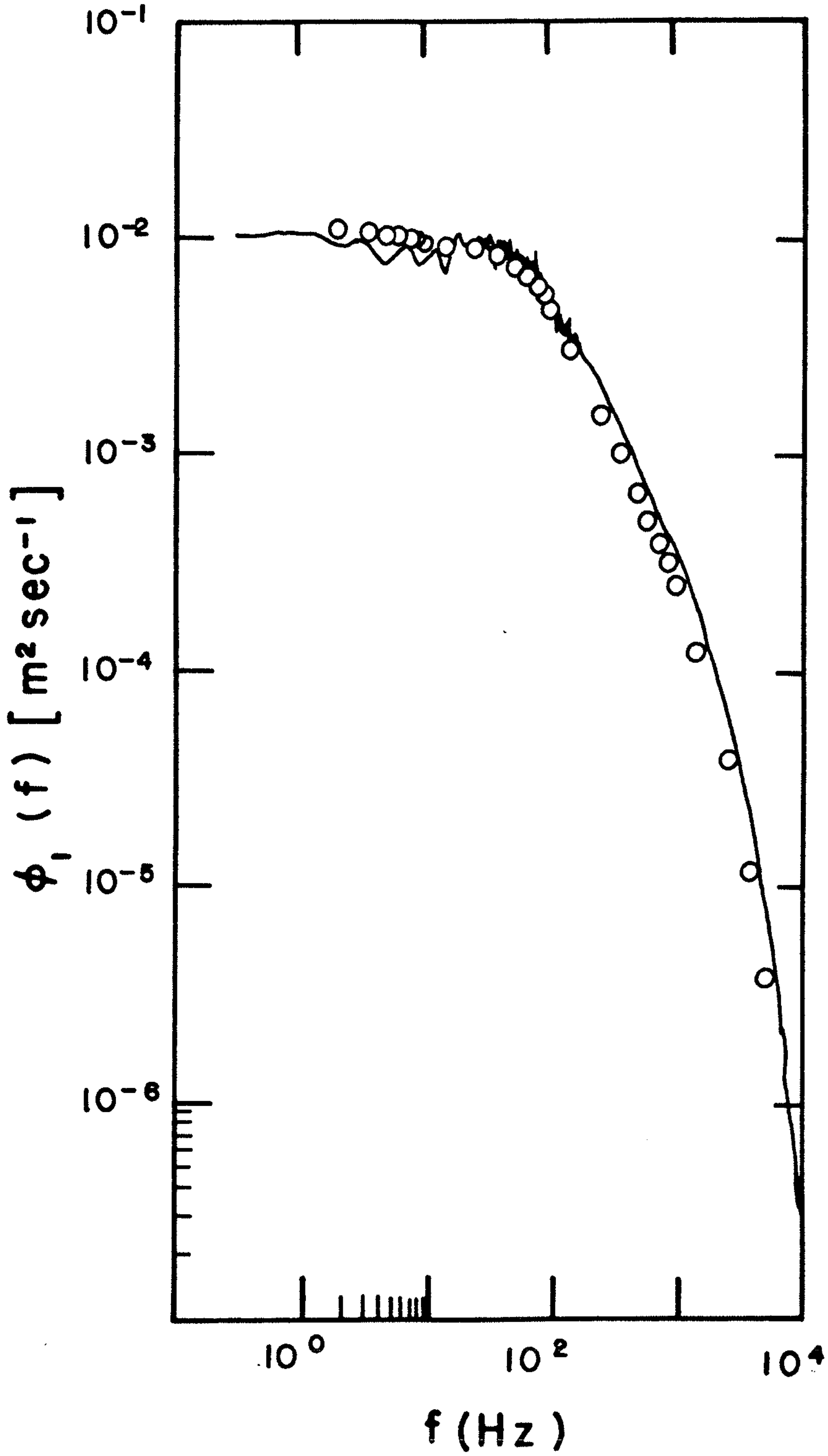

Figure 5.75: Cross wire v-spectra at y = 70 mm

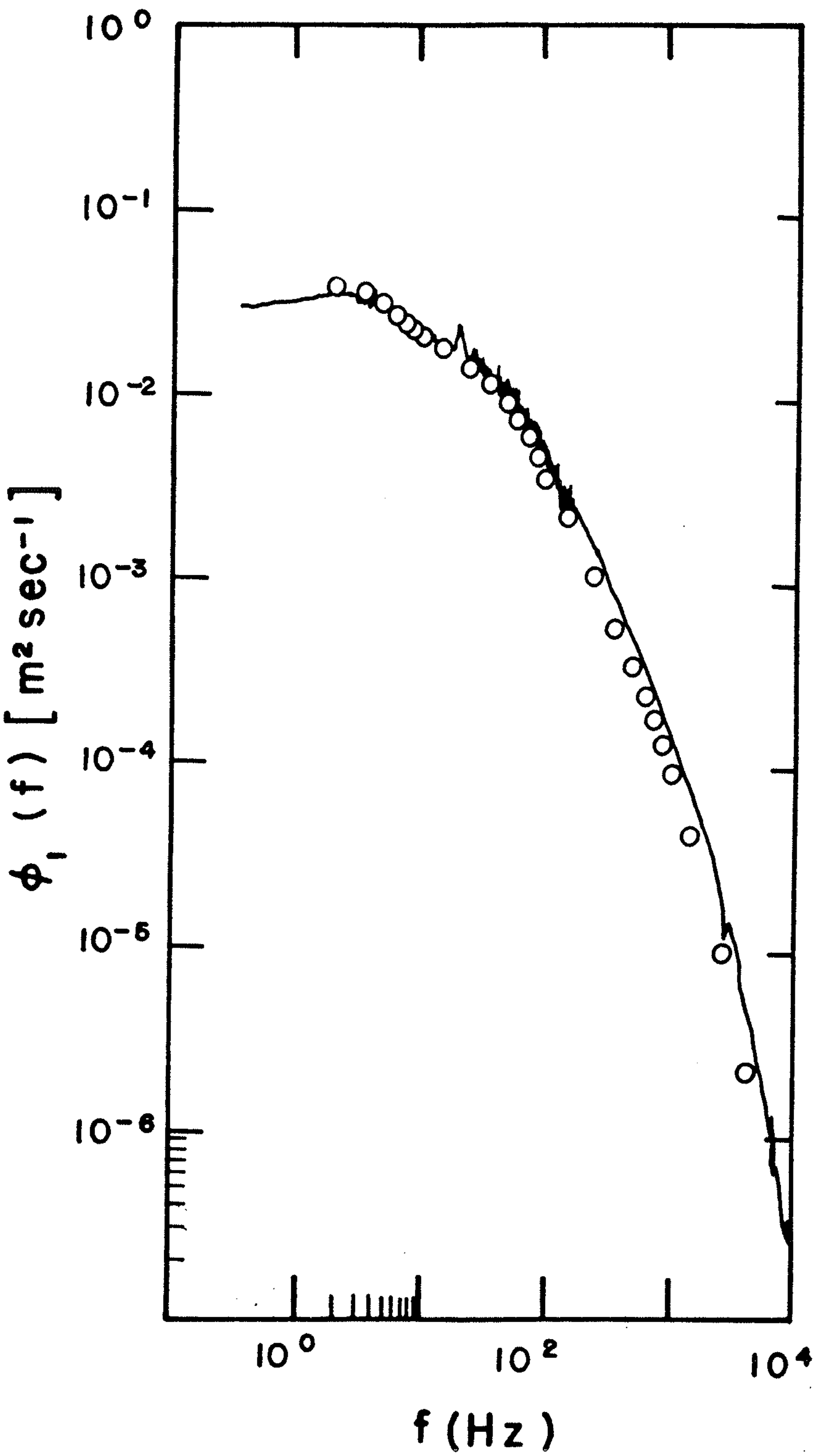

Figure 5.76: Single wire u-spectra at y = 95 mm

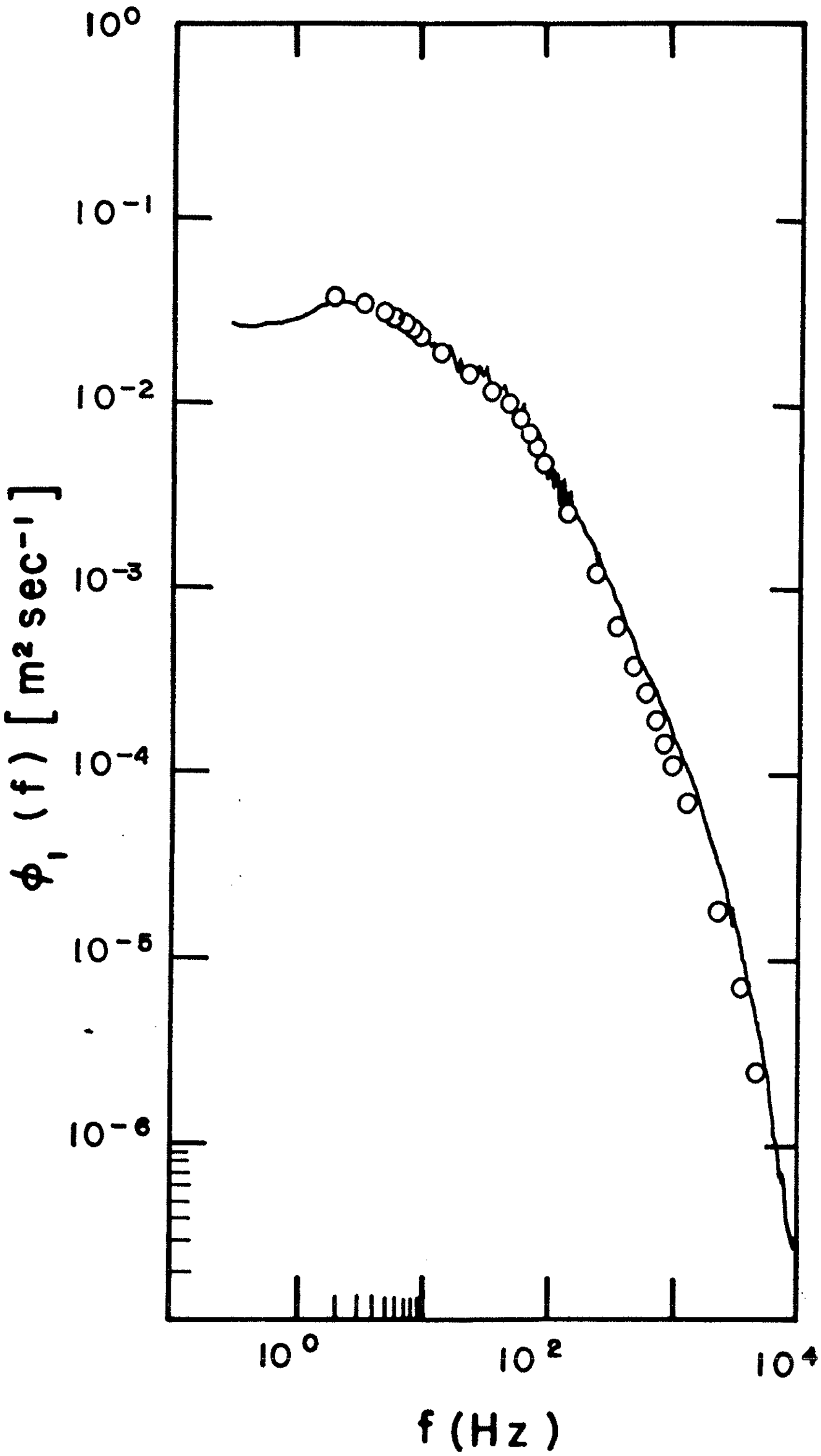

Figure 5.77: Cross wire u-spectra at y = 95 mm

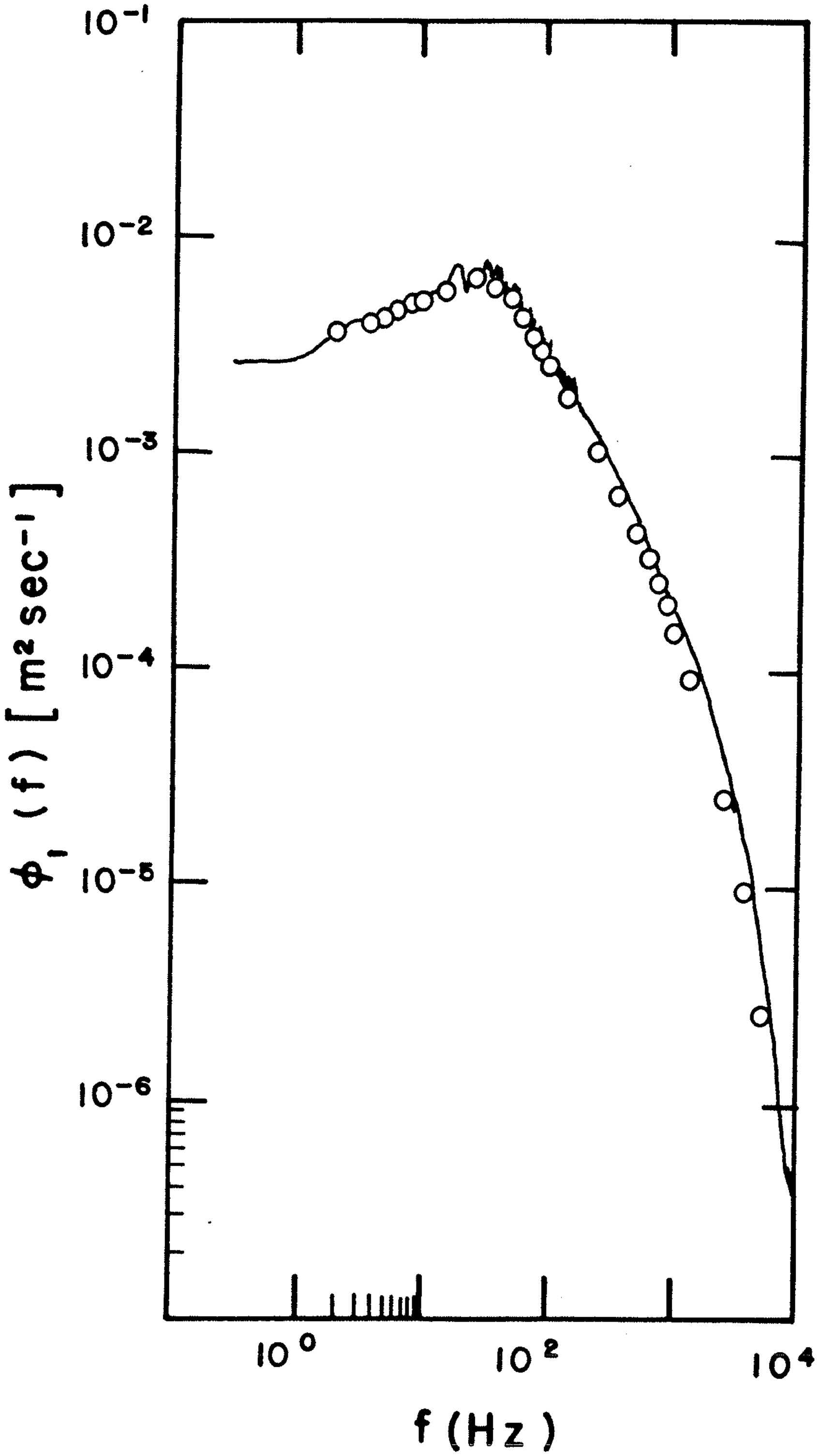

Figure 5.78: Cross wire v-spectra at y = 95 mm

Chapter VI

CONCLUDING REMARKS

An experimental investigation of analog and digital data for measurement of various flow parameters has been undertaken. Comparisons between the two techniques were made in two types of flow:

1. turbulent boundary layer flow.
2. diffuser flow with fully developed pipe flow at entry to an 8° conical diffuser.

Analog data in the boundary layer flow was determined previously by other investigators. The digital data taken in the same flow compared well with the analog data. Discrepancies in proximity to the wall may be attributed to effects of imperfect spatial resolution of the hot wire and small fluctuations in the Reynolds number. Discrepancies further from the wall may be attributed to the intermittent nature of the flow.

Analog and digital data in the conical diffuser, with the exception of the spectral measurements, were taken at the 'same' time to eliminated the problems associated with inaccurate spatial resolution. The analog and digital data compared well in most parameters measured. A point of difference came in such measurements as skewness and certain fourth order mixed moments of the velocity. The digital data crossed the zero value ahead of the corresponding analog data in such measurements as S(u), S(v), $\overline{uv^3}/u'v'^3$, and $\overline{u^3v}/u'^3v'$. Skewness of the velocity derivative in proximity to the wall showed some scatter, with the digital results slightly larger in magnitude than corresponding analog results. Some scatter between points was observed in the higher order moments. Discrepancies in the data may be attributed to small fluctuations in the tunnel Reynolds number and the intermittent nature of the flow.

Both analog and digital data are subject to the effects of imperfect amplification, and with the cross wire, imperfect matching of the frequency and sensitivity of the input signals. Under amplification of the signal results in poor resolution while over amplification results in a clipped signal. Imperfect matching of the cross wire signal results in one component overpowering or contaminating the other. Either occurance produce inaccurate values of the processed signal.

Since no major difference in data exists between the analog and digital techniques, other factors such as time, versatility, and convenience may be considered.

In this study, no difference in time required to collect and process the signal for single wire group measurements of the skewness and flatness factor was apparent. However, the analog cross wire results for group measurements of skewness, flatness factors, and mixed moments of the velocity components required more time than the corresponding digital results. The digital spectras were collected, processed and plotted before the raw data used in the analog spectras was collected.

The analog techniques do have the advantage of time in measurements of single parameters. Once an analysis package is established, the time advantage with the digital techniques occurs with increased numbers of desired parameters to be calculated.

The digital techniques have a wider base as to the kinds of measurements that can be made. Here, data for fifth and sixth central moments and probability densities were produced by existing digital techniques. No analog circuit was available with which to process the signal to obtain these results.

The digital techniques have the advantage that once the data has been collected and stored on tape, it can be re-analyzed at a later date to investigate additional parameters or other hypothesis. A 'recalibration' or re-zeroing of the measuring equipment is not needed for the digital analysis, but is required prior to each analog analysis. Problems of spatial resolution and Reynolds number fluctuation could be greatly reduced with an established library of good raw data.

REFERENCES

Arora, S. C., 1978: An experimental study in the turbulent kinetic energy and the vorticity in a conical diffuser, Ph.D. thesis, University of Manitoba.

Azad, R. S. and Burhanuddin S., 1983: Measurements of some features of turbulence in wall-proximity, Experiments in Fluids 1, 149-160.

Azad, R. S. and Hummel, R. H., 1971: Measurements of the intermittency factor in diffuser flow, Canadian Journal of Physics, Vol. 49, 2917 - 2930.

Azad, R. S. and Hummel, R. H., 1979: Similarities of turbulence structure in a conical diffuser with other wall bounded flows, A I A A Journal, Vol. 17, 884 - 891.

Bearman, P. W., 1968: Digital analysis of hot-wire data, N P L Aero Report, No.1273.

Beauchamp, K. G. and Yuen, C. K., 1979: Digital Methods for signal analysis, George Allen and Unwin, London.

Bendat, J. S. and Piersol, A. G., 1966: Measurement and analysis of random data, John Wiley and Sons, New York.

Blackman, R. B. and Tukey, J. W., 1958: The measurement of power spectra from the point of view of communications engineering, Bell System Technical Journal, Vol. 37 (republished 1959: Dover Pub., N. Y.).

Bradshaw, P., 1970: Experimental fluid mechanica, second edition, Pergamon Press Ltd., Oxford.

Bruun, H. H., 1979: Interpretation of hot-wire probe signals in subsonic flows, J. Phys. E: Sci. Instrum. 12, 1116 - 1128.

Bryer, D. W. and Pankhurst, R. C., 1971: Pressure probe methods for determining wind speed and flow direstion, Her Majesty's Stationary Office, London.

Burhanuddin, S., 1980: Measurement of wall shear stress with hot-wire anemometer, M.Sc. Thesis, University of Manitoba.

Champagne, F. H., 1965: Turbulence measurements with inclined hot-wires, Boeing Scientific Research Laboratories, Flight Science Laboratory, Rep. 103.

Chen, C-T., 1979: One-dimensional digital signal processing, Marcel Dekker, New York.

Coles, D. E., 1956: The law of the wake in the turbulent boundary layer, J. Fluid Mech. 1, 191 - 226.

Compte-Bellot, G., 1965: Ecoulement turbulent entre deux parois parallels, Publ. Sci. et Tech., Min. Air No. 419, Paris (English translation 1969 by Bradshaw, P., ARC No. 31609).

Cooley, J. W. and Tukey, J. W., 1965: An algorithm for machine calculation of complex Fourier series, Math. Comput., Vol. 19, 297-301.

Dang, T., 198_: Substrate influence on flush mounted probes, M.Sc. thesis, University of Manitoba (in progress).

Derksen, R. W., 1981: The response of a hot-wire of finite length to fine-scale structure in a turbulent flow, M.Sc. thesis, University of Manitoba.

Derksen, R. W., 1986: An experimental investigation of the fluctuating wall shear stresses in an eight degree conical diffuser, Ph.D. Thesis, University of Manitoba.

Eckhouse, R. H. and Morris, R. L., 1979: Minicomputer systems - organization, programming and applications (PDP-11), Prentice-Hall, Inc., Englewood Cliffs, New Jersey.

Frei, D. and Thomann, H., 1980: Direct measurements of skin friction in a turbulent boundary layer with a strong pressure gradient, J. Fluid Mech. 101, 79-95.

Frenkiel, F. N. and Klebanoff, P. S., 1967 a : High-order correlations in a turbulent field, Phys. Fluids 10, 507-520.

Frenkiel, F. N. and Klebanoff, P. S., 1967 b : Correlation measurement in a turbulent flow using high-speed computing methods, Phys. Fluids 10, 1737-1747.

Freymuth, P., 1982: A bibliography of thermal anemometry, TSI Incorporated.

Gibson, C. H., Stegen, G. R., and McConnell, S., 1970: Measurements of the universal constant in Kolmogoroff's third hypothesis for high Reynolds number turbulence, Phys. Fluids 13, 2448-2451.

Gibson, C. H., Stegen, G. R., and Williams, R. B., 1970: Statistics of the fine structure of turbulent velocity and temperature fields measured at high Reynolds number, J. Fluid Mech. 41, 153-167.

Goldstein, S., ed., 1938: Modern developments in fluid dynamics, Vol. 1, Clareden Press, Oxford (rereleased 1965: Dover Pub.).

Gupta, B. L., 1927: Application of thermionic valves to hot-wire anemometry, J. Sci. Instrum. 4, 202-205.

Helland, K. N. and Van Atta, C. W., 1976: Response of constant-current and constant-temperature anemometers to artificial turbulence, Phys. Fluids 19, 1109-117.

Hinze, J. O., 1959, 1975: Turbulence, second edition, McGraw-Hill, Inc., U.S.A.

Hummel, R. H., 1978: Turbulence structure in a conical diffuser, Ph.D. thesis, University of Manitoba.

Johnson, F. D. and Eckelmann, H., 1984: A variable angle method of calibration for X-probes, applied to wall bounded shear flows, Exp. in Fluids 2, 121 - 130.

Jørgensen, F. E., 1971: Directional sensitivity of wire and fiber film probes, an experimental study, DISA Inf. 11, 31 - 37.

Kassab, S. Z., 198_ : Turbulence structure in axis-symmetry-wall bounded flows, Ph.D. thesis, University of Manitoba (in progress).

Kendal, J. M., 1970: The turbulent boundary layer over a wall with progressive surface waves, J. Fluid Mech. 41, 259 - 281.

Kuo, A. Y.-S. and Corrsin, S., 1971: Experiments on intermittency and fine structure distribution functions in fully turbulent field, J. Fluid Mech. 50, 285 - 319.

Laufer, J., 1954: The structure of turbulence in fully developed pipe flow, N.A.C.A., Rep. No. 1174.

Lawn, C. J., 1969: Turbulence measurement with hot wires at B.N.L., Central Electricity Generating Board., Berkeley Nuclear Laboratories, Rep. RD/B/M 1277.

Lawn, C. J., 1970: Application of the turbulence energy equation to fully developed flow in simple ducts, Central Electricity Generating Board., Berkeley Nuclear Laboratories, Rep. RD/B/R 1575(A).

Morris, J. T., 1912: The electrical measurement of wind velocity, Engineering 44, 892-894.

Okwuobi, P. A. C., 1972: Turbulence in a conical diffuser with fully developed pipe flow at entry, Ph.D. thesis, University of Manitoba.

Oppenheim, A. V. and Schafer, R. W., 1975: Digital signal processing, Prentice-Hall.

Overbeck, A., 1895: Ueber die abkuehlende Wirkung von Luftstroemen, Annalen d. Phys. u. Chem. 56, 397-411.

Panton, R. L., 1984: Incompressible flow, John Wiley and Sons, Inc., New York.

Patel, V. C.,1965: Calibration of the Preston tube and limitations on its use in pressure gradients, J. Fluid Mech. 23, 185 - 208.

Preston, J. H., 1954: The determination of turbulent skin friction by means of Pitot tubes, J. Roy. Aero. Soc. 58, 109 - 121.

Pierce, R. E., 1972: Statistical analysis of turbulence using a large scale digital computing system, Ph.D. thesis, The Pennsylvania State University.

Sastry, M. S., 1984: Comparison of turbulence data obtained from hot-wire signals by different methods, Proceedings of the Western Michigan Conference on Mechanical Engineering, Kalamazoo, Michigan, 284-289.

Schlichting, H., 1979: Boundary - layer theory, seventh edition, McGraw-Hill, Inc., U.S.A.

Serag, M. A.-A. E.-S., 1978: The influence of the length and diameter on the response characteristics of a hot-wire probe to the fine scale structure of turbulence, M.Sc. thesis, University of Manitoba.

Sovran, G. and Klomp, E. D., 1967: Experimentally determined optimum geometries for rectilinear diffusers with rectangular, conical or annular cross-section, Proc. of Gen. Motors Symposium on Internal Flow, Amsterdam, Elsevier Pub. Co.

Tennekes, H. and Wyngaard, J. C., 1972: The intermittent small-scale structure of turbulence: data processing hazards, J. Fluid Mech., 55, 93 - 103.

Van Atta, C. W. and Chen, W. Y., 1968: Correlation measurements in grid turbulence, J. Fluid Mech. 34, 497-515.

Webster, C. A. G., 1962: A note on the sensitivity to yaw of a hot-wire anemometer, J. Fluid Mech. 13, 307 - 312.

Wyngaard, J. C. and Lumley, J. L., 1967: A sharp cutoff spectral differentiator, J. Appl. Meteorol., Vol. 6, 952 - 955.

Ziegler, M. A., 1931: A complete arrangement for the investigation, the measurement and the recording of rapid airspeed fluctuations with very thin and short hot wires, Proc. Koninkl. Akad Van Wetenschap, Te Amsterdam 34, 663-673.

Appendix A

DIRECTIONAL SENSITIVITY OF THE CROSS WIRE PROBE

Response of a hot wire probe depends on the flow angle to the wire axis. Various techniques have been developed to take this effect into account. Early investigations by Champagne [1965] and others have shown the importance of a yaw factor k_1, which is included in the correction term for the tangential cooling velocity.

The effective cooling velocity acting on a sensor may be expressed as:

$$U(eff)^2 = U_1{}^2+k_1{}^2U_2{}^2 + k_2{}^2U_3{}^2$$

where U_1 is the velocity parallel to the probe supports, U_2 is the velocity parallel to the probe sensor, U_3 is the binormal velocity, perpendicular to both the sensor and probe supports, k_1 is the yaw factor, and k_2 is the pitch factor.

Hinze [1975] proposed the effective value of U can be approximately determined by the two dimensional equation:

$$U(eff)^2=U^2(\cos^2\alpha + k_1{}^2\sin^2\alpha)$$

where α is the flow angle with respect to the U_1 direction and the yaw factor k_1 takes on a small value. In the limiting case of an infinitely long wire, the angle sensitivity of the hot wire is expressed by the cosine law:

$$U(eff) = U \cos \alpha \quad .$$

The dimensionless yaw correction k_1, generally taken to be constant, is an empirically determined scalar which characterizes the sensor. It is a measure of sensor sensitivity to parallel flow. In the idealized case where only the normal component U_1 is responsible for cooling, k_1 is taken to be zero. When the flow is parallel to the sensor, cooling is less effective than for perpendicular flow resulting in $k_1 < 1$.

Although k_1 is not a true constant for all velocities and values of α, a fixed value works well within a limited range. Webster [1962] suggests k_1 takes a value between 0.1 and 0.3 depending on the magnitude of the velocity, decreasing as the velocity is increased. Champagne [1965] found that k_1 decreases nearly linearly with l/d from $k_1 = 0.2$ at $l/d = 200$ to $k_1 = 0$ at $l/d = 600$ to 800 where l is the sensitive length of the sensor and d is the diameter of the sensor.

Jørgensen [1971] tested several DISA wires in order to determine the variation of k_1 and k_2 with flow angle and velocity. He found the yaw factor k_1 depends on the sensor geometry and the angle of inclination, decreasing with increasing angles of α. He also found the pitch factor k_2 varied between 1.05 and 1.12, depends on sensor geometry, prong length, and slightly on velocity but is nearly independent of the pitch angle.

The directional sensitivity of the sensor is the basis for a cross wire probe used to measure the instantaneous U and V velocity components in the x-y plane of the cross wire probe. Based on the validity of the cosine law, a simple sum and difference solution to determine U and V exists. For negligible binormal flow component and k_1 approaching zero, the effective cooling velocities of hot wires 1 and 2 of an X-wire probe may be written as:

$$U(1, eff) = U \cos \alpha - V \sin \alpha$$
$$U(2, eff) = U \sin \alpha + V \cos \alpha$$

from which the instantaneous U and V velocity components in the x and y directions are obtained as:

$$U = [U(1, eff) + U(2, eff)] / 2 \cos \alpha$$
$$V = [U(1, eff) - U(2, eff)] / 2 \sin \alpha.$$

However, the yaw dependence of a hot wire probe deviates from a cosine law. Complicated exact solutions have been developed for yaw dependence. Bruun [1979] states a first order solution for the yaw correction factor as:

$$\cos^2\alpha \ (1-k_1{}^2)/[\cos^2\alpha(1-k_1{}^2) + k_1{}^2] \ .$$

Lawn [1969, 1970], based upon previous studies, proposed the yaw sensitivity coefficient for a DISA cross wire probe to be $k_1 = 0.23$ and used the yaw correction factor in deriving the turbulence velocities and shear stresses from the voltage signals where the correction factor for the DISA X-array probe ($\alpha = 45°$) is:

$$(1 - k_1^2) / (1 + k_1^2) \quad .$$

For $\alpha = 45°$ and $k_1 = 0.23$, the yaw correction factors proposed by Bruun and Lawn are equal to 0.8995. Reynolds shear stress measurements, uv, in fully developed pipe flow by Dang [198_], also support the yaw correction value, $k_1 = 0.23$, given by Bruun and Lawn.

As the yaw factor is a necessary correction to be taken into account due to the tangential cooling for inclined hot wires, v', w', $\overline{uv}$, and $\overline{uw}$ values are multiplied by a factor of 1.1117, the reciprocal of Lawn's proposed correction factor, as a correction for yaw. In general, the yaw correction is used with mixed stresses such that the corrected mixed correlations become:

$$\overline{u^m v^n} \text{ (cor)} = [(1+k_1^2)/(1-k_1^2)]^n \, \overline{u^m v^n} \text{(meas)}$$

However, when using the central moments, the yaw correction factor cancels since the mixed correlations are divided by appropriate powers of the rms values. That is:

$$\frac{\overline{u^m v^n} \text{ (cor)}}{u'^m v'^n \text{ (cor)}} = \frac{[(1+k_1^2)/(1-k_1^2)]^n \, \overline{u^m v^n} \text{(meas)}}{[(1+k_1^2)/(1-k_1^2)]^n \, u'^m v'^n \text{ (meas)}}$$

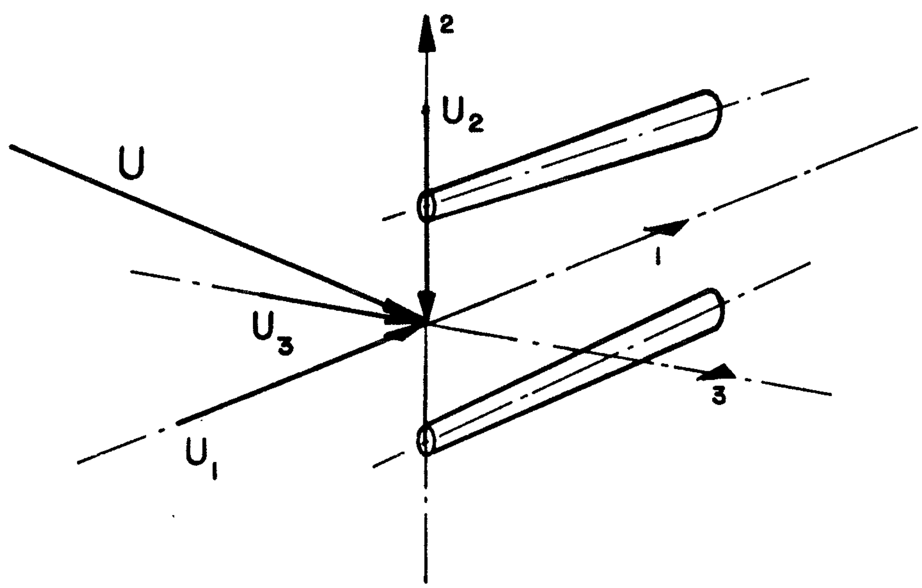

Figure A.1: Velocity Components

Appendix B

CORRECTIONS IN WALL PROXIMITY

Many factors affect the readings of a hot wire very close to a solid surface. The distance between the hot wire and the wall, the flow velocity, aerodynamic effects near the wall, the thermal nature of the wall material, and the calibration of the anemometer all influence the anemometer readings in the vicinity of the wall.

The hot wire gives higher than its true readings in approximately the first millimeter from the wall, or in terms of wall variables in the range $Y_+ \leq 5$ for the linear region of velocity. As a definite relationship exists between the voltage output from the anemometer and the distance between the wall and the hot wire, the signal from the hot wire may be used to measure the distance between the wire and the wall within the linear velocity region. The actual distance that can be measured is affected by the Reynolds number of the flow since as the flow Reynolds number or velocity increases, the amount of excessive heat loss and hence the linear distance in the sublayer region of the flow measurable by the anemometer is decreased.

As the rate of heat loss from the hot wire increases with decreasing distance to the solid surface, the flow velocity as determined directly from the anemometer output signal is over estimated. In addition, as there is no proper method of calibrating the hot wire near a solid surface, linearization must be performed in situ beyond the region of the sublayer or in some other 'ideal' calibration facility. A method of correcting for the wall effect must be used.

In this set of measurements, the wall correction used to account for the higher heat transfer close to the solid wall was similar to that used by Van Der Hegge Zijnen [1924]. A velocity difference was determined from the linearized anemometer output signal during the flow and no flow conditions imposed at each measuring position in the sublayer region of the turbulent flow in the test tunnels. The velocity difference was then taken to be the true flow velocity for that position in the flow. As a linear velocity gradient exists next to the surface in any turbulent flow, the distance between the hot wire and the wall was also corrected from the no slip condition or $U = 0$ at the wall and the linear velocity profile in the sublayer region of the flow for $Y_+ \leq 5$.

Even with the wall correction, severe errors can exist in measurements of small distances close to the wall and velocities of less than 0.5 m/sec. Special care is necessary for measurements in close proximity to the wall in order to insure reliable results.